The Cytotoxic Effects of Malondialdehyde on Human Lung Fibroblast Cells

Sally Ann Yates

A thesis submitted in partial fulfilment of the requirements of
Liverpool John Moores University for the degree of
Doctor of Philosophy

March 2015

ABSTRACT

Malondialdehyde (MDA) is a mutagenic and carcinogenic product of lipid peroxidation which has also been found at elevated levels in smokers. MDA reacts with nucleic acid bases to form pyrimidopurinone DNA adducts, of which 3-(2-deoxy-β-D-erythro-pentofuranosyl)pyrimidol[1,2-α]purin-10(3*H*)-one (M_1dG) is the most abundant and has been linked to smoking. Mutations in the *TP53* tumour suppressor gene are associated with half of all cancers. This research applied a multidisciplinary approach to investigate the toxic effects of MDA on the human lung fibroblasts MRC5, which have an intact p53 response, and their SV40 transformed counterpart, MRC5 SV2, which have a sequestered p53 response.

Both cell lines were treated with MDA (0-1000 μM) for 24 and 48 h and subjected to a variety of analyses to examine cell proliferation, cell viability, cellular and nuclear morphology, apoptosis, p53 protein expression, DNA topography and M_1dG adduct detection. For the first time, mutation sequencing of the 5' untranslated region (UTR) of the *TP53* gene in response to MDA treatment was carried out.

The main findings were that both cell lines showed reduced proliferation and viability with increasing concentrations of MDA, the cell surface and nuclear morphology were altered, and levels of apoptosis and p53 protein expression appeared to increase. A LC-MS-MS method for detection of M_1dG adducts was developed and adducts were detected in CT-DNA treated with MDA in a dose-dependent manner. DNA appeared to become more fragmented with increasing MDA concentration, and the number of mutations in the 5' UTR region of the *TP53* gene also increased. The majority of mutations observed were insertions, compared to lung cancer mutation data where the majority were G to T transversions. This was unexpected, suggesting that tobacco smoke compounds have a different role in mutagenesis than endogenous lipid peroxidation. Thus, MDA has been found to have a clear effect on human lung fibroblasts at both the cellular and DNA level.

ACKNOWLEDGEMENTS

I would like to express my sincere gratitude to my supervisors, Dr Sharon Moore and Dr Mark Murphy, for their continued patience, support and guidance throughout the course of my project.

I would also like to thank Dr Nicola Dempster for her assistance with LC-MS and LC-MS-MS, Campbell Woods and Phil Salmon for their help with HPLC, and Pete Hamlett for his help and guidance.

I would like to thank Lieslot Hemeryck and Dr Lynn Vanhaecke of Ghent University, Belgium, for analysing a number of my samples by LC-MS-MS for independent verification.

Finally, I would like to thank my husband, family and friends for their patience, encouragement and support throughout all of my years of study, in particular during my PhD.

TABLE OF CONTENTS

LIST OF FIGURES

LIST OF SCHEMES

LIST OF TABLES

LIST OF ABBREVIATIONS

$2^{-\Delta\Delta Ct}$	**Comparative Cycle Threshold Method**
^{32}P	**Phosphorus 32 Isotope**
3-D	**3-Dimensional**
8-oxo-dG	**8-oxo-7,8-dihydro-2'-deoxyguanosine**
AFM	**Atomic Force Microscope**
AIDS	**Acquired Immune Deficiency Syndrome**
ANOVA	**Analysis of Variance**
Apaf-1	**Apoptotic Peptidase Activating Factor 1 Gene**
ARF	**Alternate Reading Frame Tumour Suppressor Gene**
ATP	**Adenosine Triphosphate**
Bax	**Bcl-2 Associated X Gene**
Bcl-2	**B-Cell Lymphoma-2 Gene**
Bcl-XL	**B-Cell Lymphoma Extra Large Gene**
bp	**Base Pair**
BPDE	**Benzo[α]pyrene diolepoxide**
BSA	**Bovine Serum Albumin**
$CaCl_2$	**Calcium Chloride**
CDKN1A	**Cyclin-Dependent Kinase Inhibitor 1A Gene (p21)**
cDNA	**Complementary DNA**
CFM	**Chemical Force Microscopy**

CO_2	**Carbon Dioxide**
CT	**Calf Thymus**
C_t	**Cycle Threshold**
DAPI	**4',6-Diamidino-2-Phenylindole**
DMSO	**Dimethyl Sulphoxide**
DNA	**Deoxyribonucleic acid**
DNP	**2,4-Dinitrophenlyhydrazine**
dNTP	**Deoxynucleotide**
dR	**Deoxyribose Residue**
ε	**Molar Absorption Coefficient**
e-	**Electron**
ECACC	**European Collection of Animal Cell Cultures**
ECM	**Extra Cellular Matrix**
EDTA	**Ethylenediaminetetraacetic Acid**
$EDTA.Na_2.H_2O$	**EDTA Disodium Salt Dehydrate**
ELISA	**Enzyme Linked Immunosorbent Assay**
EM	**Electron Microscope**
ERK	**Extracellular-Signal-Regulated Kinase Gene**
ES^+	**Positive Ion Mode**
Fas	**Fas Cell Surface Death Receptor Gene**
FBS	**Foetal Bovine Serum**
FLD	**Fluorescence Detection**
g	**Acceleration due to Gravity**

G_1 phase	**Growth 1 Phase of the Cell Cycle**
G_2 phase	**Growth 2 Phase of the Cell Cycle**
GAPDH	**Glyceraldehye-3-Phosphate Dehydrogenase**
GC-MS	**Gas Chromatography-Mass Spectrometry**
H_2O_2	**Hydrogen Peroxide**
HCl	**Hydrochloric Acid**
HClO	**Hypochlorous**
HEPES	**4-(2-hydroxyethyl)-1-Piperazineethanesulfonic Acid**
HO_2•	**Hydroperoxyl Radical**
HPLC	**High Performance Liquid Chromatography**
HR	**High Resolution**
IAP	**Inhibitor of Apoptosis Gene**
ISB	**Immunoslot Blot**
JNK	**c-Jun N-Terminal Kinase Gene**
k	**Growth Rate**
K_2HPO_4	**Dibasic Potassium Phosphate**
KCl	**Potassium Chloride**
KH_2PO_4	**Monobasic Potassium Dihydrogen Phosphate**
KOH	**Potassium Hydroxide**
LC-APCI-MS-MS	**Liquid Chromatography- Atmospheric Pressure Chemical Ionisation Tandem Mass Spectrometry**
LC-MS	**Liquid Chromatography-Mass Spectrometry**
LC-MS-MS	**Liquid Chromatography-Tandem Mass Spectrometry**

LM	**Light Microscope**
LOD	**Limit of Detection**
LOQ	**Limit of Quantitation**
M phase	**Mitotic Phase of the Cell Cycle**
m/z	**Mass to Charge Ratio**
M_1dG	**3-(2-deoxy-β-D-erythro-pentofuranosyl)pyrimidol[1,2-α]purin-10(3*H*)-one**
M_1G	**Pyrimido[1,2-*α*]purin-10(*3H*)-one**
M^{2+}	**Divalent Cation**
MDA	**Malondialdehyde**
MDM-2	**E3-Ubiquitin-Proein Ligase Gene**
MEM	**Minimum Essential Medium Eagle**
$MgCl_2.6H_2O$	**Magnesium Chloride Hexahydrate**
MH^+	**Molecular Ion**
M_R	**Relative Molecular Mass**
MRM	**Multiple Reaction Monitoring**
mRNA	**Messenger Ribonucleic Acid**
MS	**Mass Spectrometry**
MS-MS	**Tandem Mass Spectrometry**
MTT	**(3-[4,5 dimethylthiazol-2yl]-2,5-diphenyl-tetrazolium bromide)**
n	**Number of Replicates**
N^2OPdG	**N^2-(3-oxo-1-propenyl)-deoxyguanosine**
N^6EtA	**1,N^6-etheno-2'-deoxyadenosine**

NaCl	**Sodium Chloride**
NEAA	**Non-essential Amino Acid**
NER	**Nucleotide Excision Repair**
NO•	**Nitric Oxide Radical**
NO_2•	**Nitrogen Dioxide Radical**
NSI	**Nanospray Ionisation**
O^{2-}	**Superoxide Ion**
•OH	**Hydroxyl Radical**
$ONOO^-$	**Peroxynitrite Ion**
p53	**Human Tumour Suppressor Protein**
PAH	**Polycyclic Aromatic Hydrocarbon**
PBS	**Phosphate Buffered Saline**
PCR	**Polymerase Chain Reaction**
PDA	**Photodiode Array**
PDT	**Population Doubling Time**
PFB	**Pentafluorobenzyl**
PI	**Isoelectric Point**
pK	**Negative Logarithm of the Dissociation Constant K**
PUFA	**Polyunsaturated Fatty Acid**
R^2	**Coefficient of Determination**
RIC	**Reconstructed Ion Chromatogram**
RNS	**Reactive Nitrogen Species**
RO•	**Alkoxyl Radical**

ROO•	**Peroxyl Radical**
ROS	**Reactive Oxygen Species**
rpm	**Revolutions Per Minute**
R_s	**Peak Resolution**
RSD	**Relative Standard Deviation**
RT-qPCR	**Reverse Transcription-Quantitative PCR**
SD	**Standard Deviation**
SEM	**Scanning Electron Microscope**
SIM	**Single Ion Monitoring**
SPE	**Solid Phase Extraction**
TBA	**2-thiobarbituric Acid**
TBARS	**Thiobarbituric Acid Reactive Substances**
TBE	**Tris/Borate/EDTA Buffer**
TE	**Tris/EDTA/$MgCl_2$ Buffer**
TEM	**Transmission Electron Microscope**
TIC	**Total Ion Current**
TLC	**Thin Layer Chromatography**
TMP	**1,1,3,3-Tetramethoxypropane**
TP53	**Human Tumour Suppressor Gene**
Tris	**Tris(hydroxymethyl)aminomethane**
UTR	**Untranslated Region**
UV	**Ultra Violet Light**

CHAPTER 1

INTRODUCTION

1.1. Cancer Incidence

Cancer is a diverse group of diseases with similar characteristics, of which there are over 200 types. One in three people will develop cancer at some point in their lives (CRUK, 2014). There is variation in cancer risk between countries, particularly between the developed and developing world, for each type of cancer, suggesting that lifestyle and diet play an important role in the aetiology of the disease (CRUK, 2011). When migrant populations are studied, the cancer rates reflect those of the new local population, rather than the country of origin, often within a single generation (Shuker and Benford, 1997). For example, breast cancer rates increased in female Italian and Polish migrants in Australia to Australian levels compared to the country of origin (Nelson, 2006). Thus, it would appear that there is a link between cancer and lifestyle.

There have been 14 major lifestyle, dietary and environmental risk factors associated with cancer: tobacco, alcohol, diet (red meat, fruit and vegetables, salt and fibre), obesity, lack of exercise, occupation, infections, radiation (ionising and solar), hormones and reproductive history. These factors were responsible for 42.7% of cancers in 2010 in the UK, with the greatest risk factor being tobacco smoke exposure which was the cause of 19.4% of new cancer cases (Parkin *et al.*, 2011). Tobacco smoking causes

cancers of the lung, larynx, pharynx, oesophagus, stomach, liver, kidney, pancreas, paranasal sinuses, oral cavity, bladder, ureter, cervix, bone marrow, colon, rectum and ovary (Ezzati *et al*.,2005; Gallus *et al*., 2003; Hannan *et al*., 2009; Jordan *et al*., 2006). Of the cases of lung cancer in the UK in 2010, 86% were due to exposure to tobacco smoke and of these 97.4% were due to smoking (Parkin *et al.*, 2011). Tobacco smoking has been linked with atherosclerosis, mutagenesis and cancer of the respiratory tract and lungs. More than 60 carcinogens are present in tobacco smoke (Pleasance *et al.*, 2010), including polyaromatic hydrocarbons, aromatic amines, aldehydes, catechols and butadiene (Arif *et al.*, 2006). It is known that changes to DNA result in the formation of cancer. These changes to DNA may be brought about by exposure to sources of oxidative stress, which may be endogenous, such as malondialdehyde (MDA) formation, or exogenous, such as exposure to tobacco smoke carcinogens.

Of the 20,000 protein-coding genes of the human genome, ~140 have been identified that promote tumorigenesis, primarily tumour suppressor genes and oncogenes. Common adult tumours, such as breast and colon, have an average of 33 – 66 genes which contain non-synonymous somatic mutations. However, other tumour types, including lung and melanoma, where mutagens are involved e.g. tobacco smoke constituents and UV light, have these mutations in around 200 genes. Moreover, there are up to ten times more non-synonymous somatic mutations in lung carcinomas from smokers than from non-smokers. Of the somatic mutations found in tumour cells, only a small number (2 – 8) play a major role in tumourigenesis (Vogelstein *et al.*, 2013). However, almost every type of human cancer exhibits DNA damage in one specific gene,

the tumour suppressor *TP53*, with mutation rates varying from 10-100% for different cancer types (Rivlin *et al.*, 2011).

Many factors are associated with cancer and the main reasons identified for further study of the influence of MDA are: the wide range of lifestyle factors linked to MDA and its association with cancer incidence; the need for sensitive and robust methods of analysis of DNA adducts resulting from MDA exposure; and to expand the knowledge of the mechanisms of cancer initiation. This chapter will consider research to date, methods and analysis, the cell lines utilised and specific regions of DNA that were studied.

1.2. Development of Cancer

Cancer develops progressively from initial abnormal cell growth and proliferation in a particular tissue, to invasion of the surrounding tissue and then metastasis. Six acquired functional capabilities of cancer cells have been described, as shown in Figure 1 (Hanahan and Weinberg, 2000). Genome instability resulting from the loss of function of tumour suppressor genes and other 'caretaker' genes enables pre-malignant cells to acquire these six capabilities. Genome instability can arise from a number of factors such as DNA damage, replication errors, chromosomal rearrangements and DNA repair deficiency. This instability can arise from chemical attack from endogenous and exogenous sources.

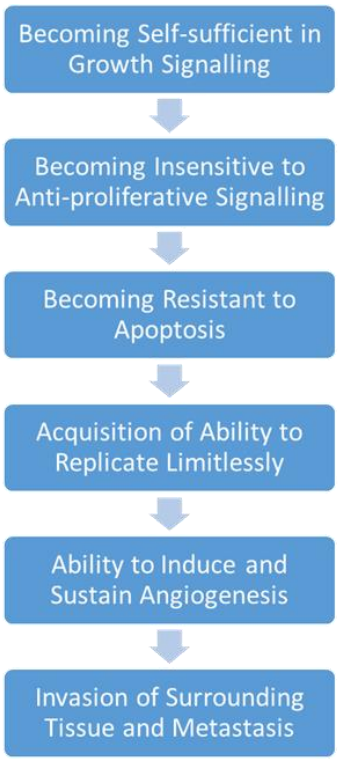

Figure 1. The six acquired functional capabilities of cancer cells (derived from Hanahan and Weinberg, 2000).

The initial stages of cancer are often induced by chemical attack to give DNA adducts, and various other types of DNA damage, that may subsequently lead to mutations. The accumulation of mutations in a number of key regulatory genes may result in cancer, of which endogenous DNA damage, a consequence of normal metabolism, is a significant cause. Additionally, exogenous DNA damage from ionising radiation, UV light and chemical agents such as those found in tobacco smoke, are also significant contributors (Jackson, 2009). The inherent chemical instability of DNA under physiological conditions, replication of sites containing DNA adducts and errors in the cellular DNA repair, replication and maintenance machinery contribute to DNA mutations (Niedernhofer *et al.*, 2003).

Genotoxic oxidizing agents, such as reactive oxygen species (ROS) may cause protein oxidation, protein degradation and lipid peroxidation. In addition, DNA damage is also caused by ROS as DNA strand-breaks, DNA cross-links with proteins and DNA adducts. The presence of ROS can directly activate the intrinsic apoptotic pathway of the cell or indirectly by ROS-induced DNA damage leading to activation of p53. The extrinsic apoptotic pathway can also be activated by ROS by activation of upstream kinases. ROS may cause mutagenesis and then alteration of the apoptosis pathway. This may lead to carcinogenic cells that are apoptosis resistant (Chen and Shi, 2002).

1.3. The *TP53* Tumour Suppressor Gene

TP53 was discovered over 30 years ago and is located on chromosome 17p13.1. and has 11 exons. It has been found to be a major tumour suppressor gene, where mutations in the gene can promote tumorigenesis. p53 plays a key role in a number of cellular pathways (Figure 2), including the DNA damage repair pathway, apoptosis , cell cycle arrest and cellular senescence (Hainaut and Hollstein, 2000).

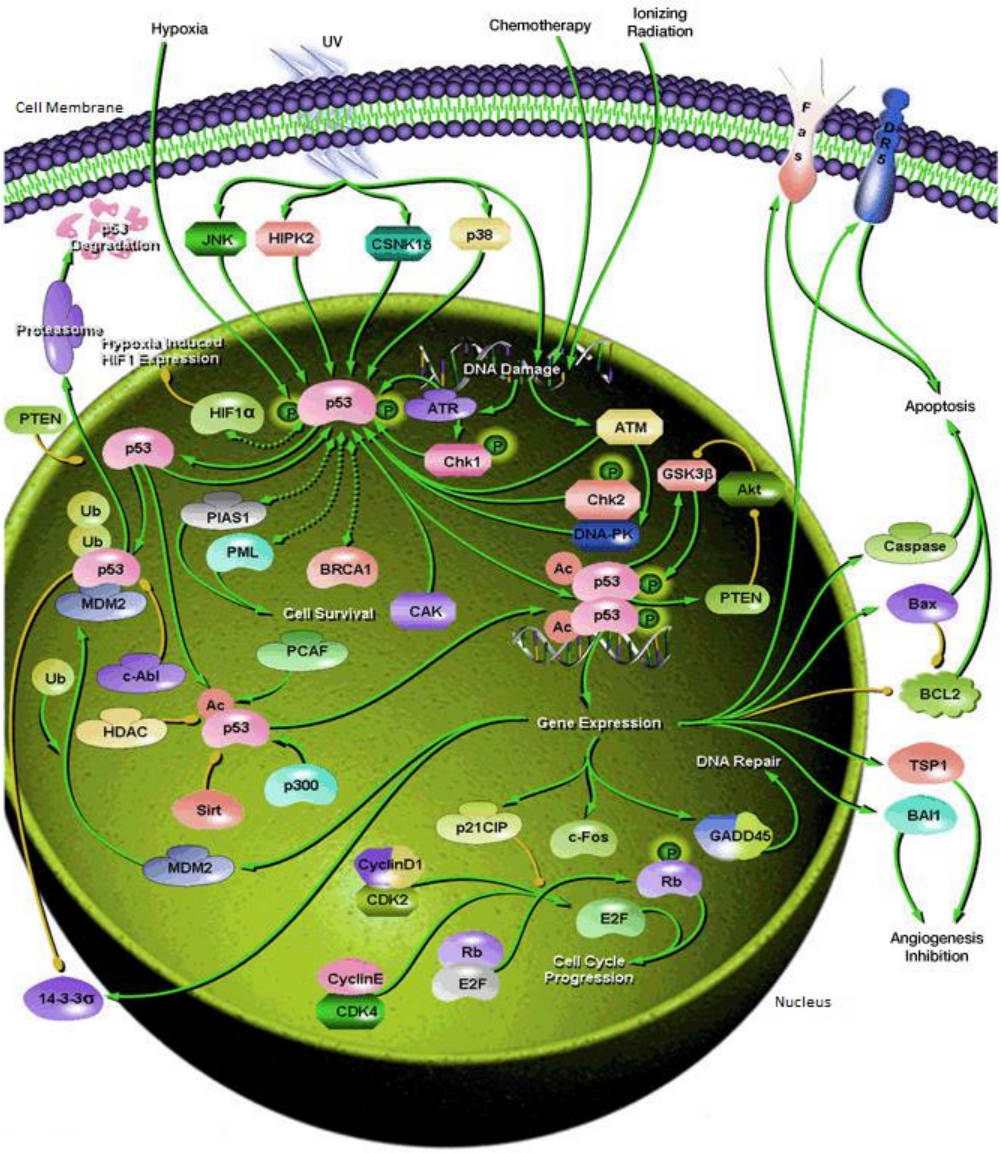

Figure 2. p53 signalling pathways in response to DNA damage. (Adapted from SABiosciences.com (2015)).

The structure was determined of the core domain of p53 tumour suppressor protein with a DNA binding site by x-ray crystallography (2.2 Å resolution), which consisted of three core domain units (Figure 3) and a 21 base pair (bp) DNA fragment in an asymmetric unit. Each of the three core domains are similar in structure with four and five β strands sandwiching two antiparallel β sheets. At one end of this sandwich is a

loop-sheet-helix motif and two large loops. The two loops are held together by a zinc atom with one histidine residue and three cysteine residues acting as ligands. The loop-sheet-helix motif and one of the large loops are involved in binding to both the major and minor grooves of DNA (Cho *et al.*, 1994).

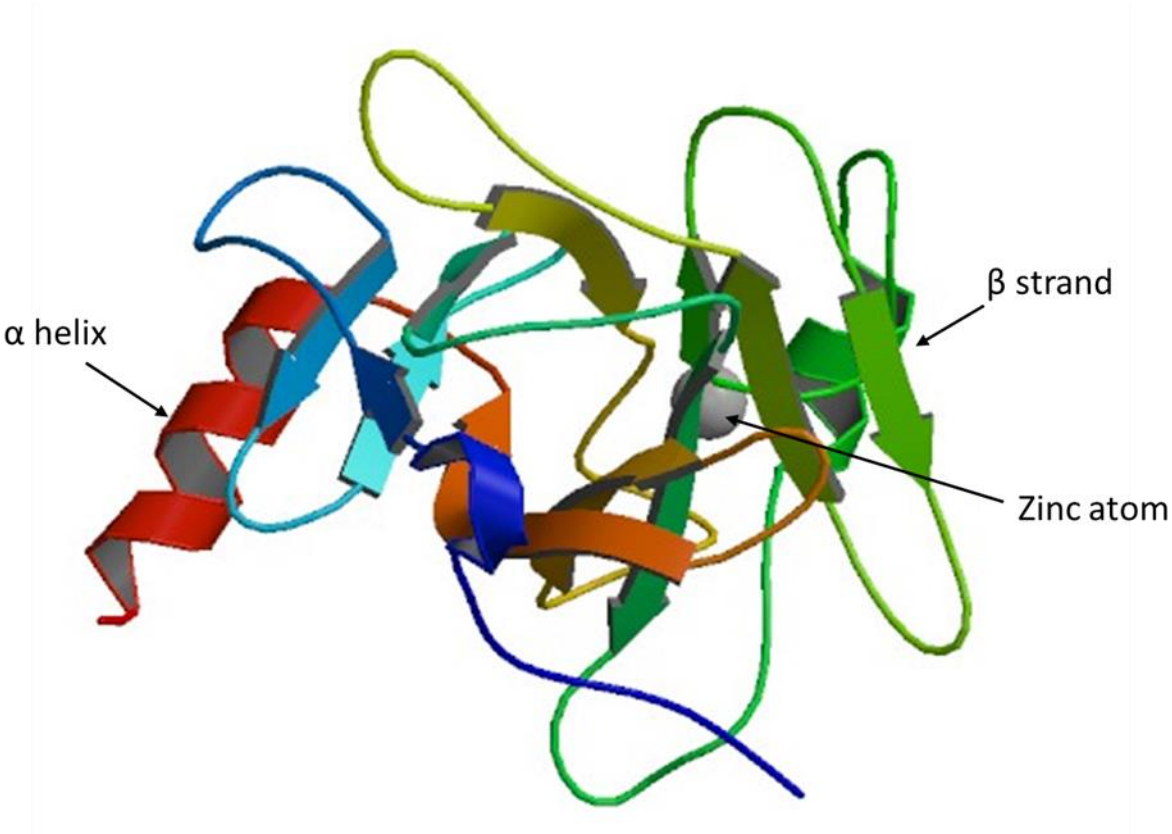

Figure 3. p53 core domain. Image from the RCSB PDB (Wang, 2007)

Apoptosis and cellular senescence are mechanisms by which p53 acts as a tumour suppressor (Levine and Oren, 2009). p53 controls the expression of over 100 genes (Nikoshkov and Hurd, 2006). It is induced rapidly to high levels in response to cellular stress in order to prevent propagation of DNA damage (Moll and Petrenko, 2003). The *TP53* gene is expressed constitutively at the basal level in almost all cell types and has a rapid turnover. To maintain p53 expression at a basal level, a negative regulator is

required. p53 promotes transcription of the *Mdm-2* gene, an ubiquitin ligase which attaches ubiquitin molecules to p53, labelling it for degradation, thus keeping p53 levels low. p53 is induced in response to DNA damaging agents such as oxidizing agents, irradiation, carcinogenic and cytotoxic compounds. Damage such as DNA strand breaks e.g. by irradiation, or DNA adduct formation by alkylating agents induce p53, as do other non-DNA damaging cellular stress factors such as hypothermia and hypoxia (Hainaut and Hollstein, 2000). When DNA damage is detected, p53 is phosphorylated which stabilises it and allows levels to rise (Dagan Feng and Zaytoon, 2006). p53 has a short half-life of 5-30 min in normal cells (Moll and Petrenko, 2003), however this can be prolonged due to missense mutations in the *TP53* gene (Cherneva *et al.*, 2009). Reconstitution of a mutant *TP53* gene to wild type *TP53* in a tumour cell line may lead to growth arrest at both G_1 and G_2/M phases of the cell cycle, thus apoptosis and cellular senescence are mechanisms by which p53 acts as a tumour suppressor (Levine and Oren, 2009).

A number of human genes have been identified that undergo alternative splicing, whereby different transcripts are generated by different combinations of exons or segments of exons, and has an important role in gene regulation, linking cell signalling and splice control. Human p53 alternative splice variants have been identified (Nikoshkov and Hurd, 2006), transcription of which are controlled by two promoters, P_1 and P_2, the latter is an alternative intragenic promoter (Wei *et al.*, 2012). At least twelve different p53 protein isoforms have been identified (including p53 (α, β and γ), Δ40p53 (α, β and γ), Δ133p53 (α, β and γ) and Δ160p53 (α, β and γ)), a number of which are shown in Figure 4, and of which the central DNA-binding domain is conserved (Courtois

et al., 2004; Wei *et al.*, 2012). These are produced by alternative splicing, use of alternative promoters and alternative initiation and translation of the p53 gene.

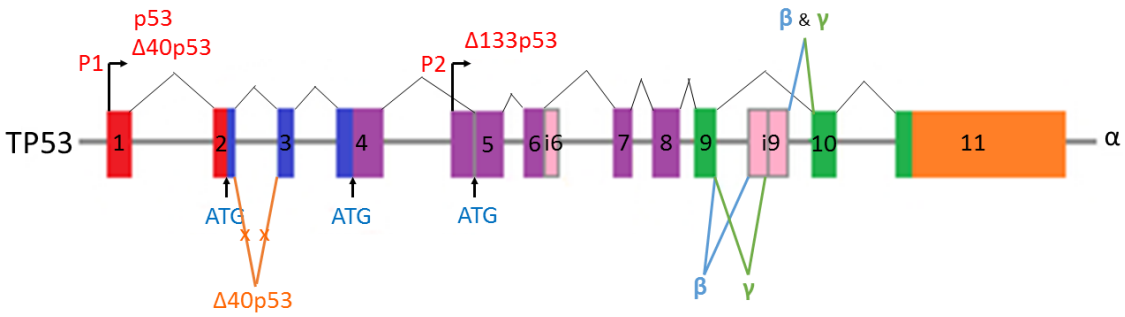

Figure 4. ***TP53*** **isoforms: exons 1 – 11 and introns 6 and 9 are shown as boxes with promoters P_1 (for p53 and Δ40p53 initiation of transcription) and P_2 (for Δ 133p53 initiation of transcription) and alternative start codons (ATG) for translation start sites. No splicing of intron 2 occurs in Δ40p53 transcripts.** ***TP53*** **α transcripts have normal splicing of exons with intron 9 fully spliced.** ***TP53*** **β and γ transcripts have alternative splicing of intron 9. (Adapted from Wei** ***et al*** **(2012)).**

The different isoforms differentially regulate gene expression in response to cellular stresses and are important for regulation of cell fate (Surget *et al.*, 2014). Alterations of some p53 isoforms have been associated with cancer, for example, p53β overexpression has been found in renal cell carcinoma, melanoma cell lines, and associated with tumour progression, whereas reduced expression has been found in breast cancer (Hu *et al.*, 2014). p53 isoforms have been found to have abnormal expression in cancers, including colon, ovarian and lung (Surget *et al.*, 2014).

1.4. Apoptosis

The cell number in multicellular organisms and tissues is highly regulated, maintaining the balance between cell division and programmed cell death (apoptosis). The apoptotic pathway involves the caspase family of proteases which cleave specific proteins, at aspartic acid residues, in the nucleus and cytoplasm. Procaspases, the inactive precursors of caspases, are activated by cleavage by other caspases, resulting in a proteolytic caspase cascade. The cascade is activated by an intra or extracellular death signal and is self-amplifying and irreversible. Adaptor proteins aggregate procaspases. An external activation signal is the Fas ligand on the surface of killer lymphocytes which binds to a Fas receptor on the cell surface, recruiting adaptor proteins and initiating a caspase cascade. An internal signal is the release of cytochrome c from mitochondria into the cytosol which binds and activates the adaptor protein Apaf-1 (Alberts *et al.*, 2002). Damage to DNA may activate the apoptotic signalling pathway (Ji *et al.*, 1998), requiring p53 to transcribe *Bcl-2* genes, initiating the release of cytochrome c into the cytosol. The *Bcl-2* gene family regulates procaspase activation, some of which inhibit apoptosis and others promote procaspase activation. The *IAP* (inhibitor of apoptosis) gene family act by binding to either procaspases, preventing activation, or to caspases, to inhibit activity.

Mdm-2 is a p53 negative regulator. DNA damage leads to a rapid increase in p53 due to inactivation of Mdm-2/p53 interaction. p53 activation leads to reversible cell cycle arrest and induction of DNA repair mechanisms to apoptosis or senescence (loss of

proliferative capacity). p53 transactivates genes that induce apoptosis e.g. *Fas* and *Bax* and genes that induce cell cycle arrest e.g. *CDKN1A* (Enge *et al.*, 2009).

Apoptotic pathway defects can contribute to a number of diseases such as cancer. For example, overexpression of *Bcl-2*, upregulation of *Bcl-x_L*, inactivation of *Bax*, and mutations in upstream and downstream components of the p53 pathway e.g. *Mdm-2*, *ARF* and *Bax* may all lead to tumorigenesis (Lowe and Lin, 2000).

1.5. Reactive Oxygen Species

ROS are species such as superoxide (O_2^-), hydrogen peroxide (H_2O_2), hypochlorous acid (HClO), hydroxyl (•OH), hydroperoxyl (HO_2•), alkoxyl (RO•) and peroxyl radicals (ROO•). The •OH free radical is a highly reactive oxidant and can attack most biomolecules (Gutteridge, 1995).

Molecular oxygen is reduced when utilised for aerobic oxidation of carbon and hydrogen rich foods to produce heat and energy for life (Scheme 1). Two of the intermediates formed by reduction of oxygen are free radicals plus H_2O_2, which readily mixes with water and diffuses rapidly across cell membranes. It can form highly reactive free radicals in the presence of the transition metal ions. Catalase and glutathione peroxidise remove unwanted H_2O_2 from the cells (Gutteridge, 1995).

$O_2 + e^- + H^+ \Longrightarrow HO_2\bullet$ (1)

$HO_2\bullet \Longrightarrow H^+ + O_2^-$ (2)

$O_2^- + 2H^+ + e^- \Longrightarrow H_2O_2$ (3)

$H_2O_2 + e^- \Longrightarrow OH^- + \bullet OH$ (4)

$\bullet OH + e^- + H^+ \Longrightarrow H_2O$ (5)

Superoxide dismutase catalyses:

$2O_2^- + 2H^+ \Longrightarrow H_2O_2 + O_2$ (6)

Scheme 1. The reduction of molecular oxygen by the stepwise addition of free electrons (equations 1-5). The enzyme superoxide dismutase catalyses the dismutation reaction of free radical superoxide in aqueous solution to hydrogen peroxide and oxygen (equation 6). (Adapted from Gutteridge (1995)).

The Fenton reaction describes the reaction between iron salts (Fe^{2+} and Fe^{3+}) and H_2O_2. The hydroxyl radicals produced go on to react with other molecules (Scheme 2) (Ayala *et al.*, 2014).

$Fe^{2+} + H_2O_2 \Longrightarrow Fe^{3+} + OH^- + \bullet OH$

$Fe^{3+} + H_2O_2 \Longrightarrow Fe^{2+} + HO_2\bullet + H^+$

Scheme 2. The Fenton reaction (adapted from Gutteridge (1995)).

In addition to ROS, there are reactive nitrogen species (RNS). NO• (nitric oxide) is a weak reducing agent and $NO_2\bullet$ (nitrogen dioxide) is a powerful oxidising agent. NO• can react

with superoxide to produce peroxynitrite ($ONOO^-$) which is a powerful oxidant (Gutteridge, 1995). Hence, there is a vast source of radicals within the body.

1.6. Oxidative Stress

Oxidative DNA damage has been associated with the pathogenesis of a number of different diseases, including cancer and aging. Oxidative stress is the result of a cellular imbalance in antioxidants and pro-oxidants, where free radicals are produced in excess of normal cellular metabolic levels following xenobiotic exposure or radiation. Free radicals, such as ROS and RNS, interact and modify biomolecules (Cooke *et al.*, 2008). A free radical is an atom, molecule or ion that contains one or more unpaired valence electrons (Gutteridge, 1995). Polyphenolic compounds such as flavinoids, isoflavinoids, anthocyanins and catechins, along with other compounds such as carotenoids and vitamins A, C and E, are found in fruits and vegetables and a diet rich in these has been associated with reduced cancer risk. It has been proposed that these compounds act as antioxidants and thereby reduce oxidative damage and thus cancer risk (Hwang and Bowen, 2007). There is a link between chronic inflammation and the aetiology of cancer. Reactive oxidants, derived from superoxide anions and nitric oxide, are generated by the inflammatory response (Marnett, 2012).

DNA damage can be formed endogenously such as DNA adduct formation produced by metabolic activation of a carcinogen, or exogenously such as DNA strand breaks and oxygen-nitrogen adducts produced by direct attack by ROS and RNS. Point mutations resulting from oxidative stress may lead to carcinogenesis, particularly when the DNA

damage involves the activation of oncogenes or the loss of tumour suppressor genes. Damage to the sugars in DNA can also occur in addition to modification of the nucleic acid bases. The action of the enzymes DNA ligase and DNA polymerase can be blocked by deoxyribose fragments (Hwang and Bowen, 2007).

Endogenous sources of oxidative stress include immune reactions, transition metal mediated oxidation, the mitochondrial respiratory chain and enzymatic reactions. Exogenous sources include chemicals and toxins such as tobacco smoke, ionizing and non-ionising radiation and air pollution. Tobacco smoke contains a large number of gas (10^{15}) and tar (10^{14}) phase oxidants, including free radicals in a single puff (Pryor and Stone, 1993).

1.7. Malondialdehyde

MDA (Scheme 3) is an example of an endogenous source of oxidative stress, as it is a product of lipid peroxidation. It has been detected a low levels in biological samples from healthy individuals (0 – 47.2 μM) and at increased levels in samples subjected to oxidative stress (Esterbauer *et al*., 1991; Nielsen *et al.*, 1997; Tug *et al.*, 2005). The numerous reactive chemicals in the tar and smoke from tobacco cause oxidative stress and lipid peroxidation, leading to an increase in MDA formation (Atasayar *et al.*, 2004). It has also been found that there was an increase in plasma MDA in individuals who smoked tobacco (Montano *et al.*, 2010).

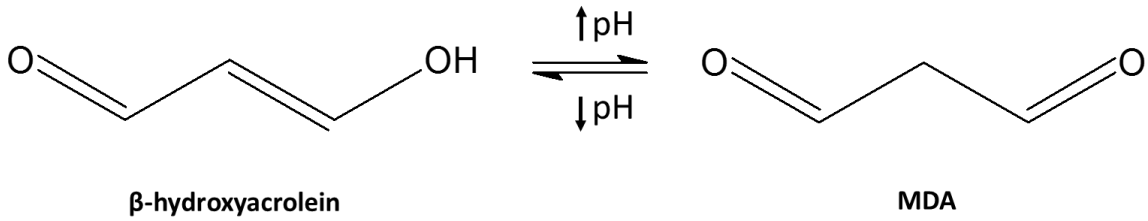

β-hydroxyacrolein **MDA**

Scheme 3. Tautomer β-hydroxyacrolein (in *trans* form) in equilibrium with MDA (adapted from Esterbauer *et al*. (1991)).

MDA exists in both its free state and also in complex with other biomolecules bound via SH and NH_2 groups (Cighetti *et al.*, 2002). Despite MDA having a low reactivity when present as an enolate ion at neutral pH, it can still react with nucleosides. MDA has been shown to induce frame shift mutations and base pair substitutions, in addition to formation of interstrand cross links in DNA. DNA-protein cross-links between DNA and histone proteins have also been reportedly mediated by MDA (del Rio *et al.*, 2005). MDA adducts with proteins and phospholipids have been identified (Agarwal and Draper, 1992). MDA reacts with bovine serum albumin (Takagi *et al.*, 2005), a key component in cell culture media, to form a protein adduct (He *et al.*, 2011). Adduction to proteins may result in denaturation due to alterations in the secondary and tertiary structure. MDA inhibited contraction of collagen in fibroblast cells when treated *in vitro*, and inhibited cell proliferation by interaction with serum proteins (Rittie *et al.*, 2002). Protein adducts can be formed by exposure of amine groups to MDA and monofunctional aldehydes, which are found in tobacco smoke (Freeman *et al.*, 2005).

MDA is hygroscopic when in the crystallised sodium salt form and only has a short storage time. In solution, at neutral and alkaline pH, the enolate anion is predominant. In acidic conditions (pH <4.5), MDA exists as the tautomeric undissociated enol form as

β-hydroxyacrolein (Scheme 3) in equilibrium with the dicarbonyl form. The C=C double bond is mainly *cis* and the cyclic chelate form is favoured due to intramolecular H bonds, although two *cis*-enols can form a dimeric complex (Esterbauer *et al.*, 1991). At physiological pH MDA exists as an enolate ion and has relatively low reactivity, with reactivity increasing as pH decreases. MDA is electrophilic and is strongly reactive towards nucleophiles, such as the basic amino acids histidine, arginine and lysine (Ayala *et al.*, 2014). MDA slowly condenses in aqueous solution under physiological conditions to form polymeric products 2-(3'-oxo-1'-propenyl)malondialdehyde and 2,4-dihydroxymethylene-3-(2,2-dimethoxyethyl)glutaraldehyde (Gomez-Sanchez *et al.*, 1993), however, although they are mutagenic, their formation is thermodynamically unfavourable under these conditions (Riggins *et al.*, 2004).

1.8. Formation of Malondialdehyde

MDA, widely used as a biomarker of oxidative stress, is the most abundant mutagenic and carcinogenic compound generated by lipid peroxiation, reacting with deoxynucleosides to produce DNA adducts (Chaudhary *et al.*, 1994). Of the biomolecular targets for oxidative stress, lipids are the more abundant and result in a number of secondary metabolites, primarily aldehydes, which can interact with biomolecules to exacerbate the oxidative damage. Two main hypotheses have been described regarding the formation of MDA *in vivo*: a radical based scheme whereby polyunsaturated fatty acids (PUFAs) form carbon-centred radicals on reaction with oxidising agents and peroxyl radicals are formed when the carbon-centred radicals react with O_2 (Scheme 4) (Marnett, 1999).

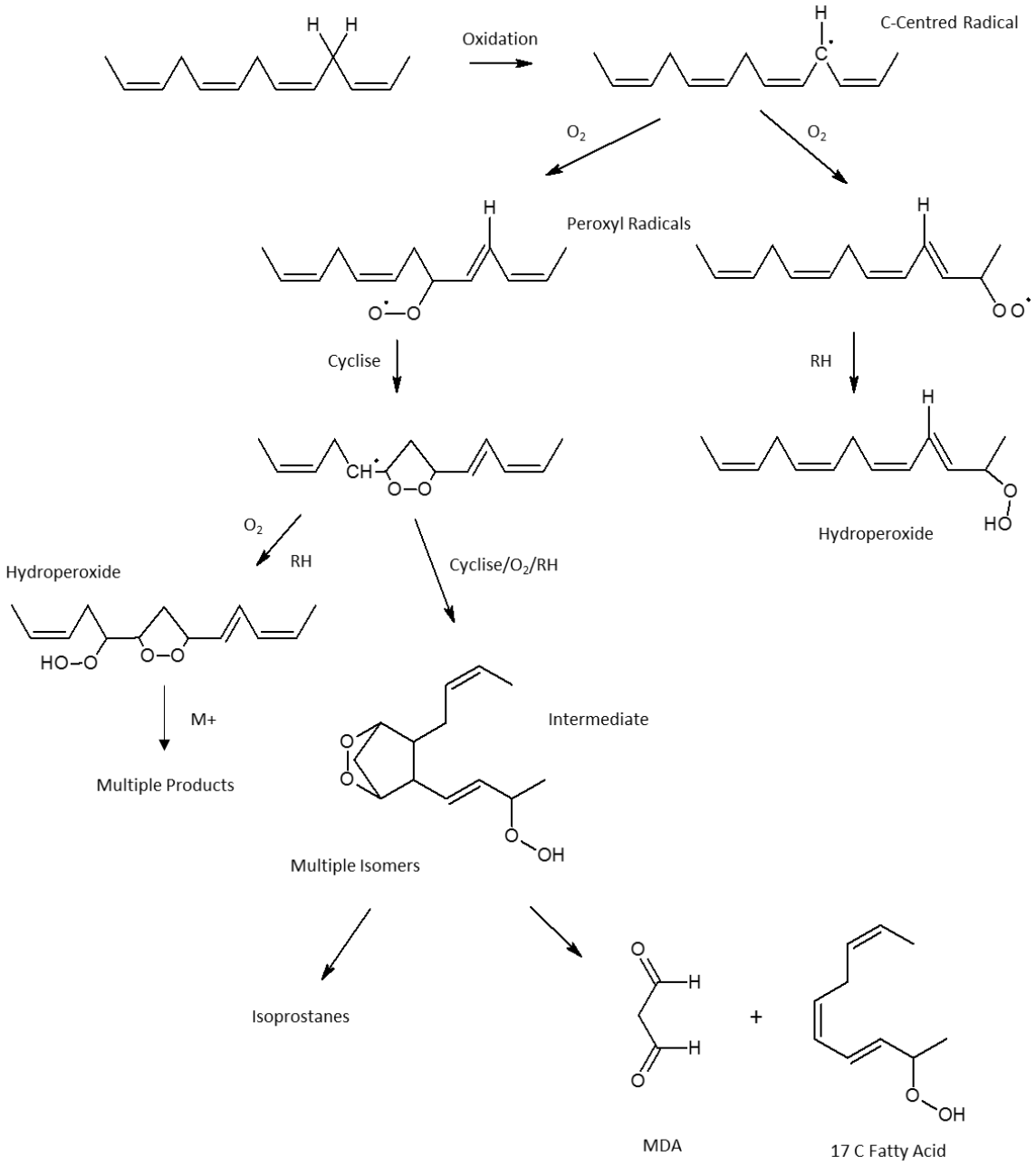

Scheme 4. Schematic of the pathways of lipid peroxidation (adapted from Marnett (1999)).

If the peroxyl radical is at one end of the fatty acid carbon chain, relatively stable hydroperoxides are formed. Initiation of a radical chain reaction can occur if the molecule that reduces the peroxyl radical to a hydroperoxide is another fatty acid e.g. in phospholipid membranes. A cyclic peroxide is produced if the peroxyl radical is within

the fatty acid carbon chain, this can either form a peroxyl radical in the presence of O_2 and be reduced to a hydroperoxide, or it can form a bicyclic peroxide after a second cyclisation event. In the presence of O_2, the bicyclic peroxide is reduced to form an intermediate compound for the production of MDA and isoprostanes. An alternative method is shown in Scheme 5 and involves the formation of successive hydroperoxides and β cleavage of the fatty acid chain (Esterbauer *et al.*, 1991). MDA is subsequently produced by β scission of the hydroperoxyaldehyde or by a hydroxyl radical reacting with the final acrolein radical (del Rio *et al.*, 2005). Other pathways of MDA formation have also been proposed that are less well understood, such as generation by prostaglandin biosynthesis (Marnett, 2002) and non-enzymatic pathways (Onyango and Baba, 2010). Overall, this shows that the mechanisms are not fully understood. However, it is known that MDA is present in the human body in variable amounts depending upon a number of factors. Moreover, it reacts with cellular components to cause damage that leads to long-term effects, including cancer.

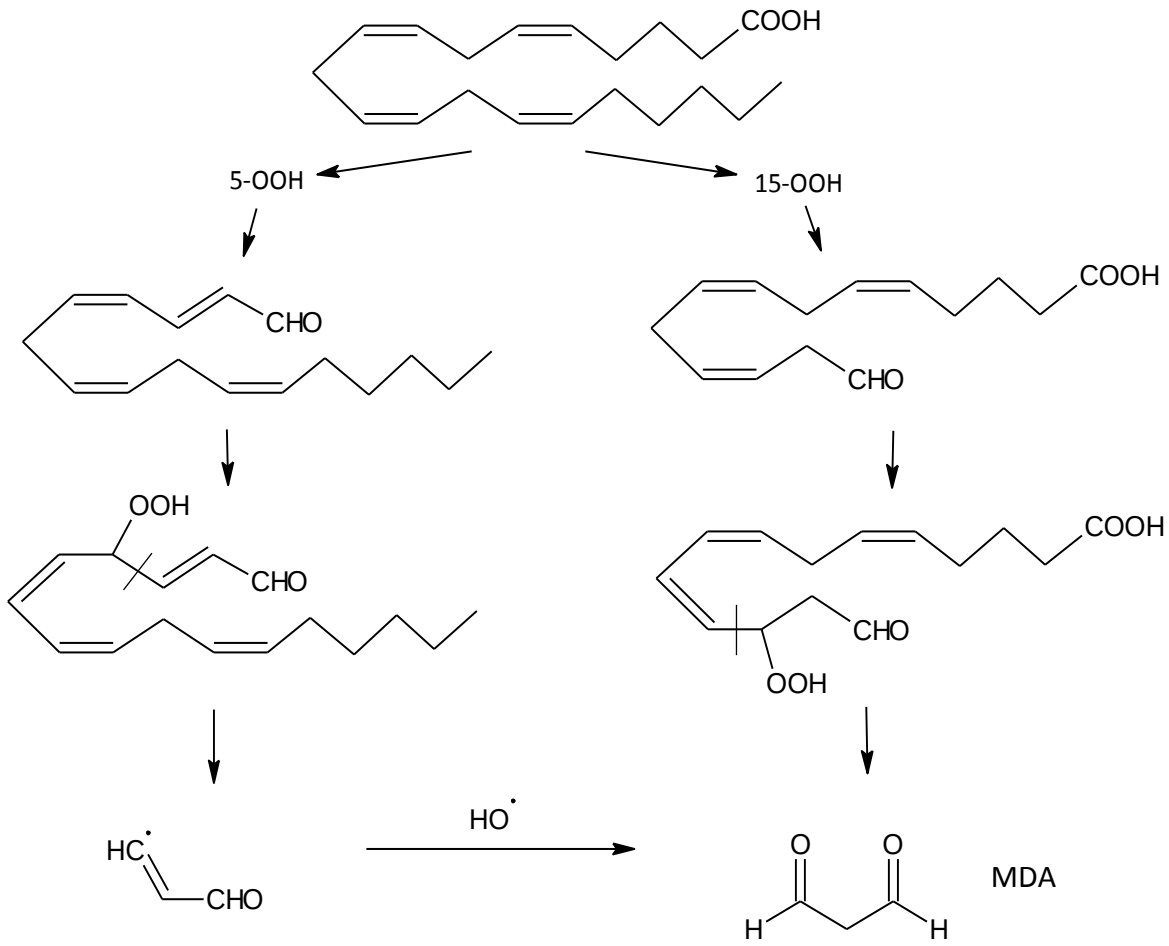

Scheme 5. Two pathways for the peroxidation of PUFAs and the formation of MDA (adapted from Esterbauer *et al.* (1991)).

1.9. Formation and Repair of the M_1dG Adduct

Endogenous and exogenous DNA adducts have been implicated in cancer (Chaudhary *et al.*, 1994). Damage to DNA by genotoxic oxidizing agents can be mutational, i.e. sequence changes/insertions/deletions, or non-mutational, e.g. telomere shortening. Direct interaction of ROS with DNA bases can lead to DNA adduct formation and DNA modification, as can the interaction of ROS with proteins and lipids forming DNA reactive intermediates e.g. by lipid peroxidation. An example of a DNA adduct formed by direct

modification of a base is 8-oxo-7,8-dihydro-2'-deoxyguanosine (8-oxo-dG), whereas those produced by a DNA reactive electrophilic intermediate include 1,N^6-etheno-2'-deoxyadenosine (N^6EtA) and 3-(2-deoxy-β-D-erythro-pentofuranosyl)pyrimidol[1,2-α]purin-10(3*H*)-one (M_1dG) (Cooke *et al.*, 2008).

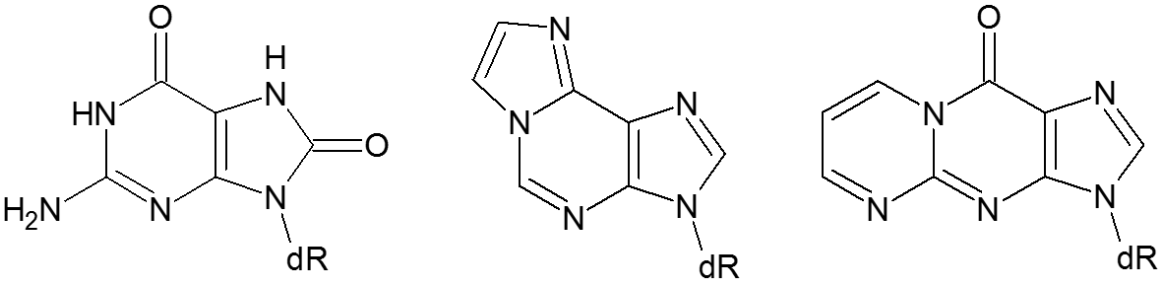

8-oxo-dG **N^6EtA** **M_1dG**

MDA reacts with nucleic acid bases e.g. deoxyguanosine to form pyrimidopurinone DNA adducts, of which M_1dG is the most abundant, with levels detected in rat liver in the region of 5000 adducts per cell (Marnett, 1999). M_1dG has been linked to a high fat diet (Moore *et al.*, 2008) and to smoking (Lykkesfeldt *et al.*, 2004). Elevated levels of M_1dG were associated with a diet high in meat (Lewin *et al.*, 2006), alcohol and saturated fatty acids, whereas reduced levels were associated with a diet rich in fruit, vegetables, wholegrains and PUFAs (Leuratti *et al.*, 2002). A decrease in urinary and plasma MDA was observed following consumption of polyphenol-rich spices, compared with a negative control, suggesting possible health benefits (Li *et al.*, 2010). Although, no association, or inverse association, was found between intake of fruits, vegetables, carotenoids and vitamins and bladder cancer incidence in tobacco smokers (Michaud *et al.*, 2002). Bronchial mucosa levels of MDA-DNA adducts, including M_1dG, were found

to be higher in smokers than non-smokers, and adduct levels were increased in lung cancer cases, but only for smokers (Munnia *et al.*, 2006).

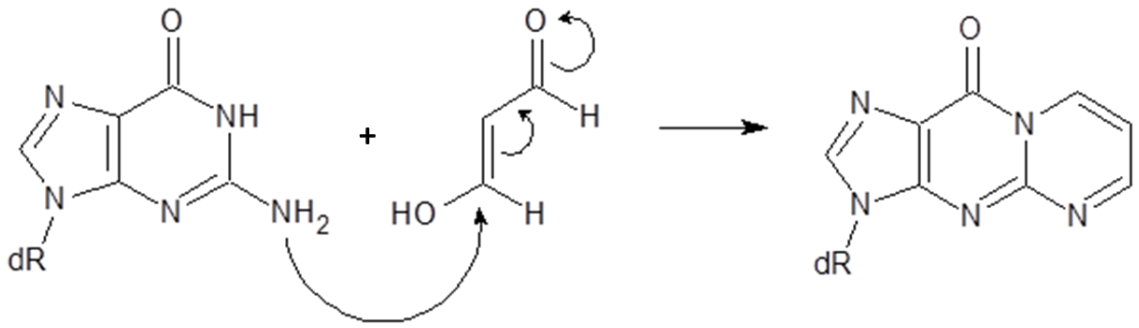

Deoxyguanosine **MDA** **M_1dG**

Scheme 6. Formation of DNA adduct M_1dG from MDA and deoxyguanosine (adapted from Marnett (1999)).

Research has suggested that the main source of M_1dG formation was by reaction of MDA from lipid peroxidation with DNA (Scheme 6) (Lykkesfeldt *et al.*, 2004). Although, other research has suggested that an alternative route of M_1dG formation is via reaction of base propenals with DNA (Sharma and Farmer, 2004; Zhou *et al.*, 2005). Base propenals e.g. adenine-N1-propenal are some of the products of direct oxidative DNA damage, for example from attack by hydroxyl radicals, and are structural analogues of MDA (Dedon *et al.*, 1998) (Scheme 7). It has been demonstrated that adenine propenal had a higher reactivity with DNA than MDA with regards to the formation of M_1dG adducts, by treatment of DNA with both compounds directly and also with two oxidising agents known to produce base propenals (Dedon *et al.*, 1998). It was suggested that base propenals are a biologically important source of M_1dG adducts, perhaps due to their proximity to DNA i.e. generated in the DNA, whereas MDA is generated by lipid peroxidation and must migrate to the DNA. However, plasma MDA levels are

significantly elevated in subjects exposed to oxidative stress, such as smoking, and M_1dG adduct levels were also increased in smokers with and without lung cancer, which suggests that M_1dG adduct formation via reaction of MDA with DNA is a biologically relevant pathway particularly in smokers (Lykkesfeldt *et al.*, 2004; Munnia *et al.*, 2006; Montano *et al.*, 2010).

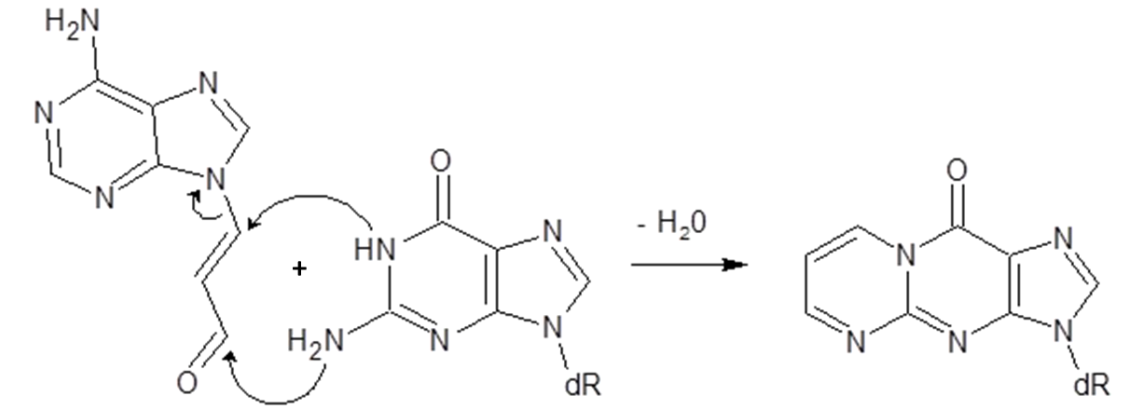

Adenine-N1-propenal **Deoxyguanosine** **M_1dG**

Scheme 7. Mechanism for the formation of M_1dG adduct from reaction of deoxyguanosine with adenine-N1-propenal (adapted from Dedon *et al.* (1998)).

In basic solution, M_1dG is subject to hydrolytic ring-opening (Scheme 8) by addition of a hydroxide ion to C8 of the exocyclic ring, breaking the C8-C9 bond (Knutson and Marnett, 2010). At physiological pH, the ring-closed M_1dG is the major form present (Mao *et al.*, 1999). Ring closure is biphasic, N^2-(3-oxo-1-propenyl)-deoxyguanosine (N^2OPdG) is protonated to 8-hydroxy-6,7-propeno-deoxyguanosine followed by acid catalysis to M_1dG (Riggins *et al.*, 2004). The ring closed form is five times more mutagenic than the ring open form, although this is difficult to determine in vivo as the two forms exist in equilibrium (Fink *et al.*, 1997).

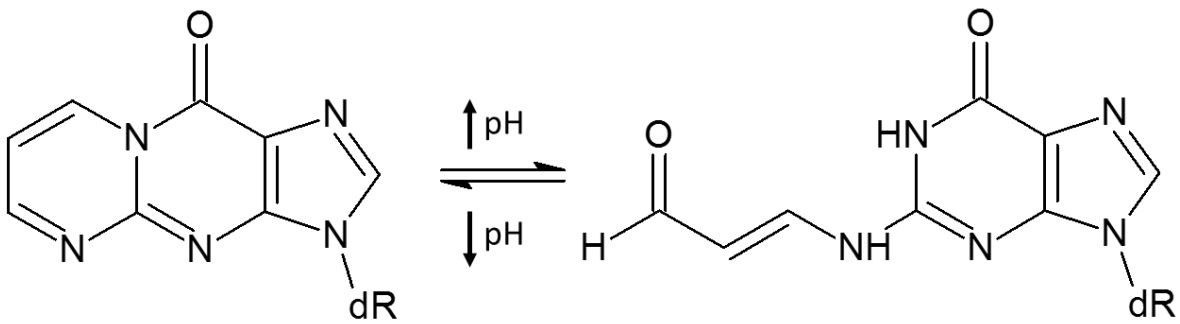

M_1dG **N^2OPdG**

Scheme 8. M_1dG exists in equilibrium with its ring-open form, N^2-(3-oxo-1-propenyl)-deoxyguanosine (adapted from VanderVeen *et al.* (2003)).

The M_1dG adduct is a substrate of nucleotide excision repair (NER) pathway (Marnett, 1999) and has been found to metabolise to 6-oxo-M_1dG for excretion in urine (Ottender *et al.*, 2006), although some M_1dG is also excreted in urine (Hoberg *et al.*, 2004). Further oxidation of 6-oxo-M_1dG to 2,6-oxo-M_1dG has also been shown to occur in rat liver extracts (Knutson *et al.*, 2007). When M_1dG was injected into rodents, the metabolite 6-oxo-M_1dG, produced by oxidation of M_1dG, was also excreted in faeces (Ottender *et al.*, 2006; Knutson *et al.*, 2007). M_1dG and 6-oxo-M_1dG, from rat urine and faeces samples, were quantified by immunoaffinity chromatography and liquid chromatography-mass spectrometry (LC-MS) and only 6-oxo-M_1dG was detected (Akingbade *et al.*, 2012).

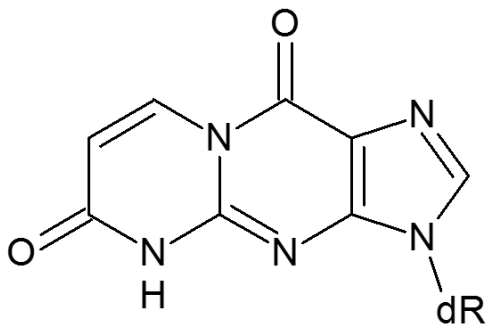

6-oxo-M_1dG

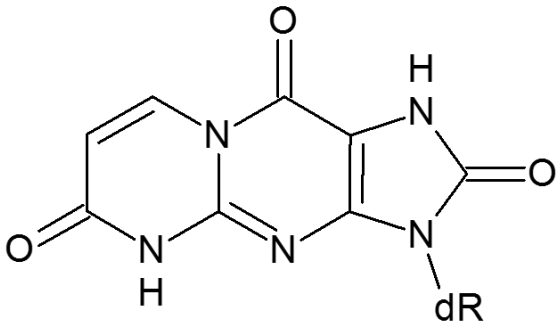

2,6-oxo-M_1dG

1.10. Analytical Methods Applied to Detection of Malondialdehyde and the M_1dG Adduct

1.10.1. Lipid Peroxidation by TBARS

The traditional measurement of lipid peroxidation is measurement of MDA by the thiobarbituric acid reactive substances (TBARS) assay. MDA reacts with thiobarbituric acid (TBA) by condensation at low pH and increased temperature by nucleophilic addition to produce a red coloured product which can easily be assessed by spectrophotometry (Janero, 1990), as shown in Scheme 9. The red MDA-TBA product is formed by a 2:1 reaction of TBA with MDA and quantified by UV-vis spectrophotometry at 532 nm (Badcock *et al.*, 1997).

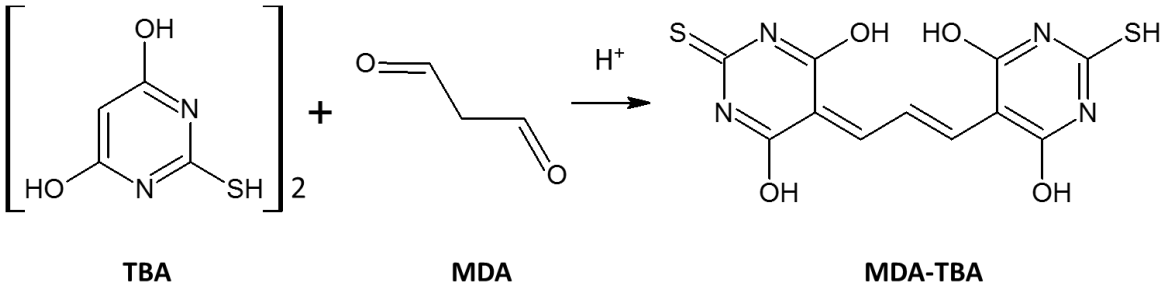

TBA **MDA** **MDA-TBA**

Scheme 9. Reaction of 2-thiobarbituric acid with MDA to produce a fluorescent red chromophore with absorbance maxima 532 nm (adapted from Atasayar *et al.* (2004)).

The TBARS assay has often been criticised for overestimation of MDA content due to reaction of TBA with other, non-MDA, exogenous and endogenous compounds found in biological specimens such as bile pigments, some proteins and carbohydrates and other aldehydes such as hexanal (Oates and Van der Kraak, 2003). Additionally, the temperature required for derivatisation of MDA by TBA is high and may cause artefactual reactions (Atasayar *et al.*, 2004) by the decomposition of lipid peroxides (Seljeskog *et al.*, 2006). However, the assay is simple, rapid and reliable.

1.10.2. Methods of M_1dG DNA Adduct Detection

Assessment of lipid peroxidation induced DNA damage needs to be both sensitive and specific. DNA damage derived from endogenous processes can occur at detectable levels in human DNA, including M_1dG adducts. A number of methods can be used for the detection and analysis of the M_1dG DNA adduct.

1.10.2.1. Immunoslot Blot Assay

The immunoslot blot (ISB) assay can be used to detect and quantify DNA adducts with the use of antibodies. The assay involves fragmentation and denaturation of the DNA sample, followed by immobilisation of the DNA on nitrocellulose. The membrane is then incubated with a primary adduct-specific antibody followed by a secondary antibody with an attached enzyme e.g. horseradish peroxidase, and detection and quantification of the DNA adduct by chemiluminescence (Leuratti *et al.*, 1998).

Several groups have used an ISB assay to assess lifestyle effects on M_1dG levels. Mean levels of M_1dG were found to be 4.3 ± 3 per 10^7 bases in men and 4.6 ± 2.9 per 10^7 bases in women, using only 1 µg colorectal DNA, with an inverse association of M_1dG adduct levels with fruit and vegetable intake and a positive association with meat and alcohol intake (Leuratti *et al.*, 2002). Higher levels of M_1dG adducts were found in human oral mucosa DNA from smokers versus non-smokers, analysed by ISB (Zhang *et al.*, 2002). Mice infected with *Helicobacter hepaticus* were found to have increased levels of M_1dG adduct (40.7 – 52.5 per 10^8 nucleotides) in their liver DNA compared to the control group (30.1 – 37.5 per 10^8 nuceotides), analysed by ISB using 1 µg DNA (Singh *et al.*, 2001).

ISB is one of the most sensitive assays for M_1dG adduct detection, requiring 1-200 µg DNA, to measure adducts in very small sample volumes, however, antibodies are required, one of which exists for M_1dG (Leuratti *et al.*, 1998). It has good relative selectivity with an antibody raised against a specific DNA adduct, although there is a risk of cross-reactivity with similar-structured DNA adducts. The technique is robust, easy to

perform and has a higher sample throughput than ^{32}P-postlabelling (Phillips *et al.*, 2000; Himmelstein *et al.*, 2009).

1.10.2.2. ^{32}P-postlabelling

^{32}P-postlabelling involves four steps: DNA digestion using enzymes; purification of the adduct by solid phase extraction (SPE), immunoaffinity or high performance liquid chromatography (HPLC); labelling of adduct with ^{32}P; and chromatographic separation by thin layer chromatography (TLC) or HPLC followed by detection of ^{32}P decay (Phillips *et al.*, 2000).

M_1dG has been found in healthy human tissues by ^{32}P-postlabelling followed by reverse phase HPLC: 3.0 ± 1.3 adducts/10^7 nucleotides in breast tissue and 2.6 ± 1.2 adducts/10^7 nucleotides in white blood cells were detected and required 10 µg DNA (Vaca *et al.*, 1995). The effect of formaldehyde exposure on M_1dG adduct levels in human leukocyte DNA was analysed by ^{32}P-postlabelling, requiring only 1-2 µg DNA. A significant increase was found in pathology workers exposed to air formaldehyde (5.7 ± 1.3 M_1dG adducts per 10^8 nucletides) versus the negative control group (2.4 ± 0.3 M_1dG adducts per 10^8 nucleotides)(Bono *et al.*, 2010). The levels of M_1dG adducts in workers and nearby residents, who had been exposed to air pollution from a Thai petrochemical industrial estate, were measured by ^{32}P-postlabelling, again using only 1-2 µg leukocyte DNA. A significant increase was found in workers (6.0 ± 0.5 M_1dG adducts per 10^8 nucletides) compared to nearby residents (3.7 ± 0.4 M_1dG adducts per 10^8 nucletides) who had significantly higher levels than a negative control group (2.9 ± 0.4 M_1dG adducts per 10^8 nucleotides) (Peluso *et al.*, 2010).

^{32}P-postlabelling is a sensitive method of DNA adduct detection, requiring only 1-10 µg DNA, and can be used to detect a wide range of adducts, although the method is more sensitive for aromatic adducts (1-100 in 10^9 nucleotides) than non-aromatic adducts (1 in 10^5 to 10^6 nucleotides) (Phillips *et al.*, 2000). However, the major drawback of this technique is that it requires the use of a radioactive substance. It also has limited specificity, low sample throughput compared to ISB and often adduct standards are required (Himmelstein *et al.*, 2009).

1.10.2.3. HPLC with Fluorescence Detection

HPLC is a separation method whereby a mixture is pumped under pressure through a column packed with a solid adsorbant phase. Different detectors can be coupled to the HPLC for detection and analysis of the fractions eluting from the column.

Reverse-phase HPLC with fluorescence detection (FLD) was used to identify the presence of M_1dG adducts in hydrolysed DNA, using synthetic M_1dG as an internal standard, however, the peaks for the sample and synthetic M_1dG could not be separated (Agarwal and Draper, 1992). Increased benzo[α]pyrene diolepoxide (BPDE)-DNA levels were detected by HPLC-FLD in DNA from human subjects exposed to high levels of polycyclic aromatic hydrocarbons (PAHs), including benzo[α]pyrene (Pavanello *et al.*, 1999).

HPLC-FLD is a simple, inexpensive, robust technique, requiring a moderate amount of sample (20-100 µg DNA), however, it can only be used for detection of fluorescent adducts and is unlikely to detect adducts at biological levels (Himmelstein *et al.*, 2009).

1.10.2.4. Detection of M_1dG Adducts by Mass Spectrometry

DNA adducts may also be detected by mass spectrometry (MS). The basic principle of MS involves sample ionisation by electron bombardment, ion separation, according to the mass/charge ratio (m/z), by acceleration and deflection using an electric or magnetic field and the detection of ions by e.g. electron multiplier detection. Two or more mass spectrometers may be coupled for tandem MS (MS-MS), whereby the ion of interest is further fragmented into daughter ion fragments (de Hoffmann and Stroobant, 2007).

The presence of M_1dG in human liver cells was investigated by derivatising cellular M_1dG with pentafluorobenzyl (PFB) and analysing with gas chromatography-electron capture negative chemical ionisation mass spectrometry. The cellular M_1dG was quantified by using selective ion monitoring relative to a dideuterated M_1dG-PFB internal standard. The average value of M_1dG adducts was 9 per 10^7 bases, i.e. 5400 per cell but required a large amount (9.3 mg) of DNA (Chaudhary *et al.*, 1994).

M_1dG is repaired by the NER pathway and can be detected in urine. The levels of free M_1dG in the urine would be a useful biomarker for lipid peroxidation and MDA exposure *in vivo* that may be implicated in cancer associated with lifestyle and diet (Marnett, 2002). Human urinary M_1dG was measured using immune-extraction purification using an M_1dG antibody, followed by chemical reduction with sodium borohydride and liquid chromatography- atmospheric pressure chemical ionisation tandem mass spectrometry (LC-APCI-MS-MS). [^{13}C,$^{15}N_2$]-M_1dG was used as an internal standard and attomole sensitivity was achieved. The average excretion rate, in 25 µl aliquots urine, over 24 hours, of M_1dG was found to be 12 ± 3.8 fmol kg^{-1} total body weight (Hoberg *et al.*, 2004).

M_1dG was quantified in urine and faeces to evaluate DNA damage by LC-MS analysis at levels of approximately 12 fmol/kg/day (Marnett, 2012). The 5,6-dihydro derivative of M_1dG was analysed by LC-nanospray ionization (NSI)-high resolution tandem MS (HRMS-MS) using 200 μg DNA. Levels of M_1dG were detected in human leukocyte DNA at 0.132 – 275 fmol/mg DNA or 0.004 – 9.15 adducts per 10^8 nucleotides, with smokers having slightly higher, although not significantly higher, levels than non-smokers (Ma *et al.*, 2015).

LC-MS and LC-MS-MS methods of DNA adduct detection have high chemical specificity, giving detailed structural information, particularly tandem MS methods. They have a high level of accuracy, particularly in multiple reaction monitoring (MRM) or single ion monitoring (SIM) modes and have high sample throughput depending on the instrumentation. Moreover, they do not require the use of antibodies or radioactive substances. However, they require expensive, specialised equipment, which are not always available in the standard laboratory, they often require the use of internal standards and they require larger sample amounts than ISB or ^{32}P-postlabelling (10-100 μg DNA) (Phillips *et al.*, 2000; Himmelstein *et al.*, 2009).

Thus, a number of methods exist for the measurement of M_1dG, however, some require the use of tissues which can be invasive and not suitable for bio-monitoring. These techniques also show overall damage rather than specific damage at sites relevant to cancer.

1.10.3. Cell Proliferation and Viability Assays

Cell proliferation and cell viability are useful measurements for the susceptibility of a cell culture to external conditions. *In vitro* assays can be used as models for *in vivo* cell populations and their reactions to, for example, therapeutic or cytotoxic agents. There are a range of techniques that measure cell proliferation and viability. Cell proliferation is important in multi-cellular organisms and failure of regulation of normal cell turnover is characteristic of a number of diseases such as cancer and AIDS. Cell proliferation is a measure of the actively dividing cells in a sample (Evan and Vousden, 2001; Macallan *et al*., 1998).

DNA labelling with stable isotope-labelled glucose was used to measure DNA synthesis and thus cell proliferation (as this is relatively specific for cell division). [6.6-$^{2}H_{2}$]-labelled glucose was administered to rats *in vivo* and after a set time genomic DNA was extracted from isolated intestinal epithelial cells, hydrolysed to deoxyribonucleosides, of which trimethylsilyl derivatives were synthesized and analysed using gas chromatography-MS (GC-MS). The relative abundance of the isotope in DNA is a measure of the rate of DNA replication i.e. cell proliferation. This method has advantages over the similar tritiated thymidine method as it does not use radioisotopes and can therefore be carried out *in vivo* in humans. An indirect measure of cell proliferation is to quantify molecules that regulate the cell cycle. This can be done directly using Western Blots or enzyme linked immunosorbent assay (ELISA), or by measuring their activity e.g. cyclin-dependent kinase assay (Macallan *et al.*, 1998).

Cell viability is a measure of the number of living cells, although it does not distinguish between those actively dividing and the quiescent which cell proliferation does distinguish. The 3-[4,5 dimethylthiazol-2yl]-2,5-diphenyl-tetrazolium bromide (MTT) assay measures the metabolic activity of the cell population, where viable cells metabolise MTT to a coloured formazan product, which can be quantified by UV-vis spectrophotometry (VanMeerloo *et al*., 2011).

There is a second type of cell viability assay, the dye-exclusion assay. This involves the exclusion of a dye from a healthy cell due to maintenance of the integrity of the cell membrane thus staining only dead, non-viable cells. Trypan blue is one such dye that can be utilised to ascertain cell viability. Cells in late apoptosis and early necrosis exhibit a loss of membrane integrity and are able to take up trypan dye and stain the cell blue. In contrast, cells with intact membranes exclude trypan blue. Cells with intact and disrupted membranes can therefore be distinguished, although cells in early apoptosis will still have an intact membrane and also exclude trypan blue (Siddique *et al.*, 2009). The trypan blue assay was compared with an assay using acridine orange and propidium iodide fluorescent dyes, which stain both viable and non-viable cells. The acridine orange and propidium iodide assay were found to have more readability and stability than the trypan blue assay (Mascotti *et al.*, 2000).

An assay used for the assessment of chromosome breakage and loss is the micronucleus assay. Chromosomal loss or non-disjunction are events associated with aging and cancer, due to spindle or centromere defects. Dividing cells containing chromosomal breaks and chromosomes that are unable to travel to the spindle poles during mitosis, often express

micronuclei which are much smaller than the main nucleus. The micronucleus assay is a method of staining and scoring these micronuclei to assess the level of DNA damage. Fluorescent stains such as 4',6-diamidino-2-phenylindole (DAPI) can be used (Fenech, 2000). Micronuclei can be used as biomarkers of cancer risk for which a non-invasive method using exfoliated epithelial cells can be used (Nersesyan *et al.*, 2006).

1.11. MRC5 and MRC5 SV2 Lung Fibroblast Cells

Human and other mammalian cell lines are used in *in vitro* studies to determine the genotoxic and carcinogenic effects of various compounds, for example, to study formation of M_1dG adducts in response to MDA levels (Sapkota *et al.*, 2014). Fibroblast cells are commonly used for *in vitro* cell culture as they are relatively easy to maintain over time.

Stromal tissue, comprised of mesenchymal cells and extra cellular matrix (ECM), is one of the fundamental features of vertebrates and is required to provide the connective, structural support for the functional parenchymal cells of an organ. Fibroblasts are the principal cells of the stroma and synthesise the majority of ECM in connective tissue and also are involved in wound healing (Tug *et al.*, 2005). Fibroblasts are identified by their spindle-shaped morphology and, although they are one of the more accessible and amenable mammalian cell types for *in vitro* tissue culture (adhere readily to plastic), they are poorly defined in terms of molecular expression in different tissue types (Chang *et al.*, 2002). Fibroblasts from different tissue types were characterised from their transcriptional patterns and it was found that fibroblasts from each site had distinct and

characteristic gene expression profiles and should be considered as separate, functional cell types (Chang *et al*., 2002). Thus, tissue-specific fibroblast cell lines should be used for *in vitro* cytotoxicity studies, for example lung fibroblasts would be used to assess the effects of tobacco smoking on the lungs. MRC5 cells are an example of a human lung fibroblast cell line.

MRC5 SV2 cells are a transformed version of the MRC5 human lung fibroblast cell line (Huschtscha and Holliday, 1983). MRC5 SV2 cells have a sequestered p53 protein, resulting from the transfection of MRC5 cells with simian virus SV40 and are thus immortalised (Zhu and Gooderham, 2002). MRC5 cells were transformed with the SV40 virus to give the MRC5 SV2 cell line, whereby the viral DNA was integrated into the cell DNA at a random integration site. The viral large T-antigen gene is expressed in transformed cells and this complexes with the p53 protein, an interaction which blocks p53 dependent gene expression by preventing association with target promoters. This T-antigen binding also stabilises the p53 protein, allowing accumulation in cells (Pipas, 2009).

Non-transformed human lung fibroblasts, when cultured *in vitro*, have a limited lifespan. In contrast, MRC5 SV2 does not senesce, and following 5 years of continuous sub-culture (passage 650) growth did not slow down, suggesting this cell line has the potential for infinite growth. Additionally, MRC5 SV2 does not exhibit contact inhibition, continuing to grow in confluent culture. Further properties of this cell line include an epithelial morphology, no tumorigenicity, and the ability to grow in methionine-free media, like non-transformed MRC5 cells, whereas other transformed cell lines require methionine

for growth (Huschtscha and Holliday, 1983). It was found that MRC5 SV2 cells are able to produce infectious SV40 viral progeny with the ability to infect both simian and human cells, a concern as SV40 is an oncogenic virus and MRC5 SV2 cells are widely used in research laboratories (Morelli *et al.*, 2004).

Previous studies have used MRC5 SV2 cells to study the effects of benzo(α)pyrene (Zhu and Gooderham, 2002) and MRC5 cells to study the effects of H_2O_2 (Caldini *et al.*, 1998). Thus these cells may be useful in determining the effects of MDA in lung cells.

1.12. Imaging Techniques

The cytotoxic effects of various compounds on the cellular morphology and subcellular structure may be examined by microscopy, of which there are numerous types. The light microscope (LM) has a maximum resolving power of 200 nm, limited by the wavelength of illumination. Larger subcellular structures, such as the nucleus, can be visualized, whereas, smaller features within the cell or on the cellular surface, such as the cytoskeletal filaments and microvilli cannot be visualized. Sample preparation is simple and low cost. Live cells can be viewed *in situ* using the inverted LM (Lodish *et al*., 2000). Cell shrinkage and pyknosis have been observed under the LM, as an indicator of the early stages of apoptosis, which is often a consequence of treatment with cytotoxic compounds (Elmore, 2007). Hence, the LM is a useful tool for preliminary identification of cytotoxicity.

Additional features, such as fluorescence, may be used in conjunction with microscopy, such as epiflourescence microscopy or with the more complex confocal microscope. The

specimen is illuminated with light of a specific wavelength which is absorbed by fluorophores, causing them to emit light of longer wavelengths. The excitation light is separated from the emitted fluorescence using an emission filter. Fluorescence microscopy has numerous applications, such as immunofluorescence, whereby antibodies labelled with fluorescent dyes bind to target molecules enabling their detection by fluorescence microscopy (Lodish *et al*., 2000). Unless molecules autofluoresce, they must be labelled with a fluorescent dye and either fixed or living cells can be imaged, for example, overexpression of p53 in a number of sinonasal squamous cell carcinoma cell lines was observed using immunofluorescence with a fluorescently labelled anti-p53 antibody (García-Inclán *et al.*, 2014). However, fluorescence fades over time, photobleaching may occur and fixatives may cause artefact formation. The confocal microscope is typically used with fluorescence. It has better resolution than regular fluorescence as it uses point illumination, so little photobleaching occurs, and allows 3-D reconstruction of whole, or parts of a specimen (Wilson and Bacic, 2012; Watkins and St Croix, 2013).

Cell surface morphology has historically been examined by electron microscopy (EM), which has the capacity to give detailed images of the cell surface e.g. membrane blebbing during apoptosis (Elmore, 2007). However, EM is very expensive and sample preparation is lengthy and fixation and coating procedures may cause artefact formation (Goodhew *et al.*, 2001; Wilson and Bacic, 2012). The atomic force microscope (AFM) is advantageous over EM techniques, as sample preparation is minimal. The AFM allows 3-D images of the surface topography of biological samples in liquid or gas over a large temperature range (Binnig *et al.*, 1986). The high resolution attained by AFM allows

imaging of biological molecules e.g. DNA and proteins and small ligands in the absence of stains, shadows and labels (Lyubchenko, 2011), allowing structure and function of biological samples to be maintained (Billingsley *et al.*, 2012). For example, altered cellular shape and morphology was observed in cells treated with different actin poisons, such as phalloidin (Lazaro-Dieguez and Egea, 2007). DNA damage was observed by AFM upon interaction of DNA with cisplatin, in a dose dependent manner (Liu *et al.*, 2010), and DNA adducts formed due to BPDE treatment were observed by AFM as 30° bends in the DNA structure (Pietrasanta *et al.*, 2000). Thus, AFM is a useful tool for examining the cytotoxic effects of compounds at both the cellular and molecular level. Resolution is in the subnanometer scale, in comparison to the optical microscopy which is in the micrometer scale, and in addition to imaging the sample, the mechanical properties e.g. surface stiffness, hardness, friction or elasticity can be measured (Alonso and Goldmann, 2003). Hence, the AFM is a versatile tool for imaging cells and DNA, although it is expensive and is not a standard tool in biological laboratories.

AFM uses a sharp tip attached to a flexible cantilever. The tip or the sample is mounted onto a piezoelectric scanner. A laser is reflected from the cantilever on to a position sensitive detector as the tip scans across the sample surface and the interactions between the tip and the sample are measured by the laser deflection. The data from the tip-sample interactions is constructed into a 3-D image of the sample. The tip scans in constant contact with the surface of the sample in contact mode, with the tip-surface force being maintained by the piezoelectric scanner. A voltage is applied to the tip causing it to oscillate across the sample surface in tapping mode, and the phase

difference and amplitude are measured to produce the data to produce the image (Figure 5) (Webb. *et al.*, 2011).

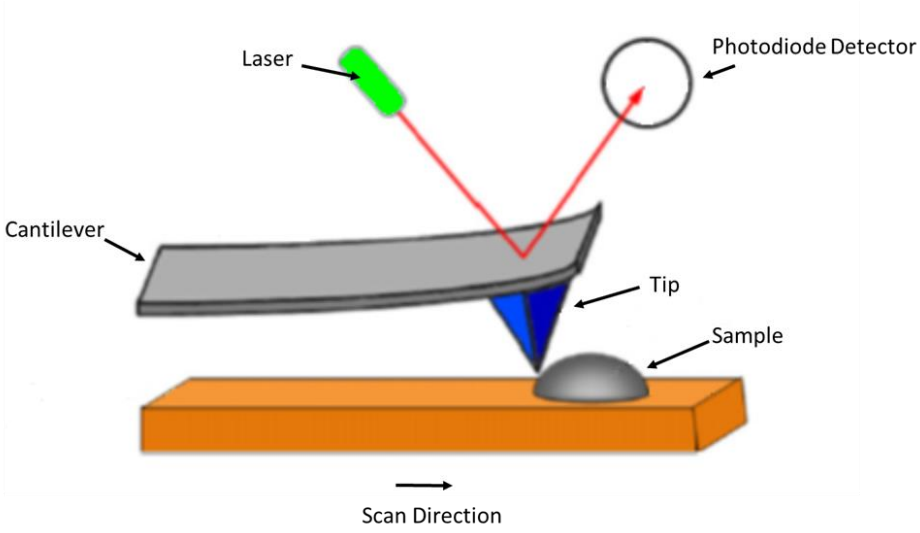

Figure 5. AFM principle: as the tip which is attached to the cantilever scans the sample surface, a laser beam is reflected off the back of the tip on to a photodiode detector which measures the deflection of the cantilever, allowing a 3-D image to be produced from the data (adapted from Billingsley *et al.* (2012)).

The flexible cantilever consists of silicon or silicon nitride of 100-500 µm in length and 0.5-5 µm in thickness. The tip is mounted on the end of the cantilever and is brought into contact with the sample surface, or taps the sample surface as it scans. An electric feedback circuit keeps the tip in constant contact with the sample surface, measuring the deflection of the cantilever tip as it scans the sample surface using a piezoelectric scanner. In tapping mode, the tip is oscillated vertically at the resonant frequency of the cantilever, and the distance the tip oscillates vertically as it scans the sample surface is measured to produce an image. Lateral shear forces, which can damage/deform the sample, are present in contact mode but are eliminated in tapping mode (Figure 6) (Alonso and Goldmann, 2003).

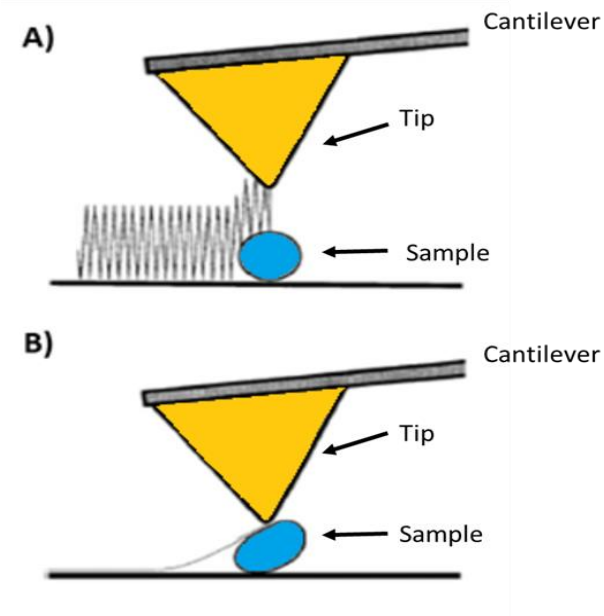

Figure 6. AFM modes: A) tapping mode and B) contact mode, showing the tips' movement over the sample surface (adapted from Santos and Castanho (2004)).

In order to image DNA by AFM, it needs to be adsorbed onto a mica surface by the sharing of counterions despite DNA and mica having similar, negative, surface charges. Cations are used to bind the negatively charged DNA molecules to the mica surface (Pastre *et al.*, 2003). Mica is used as it is atomically flat and biologically compatible as a support surface (Figure 7) (Billingsley *et al.*, 2012).

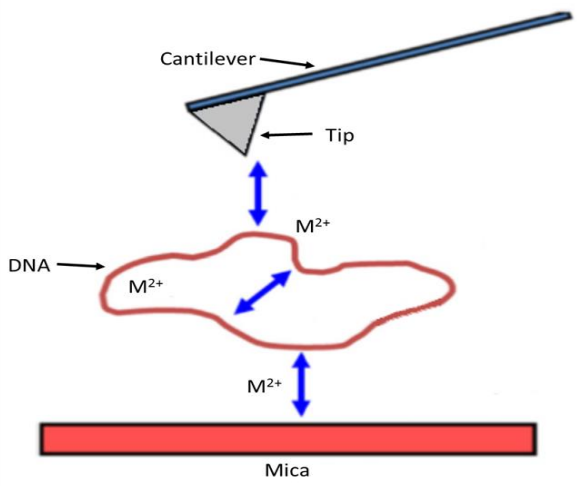

Figure 7. Divalent cations (M^{2+}) in the DNA buffer allow the DNA to interact with the mica substrate to prevent the DNA sample from moving as a result of the motion of the tip. Interactions (blue arrows) between the DNA and mica substrate must be greater than the interaction between the DNA and the tip to prevent sample movement (adapted from Billingsley *et al.* (2012)).

1.13. Summary

As levels of M_1dG adducts have been found at increased levels in smokers, the human lung fibroblast strain MRC5 and its transformed counterpart, MRC5 SV2 were chosen for the initial stages of this research. Treatment with genotoxic agents such as MDA, may serve to mimic one of the effects of smoking on the cellular response of these cell lines. MRC5 SV2 cells have a sequestered p53 response, resulting from the transfection of MRC5 cells with SV40 and are thus immortalised (Zhu and Gooderham, 2002). The differences in cellular response of both cell lines to treatment with genotoxic agents may be attributed to the p53 response.

It is well established that MDA is mutagenic and carcinogenic. However, there is a discrepancy in whether it is responsible for M_1dG adduct formation. The aim was to examine the mutation spectra in MRC5 and MRC5 SV2 cells and compare with known mutation spectra in order to establish if MDA is linked to lung cancer. In order to achieve this, sensitive methods of analysis needed to be developed.

1.14. Experimental Design

Given the link between MDA, M_1dG adduct formation and mutagenesis, and the link between *TP53* damage and carcinogenesis, further research was required to provide an overall picture of the effect of MDA at the cellular and molecular levels. The research here, focusses on the effect of MDA on the human lung fibroblast MRC5 cell line and its SV40 transformed counterpart, MRC5 SV2, which has a sequestered p53 response. These cell lines were chosen as they are human lung cell lines and MDA, linked to cellular stress, may mimic the genotoxic effects of smoking and thus lung cancer. Additionally, the differing p53 responses of the two cell lines may allow comparison of the effect of MDA on the cellular responses of healthy cells versus transformed cells.

Initially, as components in foetal bovine serum (FBS) (which contains growth supplements required for cell proliferation) have been found to interact with MDA (Rittie *et al.*, 2002), it was necessary to determine the effect of omitting FBS from the cell media on cell proliferation. This was examined in order to determine whether this would have an effect on the assays utilized in this research. The effect of MDA on cell

proliferation in the absence of FBS was also examined to determine the upper limit of MDA concentration that could subsequently be used.

A positive control was chosen to show that the cytotoxic effects of treatment with MDA were due to the oxidative stress caused by MDA and no other external cause. The ideal candidate for this was H_2O_2 as this is known to cause oxidative stress (Gutteridge, 1995) and has been shown to elicit a similar response to MDA.

A number of cytotoxicity assays were carried out, in order to demonstrate the effects of MDA on the two cell lines, and to complement each other, to build an overall cytotoxicity profile for MDA on these cell lines. A MTT assay was carried out, as this is the most widely adopted assay for cell viability. The effect of MDA on cell morphology was carried out using two imaging techniques: inverted LM, to view the live cells *in vitro*, and AFM to view the cell surface morphology. Nuclear morphology was investigated using fluorescence microscopy, and also apoptosis and p53 protein expression by immunofluorescence. p53 expression was also determined by reverse transcription-quantitative polymerase chain reaction (RT-qPCR) for comparison with p53 immunofluorescence detection.

Following characterisation of the effects of MDA at the cellular level, the effects of MDA were examined at the DNA level to determine whether the alterations observed would lead to mutagenesis or other outcomes. Initially, DNA adduct analysis was carried out to determine whether M_1dG adducts could be detected in the genomic DNA extracted from cells treated with MDA. This was carried out by synthesis and purification of a M_1G standard, to be used for quantitative analysis, followed by optimisation of a HPLC

separation method using this standard. Development and optimisation of LC-MS and LC-MS-MS techniques for M_1dG adduct analysis were carried out prior to analysis of DNA samples.

The genomic DNA extracted from the MRC5 and MRC5 SV2 cells treated with MDA was examined using AFM, to visualise any obvious large scale changes to the DNA and fragmentation levels. A feasibility study using AFM was also carried out using M_1dG antibodies to try and detect the presence of M_1dG adducts on the DNA molecules.

Finally, a section of the *TP53* gene was amplified by PCR and sequenced to look for mutations. The segment of DNA chosen included the 5' untranslated region (UTR), encompassing exon 1, of the *TP53* gene, a region previously thought to have no or little biological functionality. A huge bias exists in the mutation data from the *TP53* gene, where the majority of data is for the protein coding exons 2-11. Thus mutation sequencing of the 5' UTR would make an important, novel, contribution to the *TP53* mutation database. An overview of the methods utilised in this research is shown in Figure 8.

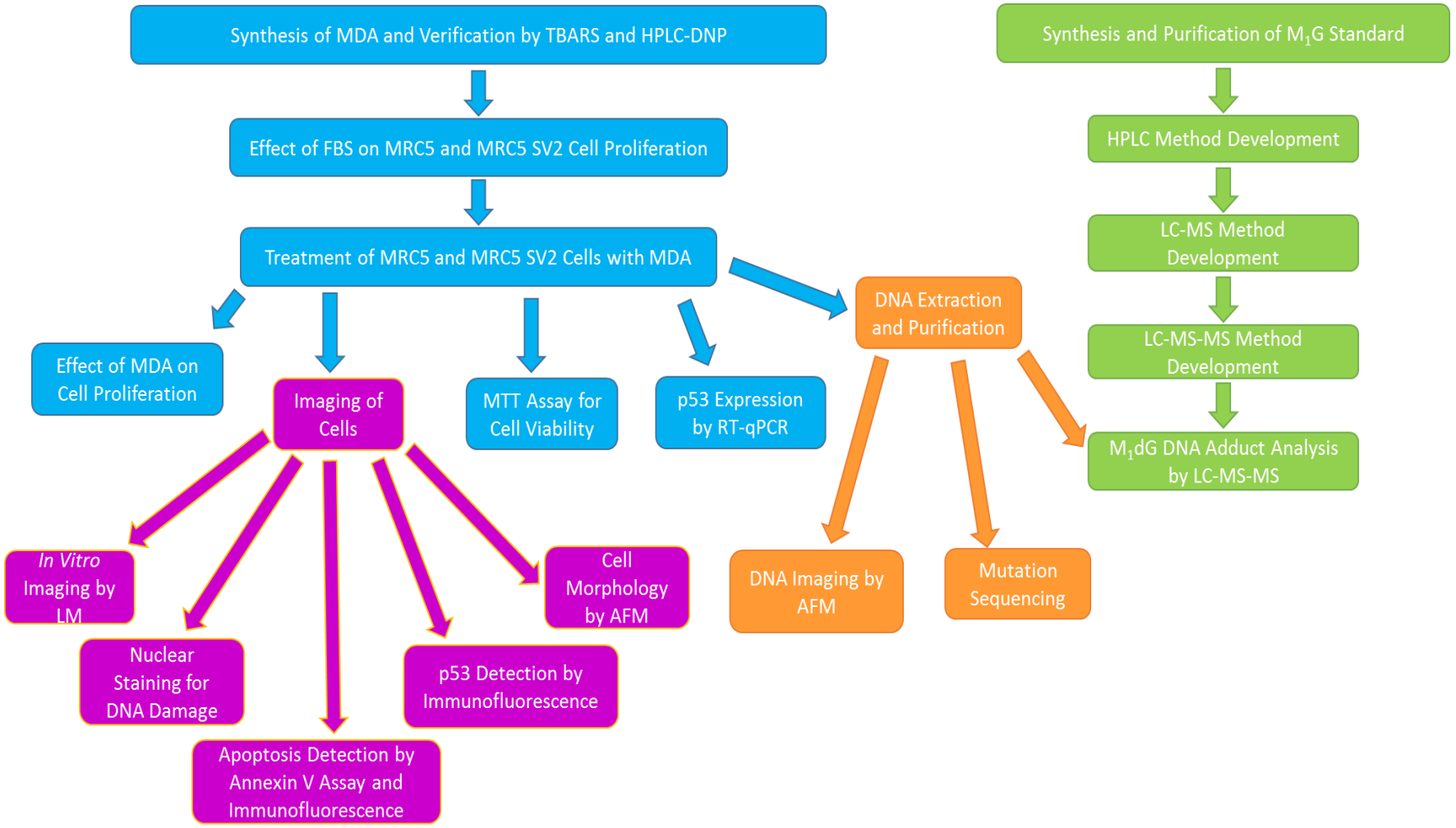

Figure 8. An overview of the methodology used in this research

1.15. Aims & Objectives

The aim of this research was to determine the effect of treatment with MDA on human lung fibroblast cells, MRC5 and MRC5 SV2, which have an intact and a sequestered p53 response respectively. This was achieved by:

- Establishing the growth characteristics of both cell lines in response to treatment with and without FBS, and with and without MDA.
- Determining the viability of the cell lines in response to treatment with MDA by MTT assay.
- Assessment of DNA damage by staining the nuclei of both cell lines following treatment with MDA, to show changes in nuclear morphology.
- Examination of cell morphology using LM and AFM following treatment of both cell lines with MDA.
- Apoptosis detection in response to MDA treatment of cells by Annexin V assay and immunofluorescence.
- p53 expression by immunofluorescence and RT-qPCR in response to treatment of cells with MDA.
- Imaging of genomic DNA from cells treated with MDA by AFM to show DNA structural changes and fragmentation.
- Development of methods to analyse M_1dG adducts in cellular DNA.
- PCR and mutation sequencing of residues 4640-5328 of the *TP53* gene.

CHAPTER 2

MATERIALS & METHODS

The materials and equipment utilized for this research are listed in this chapter, along with detailed experimental procedures and protocols.

2.1. Materials

2.1.1. Reagents and Disposable Items

The following materials were obtained from the following suppliers: 25% glutaraldehyde (EM grade) was purchased from Agar Scientific, Stansted (UK); sterile pipette tips, 0.2 µl thin-wall 8-tube strips and thin-wall tube (high profile) with an optical flat cap were from Appleton Woods, Birmingham (UK); sterile vented petri dishes were from BD Falcon, Oxford (UK); hyperladder II (included DNA loading buffer) was purchased from Bioline, London (UK); FBS was from Biowest, Nuaillé (France); *TP53* primers (forward 5'TCTGGGAGAAAACGTTAGGG3' and reverse 5'ATCCCTCTAGCCAAGCTTCC3'), p53 complementary DNA (cDNA) primers (forward 5'AGATGAAGCTCCCAGAATGC3' and reverse 5'TCTTGCGGAGATTCTCTTCC3') and glyceraldehyde-3-phosphate dehydrogenase (*GAPDH*) primers (forward 5'GGTGAAGGTCGGAGTCAACGG3' and reverse 5'GGTCATGAGTCCTTCCACGAT3') were purchased from Eurofins MWG Operon, Ebersberg (Germany); prolong gold anti fade, molecular-grade water and a purelink

messenger ribonucleic acid (mRNA) mini kit were from Life Technologies, Paisley (UK); mica was from Novascan Technologies, Ames, Iowa (USA); AC240 and TR400PSA AFM cantilevers were from Olympus, Southend-on-sea (UK); RNasin Plus RNase inhibitor, GoScript reverse transcriptase and GoTaq 2-step RT-qPCR system were purchased from Promega, Southampton (UK); random hexamers were from Qiagen, Manchester (UK); ethylenediaminetetraacetic acid (EDTA) 500 mM solution, tris(hydroxymethyl)aminomethane (tris) were from Severn Biotech, Kidderminster (UK); SPE Supelclean ENVI-18 Tubes, H_2O_2 (30%), glacial acetic acid, Cellomics p53 detection kit (included hoechst dye), nylon membrane filters (47 mm diameter, 0.2 µm pore), ethidium bromide, boric acid, deoxynucleotide (dNTP) mix, 11 mm clear glass crimp top HPLC vials and aluminium crimp caps, screw top fixed insert borosilicate glass clear 0.3 ml HPLC vials and blue plastic screw caps were purchased from ThermoFisher, Loughborough (UK); methanol HiPerSolv and water HiPerSolv were from VWR International Ltd, Lutterworth (UK).

Sterile items: serological pipettes (5 ml and 10 ml), universal tubes (25 ml), conical centrifuge tubes (15 ml), cell culture flasks (25 and 75 cm^2), 8 chamber cell culture slides, tissue culture treated 96 well, 12 well and 6 well plates with lids, cover slips (15 mm^2), glass microscope slides (75 x 25 x 1.1 mm) and glass pasteur pipettes, PCR tubes were purchased from Scientific Laboratory Supplies Ltd, Nottingham (UK).

Dimethyl sulphoxide (DMSO), minimal essential medium Eagle (MEM), L-glutamine (200 mM), penicillin-streptomycin (10,000 units/ml penicillin and 10 mg/ml streptomycin), non-essential amino acids (NEAA), phosphate buffered saline (PBS),

trypan blue solution (0.4% w/v), trypsin/EDTA Solution (0.25%), thiazolyl blue tetrazolium bromide (MTT, 97.5%), 1,1,3,3-tetramethoxypropane (TMP, 6.01 M), 2-thiobarbituric acid powder (TBA), concentrated hydrochloric acid (HCl), potassium hydroxide (KOH), potassium chloride (KCl), DAPI (10 mg/ml), 2,4-dinitrophenylhydrazine (DNP), phosphoric acid (85%), acetonitrile (HPLC-grade), methanol, 100% ethanol, calf thymus (CT) DNA, monobasic potassium dihydrogen phosphate (KH_2PO_4), dibasic potassium phosphate (K_2HPO_4), cytochalasin B, guanine, Reddymix PCR mastermix, GenElute mammalian genomic DNA mini prep kit, Annexin V-CY3 apoptosis detection kit, agarose, fluoromount, trizma hydrochloride, EDTA disodium salt dihydrate ($EDTA.Na_2.H_2O$), magnesium chloride hexahydrate ($MgCl_2.6H_2O$), 2-mercaptoethanol, araldite were purchased from Sigma-Aldrich, Gillingham (UK).

The primary antibody to M_1dG was a gift provided by Lawrence J. Marnett, Marnett Research Laboratory, Vanderbilt School of Medicine, Vanderbilt Univeristy, USA.

The M_1dG DNA standard was provided by Dr Sharon A. Moore, School of Pharmacy and Biomolecular Sciences, Liverpool John Moores Univesity and prepared as previously described (Leuratti *et al.*, 1998). M_1dG adduct levels in undiluted DNA were 21 pmol/µg DNA.

2.1.2. Cell Lines and Cell Line Maintenance

Cell lines were obtained from the European Collection of Animal Cell Cultures (ECACC), Porton Down, Salisbury, UK. MRC5 cells were adherent human lung fibroblasts, ECACC number 05090501, derived from normal human lung tissue of a 14 week old male,

requiring MEM supplemented with 10% FBS (v/v), 2 mM L-glutamine (with penicillin-streptomycin) and 1% NEAA (complete media). Growth conditions were humidified 5% carbon dioxide (CO_2)/95% air and 37°C. Cells were sub-cultured 1:3 to 1:6 when 70-80% confluent and seeding density was 2-4 x 10,000 cells/cm^2. MRC5 SV2 cells, ECACC number 84100401, were derived from the parental cell line MRC5 by transformation with the SV40 virus. Culture medium and growth conditions required were the same as for MRC5 cells. Cells were sub-cultured 1:5 to 1:10 when 70-80% confluent and seeding density was 1-2 x 10,000 cells/cm^2.

2.2. Equipment

Cell Culture: Grade II biological safety cabinet was from ESCO, Hatboro, Pennsylvania (USA); Spectramax 190 ROM absorbance microplate reader from Molecular Devices, Sunnyvale, California (USA); Cary eclipse fluorescence spectrophotometer was from Agilent Technologies, Wokingham (UK);

Microscopy: The inverted optical microscope (CK2) was from Olympus, Southend-on-sea (UK); the laser scanning confocal microscope (510 META) was from Zeiss, Cambridge (UK); haemocytometer from Sigma-Aldrich, Gillingham (UK); Lightsource monochrome CCD camera; molecular force probe 3D microscope (MFP-3D) was from Asylum Research, Santa Barbara, California (USA);

PCR: Veriti 96 well thermal cycler and 7500 real time PCR system were from Applied Biosystems, Paisley (UK); electrophoresis system and power supply were from Fisher Scientific, Loughborough (UK); Gel Doc XR image analysis system from BioRad, Hemel

Hempstead (UK); Nanophotometer 7122 v1.3 from NanoDrop, Wilmington, Delaware (USA);

Chromatography and Mass Spectrometry: Agilent 1200 series HPLC separations module with photodiode array detector (PDA), fluorescence detector (FLD), degasser, quaternary pump, column module and autosampler were from Agilent, Stockport (UK); Alliance Micromass liquid chromatography – time of flight – mass spectrometer (LC-MS), Waters 2695 separations module and a Waters 486 tunable absorbance detector were from Waters, Elstree (UK); Phenomenex Luna C18 250 mm x 4.6 mm HPLC column (Column A), Phenomenex Gemini NX 3u C18 110A 100 x 2.00 mm HPLC column (Column B), Phenomenex security guard cartridge guard column and A50-4288 4 mm L x 2.00 C18 guard cartridge were from Waters, Elstree (UK). Waters 2690 HPLC separation module with a Waters 996 photodiode array detector and a Waters Micromass Quattro Premier Triple Quadrupole Mass Spectrometer (LC-MS-MS) were from Waters, Elstree (UK), operated by MassLynx v. 4.1 software.

2.3. Methods

All statistical analysis was carried out using Microsoft Excel 2007 software and results were significantly different if $P < 0.05$, unless otherwise stated. HPLC- grade water was used in all protocols unless otherwise stated.

2.3.1. Synthesis of Malondialdehyde

A 100 mM stock solution of MDA was prepared by acid hydrolysis of TMP (M_R 220.31). A 166.4 µl aliquot of TMP was added to 4690 µl 0.1 M HCl and incubated at room temperature for 40 min. The solution was then neutralised by the addition of 4690 µl 0.1M KOH and the volume made up to 10 ml with water.

2.3.2. Analysis of Malondialdehyde Standards by TBARS

A 100 mM MDA stock solution was diluted with water to give standards in the range 0-1000 µM MDA. TBARS reagent was prepared by dissolving 0.375 g TBA in 100 ml 0.25 M HCl. A 0.125 ml aliquot of each standard was added to 1 ml TBARS reagent and incubated at 95°C for 10 min, followed by cooling to room temperature on ice. The samples were centrifuged at 2000 g for 10 min and the supernatant transferred to wells of a 96 well plate. The absorbance at 532 nm was read using a Spectramax 190 ROM plate reader and SoftMax Pro v5.2 software.

2.3.3. Analysis of Malondialdehyde Standards by HPLC

A 100 mM MDA stock solution was diluted with water to give standards in the range 0-20 mM MDA. Brady's reagent was prepared by dissolving 0.26 g DNP in 100 ml 6M HCl (Vogel, 1956). The MDA standards were derivatised by adding 1 ml standard to 1 ml Brady's reagent and incubating at room temperature for 15 min, 2 ml HPLC grade acetonitrile was added and 1 ml was transferred to a HPLC vial. The HPLC method was

as shown in Table 1. Column A (Section 2.2) was used with an Agilent HPLC separator module with PDA and FLD detectors.

Table 1. HPLC method for DNP derivative analysis. Temperature 37°C, flow rate 1 ml/min, sample volume 20 µl.

Time (min)	H_2O (%)	Acetonitrile (%)	0.1 M H_3PO_4 (%)
0	80	10	10
30	0	90	10
30-35	0	90	10
35-45	80	10	10

2.3.4. Routine Maintenance of Cells

All cell culture was carried out under aseptic conditions in an ESCO grade II laminar flow cabinet. Cells were sub-cultured when 70-80% confluent by removal of the spent media, washing with PBS and addition of trypsin/EDTA. Complete media was added to neutralise the action of the trypsin. The cell suspension was centrifuged at 1500 rpm for 5 min. The pellet was re-suspended in complete media. Cells were seeded into T-75 flasks or re-suspended in freezing mixture (70% MEM, 20% FBS and 10% DMSO) and stored in liquid nitrogen at -196°C. Cells were grown in an incubator at 37°C with 5% CO_2 unless otherwise stated.

2.3.5. Effect of Foetal Bovine Serum and Malondialdehyde on Cell Proliferation

Cell proliferation was determined for both cell lines in both the presence and absence of FBS. FBS-free media was prepared by addition of 1% NEAA and 2 mM L-glutamine (with penicillin-streptomycin) to MEM. Complete media was prepared as described in Section 2.1.2. Cells were suspended in both media and seeded at 1 x 10^4 cells per well of a 96 well plate. A viable cell count was carried out at 24 h intervals in triplicate by application of a 1:1 mixture of cell suspension:trypan blue to a haemocytometer. Cells stained blue were regarded as non-viable and were not counted. The growth of each cell line was also determined in the presence of MDA (0-1000 µM) diluted in FBS-free media. Mean cell number versus time was plotted, all data was shown as ± 1 SD from the mean, unless otherwise stated. The population doubling time (PDT) (h) was calculated from the log phase of growth as follows:

$$\mathrm{PDT} = \frac{t_2 - t_1}{3.32(\log n_2 - \log n_1)}$$

Where n_1 = initial cell number at time t_1 (h) and n_2 = final cell number at time t_2 (h).

The growth rate (k) (h^{-1}) was calculated by:

$$k = \frac{\ln 2}{\mathrm{PDT}}$$

2.3.6. Cell Viability using a MTT Assay

The viability of both cell lines when treated with MDA (0-1000 µM) and positive control H_2O_2 (0-100 µM), diluted in FBS-free media, was assessed using an MTT assay. A 1 mg/ml MTT solution was prepared by dissolving 10 mg MTT in 1 ml PBS and then made up to 10 ml with FBS-free media. Cells were seeded at 1 x 10^4 cells per well of 96 well plates and left to attach for 24 h. The media was removed and the cells were treated with each MDA solution in triplicate and incubated for 24, 48 or 72 h. The media was removed and MTT reagent was added to each well and incubated for 3 h. DMSO was added to each well, to solubilise the purple formazan product. MTT and DMSO were also added to 3 cell-free wells to determine the background absorbance. The absorbance of each well was read using a Spectramax 190 ROM microplate reader at 540 nm. The mean absorbance and standard deviation were calculated for each MDA concentration and control, and the mean absorbance of the MTT-DMSO only wells was deducted. The mean % cell viability was calculated as follows.

$$\text{Mean \% Cell Viability} = \frac{\text{Mean Absorbance Sample}}{\text{Mean Absorbance Control}} \text{ x } 100\ \%$$

Data was normalized to the untreated (control) cells at 100% viability. Student's t-test was used to compare each cell line treated with each concentration of MDA at each time period.

2.3.7. *In vitro* Imaging of Cells

Cells from each cell line were seeded at 1 x 10^4 cells /cm^2 into 12 well plates and allowed to grow in complete media for 48 h. Cells were treated in triplicate with MDA (0-1000 µM) and H_2O_2 (50 µM) in FBS-free media and incubated for 24 h and 48 h. Light microscope images of live cells were captured after treatment using a Lightsource monochrome CCD camera coupled to an Olympus CK2 inverted optical microscope.

2.3.8. Effects of MDA on Nuclear Morphology

Cells from each cell line were seeded at 1 x 10^4 cells /cm^2 onto 8 chamber microscope slides and allowed to attach for 24 h. Cells were treated in triplicate with MDA (0-1000 µM) and H_2O_2 (50 µM) in FBS-free media and incubated for 24 h and 48 h. The media was removed from the wells. A 1 mg/ml cytochalasin B in DMSO solution was diluted 1.5:100 in complete media and was added to each well. Following 24 h incubation, the wells were removed from the chamber slides and the media discarded. The cells were washed in PBS and then fixed as follows: the microscope slides were placed in hypotonic solution (0.4% Na-citrate + 0.4% KCl in distilled water) containing 4% formaldehyde and incubated at 4°C for 8 min. The slides were removed from the solution and placed in hypotonic solution only. A fixative solution of 4:1 methanol : glacial acetic acid was prepared. An equal volume of fixative was added very slowly to the hypotonic solution whilst gently shaking. Next, 50% of the hypotonic/fixative mixture was removed and an equal volume of fixative was then added slowly. The hypotonic/fixative mixture was removed and 100% fixative was added for at least 1 min. The fixative was removed and the slides were allowed to air dry. The

slides were incubated in DAPI (50 µg/ml in distilled water) for 15 min at room temperature and then washed (x5) in PBS. The slides were then viewed using a Zeiss 510 META laser scanning confocal microscope (excitation 350 nm, emission 470 nm).

The area of 10 nuclei from each cell line and each MDA treatment were measured using ImageJ software (Rasband, 1997). Student's t-test was used to compare each cell line treated with each concentration of MDA at each time period.

2.3.9. Apoptosis Detection using Annexin V Fluorescent Assay

Cells from each cell line were seeded at 1 x 10^4 cells /cm^2 onto 15 mm coverslips placed in 12 well plates and allowed to attach for 24 h. Cells were treated in triplicate with MDA (0-1000 µM) and H_2O_2 (50 µM) in FBS-free media and incubated for 24 h and 48 h. The media was removed from the wells by aspiration and the cells were washed (x2) with PBS and the solution aspirated. Cell were stained using an Annexin V-CY3 apoptosis detection kit as follows. Cells were washed (x3) with binding buffer (10 mM 4-(2-hydroxyethyl)-1-piperazineethanesulfonic acid (HEPES), pH 7.5 containing 140 mM sodium chloride (NaCl) and 2.5 mM calcium chloride ($CaCl_2$)), diluted 1:10 in deionized water, each time removing excess solution by blotting the edge of the coverslip with a tissue. Double staining solution (1 µg/ml annexin-Cy3.18 and 500 µM 6-carboxyfluorescein diacetate in 1:10 dilution of binding buffer) was added to the coverslip to cover the cells, and the plate was incubated in the dark at room temperature for 10 min. Cells were washed (x5) in aliquots of 1:10 dilution of binding buffer. The coverslips were mounted onto microscope slides using ProLong gold anti-fade mounting

medium and the cells were imaged using a Zeiss 510 META laser scanning confocal microscope.

2.3.10. p53 Expression using Immunofluorescence

Cells from each cell line were seeded at 1 x 10^4 cells /cm^2 onto 15 mm coverslips placed in 12 well plates. Cells were allowed to attach for 24 h. Cells were treated in triplicate with MDA (0-1000 µM) and H_2O_2 (50 µM) in FBS-free media and incubated for 24 h and 48 h. The media was removed from the wells by aspiration and the cells were stained using a Cellomics p53 detection kit as follows: Fixation solution (4% paraformaldehyde in 1:10 dilution of wash buffer) was added to each well and incubated in a fume hood at room temperature for 15 min. The fixation solution was aspirated completely and 1:10 diluted permeabilization buffer (in 1:10 diluted wash buffer) was added to each well and incubated for 15 min at room temperature. The permeabilization buffer was aspirated and the cells were washed (x2) with 1:10 diluted blocking buffer (in 1:10 diluted wash buffer). The blocking buffer was aspirated and further aliquots of diluted blocking buffer were added to each well and incubated for 15 min. The blocking buffer was aspirated and primary antibody solution (1:100 dilution of anti-p53 antibody in diluted blocking buffer) was added to each well and incubated for 1 h. The primary antibody solution was aspirated and the cells were washed (x2) with diluted blocking buffer. The blocking buffer was aspirated and staining solution (1:1000 hoechst dye and 1:100 DyLight 549 goat anti-rabbit in diluted blocking buffer) was added to each well and incubated in the dark for 1 h. The staining solution was aspirated and the cells were washed (x2) in diluted wash buffer. The coverslips were removed from the 12 well plates and mounted onto

microscope slides using ProLong gold anti-fade mounting medium and the cells were imaged using a Zeiss 510 META laser scanning confocal microscope.

2.3.11. p53 Expression using Reverse Transcription Quantitative Polymerase Chain Reaction

TP53 gene expression was assessed by quantitative analysis of p53 mRNA using a GoTaq two-step reverse transcription-quantitative PCR (RT-qPCR) as follows: Cells from each cell line were seeded into T-75 flasks and allowed to grow until 70-80% confluent in complete media. Cells were treated in duplicate with MDA (0-100 µM) and H_2O_2 (50 µM) in FBS-free media and incubated for 24 h and 48 h. The growth media was removed and the cells were washed with PBS and trypsin/EDTA was added to detach the cells. Complete media was added to neutralise the action of the trypsin. The cell suspension was transferred to an RNase-free tube and centrifuged at 2000 x g for 5 min, the supernatant was discarded, leaving the pellet for mRNA extraction.

2.3.11.1. mRNA Extraction and Purification

mRNA was extracted and purified using a PureLink RNA mini kit, as follows: Lysis Buffer (containing 1% 2-mercaptoethanol) was added to the cell pellet and vortexed thoroughly to disperse the cells and they appeared lysed. The lysate was passed through a 21-gauge syringe needle (x10) to homogenise. Next, 70% ethanol was added to each sample and vortexed. The sample (including precipitate) was transferred to a spin cartridge and collection tube and centrifuged at 12000 x g for 15 s at room temperature, and the flow-through was discarded. This step was repeated until all of the sample was

used up. An aliquot of wash buffer I was added to the spin cartridge, centrifuged at 12000 x g for 15 s at room temperature and the flow through and collection tube were discarded. The spin cartridge was transferred to a clean collection tube and wash buffer II (containing ethanol) was added and then centrifuged at 12000 x g for 15 s at room temperature, the flow through was discarded and this step was repeated. The spin cartridge was centrifuged for 1-2 min at 12000 x g to dry the membrane with bound RNA. The collection tube was discarded and the spin cartridge was inserted into a recovery tube. Finally, RNase-free water was added to the centre of the cartridge and incubated at room temperature for 1 min, then centrifuged at room temperature for 2 min at 12000 x g and this step was then repeated. The purified RNA was stored at -80°C.

2.3.11.2. Quantification of p53 by RT-qPCR

The concentration of RNA in each sample was quantified using a NanoDrop spectrophotometer (absorbance at 260 nm) and then diluted with RNase-free water so that all samples contained the same concentration of RNA. Next, each RNA sample was added to a 50 µl PCR tube with random hexamers (final concentration 0.025 µg/µl random hexamers), each sample in triplicate. Two negative controls were also set up, one without an RNA template (replaced by RNase-free water) and one without reverse transcriptase (for later in the protocol) using any of the RNA samples. The sealed tubes were placed in a heat block at 70°C for 5 min to denature, followed by chilling to 4°C for 5 min and centrifuging briefly to collect any condensation. The samples were held on ice.

A reverse transcription master mix was prepared on ice as follows, adding the reagents in the following order, the volume per reaction was: 1.5 µl RNase-free water, 4 µl

GoScript reaction buffer, 2 µl $MgCl_2$, 1 µl dNTP's, 0.5 µl RNase inhibitor, 1 µl reverse transcriptase (the reaction without reverse transcriptase had 2.5 µl RNase-free water instead). The reaction mix was mixed thoroughly by inversion. 10 µl of the reverse transcription reaction mix was added to 10 µl RNA sample and the reverse transcriptase-free reaction mix was added to the correct RNA sample. cDNA was synthesized in a thermal cycler, according to Table 2. The cDNA was stored on ice for immediate use, or at -20°C for later use.

Table 2. Steps for the synthesis of cDNA by reverse transcriptase.

Step	**Temperature (°C)**	**Time**
Anneal	25	5 min
Extend	42	1 h
Inactivate	70	15 min
Chill	4	Hold ∞

To quantify the *TP53* cDNA by qPCR, two sets of cDNA primers were used. *GAPDH* was used as a reference gene, the primers for this were: forward 5'GGTGAAGGTCGGAGTCAACGG3' and reverse 5'GGTCATGAGTCCTTCCACGAT3'. The *TP53* cDNA primers were: forward 5'AGATGAAGCTCCCAGAATGC3' and reverse 5'TCTTGCGGAGATTCTCTTCC3'. Primers were designed using Entrez Gene (Maglott *et al.*, 2010), Primer3 (Untergasser *et al.*, 2012) and primer BLAST (Ye *et al.*, 2012) bioinformatics and 1 µM stock solutions of each primer were prepared using RNase-free water and held on ice.

A qPCR reaction mix was prepared on ice, containing 10 µl GoTaq qPCR Master Mix 2X, 4 µl RNase-free water and 1µl each of either *TP53* forward and reverse cDNA primers or *GAPDH* forward and reverse cDNA primers. Each RNA sample was prepared in triplicate and 2 reactions were set up for each triplicate, one for *TP53* and one for *GAPDH*, plus 2 reactions for the template-free control (*TP53* and *GAPDH*) and 2 reactions for the reverse transcriptase-free control (*TP53* and *GADPH*). A 4 µl aliquot of RNA sample/control was added to a well of a 96 well qPCR reaction plate on ice and 16 µl qPCR reaction mix was added to each sample, to give a final volume of 20 µl. The reaction plate was centrifuged using a swinging-bucket centrifuge at low speed for 1 min. The real-time qPCR thermal cycler was programmed with SYBR as the detection dye and CXR as the reference dye. The cycling conditions are shown in Table 3.

Table 3. Real-time qPCR thermal cycling conditions.

Step	Cycles	Temperature (°C)	Time
GoTaq Hot Start Polymerase Activation	1	95	2 min
Denaturation Annealing/Extension	40	95 60	15 s 1 min
Dissociation	1	60-95	-

Expression of *TP53* (target gene) relative to *GAPDH* (endogenous control gene) expression was calculated using the $2^{-\Delta\Delta Ct}$ Comparative Cycle Threshold (Ct) method (Livak and Schmittgen, 2001). Samples were normalised to a RNA–free negative control

and referenced against *GADPH*. Student's t-test was used to compare each cell line treated with each concentration of MDA at each time.

2.3.11.3. Agarose Gel Electrophoresis

Gel electrophoresis of the qPCR products was performed to check that the cDNA fragments were the correct size and that no DNA could be detected in the negative controls. Agarose gels (1%) were prepared as follows: Tris/Borate/EDTA (TBE) buffer was prepared with 10.8 g/l tris base, 5.5 g/l boric acid and 4 ml/l 0.5 M EDTA (pH 8). Next, 1 g agarose was added to 100 ml TBE buffer and stirred on a magnetic stirrer at 100°C until the agarose dissolved. The solution was cooled to approximately 60°C and 3 µl ethidium bromide was added. The gel was cast, a horizontal gel comb was inserted and the gel was allowed to set for 60 min. The gel was then placed into the electrophoresis tank and just covered with TBE buffer. A marker was loaded into the first lane (HyperLadder II, 500 – 2000bp) and 9 µl samples were loaded into the wells with 1 µl DNA loading buffer. The electrophoresis was carried out at 95 V for 45 min to 1 h. The gels were viewed with a gel imager and BioRad Quantity One software.

2.3.12. Effect of Malondialdehyde on DNA Sequence

To assess whether MDA had an effect on the integrity of the DNA sequence, both cell lines were treated with MDA and H_2O_2 (positive control) for 48 h, DNA was extracted and purified and residues 4640-5328 of the *TP53* gene were amplified by PCR and sequenced as follows: Cells from each cell line were seeded into T-75 flasks and allowed to grow until 70-80% confluent in complete media. Cells were treated in duplicate with

MDA (0-1000 µM) and H_2O_2 (0 - 100 µM) in FBS-free media and incubated for 48 h. The growth media was removed and the cells were washed with PBS and trypsin/EDTA was added to detach the cells. Complete media was added to neutralise the action of the trypsin. The cell suspension was transferred to a nuclease-free tube and centrifuged at 2000 x g for 5 min, the supernatant was discarded, leaving the pellet for DNA extraction. The cell pellets were frozen at -80°C until required.

2.3.12.1. DNA Extraction, Purification and Quantification

Genomic DNA was extracted and purified using a GenElute Mammalian Genomic DNA Miniprep Kit as follows: The cell pellets were allowed to thaw and were then resuspended in Resuspension Solution. RNase A solution was added and incubated at room temperature for 2 min. Proteinase K solution (20 mg/ml) was added to each sample, followed by Lysis Solution C, the samples were vortexed thoroughly and incubated in a water bath at 70 °C for 10 min to lyse the cells.

The columns were prepared by adding Column Preparation Solution to each pre-assembled GenElute Miniprep Binding Column and centrifuged at 12000 x g for 1 min and the flow through was discarded. Next, 100% ethanol was added to the cell lysates and mixed thoroughly by vortexing for 15 s. The cell lysates were transferred to the binding columns using wide bore pipette tips to prevent DNA shearing. The columns were centrifuged at 6500 X g for 1 min and the flow through and collection tube were discarded. The column was placed in a new 2 ml collection tube.

Wash Solution Concentrate was diluted 1:5 with 100% ethanol. The diluted Wash Solution was added to the binding columns and centrifuged at 6500 x g for 1 min. The collection tube and flow through were discarded and the binding column was placed in a new collection tube. Another aliquot of diluted Wash Solution was added to the binding columns and centrifuged at maximum speed for 3 min to dry the columns and remove residual ethanol. The collection tube and flow through were discarded and the binding columns were placed in new collection tubes.

To elute the DNA, Elution Solution (10 mM Tris-HCl, 0.5 mM EDTA, pH 9.0) was added to the centre of the binding columns, incubated at room temperature for 5 min and centrifuged for 1 min at 6500 x g. This step was repeated and the DNA was quantified using a NanoDrop spectrophotometer (260 nm absorbance). The DNA solutions were stored at -20°C until required.

2.3.12.2. Polymerase Chain Reaction of *TP53* Gene

The following *TP53* primers were used for PCR. The forward primer 5'TCTGGGAGAAAACGTTAGGG3' and reverse primer 5'ATCCCTCTAGCCAAGCTTCC3' flank residues 4640-5328 of the human *TP53* gene (GenBank Accession Number NG_017013). Primers were designed using Ensembl (Flicek *et al.*, 2012), Primer3 (Untergasser *et al.*, 2012) and BLAST (Madden, 2002) bioinformatics. PCR was carried out on the genomic DNA samples as follows.

DNA samples in aliquots of 5 µl were added to 50 µl PCR tubes and a negative control of 5 µl molecular grade water was also prepared. A reaction master mix was prepared,

containing 25 µl ReddyMix PCR Mastermix, 0.5 µl each of forward and reverse primers, 19 µl molecular grade water for each DNA sample. A 45 µl aliquot of reaction master mix was added to each DNA sample and the negative control and the tubes were sealed and placed in a thermal cycler. The PCR cycle is shown in Table 4. The PCR products were stored at -20°C until required.

Table 4. PCR cycle conditions for amplification of *TP53* DNA fragment.

Step	Temperature (°C)	Time	Number Cycles
Hot Start	95	3 min	1
Denaturation Annealing Extension	95 57 72	30 s 1 min 40 s	40
Final Extension	72	5 min	1
Hold	4	∞	1

2.3.12.3. Agarose Gel Electrophoresis

Gel electrophoresis of the PCR products was performed to check that the DNA fragments were the correct size and that no DNA could be detected in the negative controls. Agarose gels (1%) were prepared as described in Section 2.3.11.3. A marker was loaded into the first lane (HyperLadder II, 500 – 2000bp) and samples were loaded into the wells. The electrophoresis was carried out at 100 V for 30 minutes. The gels were viewed with a gel imager and BioRad Quantity One software.

2.3.12.4. Mutation Sequencing

Sanger DNA sequencing was carried out on the non-purified PCR products (using the same primers as in Section 2.3.12.2) by Beckman Coulter Genomics, UK, by double stranded primer walking using an ABI Prism 3730XL DNA sequencer.

The DNA sequences were analysed and processed using CLC Main Workbench 6 software (CLCBIO, 2014). A consensus sequence combining both the forward and reverse sequences from each sample was created. The consensus sequence was then aligned to the *TP53* reference sequence and any unknown nucleotides were assigned. Conflicts between the *TP53* reference sequence and the sample consensus sequence were identified and duplicate sample sequences were merged to include all possible mutations for that sample. A multiple alignment for each cell line was carried out, referenced to the *TP53* reference sequence. Each sample sequence was converted to the corresponding amino acid sequence and a multiple alignment of the amino acid sequence for each sample and cell line was carried out. The secondary structure of the amino acid sequence was also shown, to indicate if any mutations had any effect on the protein structure. Using the amino acid sequences, protein hydrophobicity was plotted and protein charge versus pH was plotted to show the effect any mutations had on the protein properties.

2.3.13. Imaging using Atomic Force Microscopy

2.3.13.1. Cell Surface Morphology

Cells from each cell line were seeded at 1 x 10^4 cells /cm^2 onto 25 mm coverslips placed in 6 well plates and allowed to attach for 24 h. Cells were treated in triplicate with MDA (0-1000 µM) and H_2O_2 (50 µM) in FBS-free media and incubated for 24 h and 48 h. The media was removed from the wells by aspiration and the cells were washed twice with PBS and the solution aspirated. Cells were fixed in 2.5% glutaraldehyde in PBS for 20 min. They were then washed (x6) in excess PBS followed by a final wash in molecular grade water. Cells were allowed to air-dry in the fume cupboard, covered enough to prevent settling of dust. The cell surface was imaged using a Molecular Force Probe 3D AFM in contact mode using an Olympus AFM V-shaped TR400PSA cantilever (spring constant 0.02-0.08 N/m, imaged at a rate of 1 Hz) and Argyle software. Integral and proportional gains were optimised empirically whilst scanning.

2.3.13.2. Effect of Malondialdehyde on DNA Topography

DNA molecules can be imaged using AFM. The DNA samples imaged were the PCR products produced in Section 2.3.12.2. To prepare the DNA samples for imaging, microscope slides with mica discs were prepared as follows. A mica disc was fixed to a clean, plain glass microscope slide with araldite and allowed to dry for 24 h in a covered petri dish. The top layer of mica was then removed using either a razor blade or sellotape. Tris/EDTA (TE) buffer was prepared by dissolving 0.4728 g Tris HCl in 10 ml HPLC-grade water, 0.1017 g EDTA.Na_2.H_2O in 10 ml HPLC-grade water and 0.6010 g $MgCl_2$.$6H_2O$ in

10 ml HPLC-grade water. The three solutions were then mixed together to make TE buffer. DNA samples were diluted in TE buffer to 2 ng/µl and 10 µl was applied to the prepared mica. The sample was left on the mica for 1 min in a covered petri dish (to prevent settling of dust and contamination). The solution was then carefully washed from the mica with HPLC-grade water and excess water blotted from the edge of the disc with tissue. The DNA was left to dry on the mica for 10 min and once dry was imaged using an Asylum Research MFP-3D microscope in tapping mode with an Olympus AC240 V tipped AFM cantilever (resonant frequency 72 kHz, spring constant 2 N/m, imaged at a rate of 1 Hz with a free-air amplitude of 0.5 V and a damping amplitude of 0.3 V) and Argyle software. Integral and proportional gains were optimised empirically whilst scanning.

2.3.13.3. Use of M_1dG Antibodies to Locate MDA-Induced Mutations by AFM

M_1dG primary antibodies (supplied by Marnett, L) were used to locate M_1dG adducts on the DNA strands using AFM. The antibodies were diluted to 10 ng/µl in TE buffer and were added to the DNA samples as follows: 5 µl of 10 ng/µl DNA solution, 13 µl TE buffer and 2 µl of 10 ng/µl antibody were added to a microfuge tube and placed on a rocker for 30 min at room temperature to allow the antibodies to bind to any adducts. Next, 10 µl of the DNA-antibody solution was applied to a mica disc as previously described in Section 2.3.13.1. The DNA-antibody solution was left to attach to the mica for 5 min and then washed with HPLC-grade water. The edge of the mica was blotted with tissue to remove excess water and the mica was allowed to dry for 10 min. Once, dry, the DNA-antibody sample was imaged using an Asylum Research MFP-3D microscope in tapping mode with an Olympus AC240 V-shaped AFM cantilever (resonant frequency 72 kHz,

spring constant 2 N/m, imaged at a rate of 1 Hz with a free-air amplitude of 0.5 V and a damping amplitude of 0.3 V) and Argyle software. Integral and proportional gains were optimised empirically whilst scanning.

2.3.14. Chromatography and Mass Spectroscopy Method Development for Adduct Analysis

The development of a method of analysis of M_1G adducts in DNA samples by LC-MS-MS is detailed in this section. Initially a HPLC method was developed, followed by a MS method and finally fine-tuning of the LC-MS-MS method prior to sample analysis. Two HPLC columns with a guard cartridge were used for method development. A standard C18 - bonded silica 250 mm x 4.6 mm column for reverse phase HPLC (Column A) was used initially for detection and qualitative analysis of M_1G, followed by a 100 x 2.00 mm narrower column (Column B) for quantitative analysis.

2.3.14.1. High Performance Liquid Chromatography

A crude pyrimido[1,2-*a*]purin-10(*3H*)-one (M_1G) sample, made by reacting 100 mM MDA with 1 ml 6.6 mM guanine for 1 h in an incubator shaker, was used to develop a method of detection by HPLC and then optimized using a pure M_1G standard (Section 2.3.15) to give the greatest sensitivity for detection. Three different buffers were chosen that were volatile enough to also be used for MS (Table 5). Six HPLC methods were used in combination with the three buffer choices in Table 5, shown in Table 6.

Table 5. Mobile phases for each buffer choice for HPLC method development.

Buffer	Mobile Phase 1	Mobile Phase 2
A – Acetic Acid	0.1 % Acetic Acid in methanol	0.1 % Acetic Acid in Water
B – Formic Acid	0.1% Formic Acid in Methanol	0.1% Formic Acid in Water
C – Ammonium Formate	Methanol	50 mM Ammonium Formate (pH 5.4)

Table 6. HPLC methods for development of M_1G detection method.

Method	Time (min)	Mobile Phase 1 (%)	Mobile Phase 2 (%)
i	0	10	90
	20	90	10
	30	90	10
	32	10	90
	40	10	90
ii	0	100	0
	20	0	100
	25	0	100
	28	100	0
	40	100	0
iii	0	25	75
	20	25	75
iv	0	25	75
	20	25	75
	30	100	0
	31	25	75
	40	25	75
v	0	10	90
	20	10	90
	30	100	0
	31	10	90
	40	10	90
vi	0	20	80
	20	20	80
	30	100	0
	31	20	80
	40	20	80

HPLC methods were carried out on an Agilent HPLC separation module with PDA (signal 254 nm, reference 500 nm) and FLD (excitation 360 nm and emission 500 nm) detectors. The photomultiplier tube gain setting was set at the highest level of 18 using Agilent software. A needle wash using 100% methanol was used between draws. Two HPLC columns, A and B, were also used, the sample flow rates were 0.5 ml/min and 0.2 ml/min respectively. The column temperature was maintained at 25 °C and the sample volume was 20 µl for each sample. Three different flow rates were tested for the narrower HPLC column B: 0.1 ml/min, 0.15 ml/min and 0.2 ml/min to determine the optimum flow rate.

The different methods were tested using the following samples: 1 mg/ml guanine in 1 M HCl, 1 mg/ml adenine in 1 M HCl, both diluted to 1:10 and 1:100, and a pure M_1G standard (Section 2.3.15), diluted 1:10 to $1:10^6$ in mobile phase 2 to 200 µl in low volume HPLC vials. A M_1dG DNA standard with known concentration of M_1dG (21 pmol M_1dG/µg DNA, 3 mg/ml DNA) was hydrolysed as in Section 2.3.16 and was used to validate the HPLC method. Standard curves of pure M_1G standard (0 – 53.4 µM) versus peak area and guanine (0 – 66 µM) versus peak area were plotted to assess the purity of the M_1G standard.

The peak resolutions (R_s) of the guanine and M_1dG peaks of the M_1dG DNA standard for columns A and B were calculated and compared using the following equation, where retention time (t), peak width (w) and baseline resolution $R_s > 1.5$.

$$\mathrm{Rs} = \frac{1.18(\mathrm{t_B} - \mathrm{t_A})}{(\mathrm{W_{0.5A}} + \mathrm{W_{0.5B}})}$$

2.3.14.2. Liquid Chromatography – Mass Spectrometry

An Alliance LC-MS was used to develop a method for detection of M_1G adducts by MS. The same samples, columns and HPLC conditions were used as in Section 2.3.14.1., with the UV absorbance set at 260 nm. The same mobile phases were used as in Table 5, with HPLC Method (iii) from Table 6, plus an additional method shown in Table 7.

Table 7. LC method for development of M_1G detection method.

Time (min)	Mobile Phase 1 (%)	Mobile Phase 2 (%)
0	2	98
5	2	98
20	98	2
30	98	2
32	2	98
40	2	98

Direct infusion of the crude M_1G sample (Section 2.3.14.1) was used to determine the optimum cone voltage for detection of M_1G by MS. The MS was performed in positive ion (ES^+) mode with the lockspray removed, with a total ion current (TIC) scan of m/z 75 to m/z 190 and reconstructed ion chromatogram (RIC) of m/z 188. The column temperature was maintained at 25 °C. The cone voltage was set at 50 V. Guanine and the pure M_1G standard, diluted 1:100 in 50 mM ammonium formate (pH 5.4) buffer,

were analysed by LC-MS using the optimized MS conditions using method C(iii) (Section 2.3.14.1.) and column B.

2.3.14.3. Triple Quadrupole Mass Spectrometry

Based on the development of the HPLC and LC-MS methods, the optimum method was used to fine tune the HPLC and MS methods and begin method development for LC-MS-MS. The HPLC method used was C(iii) (Section 2.3.14.1.). Column B was used and this was maintained at 25 °C. The sample flow rate was 0.2 ml/min with sample injection volume 10 µl, and UV absorbance at 254 nm. Different run times were tested, from 8 min to 15 min. The final run time of 10 min was chosen, with a blank run in between each sample to remove any residual sample from the column.

Direct infusion of the pure M_1G standard was used to determine the optimum collision energy for analysis. Two MS-MS methods were used in conjunction: 1) a products of m/z 188 scan in ES^+ mode, scanning from m/z 75 to m/z 190, with 10 min data collection, 0.5 s scan time, 0.1 s inter-scan delay, 28 eV collision energy and 50 V cone voltage; 2) a MRM scan of 2 mass pairs, with 10 min data collection in ES^+ mode, as shown in Table 8.

Table 8. MRM parameters for MS-MS scan

Precursor m/z	Product m/z	Dwell (s)	Cone (V)	Collision Energy (eV)
188	79	0.05	50	28
188	106	0.05	50	28

A full scan was also set up in MS mode of m/z 145 to 300 in ES^+ mode, scan duration 0.5 s, inter-scan delay 0.1 s and cone voltage 50 V. The data was processed from the TICs produced by the products of m/z 188 scan and the full scan to give RICs and mass spectra.

The same samples were used as in Section 2.3.14.1 to test the parameters and develop the optimum method for M_1G detection by LC-MS-MS. Different flow rates were tested, including 0.1 ml/min, 0.125 ml/min, 0.15 ml/min, 0.175 ml/min and 0.2 ml/min. Flow rate 0.15 ml/min was chosen for sample analysis.

2.3.15. Preparation of Standards

2.3.15.1. Synthesis of Pyrimido[1,2-*a*]purin-10(*3H*)-one Standard

A procedure adapted from Singh *et al.* (2001) was used produce M_1G. A number of different conditions were tried in order to optimize the method to produce the greatest yield of M_1G crystals, including reaction of guanine with either MDA, as prepared in Section 2.3.1., or TMP directly and variations in the temperature used and length of reaction. The optimized method was as follows: 0.66 mmoles guanine was added to 10 ml 1M HCl in a conical flask and heated on a hot plate to dissolve. The solution was then cooled, but not lower than 40 °C as the guanine precipitated. Next, 3 equivalents of TMP (2 mmoles) were very slowly added to the reaction mix and the flask was covered in foil and allowed to react for 2 h at 40 °C in a shaker incubator.

The reaction mix was filtered using filter paper and the yellow M_1G crystals were then washed with 0.1 M HCl to remove any impurities. The crystals were then rinsed with

water and allowed to dry overnight in a fume hood covered with a funnel to prevent contamination. The crude M_1G crystals were collected and weighed.

2.3.15.2. Purification of Pyrimido[1,2-*a*]purin-10(*3H*)-one Standard

M_1G crystal solubility was found to be pH dependent, increasing in basic conditions. However, a neutral or slightly acidic solution was required in order to prevent hydrolytic ring-opening of the M_1G. Combinations of KOH with HCl and ammonia with formic acid were used to dissolve the M_1G crystals, with differing final pHs. These solutions were analysed by HPLC to identify the acid/alkali combination and pH that gave the largest peak for the ring-closed form of M_1G, which was formic acid/ammonia at pH 5.

To purify the M_1G crystals, 10.0 mg M_1G crystals were dissolved in 1 ml concentrated ammonia solution and then diluted 1:10 in water. The pH was adjusted with concentrated formic acid to approximately pH 5, using litmus paper to check pH.

A SPE cartridge was conditioned with 2 ml methanol followed by 2 ml 50 mM ammonium formate buffer (pH 5.4), taking care not to allow the column to dry out. All of the M_1G solution was added to the SPE cartridge and fractions of approximately 250 µl were collected, cooled immediately, labelled and frozen at -20°C. Next, 1 ml aliquots of the following were added to the SPE cartridge – 50 mM ammonium formate (pH 5.4) with an increasing % of methanol in 5 % increments from 0 – 100 %.

Fractions were analysed by HPLC using method C(iv) as detailed in Section 2.3.14.1, using column B. Fractions with M_1G peaks were identified, combined, and freeze-dried overnight. The freeze-dried crystals were then weighed.

The M_1G crystals were dissolved in 1 ml concentrated ammonia solution and then diluted 1:10 in water. The pH was adjusted with concentrated formic acid to approximately pH 5. The SPE was repeated as above for additional purification.

2.3.16. Treatment of DNA with Malondialdehyde

CT-DNA was dissolved in 0.1 M KH_2PO_4 buffer (1.35 g/l KH_2PO_4 in water) at 60 °C to 5 mg/ml. DNA from MRC5 (51.5 µg/ml) and MRC5 SV2 (86.0 µg/ml) cells untreated with MDA or H_2O_2 (negative controls), from Section 2.3.12.1., were treated post-DNA extraction as follows: A 100 mM stock solution of MDA was prepared as in Section 2.3.1. Aliquots of 100 µl DNA were reacted with MDA (0 – 50 mM) and H_2O_2 (100 µM), to give a final volume of 500 µl, in triplicate for 5 days in the dark at 37 °C in a shaker incubator. All DNA samples extracted from MRC5 and MRC5 SV2 cells treated with MDA and H_2O_2 in Section 2.3.12.1., the concentrations of which are shown in Table 9 (previously quantified by Nanodrop spectrophotometry (absorbance 260 nm)), were then precipitated and hydrolysed for LC-MS-MS analysis.

A 500 µl aliquot of the DNA sample (500 µg CT-DNA samples, 5.15 µg MRC5 and 8.6 µg MRC5 SV2 DNA samples treated post-extraction, and 1.75 µg MRC5 and 24.5 µg MRC5 SV2 DNA samples from treated cells) was added to 500 µl cold isopropanol and centrifuged for 10 min at 12,000 x g. The supernatant was removed and 500 µl cold 100% ethanol was added to wash the pellet and then centrifuged at 12,000 x g for 10 min. The supernatant was removed and 500 µl cold 70% ethanol was added to wash the pellet and then centrifuged for 10 min at 12,000 x g. The supernatant was removed and the pellet was re-suspended in 500 µl 0.1 M formic acid and then incubated for 1 h at 70 °C

in a water bath. The samples were then dried overnight at 40 °C in a centrifugal dryer. The dried DNA samples were then re-suspended in 100 µl 0.01 M formic acid and sonicated for 20 min to re-dissolve ready for analysis.

Table 9. DNA concentrations of MRC5 and MRC5 SV2 DNA from cells treated with MDA and H_2O_2 used for LC-MS-MS analysis.

MDA Treatment (µM)	DNA Concentration (µg/ml)	
	MRC 5	MRC 5 SV2
0	17.0	49.0
10	25.5	29.5
50	13.5	39.0
100	13.0	30.0
200	24.0	37.5
500	16.5	14.5
1000	20.0	47.0
50 H_2O_2	37.0	3.5
100 H_2O_2	12.0	4.5

2.3.17. DNA Adduct Analysis by Triple Quadrupole Mass Spectrometry

2.3.17.1. Analysis of Pyrimido[1,2-*a*]purin-10(*3H*)-one Standard

A series of M_1G standards was made using the purified M_1G crystals (Section 2.3.15.2.). 0.1 mg M_1G crystals were dissolved in 500 µl 50 mM ammonium formate buffer (pH 5.4), sonicated for 20 min and then made up to 1 ml with more buffer, to give a 0.1 mg/ml solution. The standard was diluted 1:10 – 1: 10^6 in buffer.

Standard curves of peak intensity versus M_1G concentration were prepared using the series of pure M_1G standards, for each of the products of m/z 188 ions and the MRM scan produced from analysis by LC-MS-MS using the method optimized in Section 2.3.14.3. The M_1dG DNA standard with a known concentration of adduct (21 pmol/µg DNA) was analysed by the same method and the standard curves were used to compare the amount M_1G detected for each product of m/z 188 ion and by the MRM scan with the known amount, to ascertain the accuracy of the method.

The limit of detection (LOD) and limit of quantification (LOQ) were determined using the calibration line method. A standard curve of peak intensity versus M_1G concentration was plotted for 1:1000 to 1:15000 dilutions of the pure M_1G standard, as prepared and analysed as above, for products of m/z 188 ions (m/z 79 and m/z 106) and the MRM scan. LOD was calculated using the following equation:

$$\text{LOD} = \frac{\text{Standard Error of Regression Line}}{\text{Gradient}} \times 3.3$$

The LOQ was calculated using the following equation:

$$\text{LOQ} = \frac{\text{Standard Error of Regression Line}}{\text{Gradient}} \times 10$$

Peak precision for the peak with the M_1G concentration closest to the LOQ was determined by calculating the % relative standard deviation (RSD), with good precision < 0.5%, as follows:

$$\%\ \text{RSD} = \frac{\text{SD}}{\text{Mean}} \times 100$$

To determine if guanine had an effect on the level of detection of M_1G adducts by LC-MS-MS, the 1:200 diluted M_1G standard was spiked with 10 µl, 20 µl, 50 µl and 100 µl 1 mg/ml solution of guanine and analysed by LC-MS-MS as previously. To determine whether the expected m/z was correct for each sample, a full scan of m/z 145 –300 was carried out on 0.1 mg/ml guanine, 0.1 mg/ml adenine, 1:10 and 1:100 dilutions of the M_1dG DNA standard (diluted as above) and the M_1G standards.

2.3.17.2. Analysis of DNA Samples

The hydrolysed CT-DNA and the MRC5 and MRC5 SV2 DNA samples treated post extraction with MDA and H_2O_2 (Section 2.3.16) and the MRC5 and MRC5 SV2 cell samples (Section 2.3.12.1) were each transferred into low volume HPLC vials and freeze dried overnight. The samples were then each dissolved in 100 µl 50 mM ammonium formate buffer (pH 5.4) in the low volume vials and then analysed by LC-MS-MS using the method developed in Section 2.3.14.3 for both the products of m/z 188 and the MRM scans.

CHAPTER 3

CELLULAR EFFECTS OF MALONDIALDEHYDE

The purpose of this chapter is to present the results from a number of assays where the effects of MDA are shown at the cellular level using an *in vitro* model. The MDA standards used in the assays were checked by the TBARS assay and HPLC with DNP derivatisation prior to treatment of MRC5 and MRC5 SV2 cells. Components in FBS (a widely used serum-supplement in *in vitro* cell culture of eukaryotic cells) have been found to interact with MDA (Rittie *et al.*, 2002). As FBS contains growth supplements that cells require for proliferation, the effect of omitting FBS from the cell media was examined in order to determine whether this would have an effect on the assays utilized in this research. The effects of MDA on cell viability, cellular morphology, nuclear morphology, apoptosis and p53 protein expression are presented here.

In all assays involving MRC5 and MRC5 SV2 cells, cells were initially grown in complete media and subsequently treated with MDA (0 – 1000 µM), or untreated as a negative control, in FBS-free media for 24 and 48 h, unless otherwise stated. H_2O_2 (0-100 µM), known to induce oxidative stress at sub-lethal doses, was used as the positive control to verify that the effects observed were due to the effect of MDA on the cells (Caldini *et al.*, 1998), the data for which is not always shown. Where confocal microscopy was used,

the detector gain was kept constant to show that differences in fluorescent intensity was due to the experimental rather than instrumental parameters.

3.1. Verification of Malondialdehyde Concentrations

MDA was synthesised by acid hydrolysis of TMP, as shown in Scheme 10.

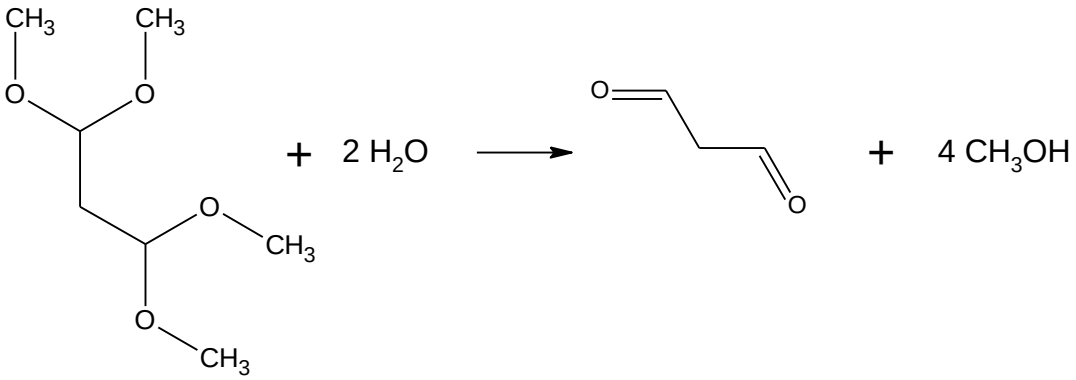

Scheme 10. Hydrolysis of TMP to form MDA

A TBARS assay to confirm the MDA concentration of MDA standards was carried out. This was then verified by reacting MDA with an acidified solution of DNP (Brady's reagent) to form MDA-DNP derivatives, which were then analysed by HPLC. In order to determine the concentration of MDA present in solutions, a TBARS assay of MDA standards (Section 2.3.2.) was carried out (Figure 9). The linear regression had a R^2 value close to 1 indicating good linearity, however, above 1000 µM the linear regression lost linearity, indicating the upper limit of detection of MDA by this assay.

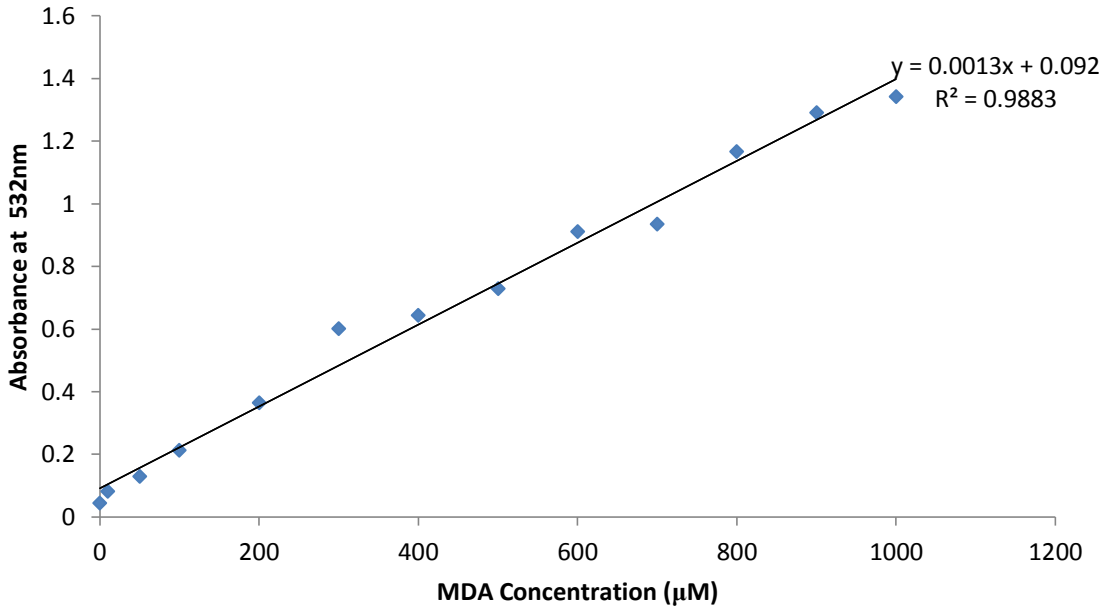

Figure 9. Standard curve of 0-1000 µM MDA measured using a TBARS assay, absorbance measured at 532nm.

The concentrations of MDA standards were verified by DNP derivatisation and HPLC (Section 2.3.3.), the derivatisation reaction is shown in Scheme 11.

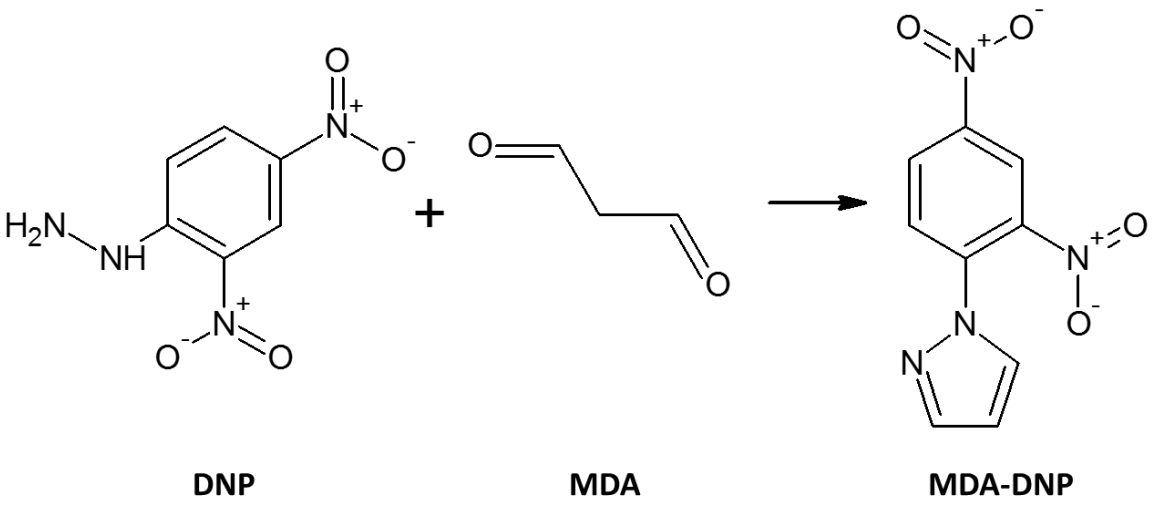

Scheme 11. DNP derivitisation of MDA to form 1-(2,4-dinitrophenyl)pyrazole (MDA-DNP) (adapted from Ekstrom *et al.* (1988)).

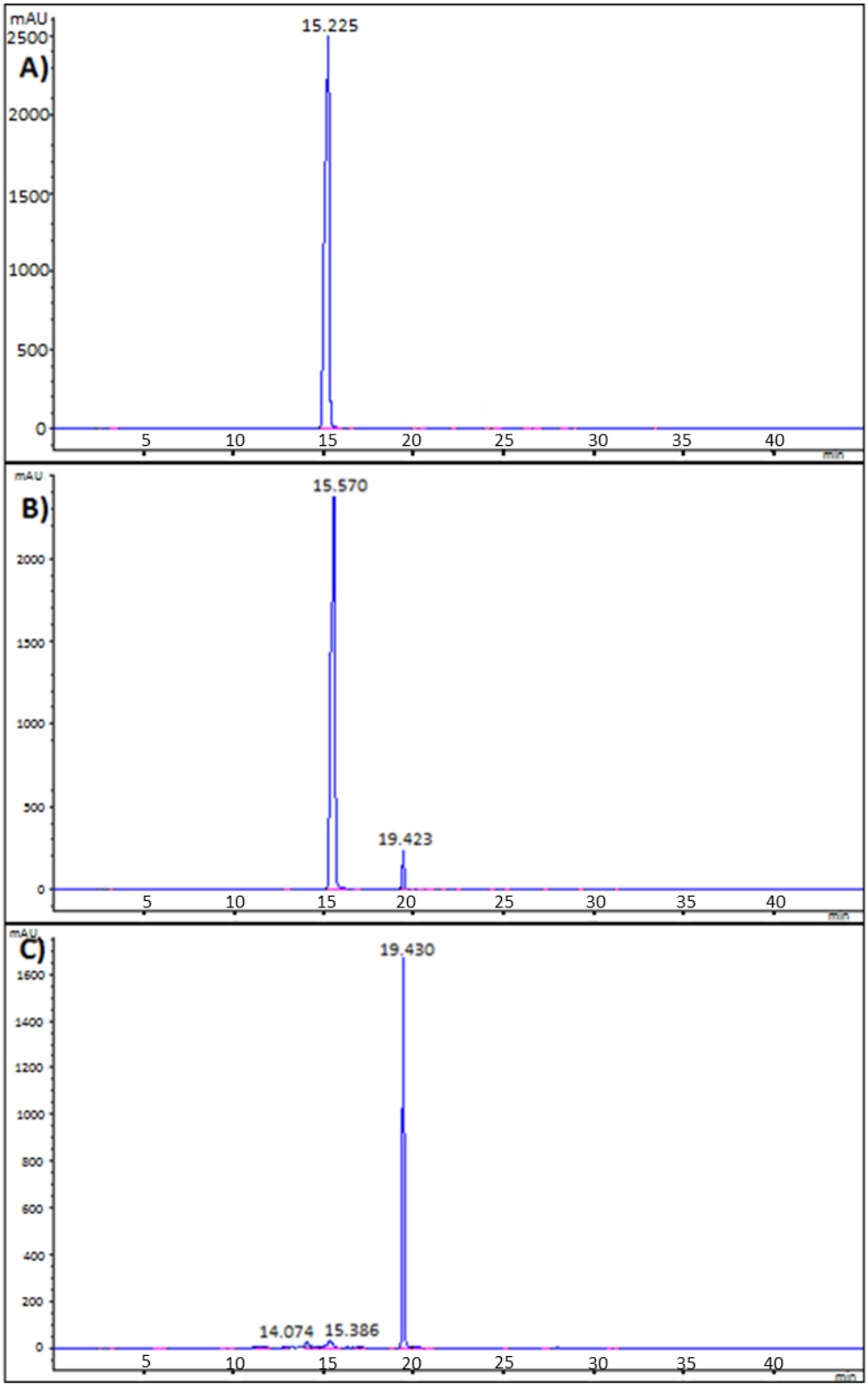

Figure 10. HPLC chromatograms of MDA analysis using derivatisation with Brady's reagent: A) blank showing the peak for Brady's reagent at 15.255 min; B) 1 mM MDA showing an additional peak at 19.423 min for the MDA-DNP derivative; C) 10 mM MDA showing only the MDA-DNP peak at 19.430 min.

The HPLC chromatograms are shown in Figure 10, where for 0 mM MDA the single peak represents Brady's reagent and at 1 mM MDA shows an additional peak that represents the MDA-DNP derivative (19.4 min). At 10 mM MDA, the Brady's reagent peak is present as a very small peak, however, the MDA-DNP peak is present (19.4 min) as a large peak, indicating that the MDA concentrations were at the upper limit for this assay, as above 10 mM the Brady's reagent is saturated and there is little further increase in peak area. This can also be seen in the calibration curve, as shown in Figure 11. The calibration curve had good linearity with a R^2 value close to 1. However, the calibration curve loses linearity above 8 mM MDA, where the R^2 value decreases indicating the upper limit of the assay due to Brady's reagent saturation. Analysis of MDA by HPLC with DNP derivatisation allows for a wider range of MDA concentrations to be analysed, up to 8 mM MDA, compared to 900 µM MDA by TBARS assay, with improved sensitivity and selectivity.

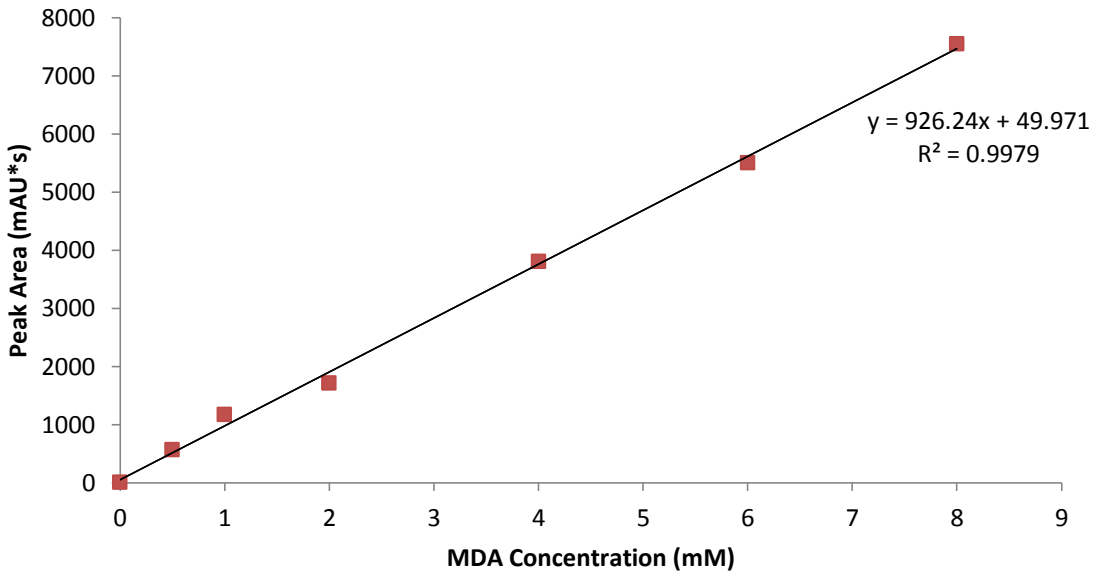

Figure 11. Standard curve of 0-8 mM MDA by DNP-derivatisation, analysed by HPLC at 350 nm.

A possible small peak at retention time 14.1 min at 10 mM MDA was observed in Figure 10. However, concentrations at this level were not used for treatment of cells. Most importantly, as the aim of this work was to ensure that the product of TMP hydrolysis was MDA, no other peaks were observed at any of the lower MDA concentrations analysed indicating that the only aldehyde that results from TMP hydrolysis is MDA. It has been suggested that MDA may polymerise at high concentrations, and in older solutions (Gutteridge *et al.*, 1977; Janero, 1990). However, as the concentration range of MDA (0 – 1000 μM) used for treatment of MRC5 and MRC5 SV2 cells and subsequent assays in this chapter was relatively low, it is unlikely that polymerisation of MDA would occur at these concentrations.

The TBARS assay had lower specificity and overestimated the MDA content compared to HPLC detection of the same MDA-TBA samples (Lykkesfeldt, 2001). Interfering chromagens are mostly eliminated by measurement of MDA-TBA by high performance liquid chromatography (HPLC). However the red product can stain the HPLC equipment and HPLC is less practical as it is less readily available as an analytical technique than TBARS (Badcock *et al.*, 1997). The traditional MDA-TBA spectrophotometric assay was compared to detection of MDA-TBA and MDA-DNP by HPLC in fish, which has high levels of PUFA and therefore highly susceptible to lipid peroxidation. The MDA-DNP method gave the greater accuracy and specificity than the MDA-TBA methods, however it had a relatively high limit of detection and lower reproducibility at lower MDA concentrations (Mendes *et al.*, 2009).

The TBARS test has low specificity for MDA as other lipid peroxidation products are also TBA positive e.g. monofunctional aldehydes, it is therefore considered to be a general indicator of lipid peroxidation rather than a specific test for MDA (Janero, 1990). Different analytical techniques for the quantification of MDA were compared (Fenaille *et al.*, 2001). MDA derivatisation with TBA, using both visible spectrophotometry and HPLC led to an overestimate of MDA content due to the elevation of temperature required which may have catalysed artefactual MDA formation. The DNP derivative of MDA measured by HPLC-UV and the phenylhydrazone derivative of MDA, measured by GC-MS gave lower MDA levels. However, the TBARS test is widely used as it is simple and can be a useful tool for MDA detection if further methods of verification are used, such as DNP derivatisation. The HPLC analysis verified that a single aldehyde was formed from TMP hydrolysis, and that quantitative hydrolysis occurred to give the required concentration of MDA for treatment of cells.

3.2. Effect of Foetal Bovine Serum and Malondialdehyde on Cell Growth and Viability

Mammalian cells, used in *in vitro* studies, are cultured in basic media which contains a number of different nutrients. The media can be supplemented according to the growth requirements of a particular cell line. Amino acids, antibiotics and FBS are examples of media supplements. Although FBS is ill-defined, it provides nutrients, macromolecular proteins and other compounds necessary for cell growth, such as hormones. It can also act as a buffer for the culture medium and it contains a high content of embryonic

growth factors. It possesses these properties as it is harvested from foetuses. Cell proliferation and growth of the foetus requires specific growth factors and nutrients which are present in the serum. Cells from solid tissues e.g. fibroblasts and epithelial cells are adherent and require a surface for the cells to attach and proliferate, whereas other cells can grow in suspension e.g. blood cells. Adherent cells need to be detached from the surface of their container when they reach a particular level of confluence (depending on the requirements of the particular cell line) and subcultured/passaged. The adhesion mechanisms of the cell are Ca^{2+} dependent and the enzyme trypsin is used (often with chelating agent EDTA) to digest the proteins from the cell surface that allow adhesion (Butler, 2004). MRC5 and MRC5 SV2 are adherent cell lines and hence growth in FBS-free media needed to be investigated to ensure adequate growth.

To characterize cell proliferation and viability, the two cell lines were grown in both complete media and FBS-free media under standard conditions, as described in Section 2.3.5. Cell proliferation was measured by viable cell count. MRC5 cells were observed to grow more slowly ($k = 0.052\ h^{-1}$) than their transformed counterpart MRC5 SV2 ($k = 0.072\ h^{-1}$) in complete media and the growth rate decreases for both cell lines when grown without FBS ($k = 0.044\ h^{-1}$ MRC5 and $0.052\ h^{-1}$ MRC5 SV2 respectively), as seen in Figure 12.

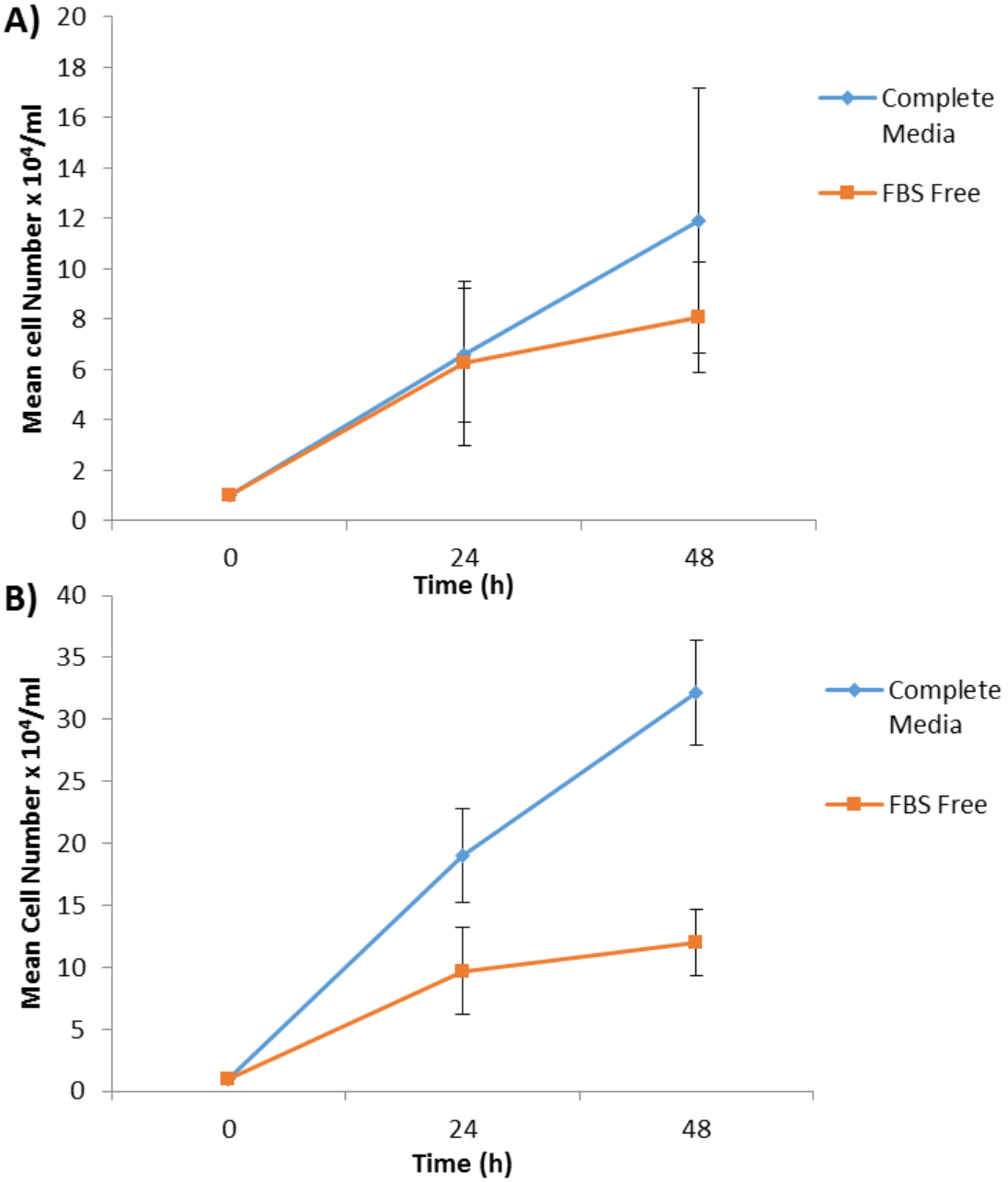

Figure 12. Growth of A) MRC5 and B) MRC5 SV2 mean cell number versus time, in complete and FBS-free media, error bars indicate ± 1SD from the mean (number of replicates n = 3).

The mean cell number of MRC5 and MRC5 SV2 cells were compared at each time point when grown with and without FBS by Student's t-test, as shown in Table 10. A significant difference was observed between cells grown with and without FBS over time, apart

from MRC5 cells after 24 h. This experiment was repeated in triplicate, giving consistent, repeatable results.

Table 10. Statistical analysis of the mean cell number of MRC5 and MRC5 SV2 cells grown in complete versus FBS free media for 24 and 48 h, by Student's t-test: P values for significance (*).

P Values for Complete vs FBS Free Media	
MRC5 24 h	0.801
MRC5 48 h	1.2×10^{-4} *
MRC5 SV2 24 h	0.041 *
MRC5 SV2 48 h	1.71×10^{-8} *

These results indicate that FBS is an important growth supplement for the proliferation of both cell lines and without FBS, and taking the large error bars in Figure 12 into account, it appears that cells were no longer proliferating at 48 h. However, cells were found to be sufficiently viable up to 48 h without FBS present in the media, indicating that FBS-free media would be suitable for further assays.

To compare the effects of MDA on cell viability, both cell lines were treated with MDA (0-1000 µM). Cell viability was measure by viable cell count and the cell number was normalised to the respective negative controls. Figure 13 shows that after 24 h treatment, there was an increase in cell viability for both MRC5 and MRC5 SV2 cells when treated with 10 µM MDA compared with the negative control. Cell viability then

decreased to a greater extent for MRC5 SV2 cells than MRC5 cells when treated with 100 µM MDA and 1000 µM.

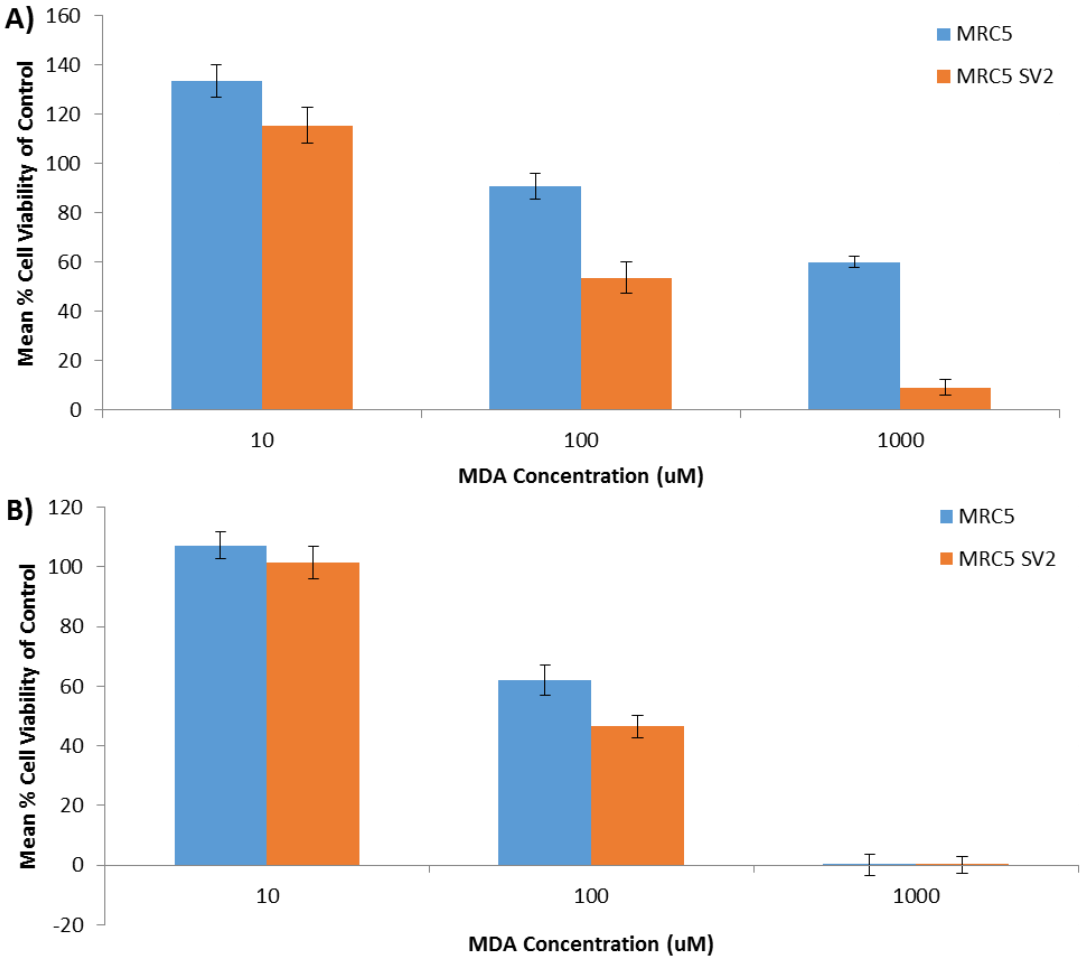

Figure 13. Viability of MRC5 and MRC5 SV2 cell lines following treatment with MDA (0-1000 µM) for A) 24 h and B) 48 h (1000 µM MDA > 0.5% in B), normalised to the negative control, error bars indicate ± 1SD from the mean (n = 12).

The mean cell number of MRC5 and MRC5 SV2 cells were compared with each other at each MDA concentration (0-1000 µM) and each time point by Student's t-test, as show in Table 11. Significant differences were observed at 24 h between the negative controls and when treated with 1000 µM MDA, which confirms the differences in growth between the two cell lines.

Table 11. Comparison of the mean cell numbers of MRC5 and MRC5 SV2 cells treated with MDA (0-1000 µM) by Student's t-test: P values for significance (*).

MDA Concentration (µM)	24 h	48 h
0	0.024 *	2.17×10^{-5} *
10	0.107	0.006 *
100	0.231	0.401
1000	0.001 *	n/a

After 48 h treatment with 10 µM MDA, cell viability remained slightly higher than the negative control for MRC5 and MRC5 SV2 cells, and these values were lower than their respective values following 24 h treatment. When treated with 100 µM MDA for 48 h, cell viability for both cell lines was reduced compared with 10 µM MDA and the negative control, but also with 100 µM MDA for 24 h. No viable cells remained following treatment with 1000 µM MDA for 48 h. Significant differences in mean cell number between the two cell lines were observed at 48 h between the negative controls and when treated with 10 µM MDA (Table 11). This experiment was repeated in triplicate, giving consistent, repeatable results.

The growth rate of MRC5 cells was found to be slower than the growth rate of MRC5 SV2 cells, both with and without FBS, and the growth rate of both cell lines is reduced in FBS-free media. Although the removal of FBS from the media reduced the growth rate of both cell lines, cells were still found to be viable up to 48 h, hence a maximum of 48 h

treatment times were used throughout this study. FBS-free media was used for treatment of cells with MDA as MDA is known to bind to bovine serum albumin (BSA) (Takagi *et al.*, 2005) *in vivo,* a major component of FBS (Rittie *et al.*, 2002). The formation of MDA-BSA adducts would effectively reduce the dose of MDA in the treatment solution, and therefore the MDA concentration would not be known, thus FBS-free media was used throughout the study.

The viability of both cell lines were compared when treated with different concentrations of MDA (Figure 13). Treatment with a relatively low MDA concentration (10 µM) appeared to induce (or failed to inhibit) the growth in both cell lines compared to the negative control (cells grown in FBS-free media). The same trend has been observed with other cell lines treated with different chemicals, for example, in LL24 human lung fibroblast cells treated with relatively low concentrations of benzene, enhanced cell proliferation was observed (Giuliano *et al.*, 2009) and it was suggested that treatment with relatively low doses caused a defect in cell cycle control, allowing cell proliferation. Increased cell proliferation was observed in MRC5 cells and A549 human adenocarcinoma cells treated with relatively low doses of the cigarette smoke products, pyrazine, 2-ethlpyridine and 3-ethylpyridine, whereas higher doses were inhibitory (Liu *et al.*, 2015).

At higher MDA concentrations (100-1000 µM), the cell viability of both cell lines gradually decreased to zero after 48 h incubation, suggesting that higher MDA concentrations have an adverse effect on cell viability, which was also observed by (Giuliano *et al.*, 2009), although in different cell lines.

Cells were counted using a dye-exclusion assay, involving the exclusion of trypan blue from healthy cells due to maintenance of the integrity of the cell membrane, thus staining only dead, non-viable cells. Cells in late apoptosis and early necrosis exhibit a loss of membrane integrity and are able to take up trypan blue. In contrast, cells with intact membranes exclude trypan blue and are therefore not stained blue. Cells with intact and disrupted membranes can therefore be distinguished and excluded from the cell count, although cells in early apoptosis will still have some membrane integrity and also exclude trypan blue (Siddique *et al.*, 2009). Therefore the cells counted as healthy and viable in these assays may be greater than expected due to early apoptotic cells being counted as well as viable cells, although the cell counts are relative to each other as the same procedure was used for each cell line and MDA treatment.

3.3. Cell Viability using a MTT Assay

The colormetric MTT assay is used as a measure of metabolic activity of a cell population. The assay was developed to measure cell proliferation, cell activation and cytotoxicity rapidly, precisely and without the use of radioisotopes (Mosmann, 1983). The principle behind the MTT assay is to add a substrate to a cell culture which is metabolised by living cells to produce a different coloured product which can be quantified by spectrophotometry. Any dead cells and the medium in which the cells are growing do not account for any change in colour/absorbance as they do not process the substrate. MTT is a tetrazolium salt which has a tetrazolium ring. Active mitochondria (i.e. living cells) cleave the ring producing the coloured product. The formation of the coloured product is therefore directly related to mitochondrial activity and can be used to

measure cell viability. MTT is yellow in colour and is reduced by mitochondria to give a purple product, a formazan. The reaction is shown in Scheme 12.

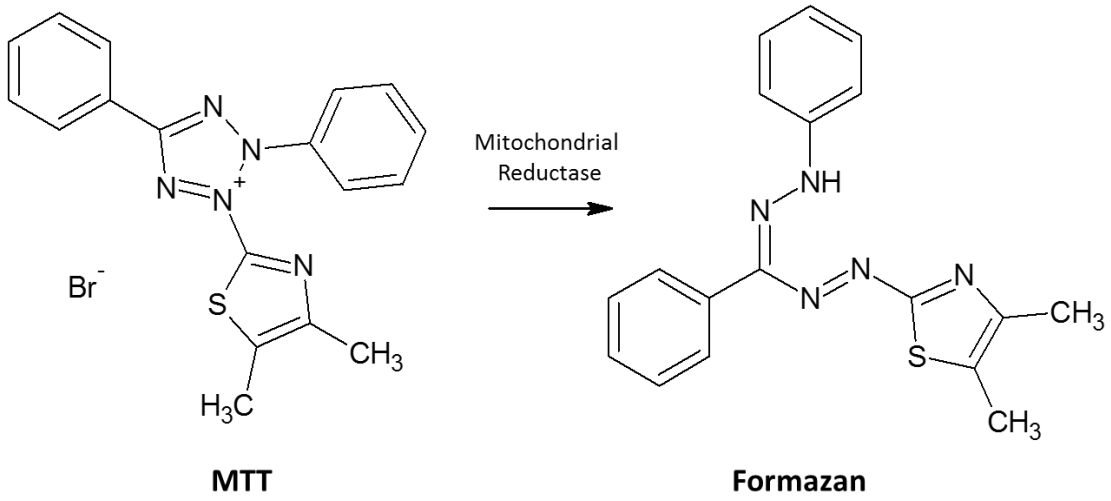

MTT **Formazan**

Scheme 12. The reaction of MTT to the purple formazan product, catalysed by mitochondrial reductase.

The mitochondrial reductase enzyme that converts the MTT to the formazan product is only active in active mitochondria. Suitable solvents, such as DMSO, are used to solubilise the insoluble formazan into a coloured solution whose absorbance is quantified using spectrophotometry (Mosmann, 1983).

The effect of MDA (0-1000 µM), and positive control H_2O_2 (0-100 µM), on the viability of MRC5 and MRC5 SV2 cells was assessed by MTT assay and the mean percentage cell viability calculated and normalised to the negative control (Section 2.3.6.). Only data for 0-450 µM MDA was recorded as above this concentration range the cell viability was very low and results were inconsistent, perhaps due to decreased cell numbers and assay sensitivity. Figure 14 shows the mean percentage viability of MRC5 and MRC5 SV2 cells treated with MDA for 24 and 48 h. After 24 h, the viability of MRC5 cells increases

when treated with 25 µM MDA and then decreases with increasing MDA concentration, although viability appears to increase when treated with 400 µM and 450 µM MDA. The viability decreases further after treatment with MDA for 48 h, compared with the respective treatments after 24 h, although there was some fluctuation in the percentage viability of cells treated with 100 µM to 450 µM MDA rather than a gradual decrease in viability. After 24 h, the viability of MRC5 SV2 cells increased when treated with 25 µM MDA and then remained at approximately 100% (the same as for the untreated cells to which the data were normalised) for 50-100 µM MDA but then decreased gradually. After 48 h, the viability of MRC5 SV2 cells decreased much more steeply than for 24 h, although there was still an increase in viability following treatment with 25 µM MDA, however, this was lower than after 24 h. Treatment of both cell lines with the positive control (H_2O_2) also showed a similar dose dependent decrease in cell viability, but to a greater extent than MDA (data not shown).

The percentage viability of MRC5 and MRC5 SV2 cells were compared with one another for each MDA concentration (0-450 µM) at each time point by Student's t-test, P values are shown in Table 12. For 24 h, the viability of the two cell lines were significantly different for each concentration of MDA. After 48 h, there was a significant difference in the viability of the two cell lines for each MDA concentration apart from 350 µM MDA. These assays were repeated (n = 4) giving consistent results.

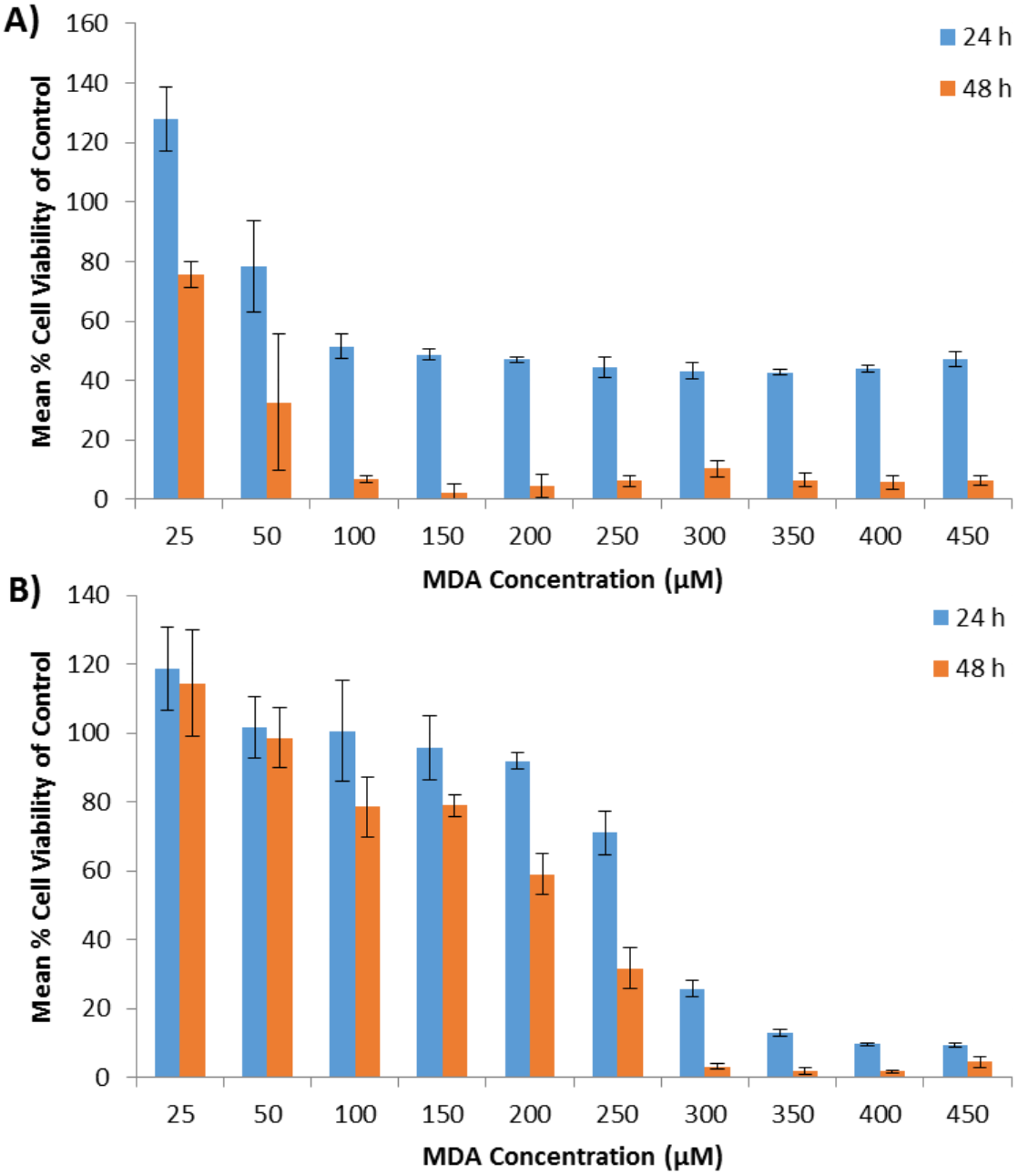

Figure 14. Viability of A) MRC5 and B) MRC5 SV2 cells treated with MDA (0-450 µM) over 24-48 h, normalised to the negative control, error bars indicate ± 1SD from the mean.

Table 12. Comparison of the viability of MRC5 and MRC5 SV2 cells treated with 0-450 µM MDA by Student's t-test: P values for significance (*)

MDA Concentration (µM)	24 h	48 h
25	0.0028 *	0.0133 *
50	0.00020 *	0.00022 *
100	0.00098 *	0.00040 *
150	0.00029 *	0.00020 *
200	0.00001 *	0.00025 *
250	0.00021 *	0.00196 *
300	0.00034 *	0.00682 *
350	0.00072 *	0.08172
400	0.00015 *	0.01439 *
450	0.00017 *	0.01628 *

MDA appeared to have less of an effect on MRC5 SV2 cells than MRC5 cells at concentrations below 250 µM MDA. In general, the viability decreased after 24 h and then decreased further after 48 h for both cell lines, but to a greater extent with MRC5 cells. When treated with 25 µM MDA, the viability of both cell lines did not follow the trend and increased to greater than the viability of the untreated controls to which the data was normalised. At higher MDA concentrations (50-450 µM), the profile of cell viability of MRC5 was very different to that of the MRC5 SV2 cells. The viability of MRC5 cells decreased after 24 h for all concentrations, and decreased further after 48 h. The viability of MRC5 SV2 cells decreased to a much lesser extent than for MRC5 cells after

both time periods for concentrations up to 300 µM MDA, but to a greater extent than MRC5 after 24 h, above 300 µM MDA.

When compared to the initial cell viability assay in Section 3.2., where a viable cell count was used to assess viability in response to MDA treatment, the cell viability of both cell lines was generally lower when assessed by the MTT assay. This was due to the inclusion of all cells with an intact cell membrane which may or may not have been viable using the viable cell count, whereas the MTT assay measures mitochondrial activity as a measure of viability.

H_2O_2 is often chosen as a positive control in cell toxicity assays as it is known to induce cytotoxic effects and DNA damage and induce oxidative stress at sub-lethal doses (Caldini *et al*., 1998). It is an intermediate molecule formed from dismutation of superoxide anions by superoxide dismutase. The positive control in this assay (H_2O_2) had a greater effect on both cell lines than MDA, with cell viability decreasing with increasing H_2O_2 concentration (0-100 µM). This effect was also seen in rat cortical neurons, where treatment with MDA and H_2O_2 produced a significant dose dependent decrease in cell viability using the MTT assay. The effect of H_2O_2 was more severe than MDA, suggesting that they have different damaging effects on the cell (Cheng *et al.*, 2011).

MRC5 cells, which have an intact p53 response, appear to be more susceptible to MDA than their transformed counterpart, MRC5 SV2 cells, which have a sequestered p53 response (Huschtscha and Holliday, 1983). The *TP53* gene acts in response to DNA damage by triggering apoptosis and cellular senescence. Lack of p53 response in MRC5 SV2 cells may allow cells with DNA damage, which would normally apoptose, to continue

to proliferate. MRC5 SV2 cells appear to be less sensitive to MDA than MRC5 cells, perhaps due to the altered p53 response of MRC5 SV2 cells, e.g. allowing cells to continue to be metabolically active despite DNA damage which would normally trigger apoptosis. Other non-transformed human cell lines have been shown to respond to MDA in a similar manner to MRC5 cells. The effects of MDA on human bone marrow mesenchymal stem cells was assessed by flow cytometry and MTT assay (Guolin *et al.*, 2006) and it was found that increasing concentrations of MDA (up to 1 mM) decreased the cell count, increased the population doubling time, decreased cell viability and triggered apoptosis. The flow cytometry also revealed that the percentage of cells in the G_2/M and S phases of mitosis increased with increased MDA concentration, suggesting MDA may trigger cell proliferation during oxidative stress, even though the rate of apoptosis also increased. As discussed in Section 3.2, enhanced proliferation was observed in cells subjected to low doses of chemical (Giuliano *et al.*, 2009; Liu *et al.*, 2015). This hermetic dose response, with contradictory low dose stimulation but high dose inhibition was described when levels of ROS, lipid peroxidation, heat shock proteins and glutathione peroxidase (the latter two being indicators of damage response) were measured in human embryo lung fibroblasts following treatment with sodium arsenite (Yang *et al.*, 2007). Cell proliferation was induced in response to low doses without cytotoxicity, but was inhibited at high doses, along with increased ROS, lipid peroxidation and cellular damage. This induction of cellular proliferation was also observed in the MTT assay (25 μM MDA) for both MRC5 and MRC5 SV2 cells, the viability increased in the initial 24 h of treatment with MDA, although this may also be due to cell proliferation before the MDA has had time to act.

The MTT assay relies on the mitochondrial reductase enzyme to catalyse the production of the formazan product, however, the enzyme may be altered by the test compound which may result in false negative or positive results, although this would depend upon the mechanism by which the test compound acts. A combination of assays, including microscopy to observe cell morphology, is therefore required to confirm the effect of the test compound on the cell (Hamid *et al.*, 2004).

3.4. *In vitro* Imaging of Cells

MRC5 and MRC5 SV2 cells are morphologically different from one another, MRC5 cells appear more elongated with finger-like projections, typical of fibroblast cells (Alberts *et al.*, 2002), whereas MRC5 SV2 cells are smaller and more rounded, typical of epithelial cells, as shown in Figure 15 and Figure 16, which may be due to their differing p53 responses.

Both cell lines were imaged using an inverted optical microscope to assess the effect of treatment with MDA and H_2O_2 on cell morphology, as described in Section 2.3.7. MRC5 cells treated for 24 h and 48 h are shown in Figure 15. MRC5 SV2 cells treated for 24 h and 48 h are shown in Figure 16. Overall, MRC5 cells appeared to be fibroblastic with multiple filopodia compared to the MRC5 SV2 cells, which appeared to display an epithelial morphology, as expected. As previously observed in Section 3.2, MRC5 SV2 cells grow more densely than their MRC5 counterparts, which can also be seen in Figure 15 and Figure 16. As the concentration of MDA increased, the number of cells decreased for both cell lines, which was also observed in Section 3.2. There was a noticeable

decrease in cell density between the positive control (50 μM H_2O_2) and negative control (no treatment) for both cell lines and both time periods.

It can be seen from Figure 15 and Figure 16 that when treated with MDA, both cell lines started to detach from their substrate (as indicated by dark/light round structures in the images). Cell detachment appeared to increase with increasing MDA concentration and exposure time, indicating loss of cell viability as previously observed in Sections 3.2 and 3.3. Similar results were observed when cells were treated with H_2O_2 (positive control). The images shown in Figure 15 and Figure 16 are representative of a number of images (n = 6) taken for each cell line and treatment, the observations were thus repeatable.

MRC5 SV2 cells have a sequestered p53 response, due to transformation of the wild type cells, MRC5, with the SV40 virus (Huschtscha and Holliday, 1983). It has not been documented as to why there is a difference in cell size and shape between the two cell lines, however, it may be assumed that the differences in morphology are due to the sequestration of p53 in MRC5 SV2 cells compared to the wild type p53 in MRC5 cells. A possible explanation for the difference may be the effect sequestration of the p53 protein has on the cytoskeleton.

The cytoskeleton is a network of protein fibres including microfilaments (actin), microtubules and intermediate filaments, that, along with cell surface receptors and the extracellular matrix, determine the morphology of the cell. Contractile stress fibres are the main actin-containing cytoskeletal structures, and give the cell tension and shape. Microtubules are involved in cell-substrate adhesion and aid cell elongation and filopodia maintenance. Intermediate filaments provide the main structure for overall

cell shape (Mermelstein *et al.*, 2003; Lazaro-Dieguez and Egea, 2007). The *TP53* gene coordinates many cellular responses and with regards to the cytoskeleton, actin regulators *RhoC* (which is involved in rearrangement of the actin cytoskeleton) and *LIM kinase 2* (which inactivates filamentous actin) have been found to be direct *TP53* target genes. Treatment of cells expressing wild type p53 with cisplatin led to an increase in RhoC and Lim kinase 2 expression, but not in cells expressing mutant p53 (Croft *et al.*, 2011).

The morphology of the cell may be affected by treatment with carcinogenic and mutagenic compounds. Actin poisons, e.g. phalloidin, have been shown to have an effect on the cytoskeleton organisation and thus the shape of the cell (Lazaro-Dieguez and Egea, 2007). MRC5 cells treated with cigarette smoke compounds exhibited altered cell morphology with increased cell rounding, shape irregularity in a dose dependent manner (Liu *et al.*, 2015), as also observed here. The carbonyl group of MDA has been found to react with nucleophilic groups of proteins, such as cysteine, lysine, arginine and histidine residues, to form protein adducts (Pamplona, 2011). MDA is known to modify β-actin, γ-actin, α-tubulin and β-tubulin (Zarkovic *et al.*, 2013), which are involved in the maintenance and integrity of the cytoskeleton and thus cell morphology.

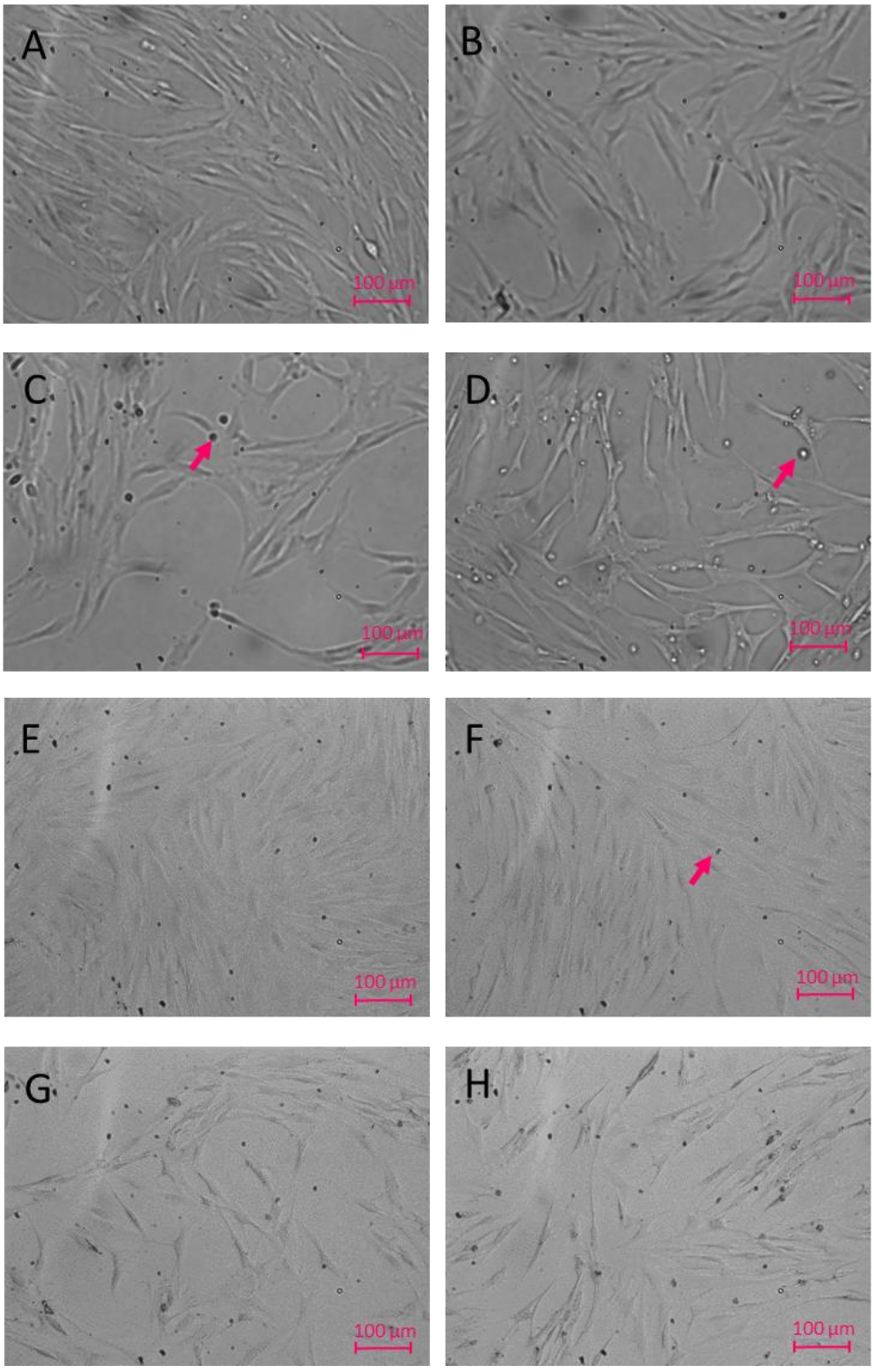

Figure 15. Light microscope images of MRC5 cells following treatment for 24 h (A-D) and 48 h (E-H) with MDA: A & E) 0 µM MDA; B & F) 100 µM MDA; C & G) 1000 µM MDA and D & H) 50 µM H_2O_2. Arrows indicate cell detachment as light/dark round structures. Magnification x20, n=6, all images are representative of each sample.

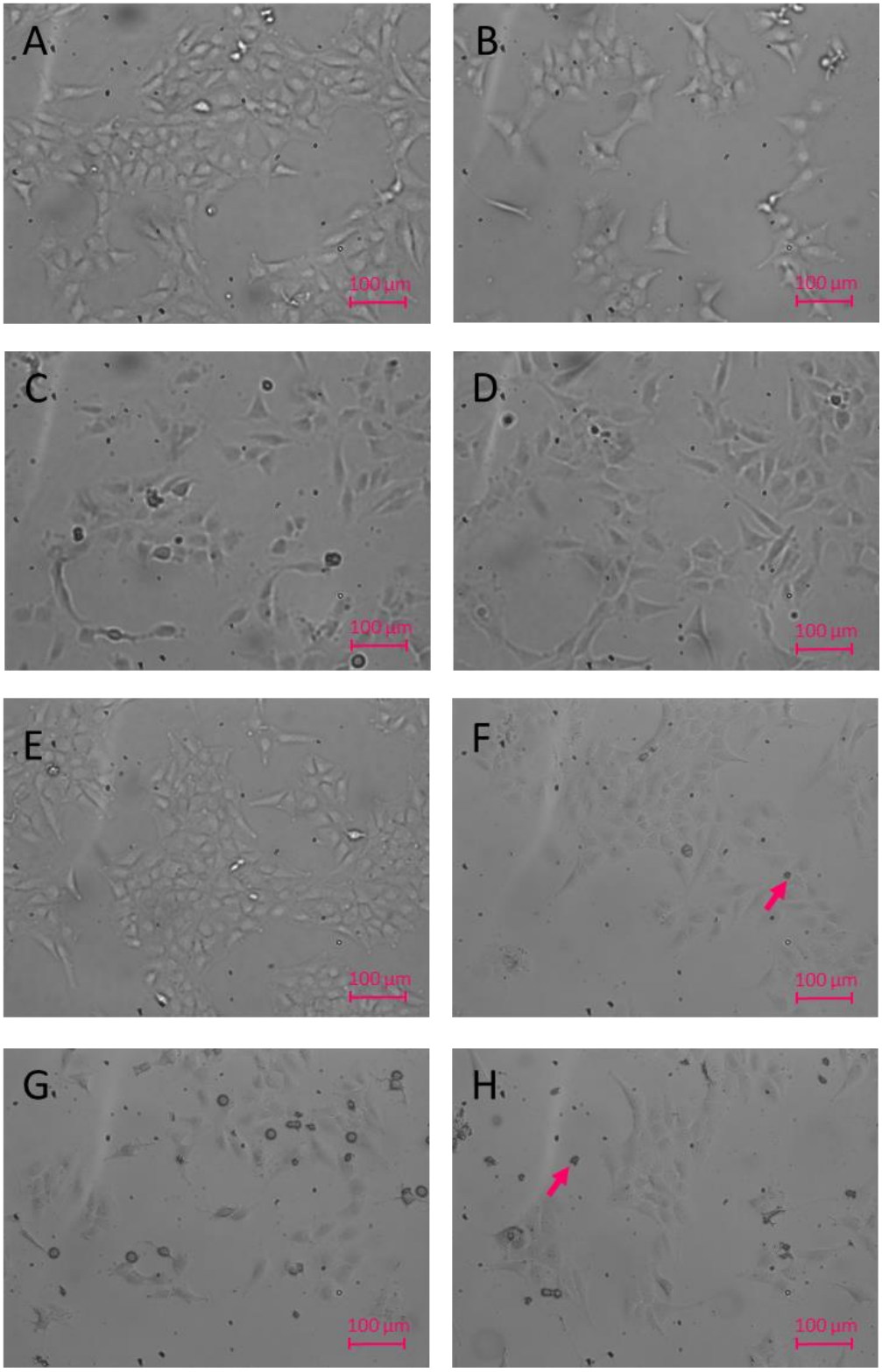

Figure 16. Light microscope images of MRC5 SV2 cells following treatment for 24 h (A-D) and 48 h (E-H) with MDA: A & E) 0 µM MDA; B & F) 100 µM MDA; C & G) 1000 µM MDA and D & H) 50 µM H_2O_2. Arrows indicate cell detachment as light/dark round structures. Magnification x20, n=6, all images are representative of each sample.

Whilst inverted light microscopy allowed imaging of live cells *in vitro*, without using fixation techniques which may alter the cellular conformation, the low magnification of the light microscope limits the amount of information obtainable from these images. The morphological differences between the two cell lines have been shown, but other than reduction in cell density and an increase in cell detachment, no other changes could be detected, hence the requirement to use more advanced imaging techniques to investigate the effects of MDA on MRC5 and MRC5 SV2 cells.

3.5. Cell Surface Morphology by Atomic Force Microscopy

AFM imaging of the cell surface was used at it allows much more cellular surface detail to be shown compared with the light microscope. Firstly, the magnification and resolution are much greater than the light microscope. Secondly, the AFM tip also scans the surface of the cell enabling the morphology of the cell surface to be mapped.

Following treatment with MDA for 24 h, the cells were fixed in glutaraldehyde, air-dried and then imaged by AFM to look for differences in cell surface morphology, as described in Section 2.3.13.1. Only images of cells treated with 0-200 µM MDA and after 24 h were captured due to the reduced cell density observed at higher MDA concentrations making AFM imaging difficult, as cells were harder to locate. All images shown are representative of a number of images (n = 10) taken for each cell line and treatment. MRC5 and MRC5 SV2 cells treated with MDA are shown in Figure 17. Untreated MRC5 and MRC5 SV2 cells both appeared to have a smoother, more rounded surface, with defined boundaries. AFM images of MRC5 and MRC5 SV2 cells treated with MDA show

increasing irregularity of the cell morphology and the cell surfaces seemed to become more 'pitted' with increasing concentrations of MDA, indicating possible damage to the cell membrane and cytoskeleton. Different actin poisons (e.g. phalloidin, which binds to, and stabilises dynamic actin microfilaments, preventing depolymerisation (Prentki *et al.*, 1979)), had an effect on the actin cytoskeleton and on cellular shape, with the surface of cells becoming more pitted and with blebbing (protrusion or bulging of the plasma membrane) (Lazaro-Dieguez and Egea, 2007), as observed here. MDA has a high capability of interacting with a number of biomolecules, forming adducts with both DNA and proteins including cytoskeletal proteins, enzymes, carrier proteins and mitochondrial proteins. These adducts may form secondary DNA or protein crosslinks, which may alter the biochemical nature of these biomolecules (Ayala *et al.*, 2014), and thus make alterations to the cell morphology.

MRC5 cells treated with cigarette smoke compounds, had increased cell rounding, altered cell morphology and shape irregularity with increased doses of the chemicals (Liu *et al.*, 2015), as also observed here. Whilst there was an obvious change in the cell surface characteristics of the MRC5 and MRC5 SV2 cells here, the cells were fixed and air-dried and so their appearance when imaged by AFM would be altered compared to that *in vitro*. AFM was used to image the morphology of developing tumour cells and it was pointed out that the drying procedure when preparing the cells for AFM imaging may have caused some flattening of the nanostructure of the cells' surface and thus there may have been an increase in the cell surface roughness as a result (Tomankova *et al.*, 2007). The different fixatives available for cultured cells in air for AFM were investigated, ideally looking for a fixative that preserved fibroblast cells in a similar state

as *in vitro* without generating any artefacts such as coating, crystals, debris etc, to preserve the topography of the cell surface (Moloney *et al.*, 2004). Glutaraldehyde, as used here, was assessed as a good fixative, with no artefact formation, however, paraformaldehyde would have been a better choice as fibroblast morphology was conserved to a greater degree. A difference in cell surface morphology was observed between untreated cells and those treated with 100 µM MDA, so although the fixative may have had an effect, MDA has a clear effect on cell surface morphology.

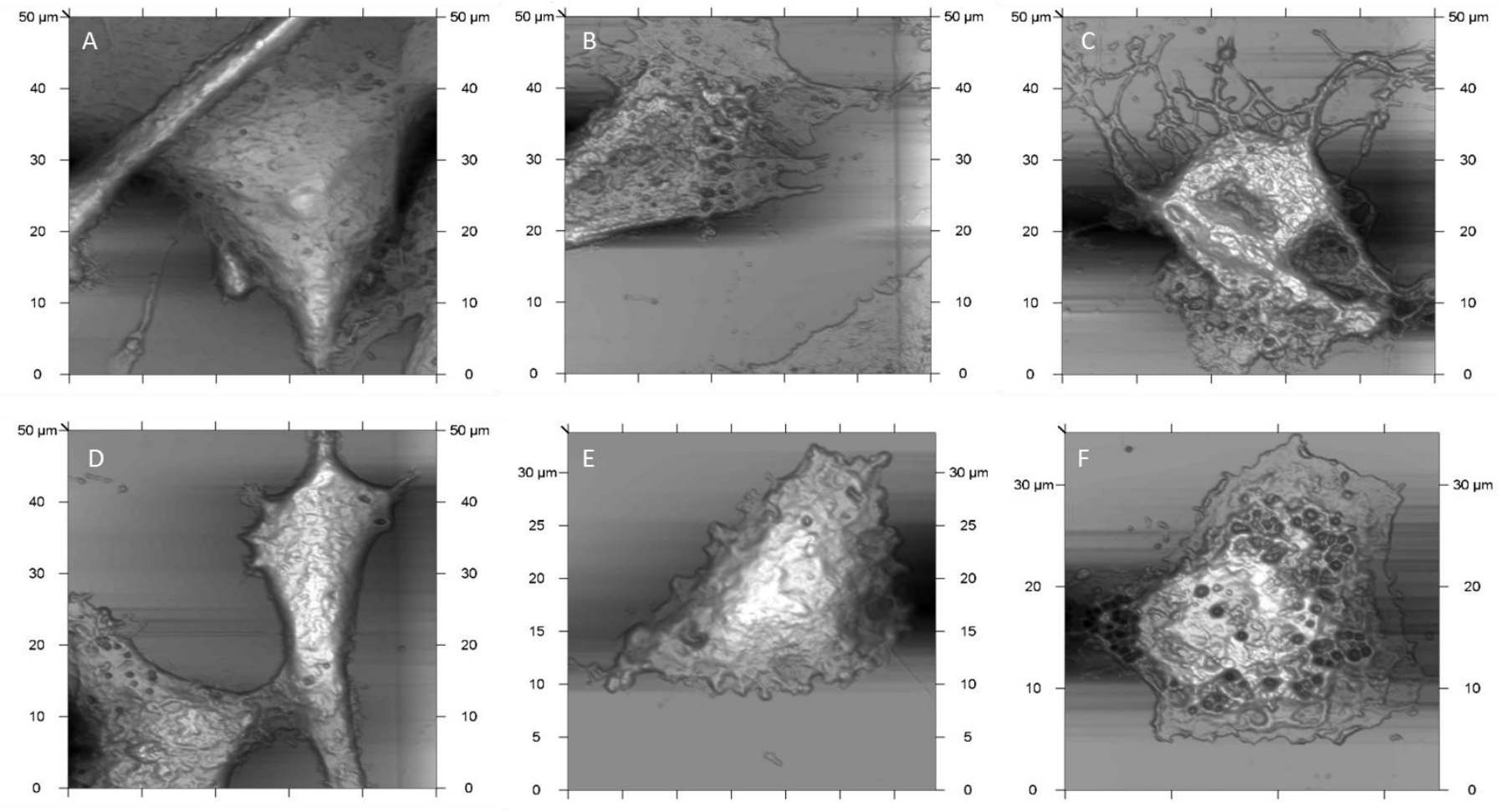

Figure 17. AFM images of MRC5 (A-C) and MRC5 SV2 (D-F) cells treated for 24 h with MDA: A &D) 0 µM, B & E) 100 µM, C & F) 200 µM. n = 10, all images were representatives of each sample.

3.6. Effects of MDA on Nuclear Morphology

In order to determine the effect of treatment of MRC5 and MRC5 SV2 cells with MDA on nuclear morphology and nuclear size, a variation of the micronucleus assay was carried out. Chromosomal mutation is an important event in carcinogenesis and this method measures both chromosomal breakage and loss. Chromosomal loss or non-disjunction are events associated with ageing and cancer, due to spindle or centromere defects. Dividing cells containing chromosomal breaks and chromosomes that are unable to travel to the spindle poles during mitosis, often express micronuclei which are much smaller than the main nucleus. The micronucleus assay involves treating cultured cells with a test compound and then inhibiting cytokinesis by using cytochalasin B, which is a microfilament assembly inhibitor, ensuring that all cells are in the bi-nucleated stage of the cell cycle as micronuclei are only expressed in cells that have completed nuclear division (Fenech, 2000). The micronucleus assay is a method of staining and scoring these micronuclei to assess the level of DNA damage. Fluorescent stains such as DAPI are used (Fenech, 2000).

Here, the protocol for the micronucleus assay was followed, to ensure that the cells were in the same stage of the cell cycle, although the aim was primarily to examine the effect that treatment of MRC5 and MRC5 SV2 cells with MDA had on nuclear morphology, rather than quantification of micronuclei (Section 2.3.8.). Fluorescent images of MRC5 and MRC5 SV2 cells treated with MDA and the nuclei stained with DAPI are shown in Figure 18 (only images for 0-200 µM MDA are shown as location of cells due to decreased cell density became more difficult at higher concentrations, and all

images are representative of each sample (n = 12)). The morphology of the nuclei were examined and as the concentration of MDA increased, the nuclei of both cell lines became more irregular in shape and what appear to be micronuclei were observed in cells treated with 100 and 200 µM MDA. Little effect was observed on the nuclear morphology of cells treated with 10-50 µM MDA. The number of possible micronuclei observed appeared to increase with increasing MDA concentration, although small blue spots can also be seen in the negative controls, albeit to a lesser extent.

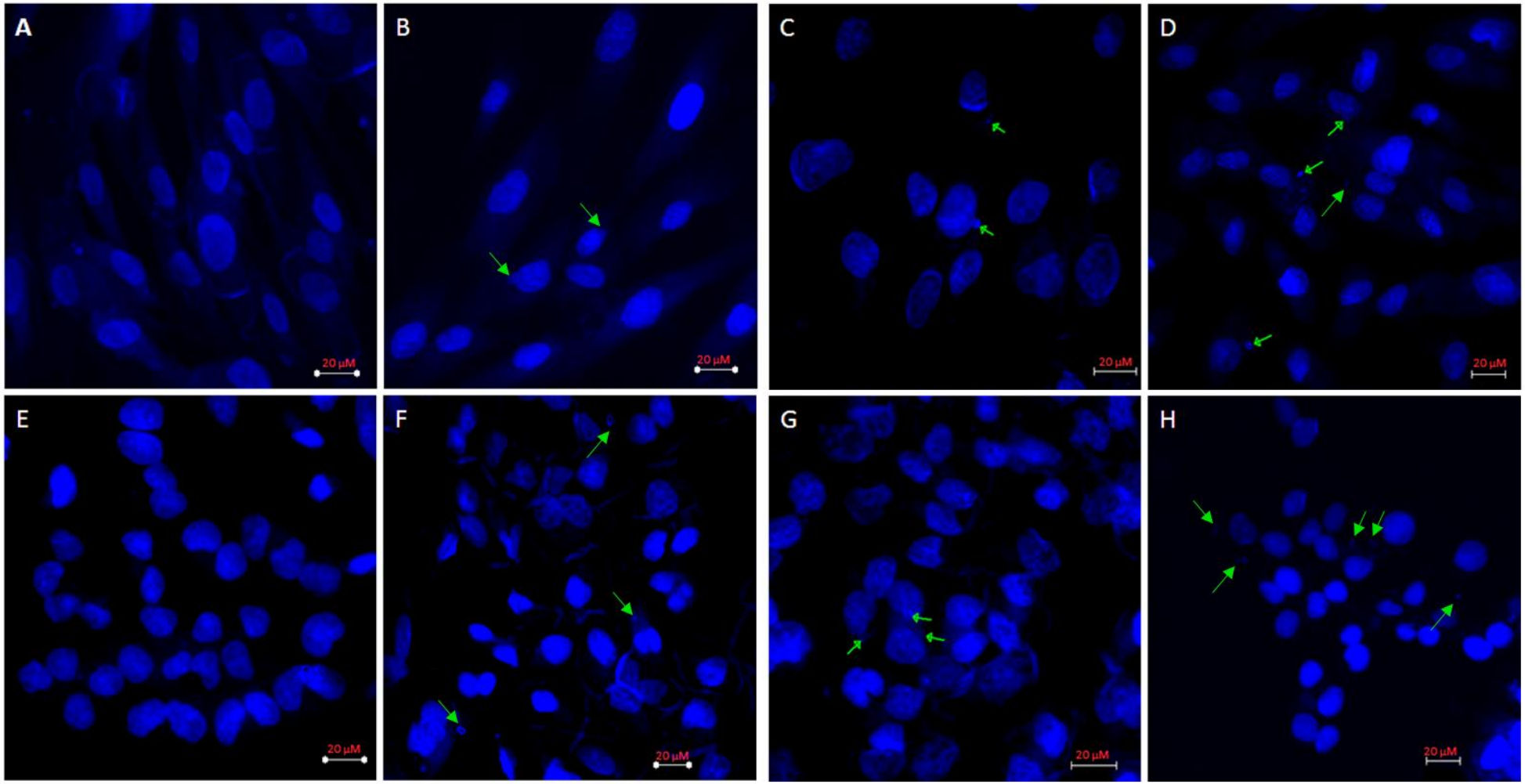

Figure 18. DAPI stain of the nuclei of MRC5 (A-D) and MRC5 SV2 (E-H) cells following treatment with MDA: A & E) 0 µM, B & F) 50 µM, C & G) 100 µM and D & H) 200 µM. The scale bars represent 20 µM. The green arrows indicate possible nuclei. (n = 12).

The mean area of the nuclei of MRC5 and MRC5 SV2 cells treated with MDA and H_2O_2 for 24 and 48 h were measured, using ImageJ software (Rasband, 1997), following staining with DAPI, to quantify the changes observed in Figure 18. Figure 19 shows the mean nuclear area of untreated MRC5 cells remained similar over 24 and 48 h. The area increased continually after 24 h treatment with increased MDA concentrations. After 48 h treatment with 50 µM MDA, the nuclear area increased more than after only 24 h and increased to a lesser extent after 200 µM MDA after 48 h than 24 h. The nuclear area of MRC5 SV2 cells increased following treatment with increasing MDA concentration for 24 h compared with the untreated control. After 48 h, the nuclear area increased further, with the largest nuclear area observed in cells treated with 100 µM MDA. Treatment with the positive control (50 µM H_2O_2, data not shown) for both cell lines showed an increase in nuclear area from 24 h to 48h.

Single factor ANOVA was used to assess the variance in nuclear area for treatments of 0-200 µM MDA at each time point for each cell line. A significant difference in nuclear area measurements were reported if $F > F_{crit}$ and $P < 0.05$. For both cell lines, for 24 h and 48 h treatment with 0-200 µM MDA, the results were all significantly different, as shown in Table 13, although significance was greater at 24 h than 48 h.

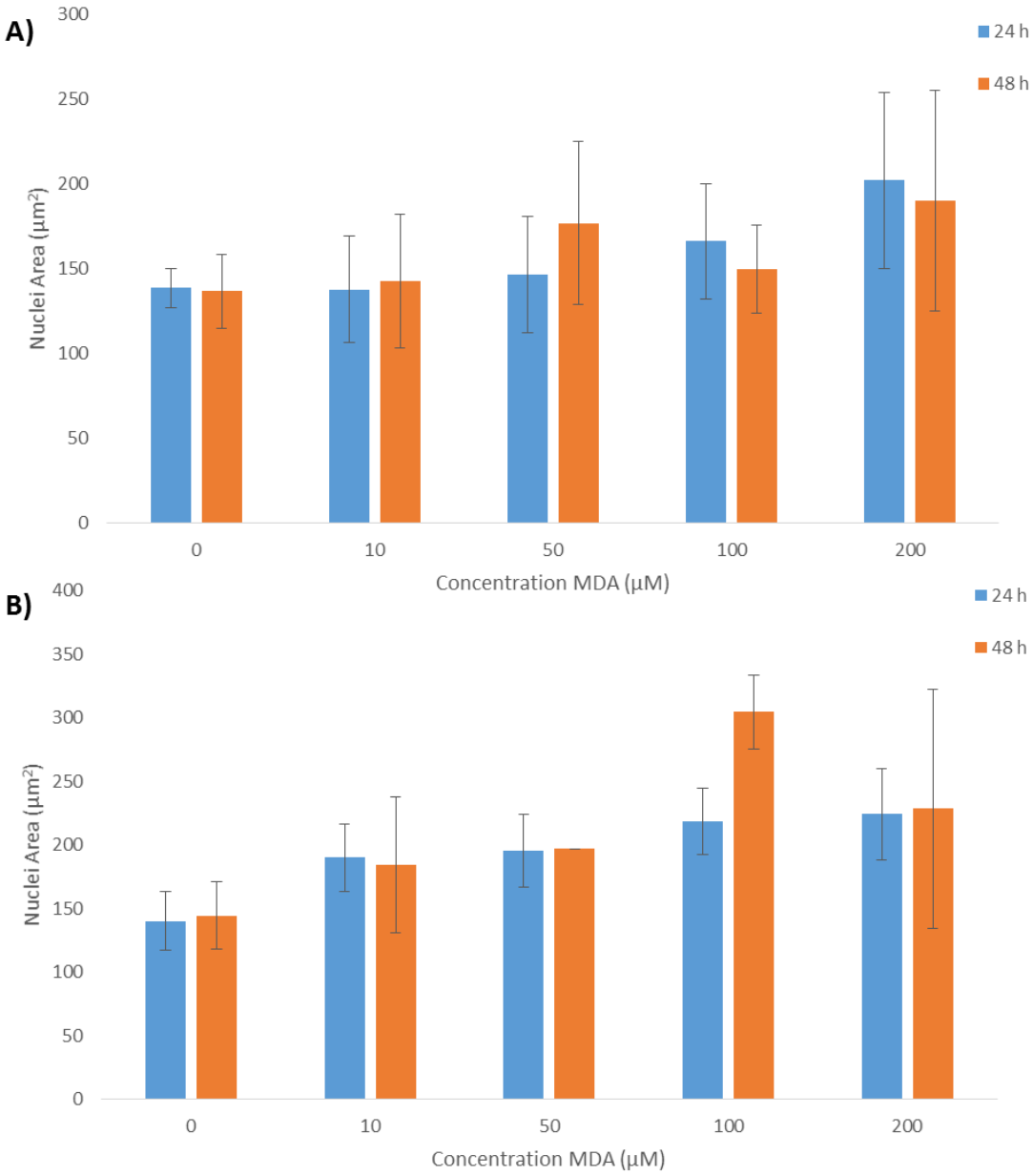

Figure 19. Area of nuclei of A) MRC5 and B) MRC5 SV2 cells treated with MDA (0-200 µM) over 24-48 h, error bars indicate ± 1SD from the mean, n=10.

Table 13. Comparison of the effect of treatment with 0-200 µM MDA for 24 h and 48 h on nuclear area of MRC5 and MRC5 SV2 cells by single factor ANOVA. P and F values for significance (*).

	MRC5		MRC5 SV2	
ANOVA	**24 h**	**48 h**	**24 h**	**48 h**
F_{crit}	2.589	2.584	2.626	2.782
F value	5.534 *	3.042 *	12.17 *	7.574 *
P value	0.001 *	0.027 *	$2.06x10^{-6}$ *	$3.02x10^{-4}$ *

The increase in the nuclear area observed in both cell lines treated with MDA compared to the negative control indicates that there had possibly been some reorganisation of the cytoskeleton, which may cause the cells to spread out and flatten, which would make the nucleus appear to be larger than it would have otherwise, or there was an increase in the volume of the nucleus. 3-D imaging and measurement of the nuclear volume would be required to confirm changes to nuclear size.

In human primary diploid fibroblasts that had senesced following treatment with H_2O_2, the cell morphology was altered, becoming enlarged, flattened and more rounded, with an increase in the size of the nucleus, whereas in apoptotic cells, the cells contracted and detached (Bladier *et al.*, 1997). As the significance of treatment with MDA on nuclear area was lower after 48 h than 24 h, this perhaps indicates that cells were starting to become apoptotic and beginning to contract. The possible damage to the

cytoskeleton as a result of MDA treatment was also observed in Section 3.5., where the cell surface morphology was imaged by AFM.

The nuclear volume is determined by cytoplasmic factors rather than DNA content and the nuclear-cytoplasmic (karyoplasmic) ratio remains constant for particular cell types and organisms (Huber and Gerace, 2007). Abnormal nuclear shape and disturbances in the ratio have been associated with some cancers (Webster *et al.*, 2009). The nuclear envelope is a double lipid bilayer, of which the outer layer is connected to the endoplasmic reticulum of the cytoplasm and the inner layer which is connected to the nuclear components and is lined by the nuclear lamina, a network of proteins including intermediate filaments (mainly nuclear lamins). The size and shape of the nucleus is influenced by the nuclear lamina (Huber and Gerace, 2007). The cytoskeleton consists of microtubules, actin microfilaments and intermediate filaments and gives the cell its shape and mechanical stability. The cytoskeleton is connected via nuclear envelope bridges to the nuclear surface and may also influence the size and shape of the nucleus (Starr and Fridolfsson, 2010). Thus damage to the cytoskeleton may alter the volume of the nucleus.

Quantification of micronuclei formed by exposure of both cell lines to different concentrations of MDA would be required to determine the level of DNA damage induced. Micronuclei can be used as biomarkers of cancer risk for which a non-invasive method using exfoliated epithelial cells can be used. The oral mucosa cells of non-smokers were compared with those of heavy smokers using a variety of DNA specific stains e.g. DAPI and non-specific stains e.g. Giemsa. There were significantly elevated

numbers of micronuclei found using the non-specific Giemsa stain but not using the DNA specific stains. However, there was an increased number of nuclear anomalies, mainly keratin bodies, which could be misinterpreted as micronuclei when using the Giemsa stain. It was concluded that micronuclei induction is not found in oral mucosa cells exposed to cigarette smoke, however the use of a more specific dye such as DAPI may have shown otherwise (Nersesyan *et al.*, 2006), as was used in this study. The micronucleus assay was used with Feulgen fast-green staining to examine the difference in micronuclei frequency in exfoliated buccal mucosa cells from non-smokers, smokers who had smoked for more than 10 years and smoker who had been smoking for less than 10 years. They found that there was a significant difference between the non-smokers and the two groups of smokers but not between the two groups of smokers (Naderi *et al.*, 2012). The data was pooled from a number of studies looking into the effect of smoking on micronuclei frequency and re-analysed, it was found that for smokers in general, there was no significant increase in micronuclei, however for those who smoked ≥30 cigarettes per day, there was a significant increase in micronuclei frequency (Fenech and Bonassi, 2011). As these studies used oral mucosa cells, there is no direct comparison with the lung fibroblast cells used in this study, and although smoking may not show a significant increase in micronuclei in oral mucosa cells, there may be a difference in lower respiratory tract cells, which will require further analysis.

3.7. Apoptosis Detection using an Annexin V Fluorescent Assay

Apoptosis is programmed cell death whereby cells initiate apoptotic signalling in response to stress (Alberts *et al.*, 2002). Morphological changes occur to the cell during apoptosis including chromatin condensation, nuclear fragmentation, membrane blebbing, collapse of the cytoskeleton and cell shrinkage. Defects in the apoptotic pathway may lead to uncontrolled cell proliferation and cancer (Lowe and Lin, 2000).

An immunofluorescence detection kit was used to detect apoptosis in MRC5 and MRC5 SV2 cells treated with MDA for 24 – 48 h, as described in Section 2.3.9. The assay involved two fluorescent dyes: Annexin V binds to phosphatidyl serine (a cell surface signal for phagocytosis (Verhoven *et al.*, 1995)) in cells that are necrotic, observed as red fluorescence, 6-carboxyfluorescein diacetate hydrolyses in viable cells to 6-carboxyfluorescein, observed as green fluorescence, and both green and red fluorescence may be observed in cells that are at an early stage of apoptosis. An increase in the amount of cells fluorescing red was observed in both cell lines after 24 and 48 h treatment with increasing concentrations of MDA, although the intensity of red was slightly less in MRC5 SV2 cells than MRC5 cells (Figure 20 and Figure 21, all images are representative of each sample, n = 6). Both cell lines show a greater intensity of red after 48 h than for 24 h, although green fluorescence was also observed in all images. This indicates that with increasing concentration of MDA and time, there were more cells in the early stages of apoptosis, compared to the untreated cells. Treatment of both cell lines with a positive control, H_2O_2 (100 µM), gave a similar result to those treated with 200 µM MDA (data not shown).

The same was observed for the green fluorescence, indicating that although the cells had begun apoptosis (as indicated by loss of membrane asymmetry), they were still viable. Some red fluorescence was observed in the untreated cells for both cell lines and time periods. This was possibly due to a background level of apoptosis, whereby a number of cell lines exhibited some background level of apoptosis (Sheridan and West, 2001). This background level of apoptosis may have been due to incubation in FBS-free media rather than full media. As BSA (a major component of FBS) interacts with MDA (Traverso *et al.*, 2004), as described in Section 3.2, FBS could not be used in the treatment of cells. However, as all cells were grown in the same media and conditions, other than the two variables of MDA concentration and time, the increase in red fluorescence with increased MDA concentration and treatment times for both cell lines may be attributed to the effect of MDA on the onset of apoptosis.

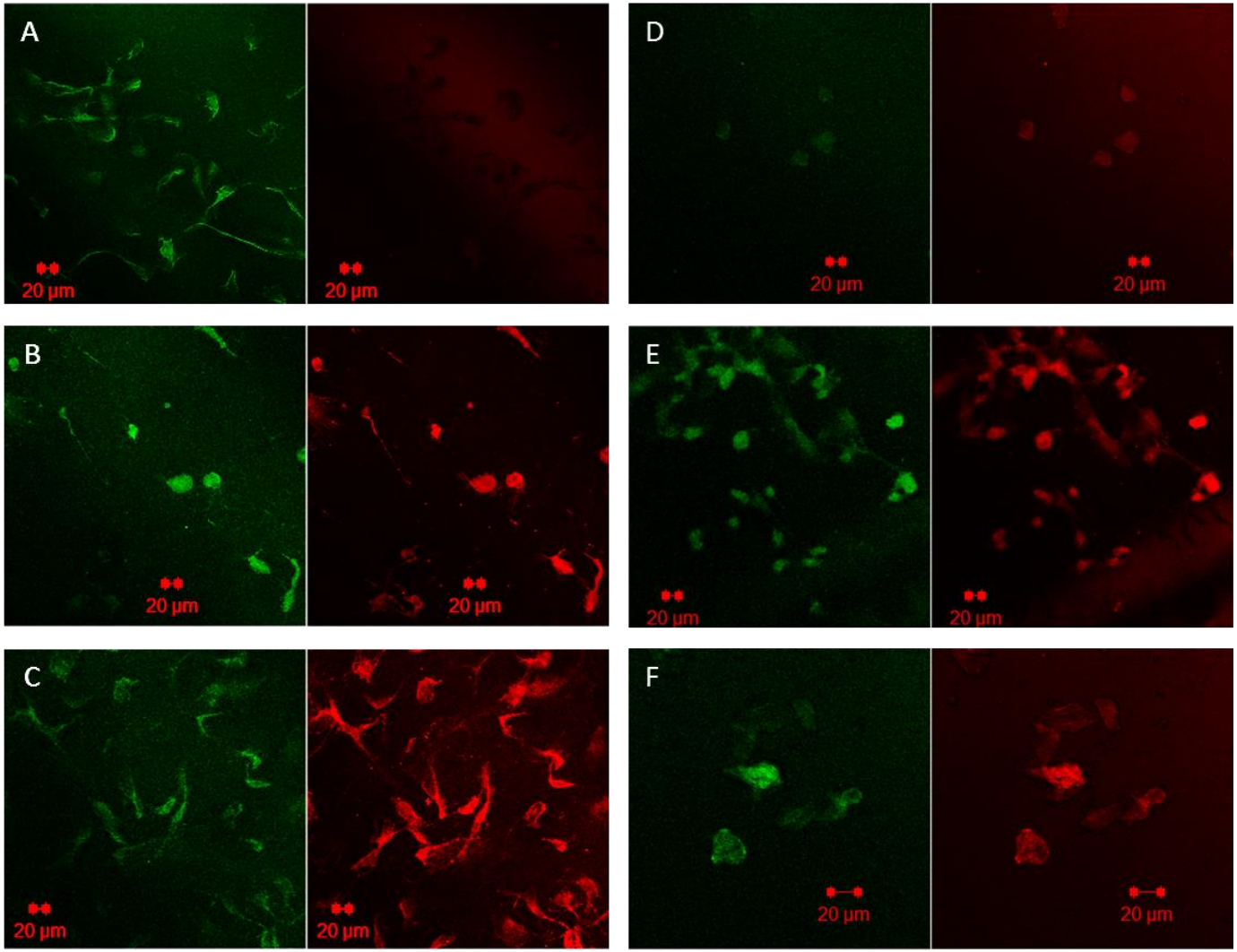

Figure 20. Apoptosis detection of MRC5 cells treated for 24 h (A-C) and 48 h (D-F) with MDA in FBS-free media: A & D) 0 µM, B & E) 50 µM and C & F) 100 µM, x20 magnification using confocal microscopy. Red indicates cells stained for apoptosis and green for viable cells.

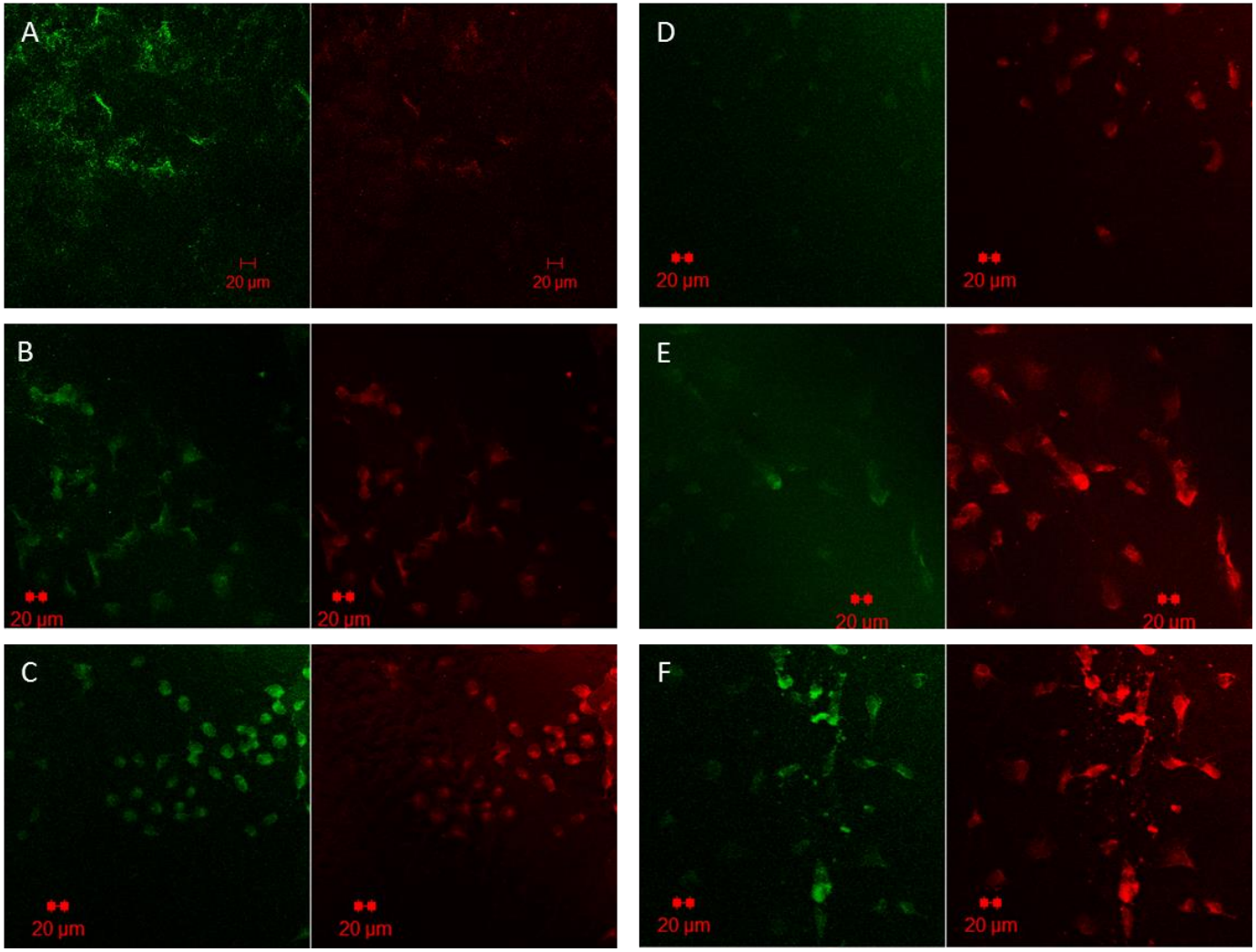

Figure 21. Apoptosis detection of MRC5 SV2 cells treated for 24 h (A-C) and 48 h (D-F) with MDA in FBS-free media: A & D) 0 µM, B & E) 50 µM and C & F) 100 µM, x20 magnification using confocal microscopy. Red indicates cells stained for apoptosis and green for viable cells.

The cell number in multicellular organisms and tissues is highly regulated, maintaining the balance between cell division and programmed cell death (Alberts *et al.*, 2002). Damage to DNA can trigger apoptosis (Ji *et al.*, 1998). DNA damage leads to a rapid increase in p53 due to inactivation of the p53/Mdm-2 interaction, which in turn leads to reversible cell cycle arrest and induction of DNA repair mechanisms and then to apoptosis or senescence (loss of proliferative capacity). p53 transactivates genes that induce apoptosis e.g. *Fas* and *Bax* and genes that induce cell cycle arrest e.g. *CDKN1A* (Ji *et al.*, 1998; Enge *et al.*, 2009). p53 transcribes *Bcl-2* genes, initiating the release of cytochrome c into the cytosol. The *Bcl-2* gene family regulates procaspase activation, some of which inhibit apoptosis, others promoting procaspase activation. The *IAP* gene family act by binding to either procaspases, preventing activation, or to caspases, to inhibit activity (Alberts *et al.*, 2002).

The caspase family of proteases cleave specific proteins in the nucleus and cytoplasm. Procaspases, the inactive precursors of caspases, are activated by cleavage by other caspases, resulting in a proteolytic caspase cascade. The cascade is activated by an intra or extracellular death signal and is self-amplifying and irreversible. Adaptor proteins aggregate procaspases. The Fas ligand on the surface of killer lymphocytes is an external activation signal which binds to Fas receptor on the cell surface, recruiting adaptor proteins and initiating a caspase cascade. The release of cytochrome c from mitochondria into the cytosol acts as an internal signal, binding and activating the adaptor protein Apaf-1 (Alberts *et al.*, 2002).

Apoptotic pathway defects can contribute to a number of diseases such as cancer. For example, overexpression of *Bcl-2*, upregulation of *Bcl-x*$_L$, inactivation of *Bax,* and mutations in upstream and downstream components of the p53 pathway e.g. *Mdm-2*, *ARF* and *Bax* may all lead to tumorigenesis (Lowe and Lin, 2000). p53 is involved in the regulation of numerous apoptotic cell functions, and damage to or sequestration of the p53 protein can have an effect on p53 dependent DNA binding and pro-apoptotic functions. This may explain the reduced red fluorescent intensity observed in MRC5 SV2 cells compared to MRC5 cells treated with the same concentrations of MDA and time. The sequestration of the p53 protein in MRC5 SV2 cells by the binding of the integral viral large T antigen (Pipas, 2009) may have reduced the level of apoptosis in this cell line due to reduced activation of p53 dependent apoptotic factors.

Two cell lines were treated with MDA, RKO (human colorectal carcinoma, wild type p53) and H1299 (human lung adenocarcinoma, p53-null), and found that there was an increase in the M_1dG adduct, but also that MDA induced an apoptotic response with irreversible cell cycle arrest at G_1/S and G_2/M and elevation p53 protein levels (Ji *et al.*, 1998). This increase in apoptotic response due to increased MDA concentration was also observed here.

The effects of MDA on human bone marrow mesenchymal stem cells were assessed by flow cytometry and MTT assay. It was found that increasing concentrations of MDA (up to 1mM) decreased the cell count, increased the population doubling time, decreased cell viability and triggered apoptosis, as also observed here with increased apoptosis and decreased cell viability and cell proliferation (Guolin *et al*, 2006).

MDA and H_2O_2 have been found to induce both apoptotic and necrotic cell death in rat cortical neurons, whereby reduced membrane integrity, increased nuclear fragmentation were observed. It was suggested that MDA induced apoptosis by protein cross-linking (Cheng *et al.*, 2011). This is in keeping with the findings in Sections 3.4., 3.5., and 3.6., where an increase in irregularity of the cell membrane, cell morphology and nuclear morphology were observed with increasing MDA and H_2O_2 concentrations, linking these observations to the increase in the early stages of apoptosis found here.

The positive control used in this research was H_2O_2, which is an intermediate molecule formed from dismutation of superoxide anions by superoxide dismutase and is known to induce apoptosis and senescence (Ayala *et al.*, 2014). Human primary diploid fibroblasts were treated with H_2O_2, inducing senescence at lower concentrations of H_2O_2 and apoptosis at higher H_2O_2 concentrations. In the senescent cells, the morphology was altered, becoming enlarged, flattened and more rounded, with an increase in the size of the nucleus. In apoptotic cells, the cells contracted and detached (Bladier *et al.*, 1997). Following treatment of human retinal pigment epithelial cells with H_2O_2, caspase 3 was activated and apoptosis was induced (Kim *et al.*, 2003). H_2O_2 induced apoptosis and decreased viability in human gastric carcinoma cells. The pro-apoptosis factor Bax was up-regulated, the anti-apoptosis factor Bcl-2 was down-regulated and the cell death receptor Fas expression increased, all of which are induced by p53 (Mao *et al.*, 2006). Thus, cellular stress due to H_2O_2 has been found to induce p53 dependent pro-apoptotic pathways, making H_2O_2 a useful positive control for the toxicity studies used here.

p53 plays an important role in apoptosis and p53 expression levels have been found to increase in response to cellular stress and DNA damage, therefore investigation of the levels of expression of p53 in MRC5 and MRC5 SV2 cells in response to treatment with MDA would supplement the previous investigations in this section.

3.8. p53 Expression using Immunoflurescence

p53 gene expression has been shown to increase in response to DNA damage by oxidising agents, irradiation and carcinogenic and cytotoxic compounds, as well as other non-DNA damaging cellular stress factors such as hypothermia and hypoxia (Hainaut and Hollstein, 2000). Increased p53 expression is part of the apoptotic response of cells (Alberts *et al.*, 2002). This assay uses immunofluorescence to detect p53 protein levels in MRC5 and MRC5 SV2 cells subject to treatment with MDA for 24 and 48 h, as a qualitative indicator of oxidative stress and possible DNA damage (Section 2.3.10.). p53 protein expression in cells was detected by immunofluorescence detection with a p53 specific primary antibody. p53 protein expression gradually increased in response to increasing MDA concentrations and treatment time (Figure 22 and Figure 23). Images for 48 h only are shown as the lower intensity of the red fluorescence at 24 h was difficult to view in this format and all images shown are representative of a number of images taken for each MDA concentration (n = 6). Treatment with the positive control (50 µM H_2O_2) also showed increased p53 expression over time compared to the negative control (images not shown), indicating that increased p53 expression was due to oxidative stress. Low levels of p53 protein were observed in the cytoplasm of both cell lines in the negative control and at 50 µM

MDA, whereas following treatment with greater MDA concentrations (100-1000 µM), increased levels of p53 protein were observed in the nuclei. p53 is synthesised in the cytoplasm and, when subject to cellular stress, p53 re-locates from the cytoplasm of the cell to the nucleus, where it is required to inhibit the growth of malignant cells (O'Brate and Giannakakou, 2003).

Low levels of p53 protein were located in the cytoplasm of cells treated with 50 µM MDA and the negative control, where it is kept at low levels by interacting with Mdm-2 in unstressed cells, preventing transport to the nucleus. It would seem that from Figure 22 and Figure 23, that p53 levels were lower in cells treated with 50 µM MDA than for the negative control. Increased levels of p53 protein were observed in the nuclei of cells treated with higher concentrations of MDA (100-1000 µM) for both 24 h and 48 h. Cleavage of p53-Mdm-2 in response to stress, for example DNA damage, activates p53 and is transported from the cytoplasm to the nucleus (Hock *et al.*, 2011).

These observations correlate with previous observations in Section 3.7., whereby treatment of cells with increasing MDA and H_2O_2 concentrations led to increased levels of apoptosis, as DNA damage leads to an increase in p53 and induction of apoptosis (Ji *et al.*, 1998), as previously described in Section 3.7. There also appears to be a greater effect for MRC5 SV2 cells than for MRC5 cells, with greater levels of red fluorescence at corresponding MDA treatment concentrations and times. This may be due to the sequestration of p53 in MRC5 SV2 cells by binding to the viral large T antigen of SV40, which had been used to transform this cell line (Huschtscha and Holliday, 1983), and

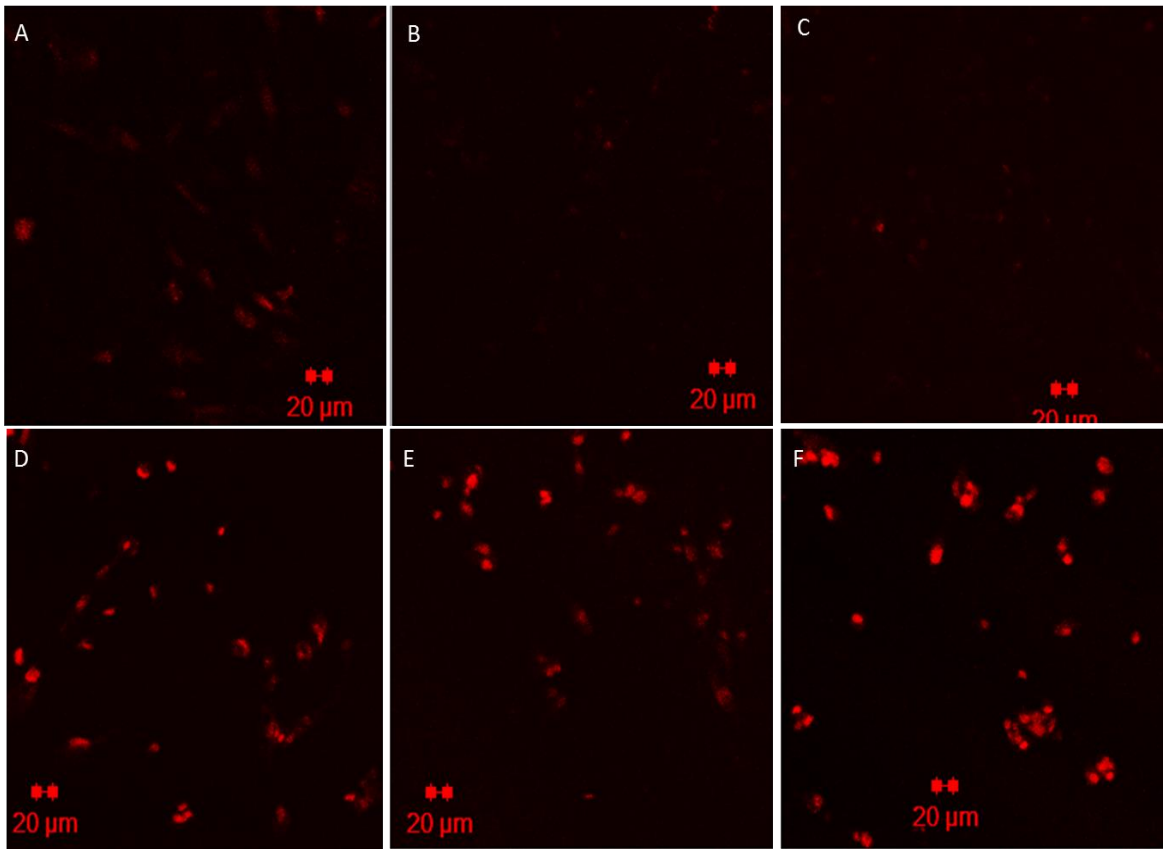

Figure 22. Confocal image of p53 protein stained red in MRC5 cells treated for 48 h with MDA: A) 0 µM, B) 50 µM, C) 100 µM, D) 200 µM, E) 500 µM and F) 1000 µM (x20 magnification).

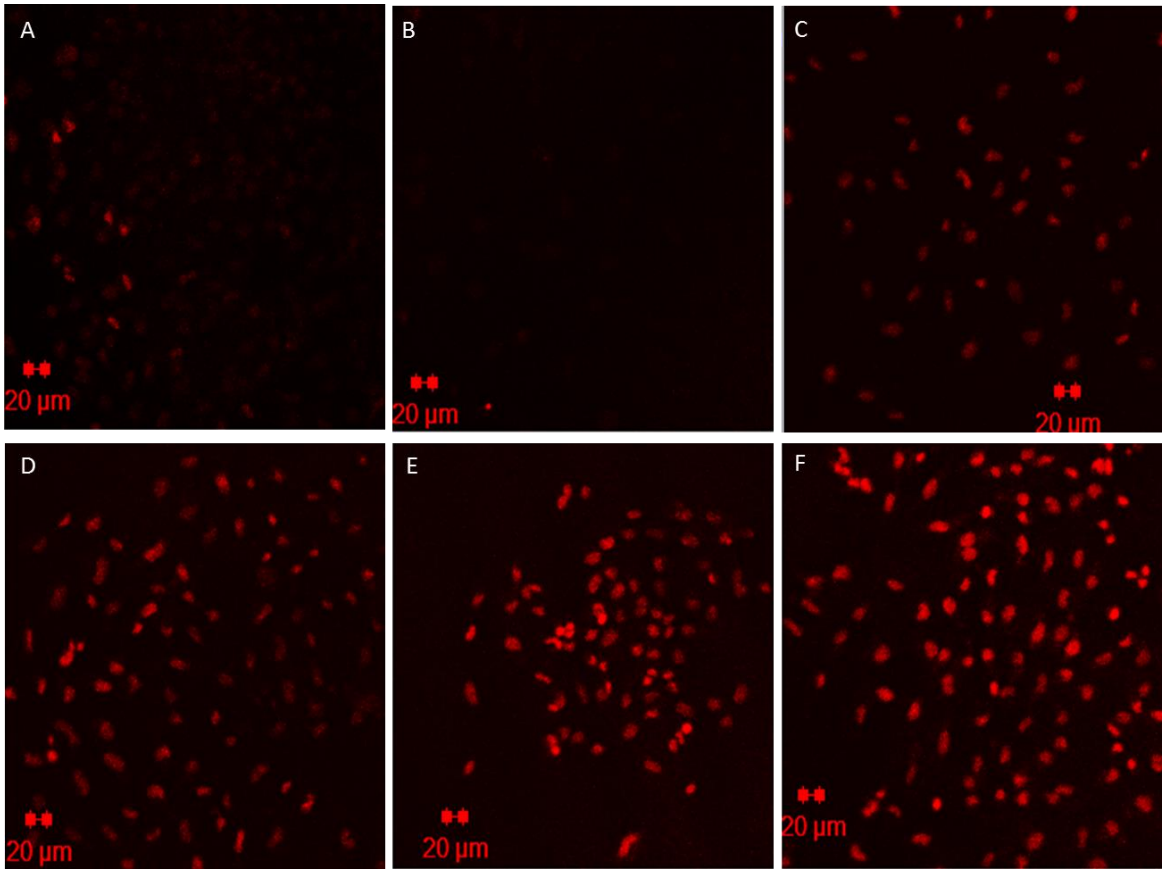

Figure 23. Confocal image of p53 protein stained red in MRC5 SV2 cells treated for 48 h with MDA: A) 0 µM, B) 50 µM, C) 100 µM, D) 200 µM, E) 500 µM and F) 1000 µM (x20 magnification).

thus may instigate an increase in p53 expression to compensate for the bound p53 in response to increased oxidative stress.

This assay shows that an increase in MDA results in increased stress and hence higher levels of p53 protein. Quantitative analysis of p53 protein expression levels in response to treatment with MDA would confirm this.

3.9. p53 Expression using Reverse Transcription Quantitative Polymerase Chain Reaction

RT-qPCR is a method used to quantify gene expression using a dual labelled fluorescent probe to measure PCR product accumulation (Heid *et al.*, 1996), and is carried out in three steps: reverse transcription of mRNA to cDNA followed by amplification of cDNA by PCR and real-time detection and quantification of PCR products (Nolan *et al.*, 2006). The data may be analysed by absolute quantification, where the transcript copy number is determined by using a standard curve, or by relative quantification, where the PCR signal of the target transcript is related to that of another sample. The $2^{\Delta\Delta Ct}$ method of relative quantification calculates the relative changes in gene expression but requires the assumption that the amplification efficiency of the target gene is equal to that of the reference gene. The data for the $2^{\Delta\Delta Ct}$ method is usually presented as the fold change (fold induction) in gene expression of the target transcript normalised to a reference gene and relative to the untreated control (Livak and Schmittgen, 2001). In this research, the fold induction was the factor by which p53 increased in response to treatment with MDA compared to the untreated control.

RT-qPCR is the method of choice for RNA quantification as it is accurate, sensitive and specific, there is no post-PCR sample handling preventing contamination and thus higher throughput, it allows analysis of small nucleic acid quantities, as low as a single cell equivalent, and it is less labour intensive than other methods (Heid *et al.*, 1996). However, the data produced depends largely on the quantity and quality of the RNA template and the results are subject to biological and technical variation (Nolan *et al.*, 2006).

The expression of p53 mRNA of cells following treatment with MDA and H_2O_2, as a positive control (data not shown), was quantified by RT-qPCR, as decribed in Section 2.3.11. Cycle threshold (Ct) values were measured for both p53 mRNA and GAPDH mRNA. The latter is a house-keeping gene, for which expression is assumed to remain constant (Barber *et al.*, 2005), and was used as the reference gene to normalize the expression data due to give the relative expression of p53 mRNA to GAPDH mRNA . This allows for any discrepancies in cell number and RNA extraction. The untreated (negative) control was used as a calibrator to which the treated samples were compared. The fold induction of p53 mRNA was calculated using the $2^{\Delta\Delta Ct}$ method and is shown in Figure 24 for MRC5 and MRC5 SV2 cells treated for 24 and 48 h. Only relatively low concentrations of MDA (10 – 100 µM) were used to treat the cells. This was because the same amount of RNA was required initially for each sample and cell number and viability remained relatively high when treated with these concentrations compared with higher concentration (Sections 3.2 and 3.3).

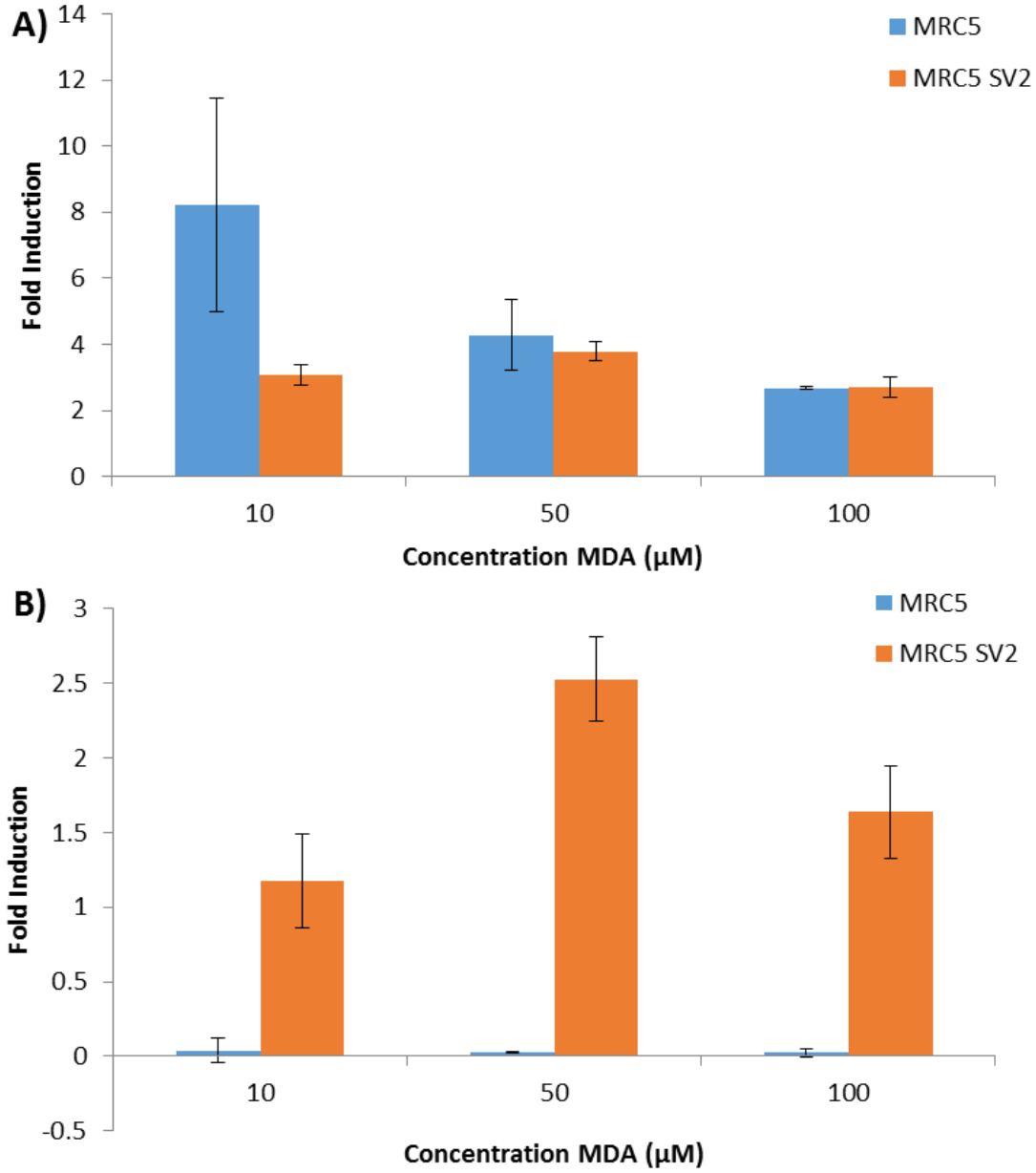

Figure 24. Induction of p53 mRNA expression relative to the negative control and reference gene GADPH, in cells treated with MDA (0 – 100 µM) for A) 24 h and B) 48 h, error bars indicate ± 1SD, n = 6.

After 24 h treatment with MDA, p53 mRNA production was induced in both cell lines compared to the negative control. Induction was greater at 10 µM MDA for MRC5 cells than MRC5 SV2 cells and gradually decreased up to 100 µM MDA, whereas for MRC5 SV2 cells, induction increased at 50 µM MDA and decreased again at 100 µM

MDA. After 48 h treatment, p53 mRNA induction was greatly reduced for MRC5 cells and slightly reduced for MRC5 SV2 cells, which follow the same pattern as for 24 h treatment.

In order to eliminate background noise due to amplification errors between samples, a cut-off point for fold induction should be applied. It has been suggested that the minimum fold change for significance is ≥ 2, with some studies suggesting up to 4 fold change as the cut-off point (Dalman *et al.*, 2012; Rajeevan *et al.*, 2001). If the minimum cut-off point of a 2 fold induction was applied to Figure 24, all results, for both cell lines, obtained after 24 h would be significant. No results obtained after 48 h were significant, apart from for MRC5 SV2 cells treated with 50 μM.

The fold induction of p53 in MRC5 and MRC5 SV2 cells was compared with one another for each MDA concentration (0-100 μM) and at each time point by Student's t-test. A significant difference was found where $P < 0.05$. No significant difference was found between the two cell lines for any MDA concentration at 24 h. All MDA concentrations were significantly different at 48 h ($P = 0.0055$, 10 μM; $P = 0.00009$, 50 μM; $P = 0.00049$, 100 μM), however, this difference may be due to amplification errors between samples as all values (other than for MRC5 SV2 cells treated with 50 μM) were above the 2 fold induction threshold.

Single factor ANOVA was used to compare all MDA concentrations (0-100 μM) for each cell line and time point, and a significant difference was found if $P < 0.05$ and $F > F_{crit}$. No significant difference was found between MDA concentrations for MRC5 cells at either 24 h or 48 h. However, significant differences were found between MDA

concentrations for MRC5 SV2 cells for 24 h ($P = 0.012$, $F = 9.91$, $F_{crit} = 5.14$) and for 48 h ($P = 0.0046$, $F = 14.98$, $F_{crit} = 5.14$), although, the difference seen at 48 h may be due to differences in amplification efficiencies between samples, as only the value for 50 µM MDA treatment was above the fold induction cut-off point.

Following treatment with 10 µM MDA, induction of p53 mRNA was increased to a greater extent compared to treatment with higher concentrations of MDA, and to a greater extent after 24 h than 48 h. This could be due to the increased cell viability at lower concentrations, as previously observed in Section 3.3. Conversely, at higher MDA concentrations (100 µM), cell number decreased and so did p53 mRNA induction. MRC5 SV2 cells survived for longer than MRC5 cells, which may be due to their altered p53 response, which would account for their continued induction of p53 mRNA after 48 h, albeit to a lesser extent than after 24 h. Perhaps due to the sequestration of p53 in MRC5 SV2 cells by the SV40 large T antigen (Pipas, 2009), inducing the cell to express a greater amount of p53 to compensate for the bound p53.

Although there was a decrease in p53 mRNA induction with increasing concentrations of MDA and over time, there appears to be an increase in p53 protein expression when viewing cells individually (Figure 22 and Figure 23). This may also be explained by cell viability decreasing with increasing MDA concentration, with the collective fluorescence decreasing with decreasing cell viability, but expression of p53 increasing in individual cells. However, only 0-100 µM MDA concentrations were tested by RT-qPCR, whereas, concentrations up to 1000 µM MDA were used for the immunofluorescence experiment, and p53 was still induced in both cell lines for both

time periods relative to the negative control. Therefore, RT-qPCR studies of the effect of higher concentrations (100-1000 μM) MDA on the fold induction of p53 would be required for a direct comparison. Levels of p53 expression in non-small cell lung carcinoma were found to be high in 90% of tumours (Cherneva *et al.*, 2009). An increase in p53 expression in human colon cancer cells treated with inositol hexaphosphate was found (Weglarz *et al.*, 2006), although a decline in p53 mRNA expression was observed in human bronchial epithelial cells in response to treatment with aflatoxin B_1 (Van Vleet *et al.*, 2006). Thus, there are differing cellular responses to oxidative stress with regards to p53 expression.

3.10. Summary

Both cell lines showed reduced proliferation and viability with increasing concentrations of MDA, but MRC5 cells to a much greater extent. Cell surface morphology was altered, becoming more pitted and irregular in shape, as shown initially by light microscopy and then by AFM. A qualitative analysis showed what appear to be micronuclei were observed in cells treated with MDA, in a dose-dependent manner. The nuclear area also appeared to increase and cells appeared to express an increased amount of phosphatidyl serine indicating the early stages of apoptosis. p53 expression was observed to increase in individual cells, treated with increasing amounts of MDA, but the overall p53 fold induction appeared to decrease when expression was measured by RT-qPCR, perhaps due to decreased cell viability, although p53 induction was still greater than the negative control.

Whilst previous studies have utilised the techniques described in this Chapter, the novel aspect of this work lies with the use of the combination of these methods to study the effects of treating MRC5 and MRC5 SV2 cells with MDA. In particular, the effects of MDA on cell surface morphology using AFM, nuclear morphology and p53 expression studies.

The above results show that treatment with MDA results in alterations at the cellular level. However, these results do not explain whether these alterations would lead to mutagenesis, carcinogenesis or other outcomes, hence the need to explain changes at the DNA level, which is the focus of the following chapters.

CHAPTER 4

ADDUCT ANALYSIS

The development of a method of analysis of M_1G adducts in DNA samples by LC-MS-MS is detailed in this chapter. A pure M_1G standard was synthesised and purified in order to proceed with developing a method of quantitative analysis. Initially, the method for HPLC separation was optimised using the M_1G standard, followed by optimisation of MS conditions using LC-MS. The method for M_1G analysis was fine-tuned by LC-MS-MS prior to analysis of DNA samples.

A standard C18 - bonded silica column for reverse phase HPLC (Column A) was used initially for detection and qualitative analysis of M_1G, followed by a narrower column (Column B) with the same length, stationary phase and conditions to give increased sensitivity for quantitative analysis.

4.1. Synthesis of M_1G Standard

A pure M_1G standard was required in order to develop a method for quantitative analysis by LC-MS-MS. The compound was synthesised and purified as described in Section 2.3.15., using a procedure adapted from the one described by Singh *et al.* (2001). A number of different conditions for synthesis of the M_1G standard were tested,

including variation of the ratio of guanine concentration to TMP concentration, the temperature and the length of the reaction to determine the reaction condition with the greatest yield of M_1G crystals. The optimum conditions for synthesis of the standard was the reaction of 0.66 mmoles guanine (in 1M HCl) with 2 mmoles TMP at 40°C for 2 h, yielding 71.3% crude M_1G crystals. The temperature was maintained above 40°C for the duration of the reaction to prevent guanine precipitation, allowing M_1G crystals to be collected after 2 h by filtration and dried.

The solubility of the crude M_1G crystals was found to be pH dependent, with greater solubility at higher pH. The pH was then decreased to approximately 5 by addition of an acid in order to prevent hydrolytic ring-opening of the M_1G (Scheme 8). The presence of M_1G in the solution was detected by HPLC using method C(iv), as described in Section 2.3.14.1., this method was used throughout the synthesis and purification stages. The optimum combination of alkali and acid for dissolving M_1G was ammonia with formic acid as this gave the largest peak area for M_1G (retention times 4.9 min PDA and 5.0 min FLD, as shown in Figure 25). The HPLC detectors were sequential resulting in a slight delay in retention times from PDA to FLD. The ring-open form of M_1G, N^2OPdG$^-$, was detected by PDA and FLD in basic conditions (pH > 8) with retention times of 4.7 min and 4.8 min respectively (data not shown). The N^2OPdG$^-$ anion eluted earlier as it was more polar than the ring-closed M_1G.

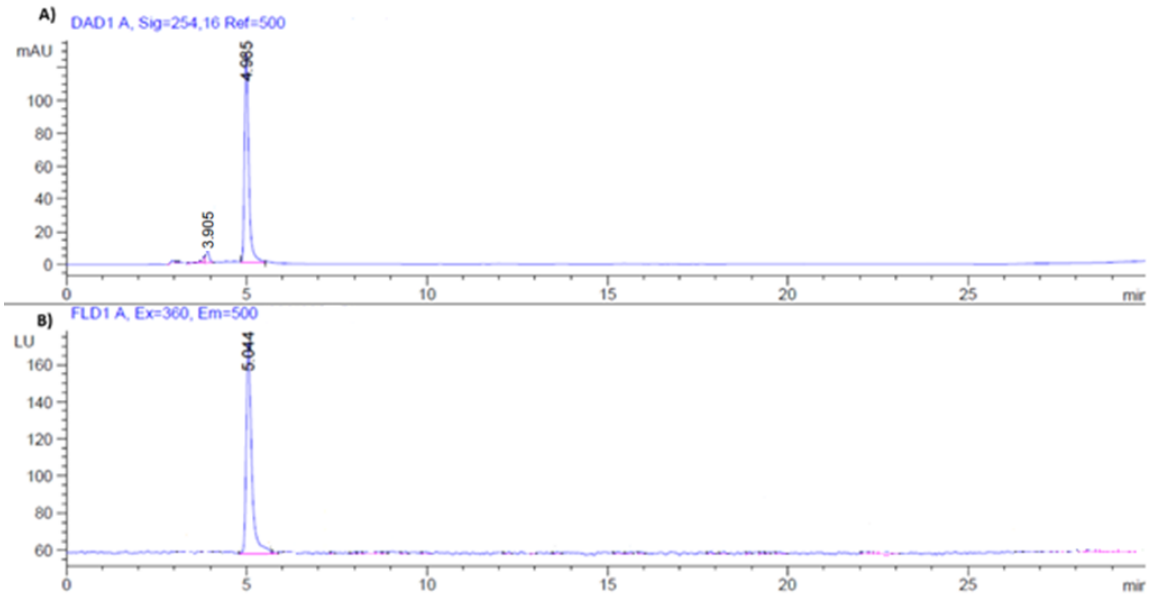

Figure 25. HPLC chromatogram of pure M_1G standard, retention time A) 4.995 min (PDA) (guanine - 3.905 min) and B) 5.044 min (FLD), using method C4 with column A, flow rate 0.5 ml/min, column temperature 25°C.

The crude M_1G was purified twice by SPE, each time collecting pure M_1G fractions identified by HPLC, as shown in Figure 25, to show that it was a pure compound. A small peak was observed at retention time 3.9 min (PDA) in addition to the M_1G peak (4.9 min). The small peak was guanine, which was identified by HPLC of a pure guanine standard (data not shown). The presence of guanine indicated that the purified M_1G was not 100 % pure, the purity was investigated in Section 2.3.14.1.

The identity of the compound that eluted at retention time 4.9 min (PDA) was confirmed by LC-MS using method C(iii) (Section 2.3.14.1.) as shown in Figure 26. The data acquired by a TIC scan of m/z 75 to m/z 190 was processed to produce a RIC of m/z 188, the ion of interest, which was further processed to produce a mass spectrum at this m/z. The TIC chromatogram shows a peak at retention time 5.1 min, corresponding to the HPLC

chromatogram (Figure 26) and the RIC chromatogram of m/z 188 also showed a peak at 5.1 min. The peak at 5.1 min on the TIC chromatogram appears to be much smaller than the RIC peak for m/z 188 due to background noise on the TIC chromatogram. RIC processing eliminated the majority of the background noise by only showing m/z 188. No guanine was detected at retention time 5.1 min (TIC) when an RIC of m/z 152 was produced. A mass spectrum (Figure 27) of the peak at 5.05 min, showed a peak with m/z 188.2 to confirm that the compound was M_1G, which has M_R 187.2 g/mol. Again, no guanine was detected on the mass spectrum as no peak at m/z 152 was detected. Any minor variation in retention time between detectors and instruments could be due to differences in tubing lengths between column and detector. The pure fractions were combined and freeze-dried to give a 0.3% yield of pure M_1G crystals. A greater yield and purity of M_1G may have been obtained with the use of preparative or semi-preparative HPLC rather than solid phase extraction (Singh *et al.*, 2001).

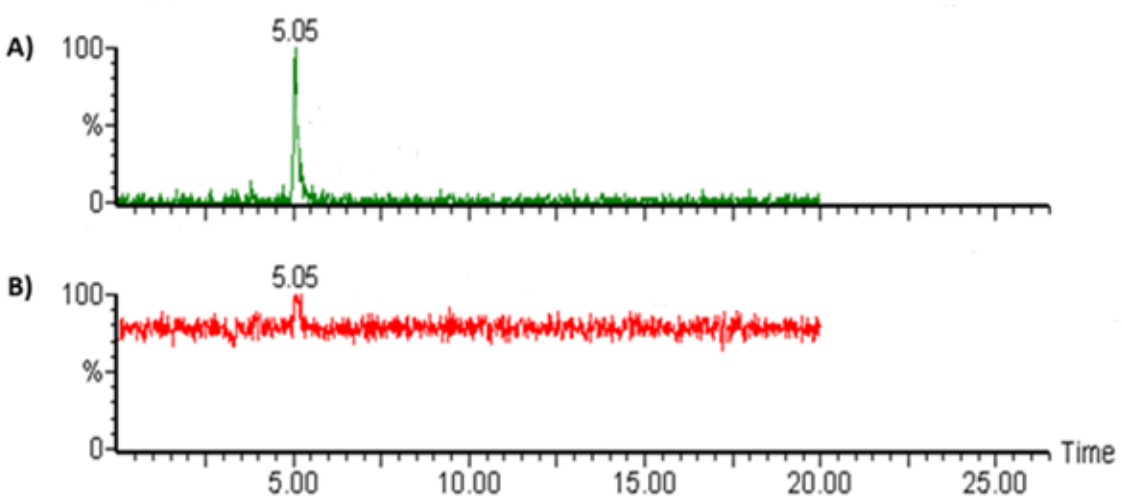

Figure 26. LC-MS mass chromatograms of pure M_1G A) RIC of m/z 188 and B) TIC scan.

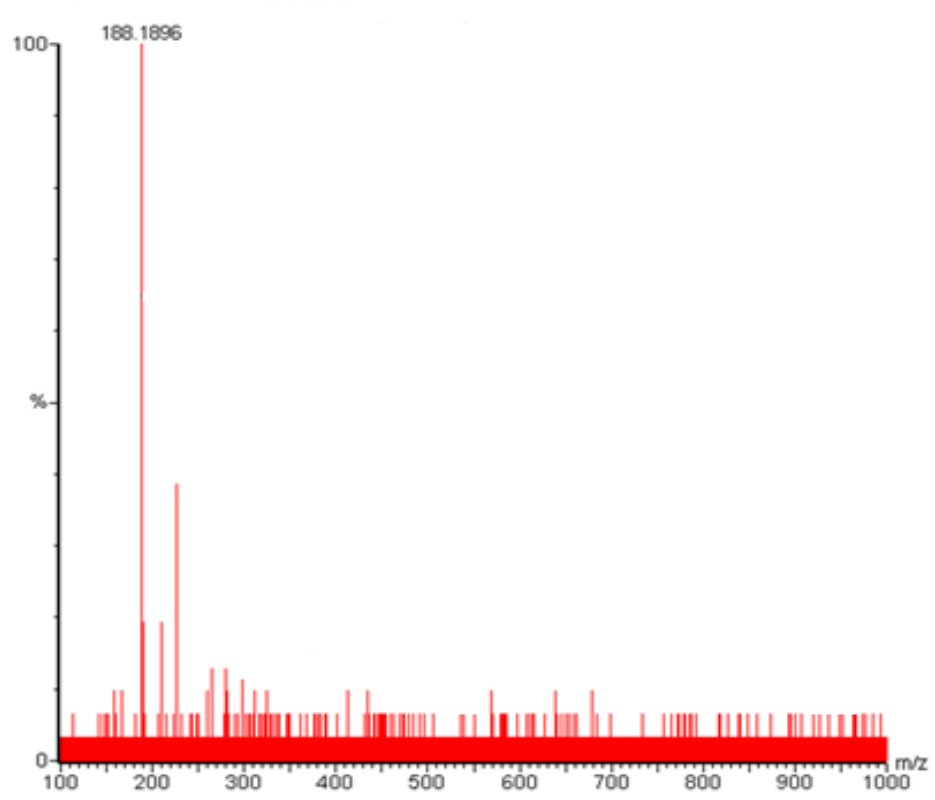

Figure 27. LC-MS mass spectrum of M_1G at retention time 5.05 min.

4.2. High Performance Liquid Chromatography Method Development

Using the pure M_1G standard, synthesised in Section 2.3.15., the HPLC separation method (reverse-phase) C(iv) (Section 2.3.14.1.) was optimised. The mobile phase additive that gave the greatest sensitivity with good peak separation was ammonium formate (50 mM, pH 5.4) compared to both acetic acid and formic acid which gave reduced sensitivity and increased peak overlap on both the PDA and FLD detectors. These additives were also chosen as they have suitable volatility for MS. The mobile phase combination that gave the optimum peak separation and greatest sensitivity for

M_1G detection was 75% 50 mM ammonium formate (pH 5.4) and 25% methanol. A 20 min isocratic run time with an additional 10 min gradient to 100% methanol and a further 10 min equilibration at the starting conditions gave the most consistent results with removal of residual analyte from the column.

The proportion of methanol at 25% gave the optimum sensitivity with sufficient retention times for peak separation, whereas lower proportions of methanol showed peak broadening and longer retention times and decreased sensitivity. Higher proportions of methanol resulted in overlap of guanine and M_1G peaks due to reduced retention times. Column B gave greater sensitivity than column A, with larger peak areas due to the narrower diameter of column B. The peak resolution ($R_{s)}$ values for the M_1G and guanine peaks in the M_1dG DNA standard were calculated for each column, as described in Section 2.3.14.1. Column A had an R_s value of 10.8, compared to column B, which had an R_s value of 2.21. Although peak resolution decreased with column B compared to column A, there was still baseline resolution ($R_s > 1.5$) and so column B was chosen for use in further analyses. The flow rate that gave the greatest sensitivity with Column B was 0.1 ml/min, however, this flow rate caused peak broadening so a higher flow rate of 0.2 ml/min was chosen for analysis of M_1G.

M_1G was detected using both FLD and PDA detectors. The excitation and emission wavelengths for detection by FLD were 360 nm and 500 nm respectively (Singh *et al.*, 2001). The wavelength chosen for detection by PDA was 254 nm as this is the standard wavelength for detection of purines, allowing for detection of guanine and adenine as well as M_1G (Rong *et al.*, 2015). DNA samples would contain high levels of purine bases

in relation to M_1G, for example 50 – 120 M_1G adducts per 10^8 nucleotides were detected by Chaudhary *et al.* (1994), of which approximately 50% of the 10^8 nucleotides would be purine bases according to Chargaff's rule (Elson and Chargaff, 1952). Therefore, it was necessary to detect guanine and adenine in order to ascertain whether they caused any interference in M_1G detection, and also to determine the purity of the M_1G standard. DNA samples and the M_1dG DNA standard were depurinated by acid hydrolyisis, so it was unnecessary to detect pyrimidine bases in addition to purines. An M_1dG DNA standard with M_1dG adduct levels of 21 pmol/µg DNA and 3 mg/ml DNA was used to determine the accuracy of the optimised methods of M_1G detection (Moore *et al.*, 2010). Chromatograms of guanine, pure M_1G standard and the M_1dG DNA standard are shown in Figure 28, using the optimised HPLC separation method. The data was acquired for 30 min, however, as all peaks eluted within the initial 5 min, only 5 min is represented on the chromatograms.

Using the optimised method for HPLC separation, retention times for guanine (A and B) were 1.6 min (PDA) and 1.7 min (FLD), and retention times for M_1G (C and D) were approximately 2.1 min (PDA) and 2.2 min (FLD), as shown in Figure 28. Adenine was detected by PDA and had a retention time of 1.8 min, however, it was not detected by FLD and would therefore not interfere with M_1G detection (data not shown). As the PDA peaks for guanine and M_1G (1.6 min and 2.1 min respectively) (Figure 28 E) are merged, adenine would be included in the peak overlap. Therefore, this PDA method would not be suitable for M_1G quantification, however, the aim was to use FLD.

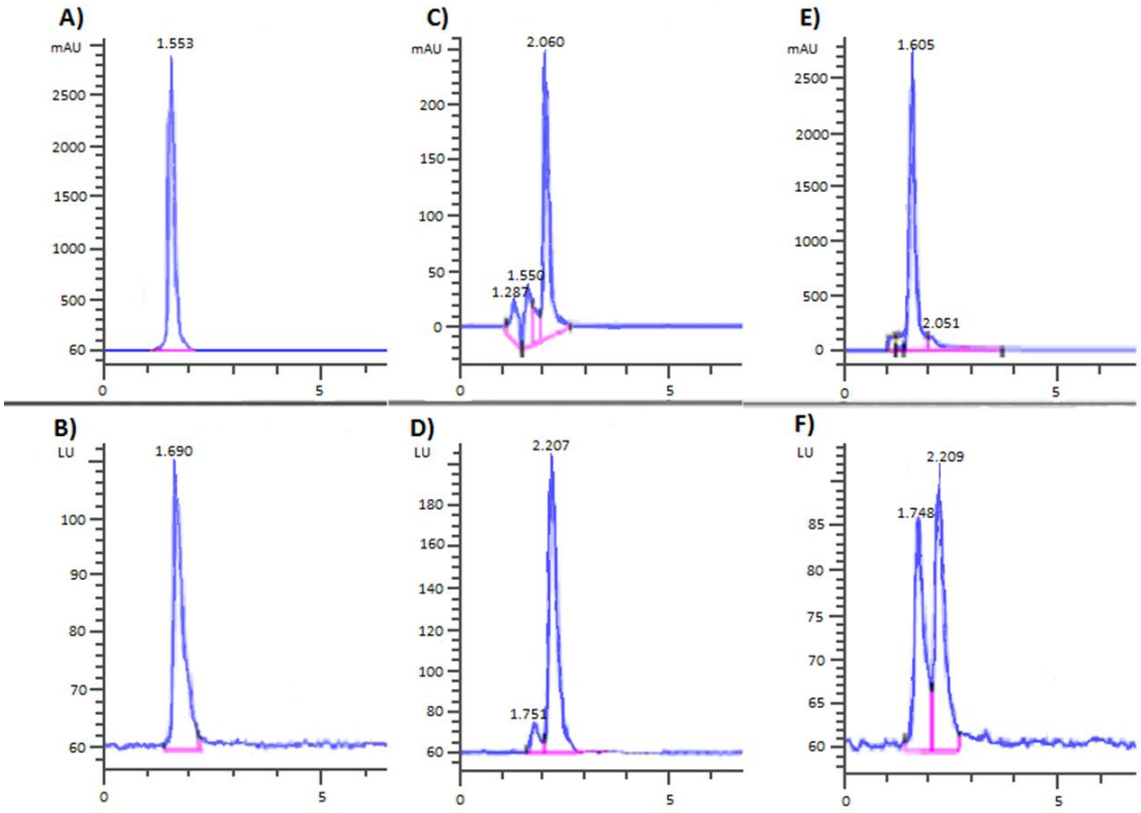

Figure 28. HPLC chromatograms with retention times for - guanine A) 1.553 min (PDA) and B) 1.690 min (FLD); pure M_1G standard - C) 2.060 min (PDA) and D) 2.207 min (FLD); and hydrolysed M_1dG DNA standard - E) 1.605 min (guanine) and 2.051 min (M_1G) (PDA) and F) 1.748 min (guanine) and 2.209 min (M_1G) (FLD).

The chromatograms in Figure 28 show minor peaks for guanine (C and D) at 1.6 min (PDA) and 1.8 min (FLD) in addition to the main M_1G peaks at 2.1 min (PDA) and 2.2 min (FLD), indicating that the M_1G standard was not 100% pure. The FLD chromatogram (Figure 28 F) of the M_1dG DNA standard showed resolution of guanine and M_1G, with a peak which corresponds to guanine at retention time 1.8 min in addition to the main peak for M_1G at 2.2 min. A peak for guanine was also detected by the PDA at 1.6 min alongside a small peak for M_1G at 2.1 min (Figure 28 E). However, as fluorescence detection is the best

method for quantitation of M_1G by HPLC compared with PDA, chromatogram F is representative of those used for M_1dG-DNA quantitation.

A standard curve was plotted using the mean FLD peak area (Figure 29). The calibration curve had a correlation coefficient R^2 value of 0.9995 demonstrating good linearity.

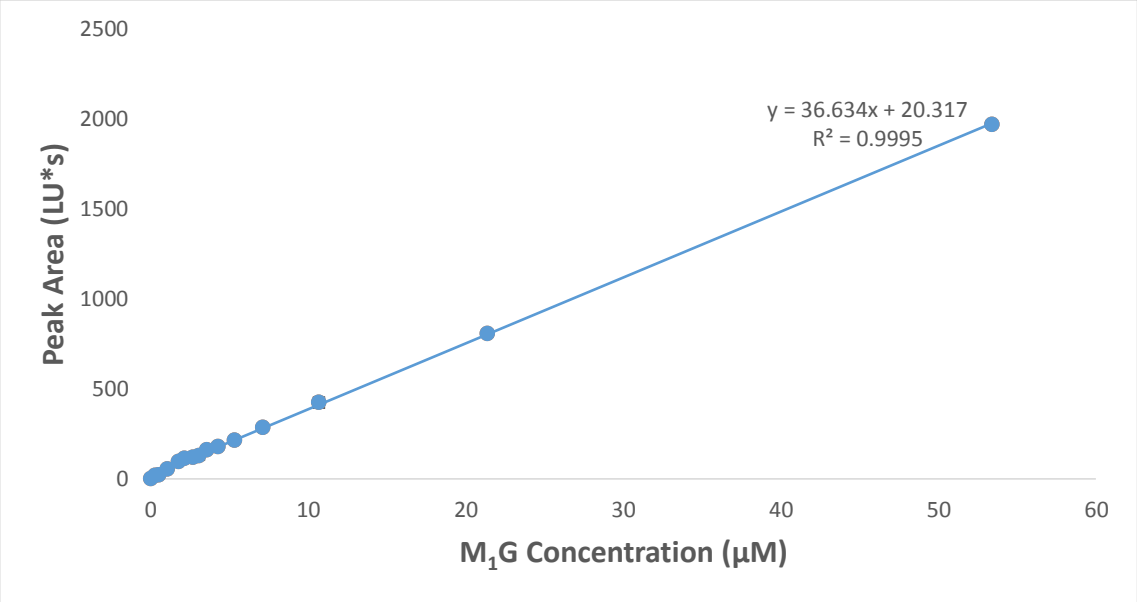

Figure 29. Standard curve 0 – 53.4 µM M_1G (retention time 2.21 min), analysed by HPLC-FLD at 360 nm excitation and 500 nm emission. Error bars (just shown) indicate ± 1SD from the mean.

As peaks corresponding to guanine had been detected in Figure 28 (C-F), the purity of the M_1G standard was assessed. The PDA detector was more sensitive for detection of guanine, however, as these peaks were poorly integrated by the software for peak area, with a large proportion of the area integrated below the baseline, the peaks were re-integrated manually and a standard curve of guanine was plotted against mean peak

area (Figure 30). The calibration curve had good linearity with a correlation coefficient R^2 value of 0.9999.

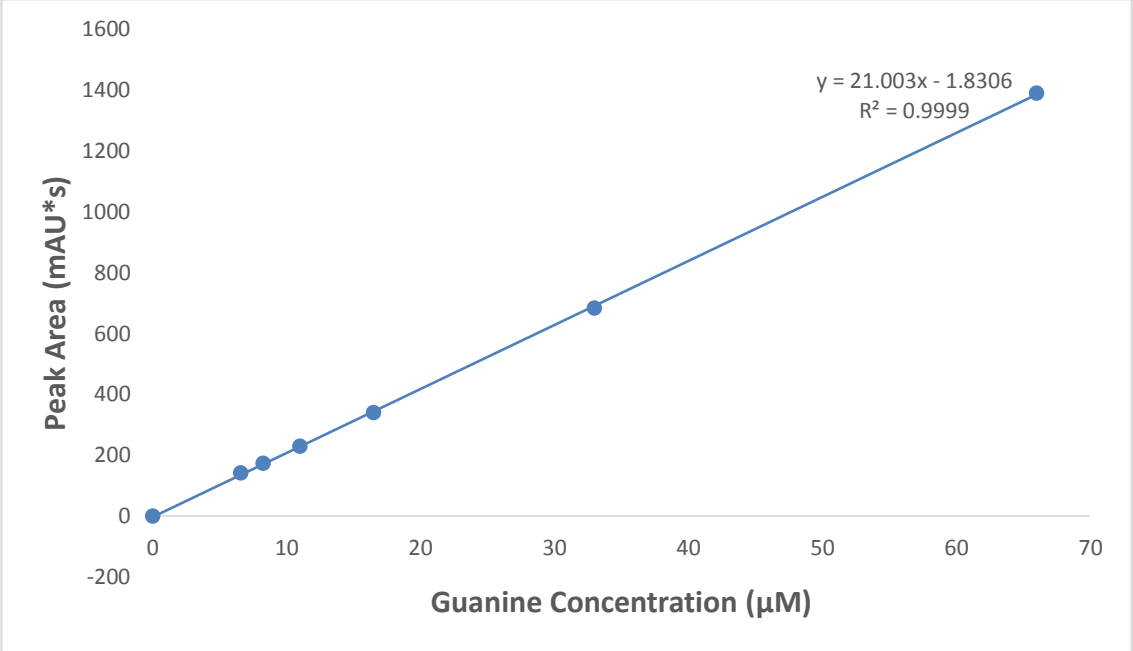

Figure 30. Standard curve of 0 – 66 µM guanine (retention time 1.55 min), analysed by HPLC-PDA at 254 nm. Error bars indicate ± 1SD from the mean.

To determine the purity of the M_1G standard with respect to guanine, the peak area of the guanine peak, detected by PDA, in the top M_1G standards were used to calculate the concentration of guanine in each standard using the guanine calibration curve equation in Figure 30:

- y = 21.003x- 1.8306, where x = guanine concentration (µM) and y = peak area (mAU*s)

The mass of guanine in each M_1G standard was calculated from the guanine concentration (x) and the mass of M_1G in each standard was calculated from the M_1G

concentration. The purity of the M_1G standard was then calculated using the following equation, using the calculated masses:

$$\%\ Purity = \frac{(Mass\ M_1G - Mass\ Guanine)}{Mass\ M_1G} \times 100\%$$

The purity of the M_1G standard was 75.6% using this method. However, overlap with M_1G was an issue as the PDA method was not optimised. An alternative method of assessing M_1G purity is by using the molar absorption coefficients (ε) of M_1G and guanine. The Beer-Lambert law was used to calculate the molar absorption coefficients:

$$A = \varepsilon cl$$

Where A is the absorbance, *c* is the concentration and *l* is the pathlength. For a graph of absorbance (or peak area) versus concentration, where the path length is 1 cm, the gradient is the molar absorption coefficient. A graph of the mean PDA peak area (mAU*s) versus 5.34 – 21.36 µM M_1G is shown in Figure 31 with the mean PDA peak area for guanine present in each of the M_1G standards.

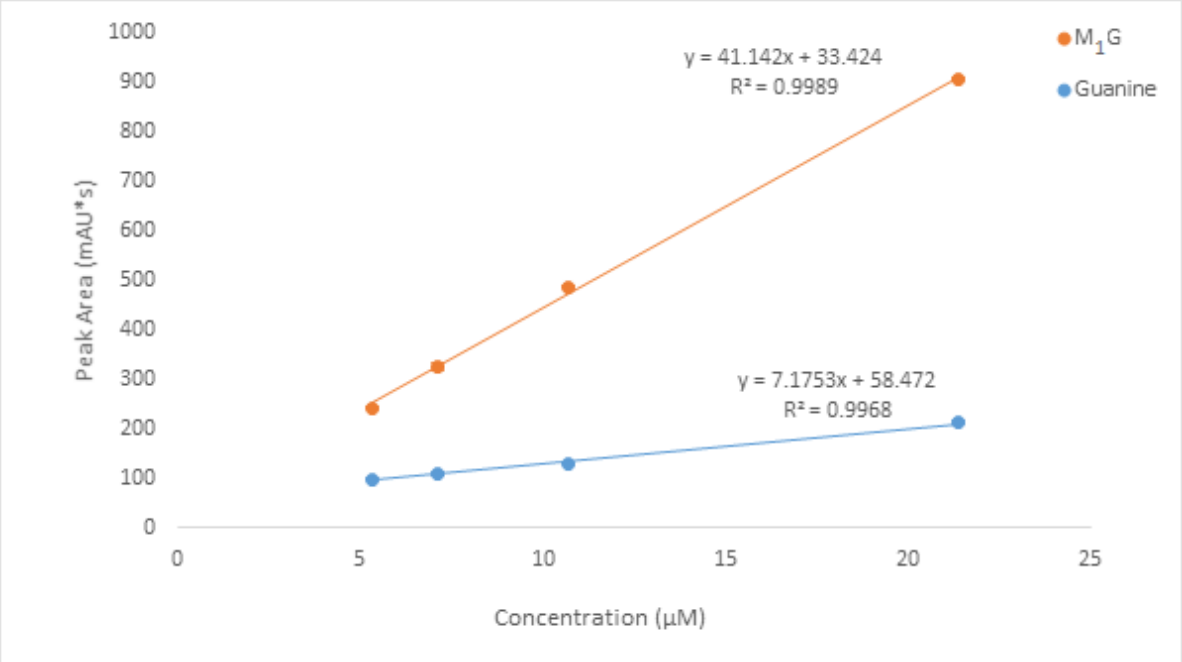

Figure 31. Standard curve of 5.34 – 21.36 µM M_1G, shown in orange (retention time 2.06 min), guanine impurities (retention time 1.64 min) are shown in blue, analysed by HPLC-PDA at 254 nm. Error bars indicate ± 1SD from the mean.

The gradient of the M_1G standard curve in Figure 31 is 41.142 mAU*s/µM and the gradient of the guanine impurities curve is 7.1753 mAU*s/µM. The purity of M_1G is calculated as follows:

$$\%\ Purity = \left[1 - \left(\frac{\varepsilon\ Guanine}{\varepsilon\ M_1G}\right)\right] \times 100\%$$

The purity of M_1G using the molar absorption coefficient method was calculated to be 82.6%. However, this method assumes that the gradients are correct and at M_1G concentrations below 5.34 µM, the gradient of the guanine impurities curve was close to zero, meaning that levels of guanine were almost constant for the M_1G standards below 5.34 µM, despite an increasing M_1G concentration. This is unexpected and

indicates that guanine formation could be occurring during analysis rather than being present in the pure standard. Taking into consideration the purity calculated by both methods at higher M_1G concentrations (>5.34 µM), it appears that the purity of the M_1G standard is in the region of 75.6 – 82.6%. Although this value was relatively low for a standard, it was anticipated that there would be some degradation of M_1G to guanine on storage and on the HPLC column and would thus have been of higher purity initially. Additionally, some of the M_1G would be present in its ring-open form, N^2OPdG, which eluted earlier then the ring-closed form and was not included in the peak areas for M_1G, suggesting that the level of guanine impurities calculated could be too high and the purity of the M_1G standard was greater than the 75.6 – 82.6% range calculated.

In order to validate the method, the M_1dG DNA standard was analysed using the optimised HPLC method. The old standard contained 21 pmol M_1G/µg DNA and, following DNA hydrolysis, was 0.5 mg/ml DNA. So:

- 0.5 mg/ml DNA = 0.5 µg/µl DNA
- 20 µl injection volume = 10 µg DNA

Therefore there were 210 pmoles M_1G/10 µg DNA i.e. total amount injected on to the column.

When analysed, the M_1dG DNA standard had a mean peak area of 521 LU*s (FLD), and using the calibration equation in Figure 29 to calculate the amount of M_1G in the M_1dG DNA standard:

- y = 3.634x + 20.317
- x = 13.67 µM M_1G = 13.67 pmol M_1G/µl
- 20 µl injection volume = 273.4 pmoles M_1G

Taking into account the 75.6 – 82.6% purity of the M_1G standard, the M_1dG DNA standard contained between 206.7 and 225.8 pmoles M_1G when analysed by this method. The M_1dG DNA standard had previously been analysed by Moore *et al.* (2010) confirming that there was 21 pmol M_1G/µg DNA. The difference in the amount analysed, mean 216.3 ± 9.6 pmoles M_1G, compared to 210 pmoles M_1G in the M_1dG DNA standard could be because the HPLC method had not been fully optimised for quantitative method validation and required further optimization prior to analysis of DNA samples. However, it is within acceptable experimental error when the standard deviation is taken into account. Additionally, there was some overlap of the M_1G peak (retention time 2.2 min) and the guanine peak (retention time 1.6 min) as shown in Figure 28 (F) and so the peak integration by the software will not have been accurate and the M_1G peak may have had a smaller peak area resulting in a reduction of the 273.4 pmoles M_1G to closer to the actual value of 210 pmoles M_1G. However, the aim was to produce a standard suitable for MS detection and the LC method would require further fine-tuning for LC-MS and LC-MS-MS analysis.

To summarize, following HPLC method development and optimization, the purity of the M_1G standard had been assessed and used to quantify an M_1dG DNA standard that had been made and analysed independently on different instruments. The results agree within 130% without taking the new M_1G standard purity into account. However, when

adjusting for a purity of 76 – 83%, then the standard values agree within 98 – 108%, which is within acceptable limits.

4.3. Mass Spectrometry Method Development

Following development of the HPLC method for M_1G analysis, the next step was to optimise the MS method, initially by LC-MS and then by LC-MS-MS prior to quantitative analysis of DNA samples.

The LC-MS method, described in Section 2.3.14.2., was further optimised by direct infusion of the M_1G standard on to the MS to determine the optimum cone voltage that gave the greatest peak intensities for the ions of interest. The optimum cone voltage was 50 V for ES+ mode m/z 152 for guanine and m/z 188 for M_1G, as at lower cone voltages, not enough ions were generated and higher cone voltages produced too much fragmentation with loss of the ions of interest. The data acquisition time was reduced from 30 min to 20 min as all of the eluents eluted in the initial 5 min (column A) or 2.5 min (column B). Greater MS peak intensities were achieved with the narrower column B than column A, thus column B was chosen for further analysis. A flow rate of 0.2 ml/min was used with this column as determined in Section 4.2.

Both guanine and the M_1G standard were analysed by LC-MS during LC-MS method optimisation, as shown in Figure 32. Guanine is shown in A – C, with a UV absorbance peak at 1.5 min and a RIC of m/z 152 a0074 1.8 min retention times. The mass spectrum

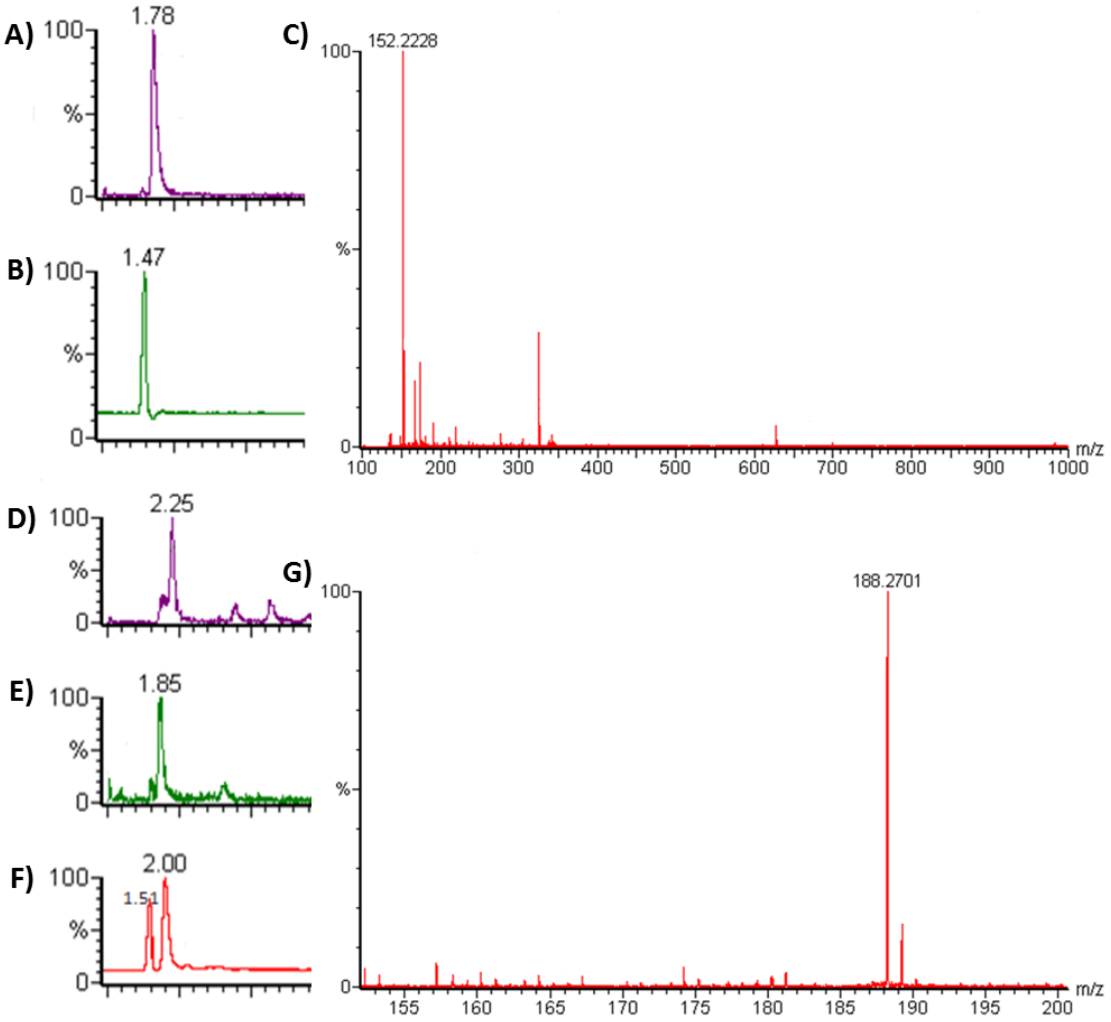

Figure 32. LC-MS chromatograms and mass spectra of guanine – A) RIC of m/z 152 for guanine, B) UV absorbance and C) mass spectrum of A; and M_1G standard – D) RIC of m/z 188 for M_1G, E) RIC of m/z 152 for guanine, F) UV absorbance retention times 1.51 min (guanine) and 2.00 min (M_1G) and G) mass spectrum of D for M_1G.

at 1.8 min shows an m/z of 152.2228, corresponding to guanine M_R 151.13 g/mol, with the addition of ~+1 by protonation of the parent ion (M) to give MH^+ as the MS was operated in ES^+ mode. The difference in retention times between UV and MS detectors was due to different lengths of tubing carrying the sample from the column to the detectors. The M_1G standard is shown in D-G, with UV absorbance peaks at retention

times 1.5 min for guanine and 2.0 min for M_1G. SIM of m/z 188 at retention time 2.3 min for M_1G and RIC of m/z 152 for guanine at retention time 1.9 min. The mass spectrum at 2.3 min shows an m/z of 188.2701, corresponding to M_1G (M_R 1.87.1582 g/mol). The relative intensities of the RIC of M_1G standard for m/z 152 (guanine) to m/z 188 (M_1G) (Figure 32, D-E) had a ratio of 0.208, which gives the M_1G standard a purity of 79.2% which is within the range previously calculated in Section 4.2., although assumes the same response per mass of analyte.

The final stage of HPLC and MS method development was LC-MS-MS, which involved fine-tuning of the methods previously optimised for M_1G analysis. The cone voltage optimised by LC-MS (50 V) was found to also be optimum for LC-MS-MS. The optimum collision energy required to fragment the precursor ion of M_1G into product ions was found to be 28 eV. The M_1G molecular (precursor) ion in ES^+ mode was m/z 188 and this fragmented into product ions m/z 79, 106, 133 and 160, as shown in Scheme 13. Szekely *et al.* (2008) used multi-stage MS/MS analysis of M_1dG in ES^+ mode with 26 eV collision energy by direct infusion. M_1dG has an m/z of 304 and neutral loss of the deoxyribose unit (116 Da) by collision induced dissociation occurred to give m/z 188 (M_1G), followed by loss of CO (28 Da) to m/z 160, followed by further loss of HCN (27 Da) to m/z 133. The two product fragments of m/z 188, m/z 160 and 133 were also detected by this research, as shown in Scheme 13. This research also produced two further product fragments, m/z 106 and m/z 79. Further loss of HCN (27 Da) from m/z 133 fragment gives the m/z 106 product fragment and subsequent loss of another HCN (27 Da) from m/z 106 leaves

product fragment m/z 79, which corresponds to a 6-membered ring and therefore the more stable of the product fragments.

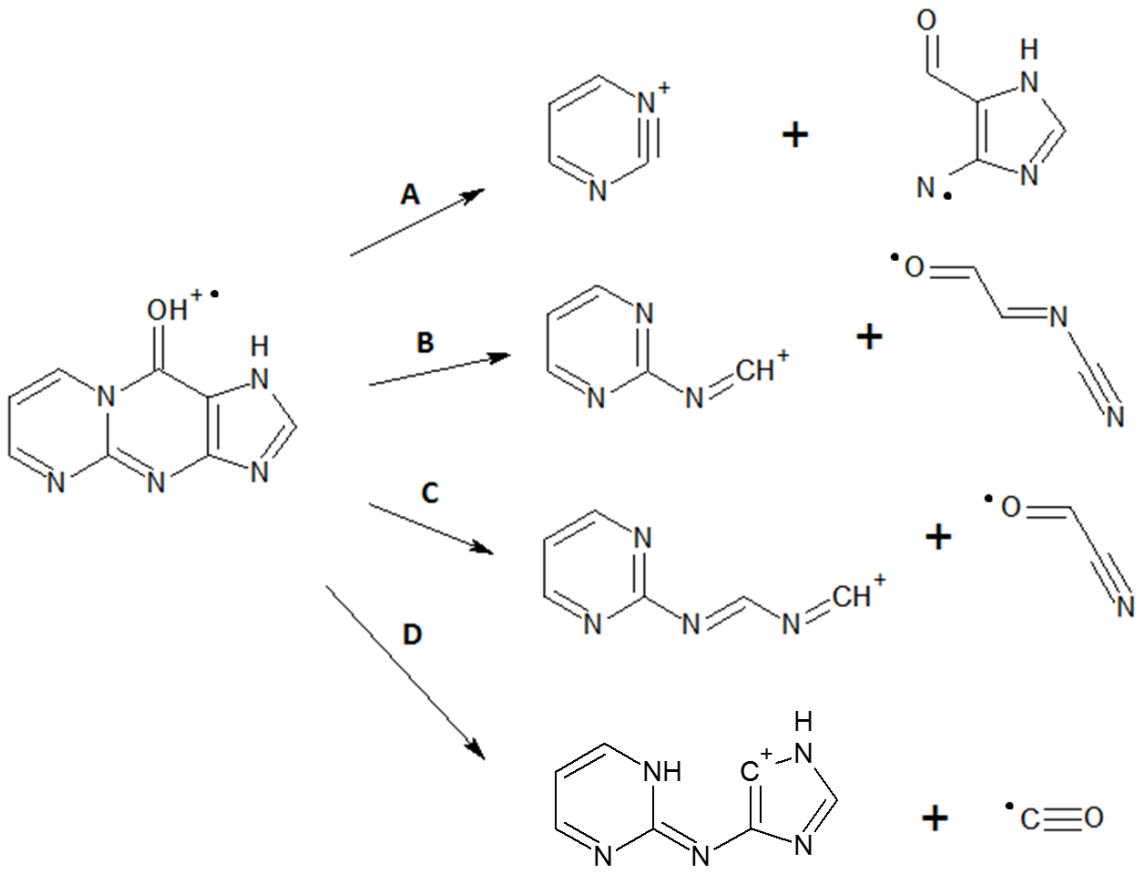

Scheme 13. LC-MS-MS fragmentation of M_1G in ES^+ mode (m/z 188) to product ions A) m/z 79 (plus 109 fragment), B) m/z 106 (plus 82 fragment), C) m/z 133 (plus 55 fragment), and D) m/z 160 (plus 28 fragment).

At 20 V collision energy, high levels of the molecular ion (MH^+) and low levels of product ions were achieved, indicating low fragmentation. However, the opposite occurred with 30 V collision energy with much lower MH^+ and higher levels of product ions. This collision energy was fine-tuned to 28 V. Next, the HPLC method was fine-tuned with a reduced run time of 10 minutes, as all eluents eluted within the initial 5 min. A blank sample (mobile phase only) was run in between samples to flush any remaining sample

from the column. The flow rate was also altered as there was some peak overlap between M_1G and guanine peaks by UV detection. Flow rates of 0.075 ml/min – 0.2 ml/min were tested and 0.15 m/min was found to be the optimum. Lower flow rates gave better peak separation, however, there was also reduced sensitivity. Although 0.2 ml/min gave the greatest sensitivity, a lower flow rate of 0.15 ml/min gave better peak separation with only a slight loss in sensitivity compared to lower flow rates.

Two scans were run concurrently by LC-MS-MS, a products of m/z 188 scan and an MRM scan. The products of m/z 188 scan, scanned for all product ions of MH^+ (m/z 188) resulting in a TIC chromatogram. The TIC data could then be processed using RIC to look for product ions of MH^+, such as m/z 79. The TIC or RIC data could be further analysed to look at the mass spectra of peaks of interest at any retention time. The four main product ions detected for M_1G were m/z 79, 106, 133 and 160, of these m/z 79 and 106 were chosen to analyse as they gave the greatest peak intensities. An MRM scan was also run of two reactions, scanning for m/z 188 to 79 and m/z 188 to 106 only.

M_1G standard (5.34 µM), guanine (66 µM) and adenine (66 µM) were analysed by the optimised LC-MS-MS method. The UV, MRM, TIC and RIC of product ions of M_1G are shown in Figure 33, along with the mass spectrum of product ions at retention time 2.9 min. An additional peak was seen on the UV chromatogram at 2.0 min which was also the only peak present when a blank containing mobile phase (50 mM ammonium formate (pH 5.4)) was run, and was absent when water only was run. This peak was therefore due to the mobile phase. A small peak corresponding to guanine (m/z 152)

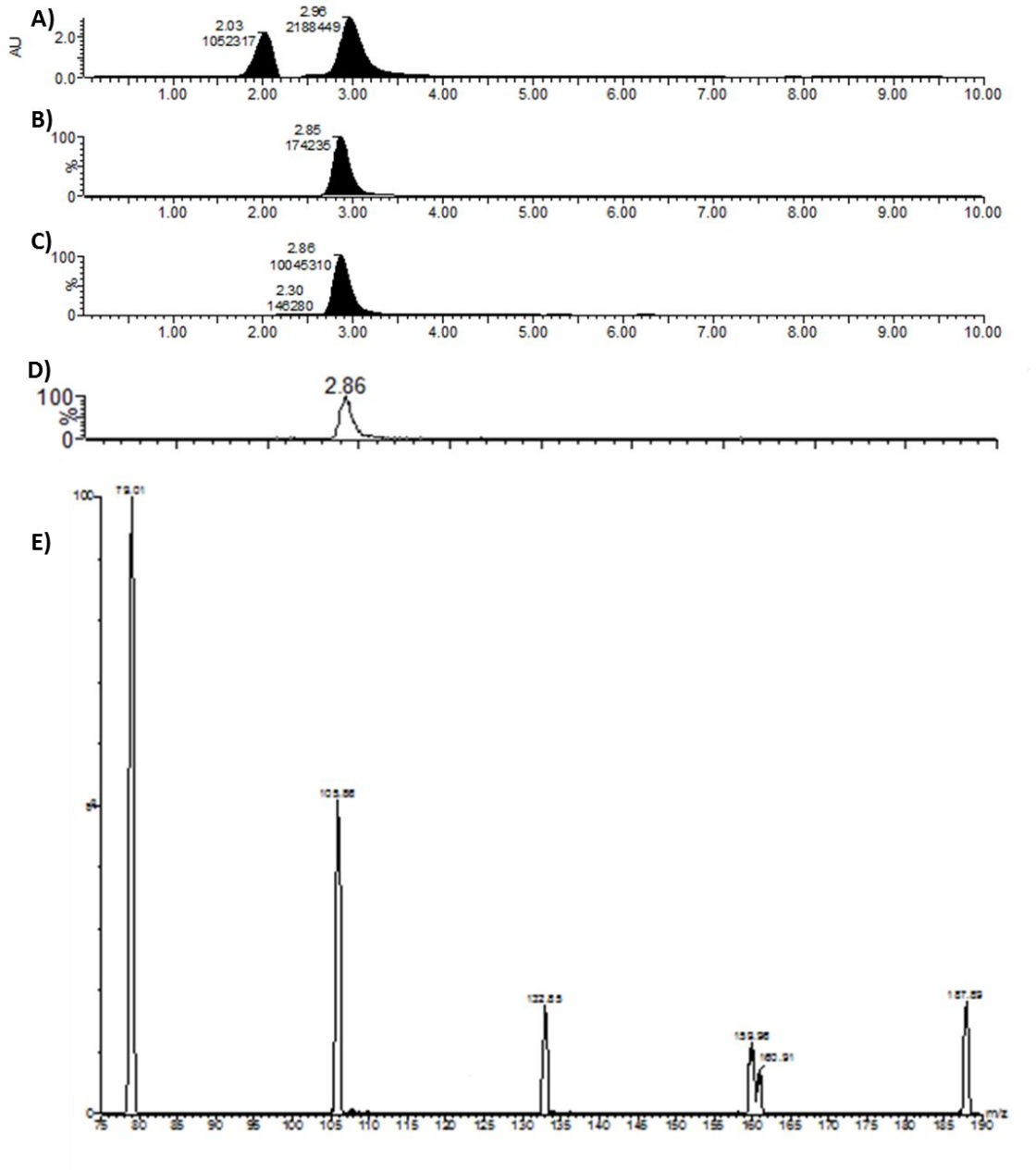

Figure 33. LC-MS-MS chromatograms and mass spectrum of 53.4 µM M_1G standard - A) UV chromatogram, retention times 2.03 min (mobile phase) and 2.96 min (M_1G), B) MRM chromatogram, retention time 2.85 min (M_1G), C) products of m/z 188 TIC chromatogram, retention time 2.86 min (M_1G) and 2.30 min (guanine), D) product ion (RIC) chromatogram from TIC, all the same for m/z 79, 106, 133, 160 and 188, retention time 2.86 min (M_1G), and E) Mass spectrum of product ion peak at 2.86 min, m/z peaks 79.01, 105.86, 132.85, 159.96 and 187.89.

was detected at 2.3 min on the TIC chromatogram Figure 33 C, the relative intensities of the guanine peak to the M_1G peak at 2.9 min gave a ratio of 0.0146, which corresponds to a purity of 98.6%, although this would assume the same response per mass of analyte.

This is a greater value for purity for the M_1G standard than previously calculated (Section 4.2), the M_1G peak in Figure 33 C was quite broad and may encompass the ring-open form of M_1G, N^2OPdG, which had previously not been included. The MS (Figure 33 E) shows the 4 main product ions and the molecular ion (m/z 188). The two ions with the greatest peak intensities were m/z 79 and 106 and were the ions chosen for further analysis of M_1G.

Guanine and adenine were also analysed by LC-MS-MS to determine if they caused any interference with M_1G detection by this method. In addition to the products of m/z 188 and MRM scans, a full scan by LC-MS was also carried out, which scans for all m/z within a specified range, m/z 70 – 1000 in this case. Figure 34 shows the products of m/z 188 scan UV chromatogram (A) and full scan (B-C) for guanine. Guanine eluted at 2.3 min and 2.3 min on the UV chromatograms for both the products of m/z 188 and full scans respectively. Guanine was not detected by the products of m/z 188 TIC scan or the MRM scan (not shown), but was detected by the full scan at 2.1 min (Figure 33 C). The MS (Figure 33 D) shows that the peak at 2.1 min had an m/z of 151.86, which corresponds to guanine. Adenine was not detected by MS for either LC-MS (full scan) or by LC-MS-MS, only by the UV detector for both scans, with a retention time of 2.7 min (data not shown). This peak was quite close to that of M_1G with regards to retention time,

however, as adenine was not detected by MS under these conditions, there would be no interference with M_1G detection.

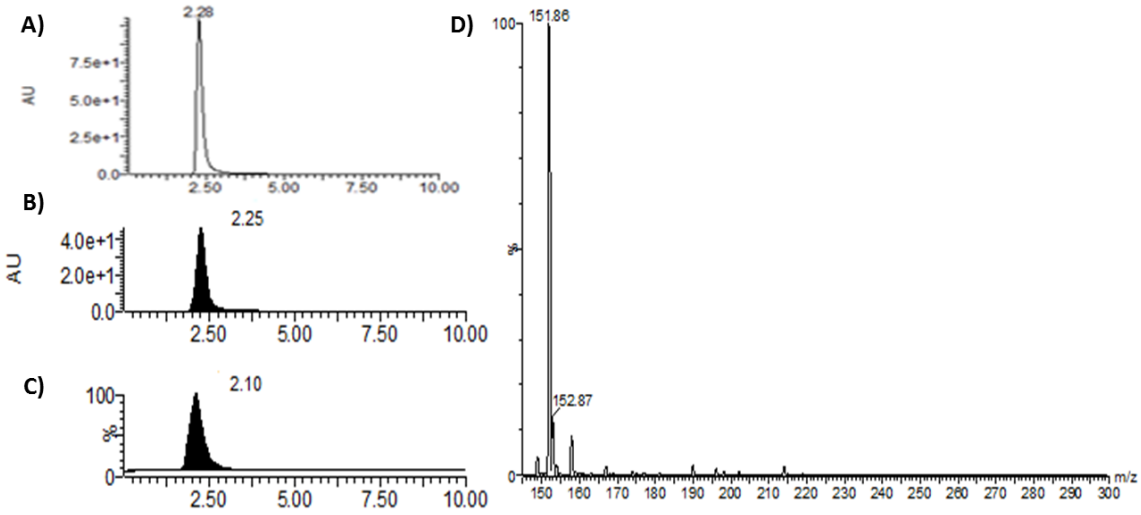

Figure 34. Products of m/z 188 and MRM (A) and full scan (B-C) chromatograms and mass spectrum (D) of 66 µM guanine – A) UV chromatogram, retention time 2.28 min, B) UV chromatogram, retention time 2.25 min, C) TIC scan, retention time 2.10 min, and D) mass spectrum of (C) at retention time 2.10 min, peak at m/z 151.86.

As guanine could be detected by LC-MS, but not LC-MS-MS, a M_1G standard was spiked with different amounts of guanine to determine if there was any interference with M_1G detection. Small differences could be seen in the peak intensities of the M_1G peak between the standards spiked with guanine and those not spiked, but not between those spiked with different amounts of guanine. The differences were < ±5% from the non-spiked M_1G standards and could be attributed to experimental and instrumental error.

A standard curve of M_1G, analysed by LC-MS-MS, was plotted of peak intensity (AU) versus M_1G concentration for product ions m/z 79 and 106 and MRM, as shown in Figure 35. All standard curves had good R^2 values (< 0.9833), with the MRM showing the best linear fit (0.9955). However, the curve for m/z 79 showed the steepest gradient. The MRM and m/z 106 curves were very similar.

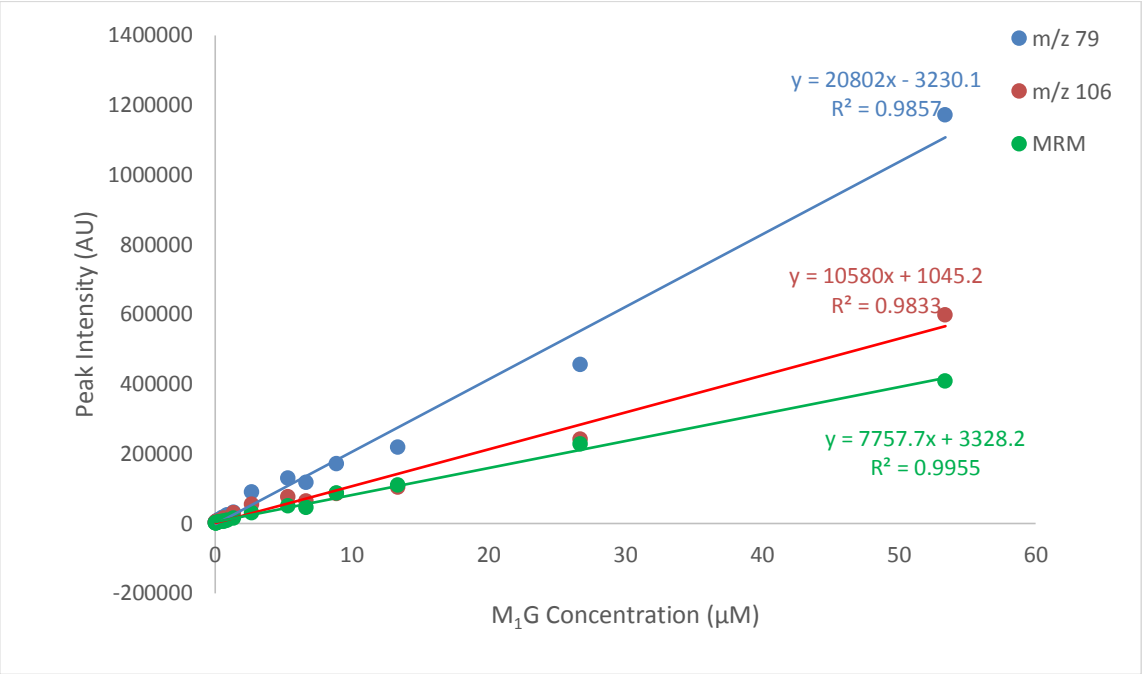

Figure 35. LC-MS-MS standard curves of 0 – 53.4 µM M_1G standard (retention time 2.85 min) product ions m/z 79 and 106 and MRM scan.

The M_1dG DNA standard was also analysed by LC-MS-MS, in order to validate the method. The UV, TIC, MRM and products of m/z 188 ion chromatograms are shown in Figure 36, as well at the MS of the M_1G peak at retention time 2.9 min on the TIC chromatogram (C), which shows the product ions of M_1G. The UV chromatogram (Figure 36 A) shows 3 peaks at 2.0 min for the mobile phase, 2.3 min for guanine and 2.8 min for M_1G. The MRM and TIC (Figure 36 B and C) chromatograms show peaks at 2.8 min

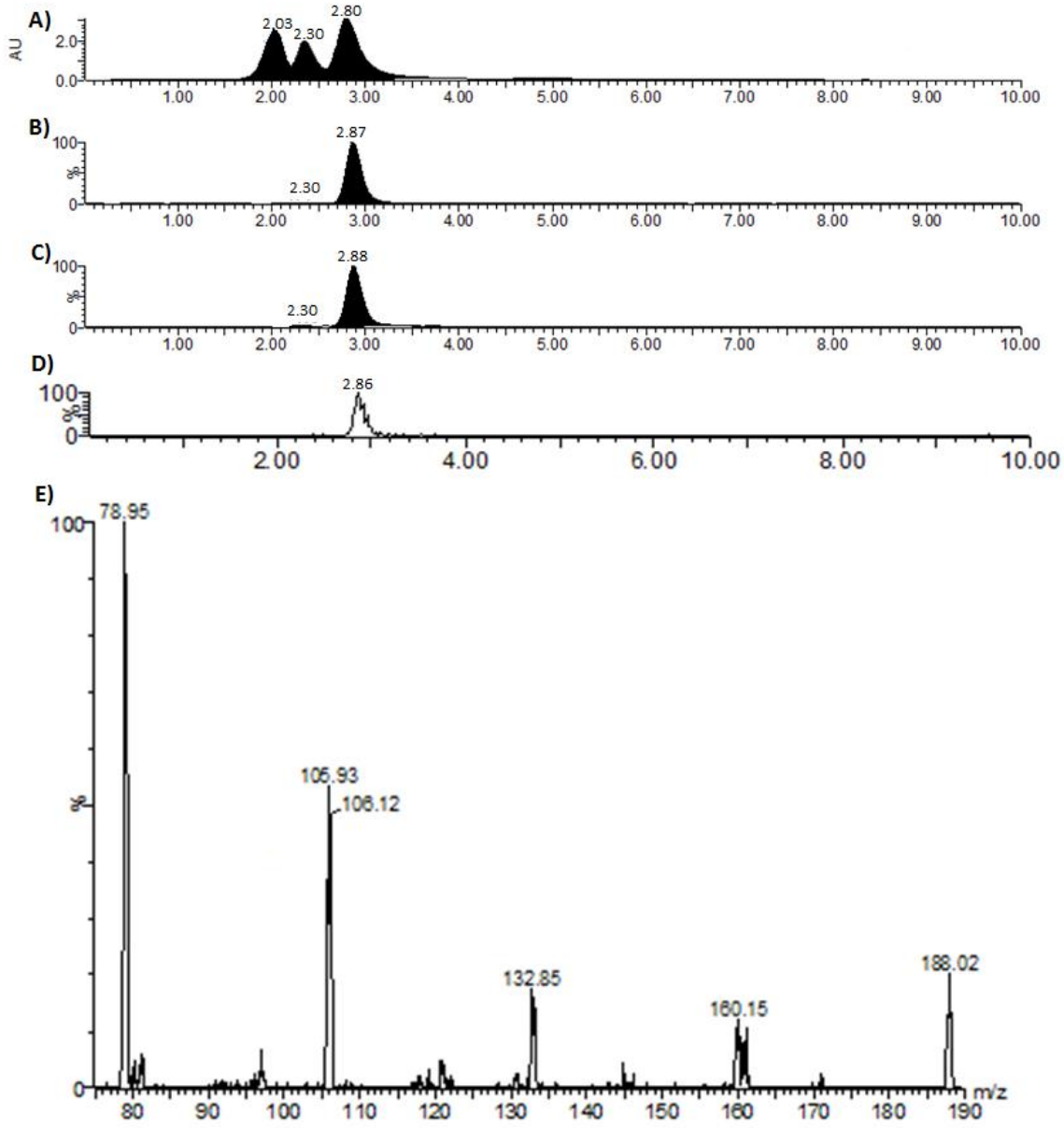

Figure 36. Products of m/z 188 and MRM LC-MS-MS chromatograms and mass spectrum of M_1dG DNA standard - A) UV chromatogram, retention times 2.03 min (mobile phase), 2.30 min (guanine) and 2.80 min (M_1G), B) MRM chromatogram, retention time 2.87 min (M_1G), C) TIC chromatogram, retention time 2.88 min (M_1G), D) product ion (RIC) chromatogram from TIC, all the same for m/z 79, 106, 133, 160 and 188, retention time 2.86 min (M_1G), and E) mass spectrum of product ion peak at 2.86 min, m/z peaks 78.95, 105.93, 132.85, 160.15 and 188.02.

and 2.9 min respectively for M_1G. The product ion (RIC) chromatogram (Figure 36 D) processed from the peak at 2.88 min on the TIC chromatogram was the same for all product ions of M_1G: m/z 79, 106, 133 and 160 as well at the molecular ion m/z 188.

The levels of M_1G adduct in the M_1dG DNA standard were calculated using the calibration equations of product ions m/z 79 and 106 and the MRM scan, as shown in Figure 35, in order to validate the detection method. The DNA standard contained 21 pmol M_1G/µg DNA and 3 mg/ml DNA, of which 30 µg DNA was used for analysis following acid hydrolysis, to quantify M_1G for method validation:

- 10 µl injection volume = 3 µg DNA
- Therefore there are 63 pmoles M_1G/3 µg DNA i.e. total amount on the column

When analysed, the M_1dG DNA standard had a peak intensity for product ion m/z 79 of 1.2 $x10^5$, and using the calibration equation in Figure 35 to calculate the amount of M_1G in the M_1dG DNA standard:

- y = 20802x – 3230.1
- x = 5.924 µM M_1G = 5.924 pmol M_1G/µl
- 10 µl injection volume = 59.24 pmoles M_1G
- 1 µg DNA = 19.75 pmoles M_1G = 94.03% of the DNA standard

The M_1dG DNA standard had a peak intensity for product ion m/z 106 of 6.41 $x10^4$, and using the calibration equation in Figure 35 to calculate the amount of M_1G in the M_1dG DNA standard:

- y = 10580x + 1045.2
- x = 5.959 µM M_1G = 5.959 pmol M_1G/µl
- 10 µl injection volume = 59.59 pmoles M_1G
- 1 µg DNA = 19.86 pmoles M_1G = 94.59% of the DNA standard

The M_1dG DNA standard had a peak intensity for the MRM scan of 3.94 $x10^4$, and using the calibration equation in Figure 35 to calculate the amount of M_1G in the M_1dG DNA standard:

- y = 7757.7x + 3328.2
- x = 4.649 µM M_1G = 4.649 pmol M_1G/µl
- 10 µl injection volume = 46.49 pmoles M_1G
- 1 µg DNA = 15.50 pmoles M_1G = 73.79% of the DNA standard

The amount of M_1G in the M_1dG DNA standard was comparable for both product ions m/z 79 and 106, however, the MRM scan gave a much lower amount due to reduced ion intensity.

LC-MS-MS had greater sensitivity for detection of the M_1dG DNA standard than HPLC (Section 4.2). Of the products of m/z 188 scan, the two product fragments that gave the greatest M_1G peak intensities were m/z 79 and m/z 106. Extraction of RIC data from the TIC for these two product fragments, gave the greatest sensitivity for detection of the M_1dG DNA standard, 94.03% and 94.59% of the M_1dG DNA standard respectively, which shows good reproducibility and is within the acceptable range of the true value. The

MRM scan of m/z 188 to 79 and m/z 188 to 106 gave a lower sensitivity than the two product fragments individually at 73.79% despite the combined ion intensities of the MRM scan, however the calibration curve for this scan of M_1G standard had a poor gradient. These scans were duplicated and gave similar results. The methods had been optimised further for the LC-MS-MS scans than for the HPLC in Section 4.2, which, along with the greater sensitivity, selectivity and accuracy of the instrumentation, may explain the differences in sample accuracy between the two instruments.

The LOQ of M_1G standard by LC-MS-MS was calculated by using the calibration line method, as described in Section 2.3.17.1., and shown in Table 14. The lowest LOQ was for m/z 79, and the closest peak on the calibration line to this was the peak at 0.267 µM M_1G. This peak had a % RSD value of 0.15%, which showed good peak precision.

Table 14. The LOD and LOQ of the M_1G standard by LC-MS-MS

Calibration Line	LOD		LOQ	
	M_1G (µM)	**M_1G (pg) in 10 µl injection**	**M_1G (µM)**	**M_1G (pg) in 10 µl injection**
m/z 79	0.09	169	0.273	511
m/z 106	0.278	520	0.841	1575
MRM	0.101	189	0.307	574

The LOD of M_1G standard by LC-MS-MS was calculated by using the calibration line method, as described in Section 2.3.17.1., and shown in Table 14. The lowest LOD was for m/z 79, with the closest peak on the calibration line corresponding to 0.089 µM M_1G

(164 pg M_1G in 10 µl injection volume). The lowest peak integrated on each calibration line was for 0.0356 µM M_1G, which corresponds to 67 pg M_1G in 10 µl injection volume.

4.4. Analysis of M_1G Adducts in DNA

DNA extracted from MRC5 and MRC5 SV2 cells and CT-DNA were treated with MDA and then precipitated and hydrolysed prior to analysis by LC-MS-MS. MRC5 and MRC5 SV2 cells were also treated with MDA and DNA was then extracted, precipitated and hydrolysed for analysis.

M_1G adducts in the DNA from the MRC5 and MRC5 SV2 cells treated and the DNA extracted and then treated were undetectable by this LC-MS-MS method and instrumentation. This may possibly be due to the low concentrations of DNA extracted from the cells and thus any M_1G present may have been below the LOD. Alternatively, cellular DNA repair mechanisms may have removed any adducts present in the DNA, possibly resulting in the formation of mutations. The elution buffer used in the DNA extraction protocol was pH 9.0, which would indicate the presence on the ring-open form of M_1dG, N^2OPdG (as previously described in Section 1.9.) (Knutson and Marnett, 2010). However, subsequent procedures, such as acid hydrolysis, would convert the ring-open form back to the ring-closed form, and hence should have been detected provided that the adduct concentration was above the LOD of the method. Other studies have used similar DNA extraction protocols for M_1dG adduct analysis (Leuratti *et al.*, 1998; Gottschalg, 2002), and is thus not thought to affect adduct levels.

The MRC5 and MRC5 SV2 DNA samples were also analysed independently by Lieslot Hemeryck and Dr Lynn Vanhaecke of Ghent University, Belgium. No M_1G was observed in the MRC5 and MRC5 SV2 DNA treated post-extraction from the cells (data not shown). However, they were able to observe very low levels of M_1G in DNA samples from cells treated with MDA. The levels detected were around the LOD and were therefore not quantifiable and were inconsistent, and it was not clear if these were method artefacts at this low level.

M_1G adducts were detected in the CT-DNA samples, the UV, TIC, MRM and products of m/z 188 chromatograms are shown in Figure 37, with the MS of the TIC (C) peak at 2.9 min retention time, which shows the 4 product ions of M_1G (m/z 79, 106, 133 and 160) and the molecular ion m/z 188. The UV chromatogram (Figure 37, A) shows a broad peak at 2.4 min for guanine, with a shoulder to the left, merging with the peak for the mobile phase (2.0 min previously). A peak at 2.8 min corresponds to M_1G. The MRM peak (Figure 37, B) at 2.9 min also indicates M_1G and the product ion (RIC) chromatogram (Figure 37, D) is representative of all of the chromatograms for the product ions of M_1G, m/z 79, 106, 133 and 160. This data is very similar to that of the M_1G standard, as shown in Figure 33, and the M_1dG DNA standard, as shown in Figure 36.

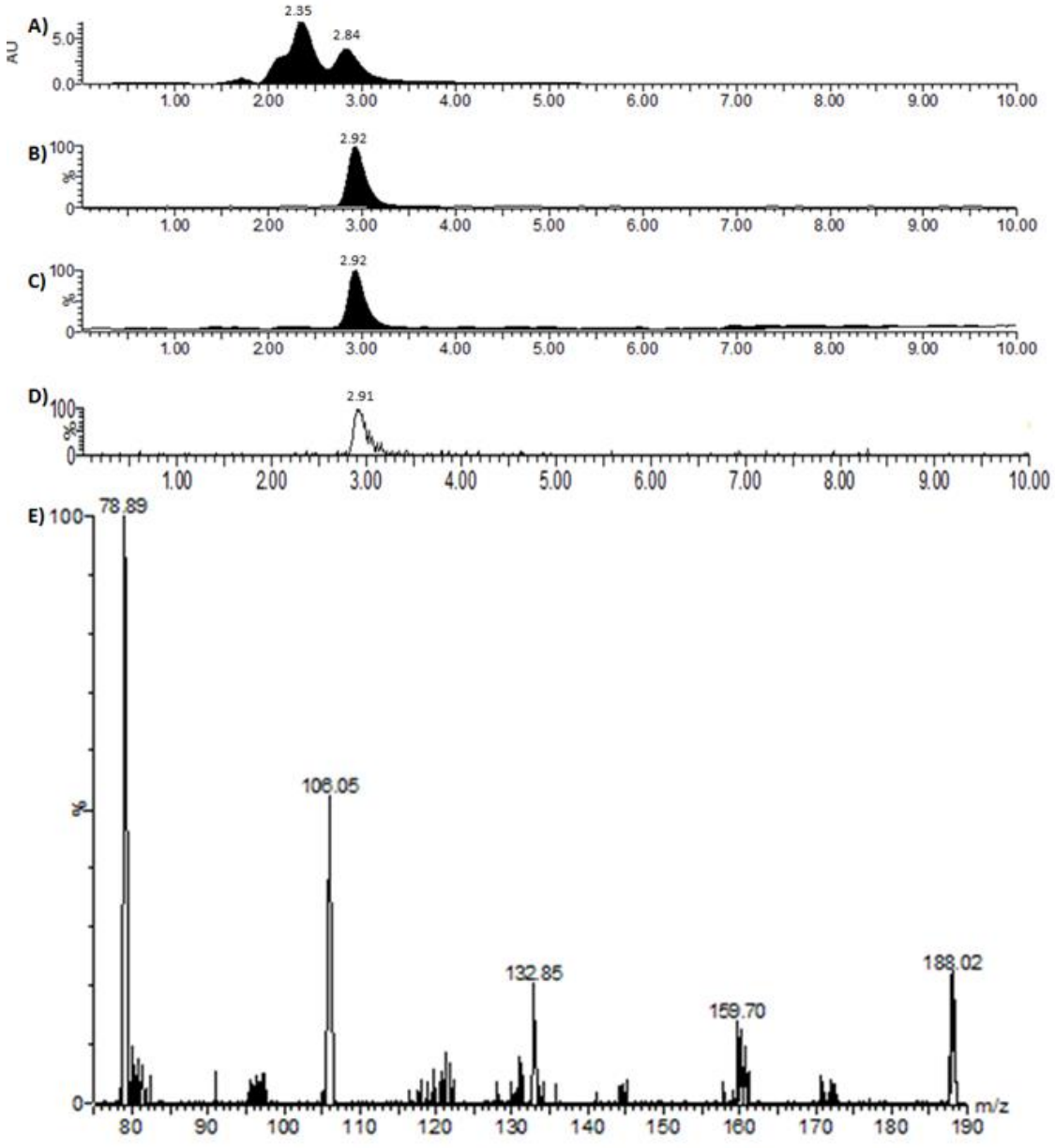

Figure 37. Products of m/z 188 and MRM LC-MS-MS chromatograms and mass spectrum of CT-DNA treated with 50 mM MDA - A) UV chromatogram, retention time 2.35 min (guanine) and 2.84 min (M_1G), B) MRM chromatogram, retention time 2.92 min (M_1G), C) TIC chromatogram, retention time 2.92 min (M_1G), D) product ion chromatogram from TIC, all the same for m/z 79, 106, 133, 160 and 188, retention time 2.91 min (M_1G), and E) mass spectrum of product ion peak at 2.86 min, m/z peaks 78.89, 106.05, 132.85, 159.70 and 188.02.

The peak intensities of product ions of M_1G m/z 79 and 106 (chosen as they gave the greater peak intensities) were measured for CT-DNA treated with MDA and the M_1G concentration in each sample was calculated using the equations from the calibration curves in Figure 35. A chart of M_1G concentration versus the MDA concentration was plotted using both product ions and is shown in Figure 38. For both product ions, the concentration of M_1G increases with the concentration of MDA, although the concentration is slightly lower for m/z 106 than m/z 79. For m/z 79, there was a low concentration (0.16 µM) M_1G adducts in untreated DNA, which is also often found for many adducts, however this is below the LOQ and just above the LOD, as shown in Table 14. For m/z 106, the untreated DNA and the DNA treated with 0.01 mM MDA have low negative values, -0.09 and -0.06 µM M_1G. The levels of M_1G detected for m/z 79 were below the LOQ for < 1 mM MDA, but all MDA concentrations were greater than the LOD. For m/z 106, the levels of M_1G detected were below the LOD for < 1 mM MDA, and above the LOQ for $\geq$ 10 mM MDA. This means that the levels of M_1G detected at the lower MDA concentrations were less reliable than for higher concentration, particularly for m/z 106, however, a clear pattern can be seen whereby levels of M_1G increased with increasing MDA concentration.

Treatment with the highest concentration of MDA (50 mM) results in 1.95 µM and 1.74 µM M_1G adducts for m/z 79 and 106 respectively, which corresponds to 0.39 pmol/µg DNA and 0.35 pmol/µg DNA respectively (or 1205 adducts per 10^7 nucleotides and 1077 adducts per 10^7 nucleotides, respectively). However, the MDA solution used here was only verified, in Section 3.1., up to 10 mM by HPLC with DNP

derivatisation, where at this concentration, an additional small peak was observed, indicating potential polymerization of MDA (Gutteridge *et al.*, 1977) which would reduce the effective dose of MDA. Thus, it only appears to be possible to detect any effect from ~ 0.1 mM MDA upwards, although this does appear to be a dose-response relationship.

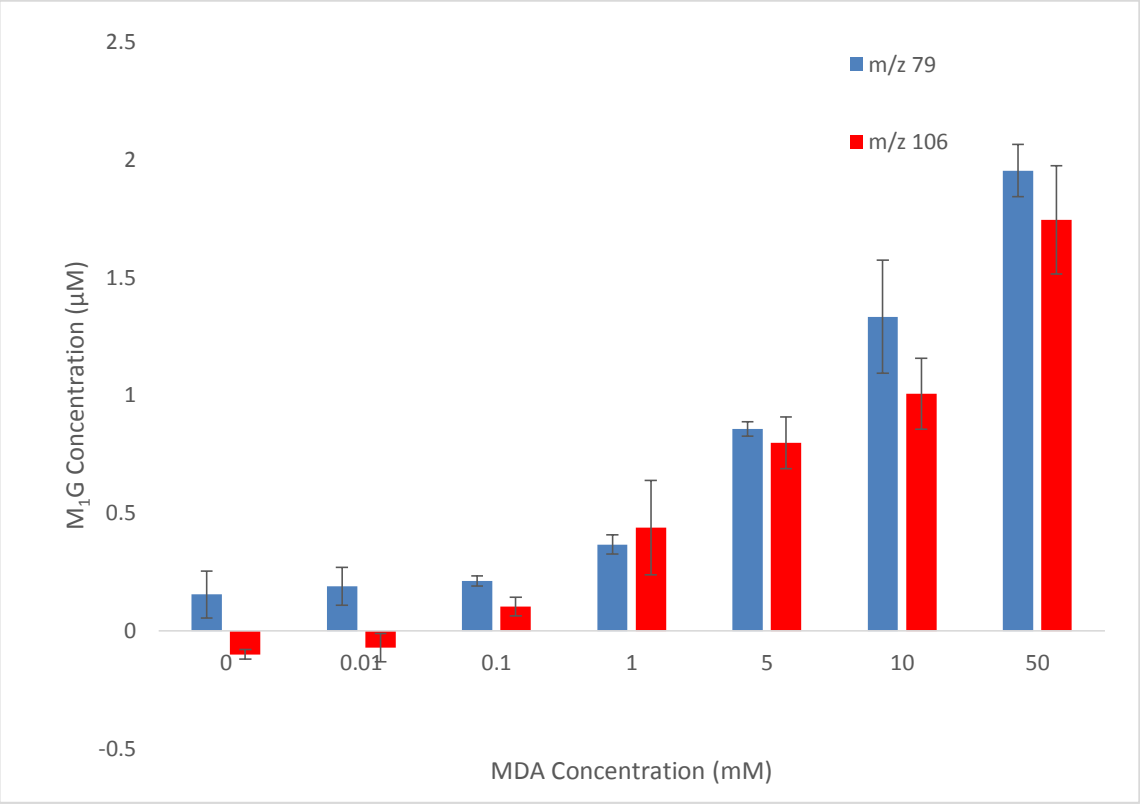

Figure 38. M_1G concentration in CT-DNA treated with 0 – 50 mM MDA for product ions of M_1G - m/z 79 and 106. Error bars show ±1 SD from the mean.

ISB was carried out as previously described Moore *et al.* (2010) (data not shown). Adducts were not detectable by ISB for the cell samples, which corroborates with the LC-MS-MS data here, indicating that cellular responses, such as DNA repair mechanisms, could be occurring. Treatment with MDA alone resulted in a dose-response relationship as expected for the CT-DNA samples, however, only DNA was involved and no cellular

responses could have repaired these adducts. Similar effects have been seen in previous studies with HT29 cell, which also showed that there was no correlation between MDA concentration and adduct levels (unpublished data) (Gottschalg, 2002).

4.5. Summary

A method of M_1G adduct detection has been developed and validated using a M_1dG DNA standard that had been made previously Moore *et al.* (2010). The standard had been analysed by independent methods and the value obtained by LC-MS-MS here was 94.03% of that expected, showing that the standard was of a high purity and this method has given good accuracy.

M_1G adducts in DNA from the MRC5 and MRC5 SV2 cells treated and the DNA extracted and then treated were undetectable by this LC-MS-MS method and instrumentation. However, the DNA concentrations were very low for the DNA from treated cells, and for MRC5 and MRC5 SV2 DNA treated post-extraction. Increasing the yield of DNA from the cells may allow for detection of M_1G adducts by this method and instrumentation, however, there would be cell culture issues with increasing the yield sufficiently as large numbers of cells would have to be cultured. Analysis elsewhere and by the ISB, which uses a lot less DNA (1 μg), also showed no quantifiable adducts. Instrumentation with much greater sensitivity may aid future quantification of adducts in cellular DNA. M_1G adducts have been quantified in CT-DNA, although with a relatively high concentration of DNA compared to MRC5 and MRC5 SV2 DNA.

MDA has been found to have an effect on MRC5 and MRC5 SV2 cells at the cellular level, as previously described in Chapter 3, with reduced cell proliferation and viability, alteration to cell and nuclear morphology, increased apoptosis and p53 expression. However, M_1dG adducts were undetectable in these cells by LC-MS-MS. Other than the possible reasons mentioned above, DNA repair mechanisms in the cell, such as NER (Marnett, 1999), may act to remove M_1dG adducts from DNA, and the M_1dG adduct is subsequently metabolised to 6-oxo-M_1dG and 2,6-oxo-M_1dG (Knutson *et al.*, 2007) for excretion. MDA has also been found to form protein adducts (Agarwal and Draper, 1992), and must encounter an array of proteins, such as actin, in the cell cytosol and nucleus prior to reaching the DNA, and thus may be sequestered as protein-MDA adducts, reducing the effective dose of MDA reacting with DNA. MDA also reacts with its own degradation product, acetaldehyde, and the amino group of proteins to form MDA-acetaldehyde-protein adducts (Tuma *et al.*, 2001). This may explain why M_1dG adducts were detected in CT-DNA and not DNA extracted from cells treated with MDA.

While analysis and quantification of M_1G adducts by LC-MS is useful as it can relate the treatment of samples of cells or DNA with a particular substance to the effect on the levels of adducts, it does not give any indication as to the effects at the DNA level due to adduct formation. It also requires very costly instrumentation for analysis, particularly for the levels of sensitivity required if biological samples were to be analysed, whereas other methods of adduct detection can be much less expensive, for example, analysis of DNA by mutation sequencing which shows the long-term effects upon DNA rather than just adducts which may be repaired or of no consequence to the cell.

CHAPTER 5

EFFECT OF MALONDIALDEHYDE ON DNA

This chapter details the effect of treatment with MDA on DNA. DNA extracted from MRC5 and MRC5 SV2 cells, treated *in vitro* with MDA, was subject to imaging by AFM and mutation sequencing of residues 4640-5328 (encompassing exon 1) of the human *TP53* gene (GenBank accession NG_017013.2). The effects of MDA on DNA topography and on DNA sequence are presented here.

5.1. Imaging of DNA by Atomic Force Microscopy

To image the effect that treatment of cells with MDA on DNA topography, AFM was utilized following immobilization of DNA on mica discs, as described in Section 2. 3.13.2. Initially, as negative controls, images were taken of the mica only and of the TE buffer that the DNA samples were diluted in, shown in Figure 39, to demonstrate the appearance of the mica without DNA attached. In Figure 39, the mica in A was approximately 0.4 nm in height, whereas the small round 'blobs' in B were most likely formed from crystals of TE buffer and were approximately 4 nm in height. The two images show that there was no DNA contamination on either the mica or in the TE buffer used.

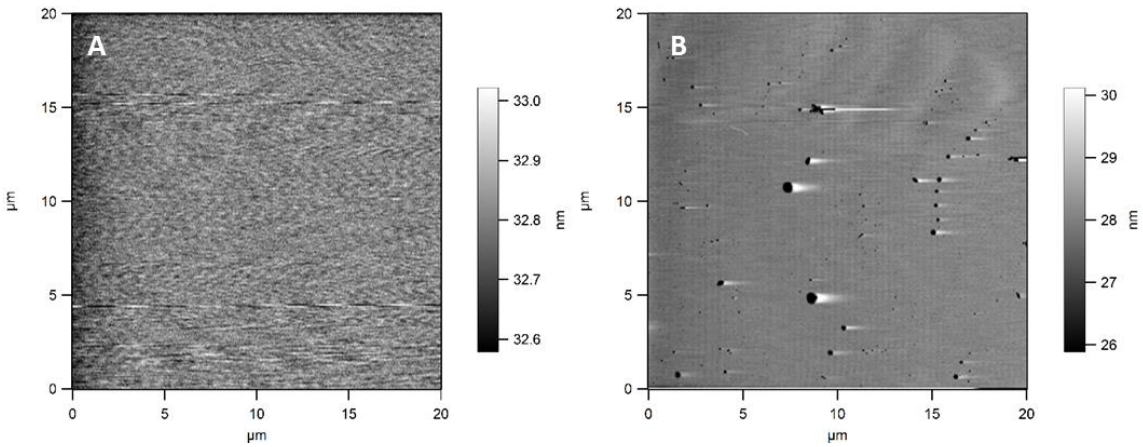

Figure 39. AFM images of A) mica only and B) TE buffer.

5.1.1. Effect of MDA on DNA Topography

The effect of treatment of cells with MDA can be seen in Figure 40 where the DNA from untreated cells was adsorbed on to the mica surface in long, double-stranded networks, and was similar for both the MRC5 and MRC5 SV2 cell lines, although the images differ in size. Whereas following treatment of cells with MDA (100-1000 µM), the DNA networks were more fragmented with increasing MDA concentration and treatment time, indicating DNA damage due to MDA treatment. The images shown in Figure 40 are representative of those from a number of samples (n = 3). The untreated controls and treatment with low concentrations of MDA (10 – 100 µM) gave similar images repeatedly, however with further increases in MDA concentration, images were difficult to obtain due to increased fragmentation and/or the clumping together of DNA making it difficult to locate areas of damaged DNA. Although images were taken for both 24 and 48 h, only images for 48 h MDA treatment are shown.

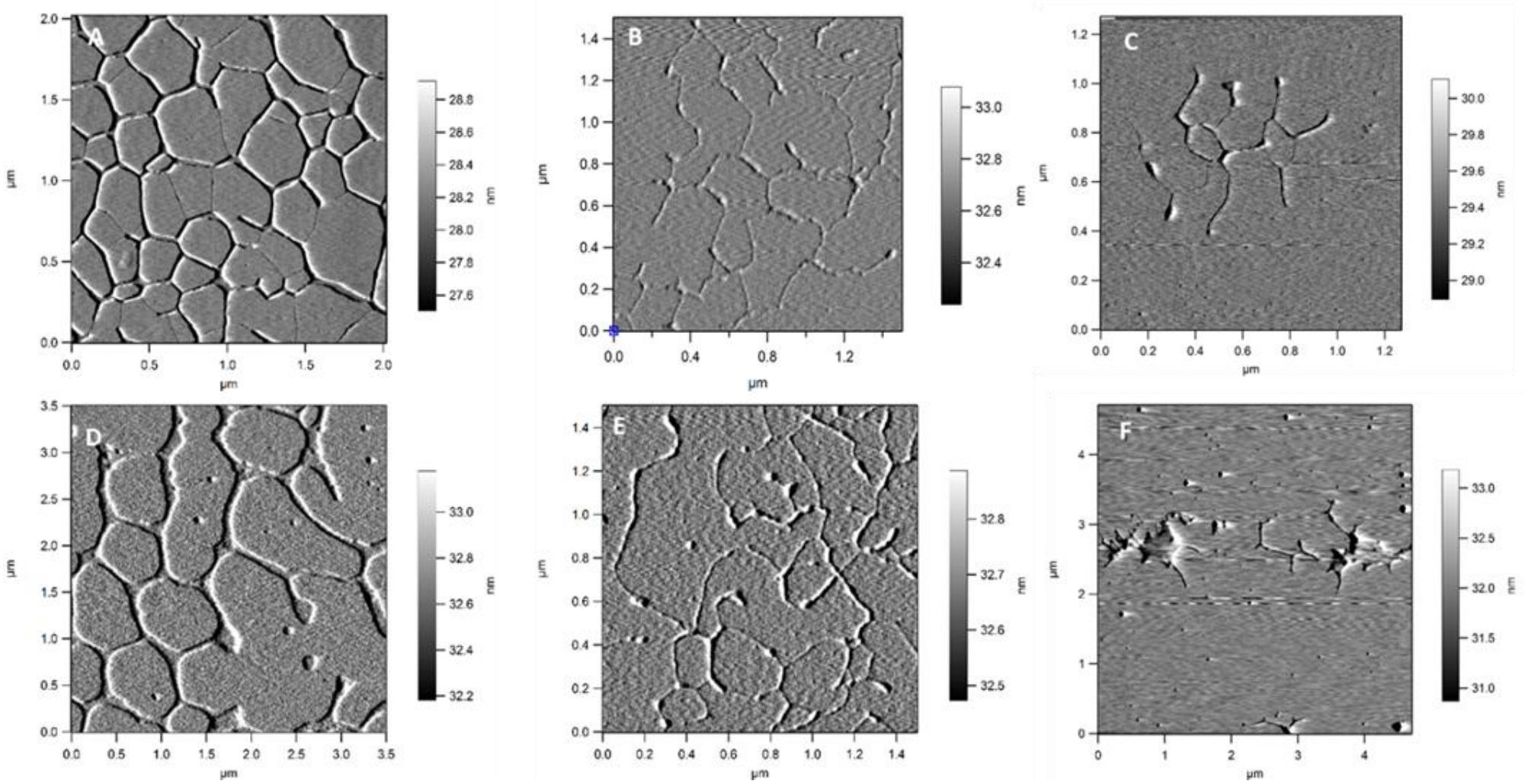

Figure 40. AFM images of DNA extracted from MRC5 (A-C) and MRC5 SV2 (D-F) cells treated for 48 h: A&D untreated, B&E) 100 µM MDA and C&F) 1000 µM MDA, immobilized on mica.

This increased DNA fragmentation due to treatment with genotoxic compounds has been observed previously. Liu *et al.* (2010) looked at DNA-cisplatin interactions by AFM and found that the appearance of DNA changed with increasing cisplatin concentration, from extended chains to bending structures, worm-like structures and flat particles, with longer DNA fragments (~48 kbp) forming loop structures. BPDE has been shown to induce the formation of DNA adducts. When using AFM in tapping mode to image the treated DNA, 30° bends were observed at the adduct sites (Pietrasanta *et al.*, 2000). It has been recently suggested that DNA dynamics rather than static DNA structure is important in gene expression control. Using high speed AFM in tapping mode, RNA polymerase has been shown moving along DNA strands by time-lapse AFM (Lyubchenko, 2011). Thus, AFM enables visualisation of DNA in an environment that may reveal its biological conformation.

The height along the length of the DNA molecules was measured, shown in Figure 41. The height varied along the length of the DNA molecule in peaks and troughs. For MRC5, the height decreased from 1.6 nm to 0.6 nm, over a 140 nm length. For MRC5 SV2, over the same distance, the height alternated between 1.0 nm and 0.4 nm with many more peaks and troughs than MRC5 DNA, although this difference may be due to differences in image size. The height profiles were representatives of a number taken for each cell line (n = 3), however, as the images are not the same size, comparison of DNA height profiles between the two cell lines cannot be quantified. The differences in height (peaks and troughs) along the length of the DNA strands maybe due to the major and minor grooves of DNA. The average diameter of double stranded DNA (B-form) is 2 nm, the height of the DNA measured in Figure 41 is less than this which could be due to the DNA

becoming flattened due to adsorption on to the mica, and no hydrogen bonds due to dehydration, meaning that the tertiary structure of the DNA molecule collapses and is therefore not the same as *in vivo* (Klinov *et al.*, 2003).

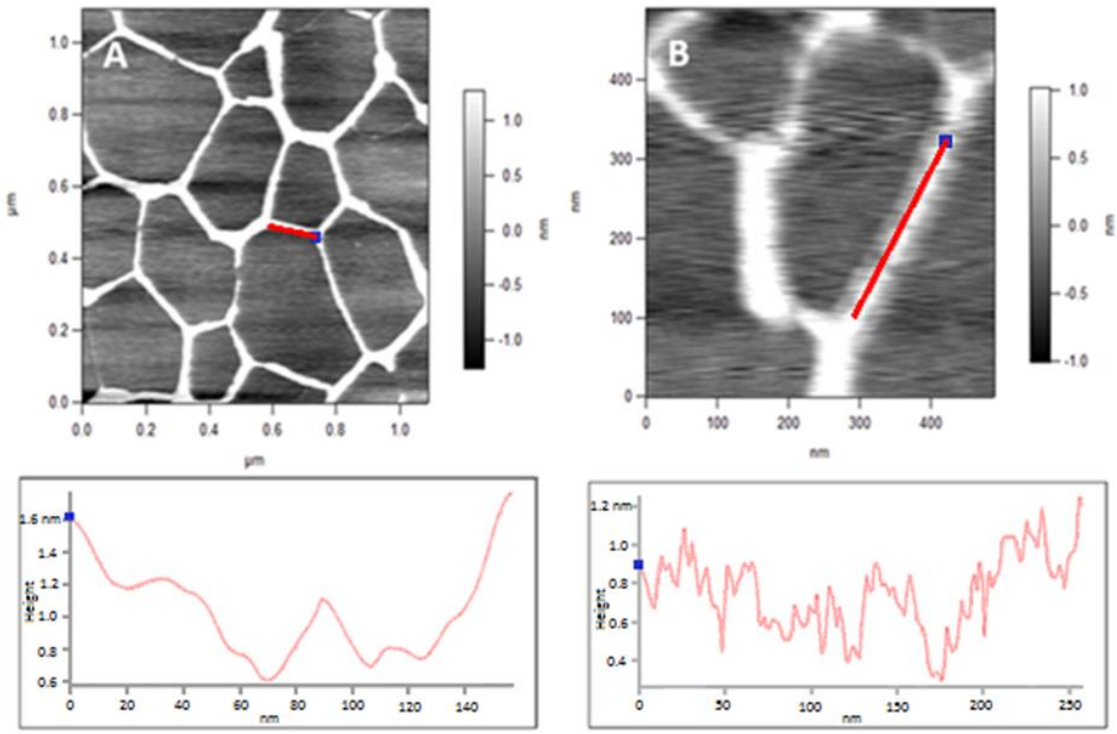

Figure 41. AFM images of DNA extracted from untreated A) MRC5 cells and B) MRC5 SV2 cells, immobilized on mica. The height along the DNA molecule is shown beneath each image.

The heights along the DNA strands, as shown in Figure 41, were measured in order to show what the height profile looked like before the addition of M_1dG primary antibodies in the following section. This was to determine whether the antibody-DNA could be detected using AFM and also whether the DNA fragments clumped together.

5.1.2. Use of M_1dG Antibodies to Locate MDA-Induced Mutations

As a feasibility study, M_1dG primary antibodies were used to see if M_1dG adducts could be located on the DNA strands using AFM, as described in Section 2.3.13.3. As the lowest concentration of M_1dG adduct that has been detected in cellular DNA is 1 per fmol DNA i.e. 1 in 10^7 bp or 0.5 in 10^7 bases (Moore *et al.*, 2010), and as 1 bp is 3.4 Å in length, or 0.34 nm (Watson and Crick, 1953), and assuming that the M_1dG adducts are evenly spaced, an adduct would be present every 3.4 mm, and therefore a large number of images may be required to detect M_1dG adducts by this method. It may therefore only be possible to see adduct-antibody binding at high MDA concentrations.

The M_1dG antibody and MRC5 and MRC5 SV2 DNA, from cells treated with MDA (0-1000 μM), incubated with the antibody were both imaged by AFM. The antibody and the antibody incubated with MRC5 SV2 DNA treated with 100 μM MDA are shown in Figure 42. Similar observations were shown with MRC5 DNA and other concentrations of MDA, although increasing DNA fragmentation with increasing MDA concentration was observed, as in the previous section, thus locating areas of damaged DNA was more difficult at higher concentrations. Antibodies imaged by AFM have been found to have greater heights then DNA, for example the anti-interleukin 10 antibody was found to be 4.2 ± 0.3 nm (Ierardi *et al.*, 2013). The height of the antibody adsorbed to mica (Figure 42 A) was 2.8 nm, smaller than the anti-interleukin 10 antibody, and the peak shown in Figure 42 B was 1.4 nm, indicative of DNA only, as seen in the previous section. The antibody can be clearly seen on mica, however, in conjunction with MDA-treated DNA, and although the image appears to have 'blobs' attached to the DNA fragments, which may possibly be the antibody, the height profile of the DNA fragment with the 'blob'

indicates that it is DNA only. This correlates with the adduct results in Section 4.4., where no adducts could be detected by any methods including the ISB which utilises the M_1dG antibody. Hence, if no adducts had formed then there could be no DNA-antibody binding and thus no adducts detected in the DNA samples by AFM. This may be due to the large number of AFM images that would be required to detect any M_1dG adducts, as discussed above, or alternatively, a rapid turnover occurred and it was not possible to find them in cell samples due to DNA repair mechanisms.

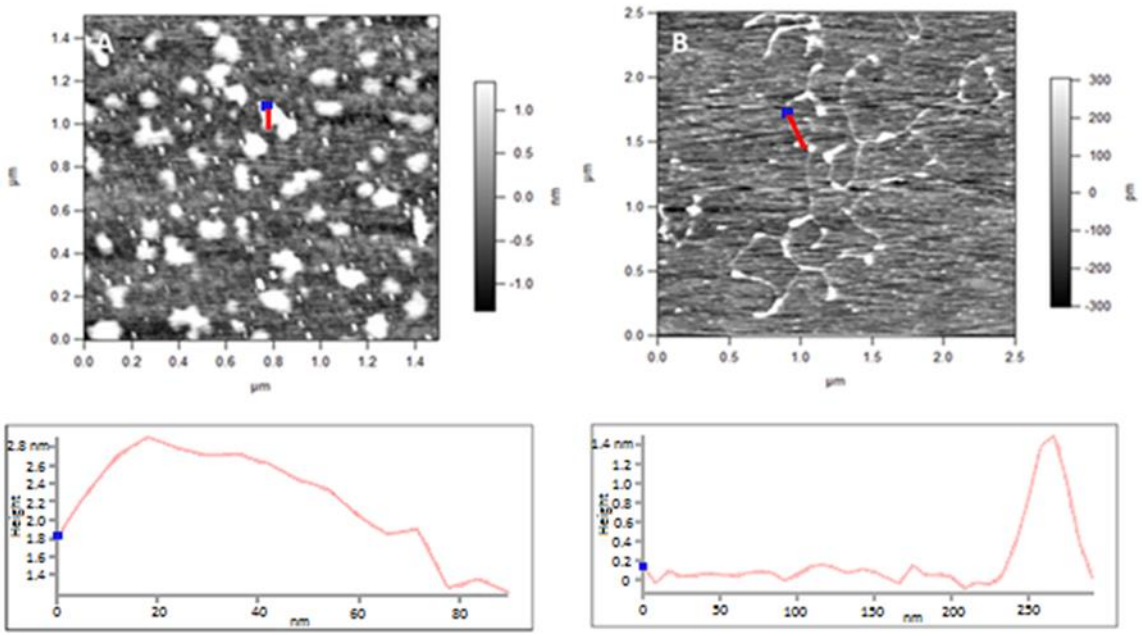

Figure 42. AFM images of A) M_1dG antibody only and B) DNA extracted from MRC5 SV2 cells treated with 100 µM MDA plus M_1dG antibody for 48 h, immobilized on mica. The height is shown below each image.

5.2. Mutation Sequencing

Missense mutations in the *TP53* gene are present in about half of all cancer cases (Martin *et al.*, 2002), with inactivation of the *TP53* gene by viral or cellular oncogenes

being associated with further cases. Most of the mutations are found in the central 200 amino acid section of the p53 protein. The functional wild-type p53 protein exhibits an anti-tumour response inhibiting neoplastic transformation, for example cell growth is arrested when p53 induces the expression of Cip1 cell cycle inhibitor. Mutations in exons 5-9 of p53 lead to inactivation of the gene in many human cancers. A major target in p53 is the DNA binding domain (Hainaut and Hollstein, 2000) which contains many of the mutation hotspots, six of which stand out: arginine residues 248, 273 (both in direct contact with DNA), 175, 249 and 282, and glycine 245 (Cho *et al.*, 1994).

The main *TP53* transcript is 2586 bases in length (Xu-Monette *et al.*, 2012) and most mutations have been found in the central DNA binding domain (Kruse and Gu, 2009). The main transcript includes a 5' UTR which covers exon 1, a large intron between exons 1 and 2, and the coding sequence from exons 2 to 11 (Xu-Monette *et al.*, 2012). A bias has been observed in the mutation screening of the human *TP53* gene, with the majority of studies focusing on the main coding regions (exons 2-11) and overlooking the 5'UTR exon 1 (Liu and Bodmer, 2006), perhaps as it is a non-coding sequence and therefore dismissed as non-functional.

Protein-coding DNA sequences make up only a small fraction of the human genome, and some non-coding sequences transcribing regulatory promoters, enhancers and silencers, RNA molecules such as tRNAs, origins of replication and telomeres and centromeres. However, the majority of the human genome has long been referred to as 'junk DNA', DNA sequences that have no biological function. However, current research suggests that much of this 'junk' DNA has been found to have, or has the potential to have, some biological functionality (Palazzo and Gregory, 2014), including regions involved in gene

regulation and control of gene expression at the post-transcriptional level (Blattner, 2008). An example of this is the 5' UTR of the human *TP53* gene, which encompasses exon 1.

Recent studies have found that regulatory elements are located in exon 1, and can regulate the translation and the stability of p53 mRNA (Pouladi *et al.*, 2013). A regulator of p53 was discovered recently, which is an antisense transcript of p53, called *Wrap53*. *Wrap53* overlaps exon 1 in the antisense direction and encodes the Wrap53α transcript that hybridises with p53 mRNA, which prevents degradation of the p53 mRNA, and is thus a form of post-transcriptional p53 control (Mahmoudi *et al.*, 2009). It has been suggested that the Wrap53-p53 interaction is required to maintain basal p53 levels in cells, as overexpression of *Wrap53* leads to increased p53 mRNA levels resulting in translation to p53 protein, whereas knockdown of *Wrap53* leads to reduced levels of p53 mRNA (Farnebo, 2009). This section of the *TP53* gene, previously overlooked in mutation studies as it is not part of the main p53 coding sequence, therefore has a role in p53 regulation in both the sense and antisense sequences.

In order to locate MDA-induced mutations and map M_1dG adduction sites, mutation sequencing was carried out. A 689 bp section of the human *TP53* gene, covering the 5'UTR and exon 1, was amplified by PCR from DNA extracted from MRC5 and MRC5 SV2 cells treated with MDA and H_2O_2 for 48 h. The DNA sequence analysed included residues 4640-5328 of the 32,772 bp *TP53* gene, located on chromosome 17 (GenBank accession NG_017013.2). The PCR products were then sequenced to look for mutations that could be attributed to treatment with MDA.

5.2.1. Agarose Gel Electrophoresis

The sizes of the PCR products were checked by agarose gel electrophoresis as shown in Figure 43. All PCR products had single bands at approximately 700 bp in size, corresponding to the PCR product length of 689 bp. The negative control, containing no DNA, had no band (lane 2), whilst the positive control (H_2O_2) produced a single band corresponding to 689 bp (lane 10).

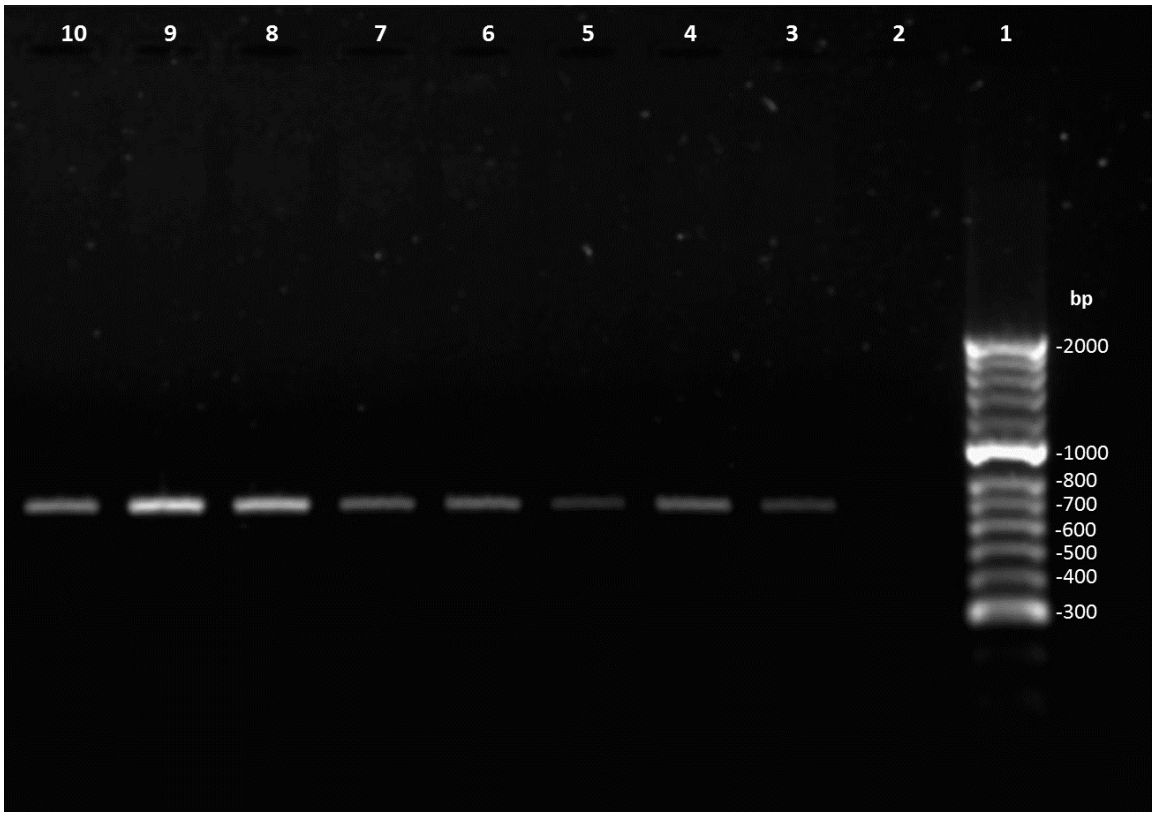

Figure 43. Agarose electrophoresis gel of MRC5 *TP53* (residues 4640-5328) PCR products. Lane 1: Hyperladder II, Lane 2: no DNA, Lanes 3 – 9: 0-1000 µM MDA, Lane 10: 100 µM H_2O_2.

5.2.2. Mutation Sequencing of the p53 Gene Segment

The DNA sequencing of the PCR products was carried out by double stranded primer walking Sanger DNA sequencing. The mutations and the type of mutations detected in MRC5 and MRC5 SV2 DNA from cells treated with MDA and H_2O_2 are shown in Appendix 1 and were compared to the same sequence from the *TP53* gene (NCBI, 2014). Conflicts were highlighted to indicate mutations in the sequences and are summarized in Table 15.

In general, more mutations were observed in MRC5 DNA (n=21 MDA, n=20 H_2O_2) than for MRC5 SV2 DNA (n=11 MDA, n=12 H_2O_2). This may be due to the altered p53 response and p53 stabilisation by the viral large T antigen in MRC5 SV2 cells compared to the wild-type MRC5 p53, as described in Section 1.11. This large T antigen - p53 binding blocks p53 dependent gene expression and may therefore have an effect upon the cellular response to DNA damage.

No mutations occurred in the negative control DNA (untreated), nor in DNA where cells had been treated with 10 µM MDA, which may be due to very low levels of mutations and DNA repair mechanisms reversing any mutations that may have formed, or no mutations were produced in this relatively short section of DNA sequence.

Table 15. Mutation type and residue number of mutations in DNA from MRC5 and MRC5 SV2 cells treated with MDA and H_2O_2. Residue numbers with repeat mutations are highlighted in bold with different, corresponding colours.

Cell Treatment (μM)	MRC5 Mutations		MRC5 SV2 Mutations	
	Residue Number	Mutation Type	Residue Number	Mutation Type
0				
10 MDA				
50 MDA	**4821**	**C to T transition**	**4724**	**G insertion**
	5149	G insertion		
	5152	G insertion		
100 MDA	**4738**	**A to G transition**	**5253**	**T insertion**
	4823	T insertion		
	4832	C to A transversion		
	5188	T insertion		
	5216	**G insertion**		
	5238	T insertion		
	5245	G insertion		
	5254	**C insertion**		
	5255	**T insertion**		
200 MDA	**4724**	**G insertion**	**4724**	**G insertion**
	5216	**G insertion**	**5216**	**G insertion**
	5256	**T insertion**	**5256**	**T insertion**
	5263	**C insertion**	**5263**	**C insertion**
500 MDA	**4714**	**A to G transition**	5222	A insertion
	4724	**G insertion**		
	5255	**T insertion**		
1000 MDA	**4724**	**G insertion**	**4724**	**G insertion**
	5254	**C insertion**	4725	A insertion
			5155	G insertion
			5253	**A insertion**
50 H_2O_2	**4714**	**A to G transition**	5215	G insertion
	4724	**G insertion**		
	5253	**T insertion**		
	5263	**C insertion**		
100 H_2O_2	**4738**	**A to G transition**	**4738**	**A to G transition**
	4819	A to G transition	4788	T insertion
	4828	T to A transversion	4791	G insertion
	4830	A insertion	4819	A to G transition
	5150	G to C transversion	4820	G to T transversion
	5209	A insertion	**4821**	**C to T transition**
	5214	G insertion	4831	C to A transversion
	5219	G to C transversion	5046	A insertion
	5224	A insertion	5154	G insertion
	5226	G to A transition	5171	G insertion
	5242	G to T transversion	5287	G to A transition
	5260	G to T transversion		
	5266	G to T transversion		
	5281	G to T transversion		
	5287	G to A transition		
	5311	G to T transversion		

For the DNA from MRC5 cells treated with MDA, the majority (43%) of mutations occurred in DNA from cells treated with 100 µM. Normal biological levels of MDA are < 50 µM, so these mutations may be representative of those occurring in human tissue subjected to oxidative stress. This was followed by a decrease in the number of mutations as MDA concentration was increased further, up to 1000 µM. This may be due to more cells being damaged due to higher MDA concentrations, resulting in increased apoptosis and decreased cell viability as previously observed in Sections 3.3 and 3.7, with increasing MDA levels. Mutations occurring in cells that have undergone apoptosis would not be detected, as only DNA from live cells, including those in the early stages of apoptosis, which remained attached to the flask wall was collected for analysis.

In both cell lines treated with the positive control, H_2O_2, the number of mutations increased with increasing H_2O_2 concentration, suggesting that the higher H_2O_2 concentration (100 µM) was enough to cause mutations in the DNA whilst retaining cell viability. For the DNA from MRC5 SV2 cells treated with MDA, the greater numbers of mutations occurred at concentrations of 200 µM and 1000 µM MDA, but were much lower in number than the respective MRC5 DNA, perhaps due to the altered p53 response of MRC5 SV2 cells.

A number of mutations observed, were repeated, as highlighted in Table 15 in different colours. These were an A to G transition appearing twice at residue 4714 in MRC5 DNA; a G insertion appearing seven times at residue 4724 in both cell lines; and A to G transition appearing three times at residue 4738 in both cell lines; a C to T transition appearing twice in both cell lines at residue 4821; a G insertion appearing three times at residue 5216 in both cell lines; a T insertion appearing twice and an A insertion appearing

once at residue 5253 in both cell lines; a C insertion appearing twice at residue 5254 in MRC5 DNA; a T insertion appearing twice in MRC5 DNA at residue 5255; a T insertion appearing twice at residue 5256 in both cell lines; and a C insertion appearing three times at residue 5263 in both cell lines. The most prominent mutation was the G insertion at residue 4724, indicating a potential mutation hotspot in this DNA sequence. Exon 1 is 224 bp in length and is located between residues 4953 and 5176 of the *TP53* gene sequence, within the 689 bp region sequenced here. Mutations found in this region were at residues 5149, 5152 and 5155 due to treatment with MDA, and residues 5046, 5150, 5154 and 5171 due to treatment with H_2O_2. The 689 bp sequence examined also aligns to residues 1841 to 1153 of the 17432 bp *Wrap53* gene sequence (GenBank reference NG_028245.1) in the antisense direction.

The type and percentage of mutations found in the DNA of both cell lines following treatment with MDA and H_2O_2 is summarised in Figure 44. In the DNA from MRC5 cells treated with MDA, the majority of mutations were insertions, of which were mainly G, T and C (81% in total) but no A insertions. The remainder were transitions, of which were A to G and C to T, and transversions, of which were C to A. All of the mutations that occurred in the DNA from MRC5 SV2 cells treated with MDA were insertions, of which the majority were G, but also A, which did not occur in MRC5 cells, and no transistions or transversions. This difference in mutation type between the two cell lines maybe due to the sequestration of the p53 protein in MRC5 SV2 cells by the viral large T antigen compared to the wild type p53 in MRC5 cells (Huschtscha and Holliday, 1983; Pipas, 2009), which may have an effect on downstream p53 dependent gene expression and subsequent alteration to DNA repair response mechanisms.

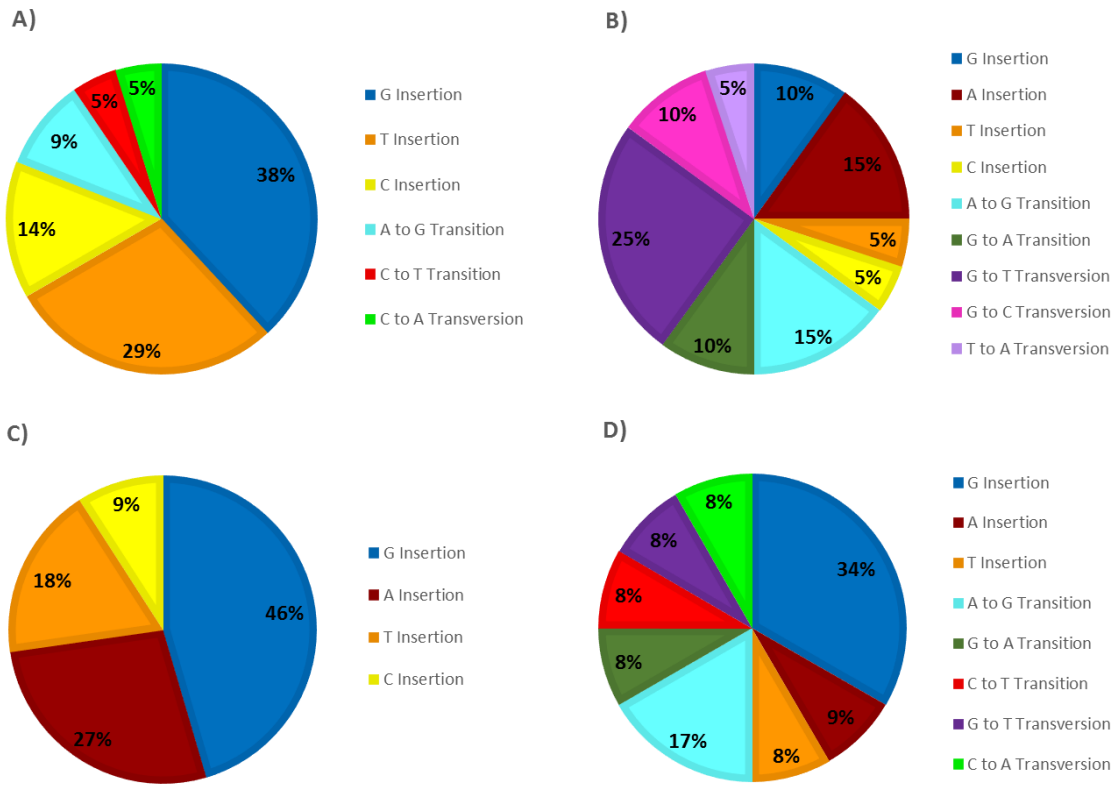

Figure 44. Type of mutations (%) in DNA from MRC5 cells treated with A) MDA and B) H_2O_2 and MRC5 SV2 cells treated with C) MDA and D) H_2O_2.

TP53 is the most commonly mutated tumour suppressor gene in lung cancer (Hecht, 2008), with mutations present in around 60% of human lung cancers. The majority of the mutations are G to T transversions, which are infrequent in other tumours except hepatocellular carcinoma. In other cancers, almost all mutations are G to A transitions (Hainaut and Hollstein, 2000; Hecht, 2008). The mutations in smoking associated lung cancers occur at a number of mutational hotspots along the *TP53* gene, particularly at codons 157 (specific for lung cancer), 249 and 273 which are found in the DNA binding domain of the p53 protein (Denissenko *et al.*, 1996). Previous studies have described DNA mutations due to MDA and M_1dG adduct formation. MDA has been shown to induce frameshift mutations and base pair substitutions (Niedernhofer *et al.*, 2003; del

Rio *et al.*, 2005). Benamira *et al.* (1995) found that the majority of mutations in *Escherichia coli* DNA were transversions consisting mainly of G to T and transitions consisting of A to G and C to T substitutions, and the remaining sequence changes were single base insertions. Whereas the data here found that the majority of mutations were insertions. M_1dG is also mutagenic in mammalian cells, with the majority of mutations occurring as base substitutions at dT and dA and the remaining as frameshift mutations (insertions or deletions) (Stafford *et al.*, 2009).

In the *TP53* gene of lung cancer cells, the majority of mutations were G:C to T:A transversions, of which there was a strong link between these types of mutation and cigarette smoking (Soussi *et al.*, 2000), whereas there was an increase in G:C to A:T transitions in *TP53* lung cancer mutation spectra in non-smokers (Kim *et al.*, 2012). An increase in frameshift mutations was observed in former or non-smokers who were exposed to passive smoking (Vahakangas *et al.*, 2001). The majority of mutations observed here, in both cell lines, were insertions i.e. frameshift, as previously observed in passive smokers, whereas in the smoking-associated lung cancer studies, the majority were transversions. Although both types occurred in MRC5 and only insertions in MRC5 SV2 cells. Some transition mutations were observed in MRC5 DNA, which holds some similarity with non-smoking-associated lung cancer studies. Additionally, the majority of mutations seen here, occurred at guanine bases, which had also been observed previously, and is in keeping with the greater reactivity of MDA with guanine to produce M_1dG adducts, compared to the other DNA bases (Marnett, 1999). The mutation hotspots for G:C to T:A transversions occurring in lung cancers of smokers were at codons 157, 158, 245, 248 and 273, which have been identified as strong binding sites

for PAHs, suggesting direct DNA damage from cigarette smoke carcinogens at these sites, rather than from endogenous sources (Hainaut and Pfeifer, 2001), as would be expected here as MDA is a product of endogenous lipid peroxidation (Chaudhary *et al.*, 1994). All of the studies above looked at the main coding regions of *TP53* (exons 2-11), whereas the 5' UTR was studied here as little mutational analysis has been carried out on this region previously (Liu and Bodmer, 2006), hence, no direct comparison may be carried out. However, mutational analysis of this region of *TP53* as a result of exposure to MDA provides a novel contribution to research.

Of the mutations that occurred in the DNA from MRC5 cells treated with H_2O_2, the majority of mutations were transversions, of which were G to T, G to C and T to A. The remainder were transitions, of which were A to G and G to A, and insertions, of which the majority were A and G. In the DNA from MRC5 SV2 cells treated with H_2O_2, half of the mutations were insertions, of which the majority were G with no C insertions. The remainder were transitions, of which were A to G, C to T and G to A, and transversions, of which were G to T and C to A. The mutation profiles for MDA and the positive control, H_2O_2, differ for both cell lines, which may be due to the different modes of action of MDA and H_2O_2, enabling the assumption that the mutations seen here were a direct effect of MDA treatment. H_2O_2 is an intermediate molecule formed by dismutation of superoxide ions by superoxide dismutase (Ayala *et al.*, 2014), and is involved in the production of hydroxyl radicals in the Fenton reaction (see Section 1.5). The hydroxyl radicals react with DNA bases resulting in DNA damage, mainly DNA strand breaks and base substitutions, mainly transversions at guanine (Termini, 2000), the majority of mutations were G to T transversions or C to T transitions (Lee *et al.*, 2002). The mutations

in MRC5 DNA due to H_2O_2 are in line with the findings in these previous studies, however, those in MRC5 SV2 DNA do not, which, again, may be due to the sequestration of MRC5 SV2 p53 by the SV40 virus (Huschtscha and Holliday, 1983).

5.2.3. Secondary Structure of the p53 Protein Sequences

The mutations were examined to determine their influence upon secondary structure of residues 4640-5328 of the wild-type p53 protein shown in Figure 45. The primary and secondary structures of MRC5 and MRC5 SV2 DNA from cells treated with MDA and H_2O_2, compared to residues 4640-5328 of the wild-type p53 protein, are shown in Appendix 2. The predicted effect of the mutations in Table 15, in the previous Section, are shown in the primary structure, where there are alterations in amino acid sequence, and consequently the secondary structure of how the pattern of hydrogen bonds between the amino and carboxyl groups of the peptide backbone of the protein is altered resulting in changes to how the protein folds into α-helices and β-strands.

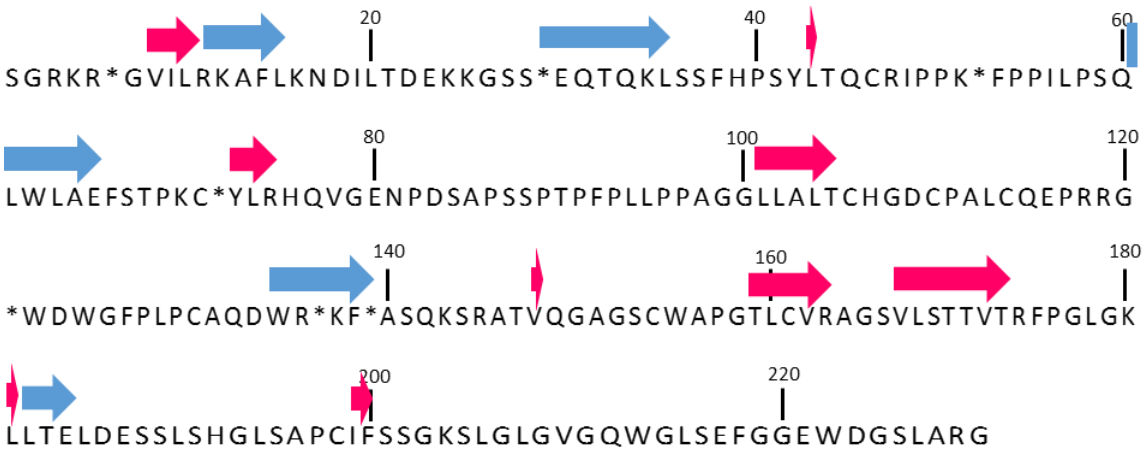

Figure 45. Primary structure of residues 4640-5328 of GenBank TP53 sequence. Secondary structures are illustrated with arrows in pink (β –strand) or blue (α-helix).

No change in the secondary structure was predicted in either cell line for untreated cells and those treated with 10 µM MDA, due to no observed mutations in these section of DNA sequence, compared to the wild type p53 sequence. Changes in secondary structure were predicted in cells treated with increasing concentrations of MDA and H_2O_2 above 10 µM MDA, with increasing irregularity. Different numbers and lengths of α helices and β strands were predicted with increasing MDA and H_2O_2 concentrations, with increasing irregularity the further along the DNA sequence, from 1 to 689 bases. This effect was predicted to be more so for MRC5 SV2 DNA than for MRC5 DNA, possibly due to the greater number of insertion mutations found in MRC5 SV2 DNA than MRC5 DNA, as described in the previous Section.

Insertion (and deletion) mutations are frame-shift mutations which alter the reading frame of the DNA sequence resulting in changes where the mutation is inserted (or deleted), but also for downstream sequences. This effect is predicted here, where there is an increased number of insertions, resulting in an increased number of changes to the secondary structure. MRC5 DNA, which had fewer insertion mutations, had an increased number of short β strands with increased MDA and H_2O_2 concentrations, and apart from the final ~60 amino acids, the stretches of amino acids were similar with similar secondary folding, compared to MRC5 SV2 DNA which had increased irregularity of secondary folding after the initial ~80 amino acids.

Table 16. Repeat mutations in residues 4640-5328 of the *TP53* gene sequence in MRC5 and MRC5 SV2 DNA form cells treated with MDA and H_2O_2.

Residue Number	Mutation Type	Amino Acid	
		Wild Type	Mutated
4714	A to G Transition	Lysine	Arginine
4724	G Insertion	Serine	Glutamic Acid
4738	A to G Transition	Threonine	Alanine
4821	G to T Transition	Glutamine	Stop Codon
5216	G Insertion	Histidine	Alanine
5253	T Insertion	Lysine	Isoleucine
5254	C Insertion	Lysine	Asparagine
5255	T Insertion	Serine	Phenylalanine
5256	T Insertion	Serine	Phenylalanine
5263	C Insertion	Glycine	Glycine

The repeated mutations described in the previous section, all apart from one (residue 5263), was predicted to result in changes to the amino acid sequence, assuming that the reading frame began at residue 1 of the 689 bp sequence (residue 4640 of the *TP53* sequence), and are summarised in Table 16.

Changes to the secondary structure also results in alteration of protein charge and the hydrophobicity of the sequence. The net charge of a protein alters with pH and is determined by the pK values of the ionisable carboxyl and amino groups of the amino acids that make up the protein. The isoelectric point (PI) is the pH at which the net charge is zero and solubility of the protein is minimal. An excess of acidic residues (e.g. aspartic acid and glutamic acid) gives a low PI and an excess of basic residues (e.g. arginine, histidine and lysine) gives a high PI (Shaw *et al.*, 2001). The PI is also important in determining the cellular localization of proteins, for example, nuclear proteins have a

neutral to basic PI (pH 7.4 to 8.1), whereas cytoplasmic proteins often have more acidic PI's (pH < 7.4) (Khaldi and Shields, 2011). The protein charge versus pH plots of the predicted amino acid sequences of MRC5 and MRC5 SV2 DNA treated with MDA and H_2O_2 are shown in Figure 46. The PI's of each sequence are shown in Figure 47 and were calculated from the protein versus charge plots. The PI of the predicted amino acid sequences of MRC5 DNA treated with MDA increased from pH 9.3 for the untreated control and 10 µM MDA, which was the same as the wild type p53 sequence, to pH 11.1 for 200 µM MDA and then decreased again to pH 10.5 for 1000 µM MDA. The PI's for MRC5 SV2 followed the same trend, however fluctuated between 50 and 1000 µM MDA. For cells treated with H_2O_2 (data not shown), the PI's increased with increasing H_2O_2 concentration, but to a greater extent for MRC5 than for MRC5 SV2 cells. The overall increase in PI for both cell lines indicated an overall increase in the number of basic amino acids (e.g. lysine) incorporated into the sequences due to mutations, compared to the wild type p53 sequence, which follows previous observations that PI can vary with sequence mutations, mainly insertions and deletions (Khaldi and Shields, 2011). When acidic residues were replaced with lysine residues in the Ribonuclease Sa protein sequence, the PI increased with increasing number of lysine residues added (Shaw *et al.*, 2001). The repeated mutations, described in the previous Section, were predicted to result in the alteration of mainly basic and polar amino acids being replaced with mostly non-polar amino acids. However, as these were mainly insertions which affect the downstream amino acid sequence, the effect on the overall amino acid sequence of this section of the *TP53* gene may have been an overall increase in basic residues resulting in increased PI's.

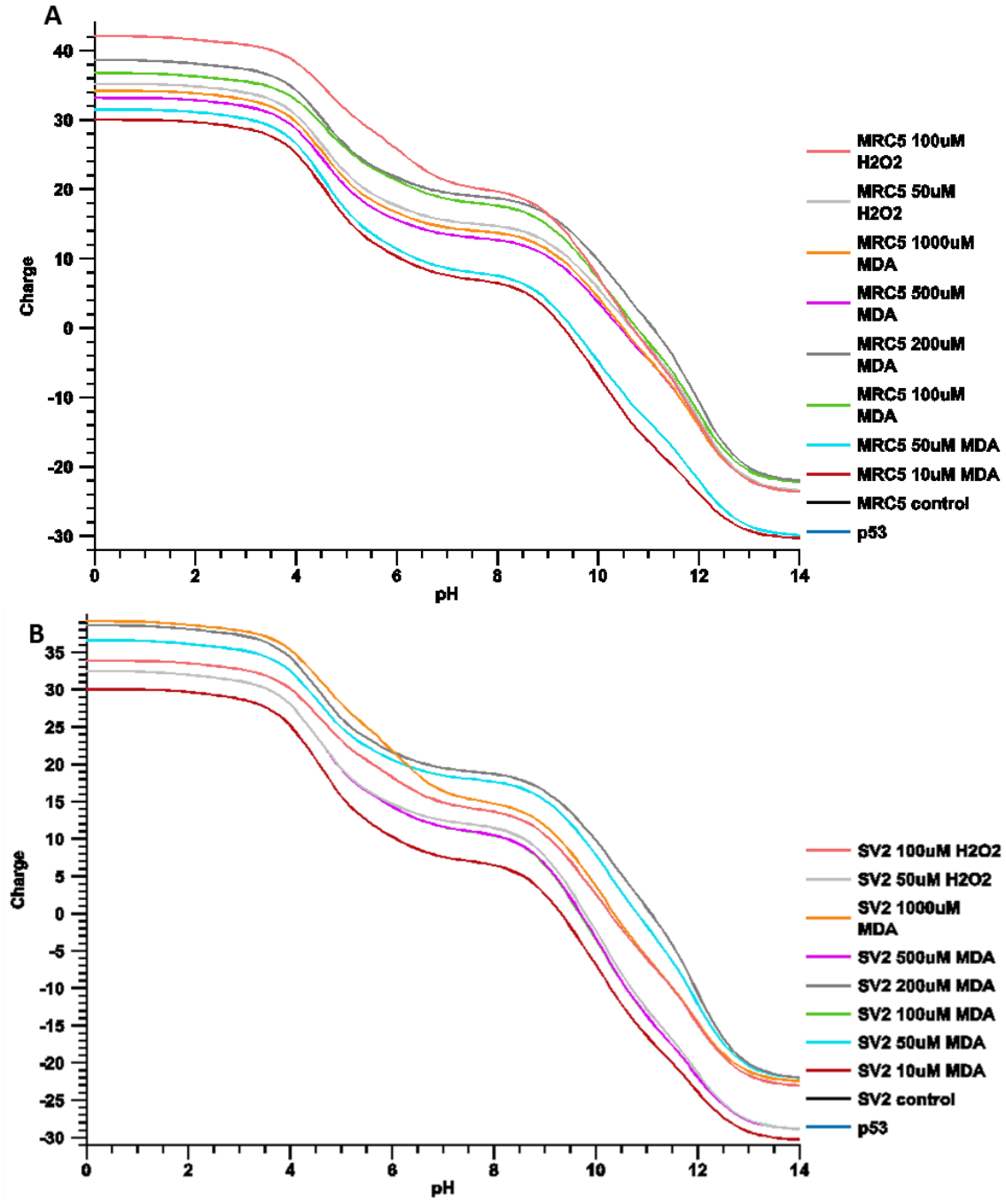

Figure 46. Protein charge vs pH plots of predicted amino acid sequences of residues 4640-5328 of the *TP53* gene extracted from A) MRC5 cells and B) MRC5 SV2 cells treated with MDA (0-1000 µM) and H_2O_2 (50-100 µM) for 48 h, compared to amino acid sequences of residues 4640-5328 of the GenBank *TP53* gene (p53).

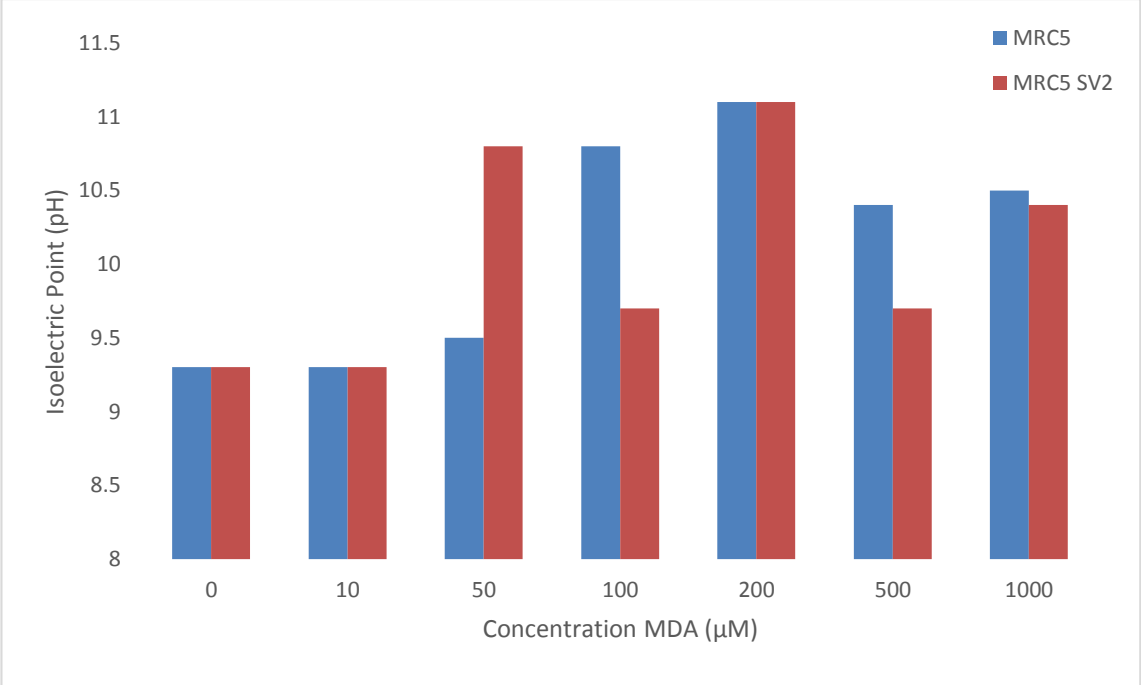

Figure 47. Isolelectric points of predicted amino acid sequences of residues 4640-5328 of the *TP53* gene extracted from MRC5 and MRC5 SV2 cells treated with MDA (0-1000 µM) and H_2O_2 (50-100 µM) for 48 h.

Mutations may also have an effect on the hydrophobicity of a protein sequence, which in turn affects the secondary and tertiary structure of the protein. The structure of a protein defines its function. The hydrophobicity of an amino acid sequence determines where each amino acid will be located in the final structure of the protein. Hydrophobic amino acids such as isoleucine and valine are non-polar and are located on the inside on globular proteins, away from the water-containing cytosol, or span the hydrophobic lipid bilayer of membranes in transmembrane proteins. Whereas hydrophilic amino acid residues such as arginine and lysine, are located on the exterior of globular proteins and on either side of the membrane of transmembrane proteins, where they interact with the water in the cytosol by hydrogen bonding (Kyte and Doolittle, 1982).

A hydrophobicity plot is a method of displaying the hydrophobic and hydrophilic regions of an amino acid sequence and can be used to predict the protein structure, potentially indicating transmembrane regions. Each amino acid is allocated a hydrophobicity score from 4.6 for the most hydrophobic (isoleucine) to -4.6 for the most hydrophilic (arginine). Hydrophobic regions are identified as peaks above the midline and hydrophilic regions as peaks below (Kyte and Doolittle, 1982). Predicted hydrophobicity plots for untreated and MDA (1000 µM) treated MRC5 and MRC5 SV2 cells are shown in Figure 48. The plots for the untreated control for each cell line are identical, and match the plot for the same section of the wild type p53 sequence (data not shown). A greater proportion of the untreated control sequences (A and C) are hydrophilic, with five main hydrophobic regions – two small regions at the beginning of the sequence, a large region in the middle which is the most hydrophobic, and two large regions towards the end of the sequence. For the MRC5 sequence from cells treated with 1000 µM MDA, there are more regions of predicted hydrophobicity (seven), with greater hydrophobicity, denoted by the increased peak size, than for the untreated control. These hydrophobic regions can be seen at the beginning of the sequence, with a main hydrophobic region spanning positions 100 to 150 of the amino acid sequence. The two hydrophobic sequences seen in the untreated control towards the end of the sequence were smaller in the treated sequence. For the MRC5 SV2 sequence from cells treated with 1000 µM MDA, the two hydrophobic regions seen at the start of the untreated sequence were much smaller in the treated sequence, with a wider region of hydrophobicity in the centre of the sequence than the untreated control. There were also more regions of hydrophobicity at the end of the treated

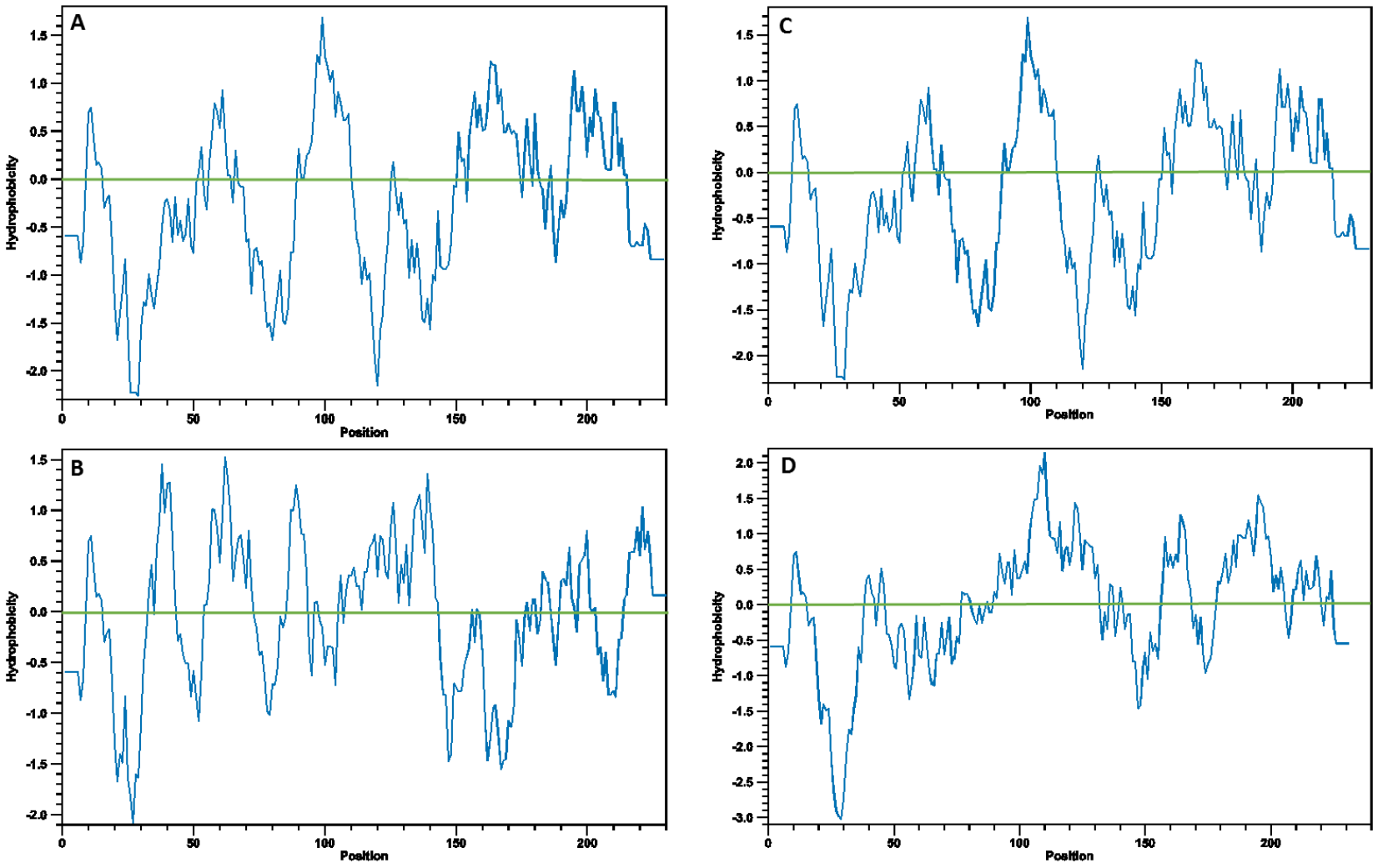

Figure 48. Kyte-Doolittle hydrophobicity plot of amino acid sequence of residues 4640-5328 of *TP53* gene from MRC5 cells A) untreated and B) treated with 1000 µM MDA and MRC5 SV2 cells C) untreated and D) treated with 1000 µM MDA for 48 h.

sequence than compared to the untreated control and also the treated MRC5 sequence. These alterations in the predicted hydrophobic regions of sequences from cells treated with MDA compared to the untreated controls, demonstrate the effect of mutations on the hydrophobicity of the protein sequences and as a result, the potential for alteration of the proteins' secondary and tertiary structure, which may impact on the functionality of the protein molecule.

5.3. Summary

Genomic DNA, extracted and purified from MRC5 and MRC5 SV2 cells which had been treated with MDA, showed increasing fragmentation with increasing MDA concentration, when imaged by AFM. A feasibility study was also carried out to see if M_1dG antibodies could be used to locate M_1dG adducts on the same DNA strands. It was not possible to locate any adducts in this study, perhaps due to cellular DNA repair mechanisms or low concentrations of adducts making location and detection of them difficult by this method. Mutation sequencing was then carried out to see if MDA had an effect on the DNA sequence.

For the first time, the 5' UTR region of the human *TP53* gene was amplified by PCR and sequenced from MRC5 and MRC5 SV2 DNA extracted from cells treated with MDA and H_2O_2. This sequence encodes exon 1 and also *Wrap53* in the antisense direction, a transcript that hybridises with p53 preventing post-transcriptional degradation. In general, a greater number of mutations were found in MRC5 DNA than in MRC5 SV2 DNA, perhaps due to the altered p53 response of MRC5 SV2 cells. No mutations were

found in either the negative control or in DNA from cells treated with 10 µM MDA for both cell lines, perhaps due to low level mutation rates and/or DNA repair mechanisms. DNA from both cell lines had an increased number of mutations with increasing concentration of H_2O_2, the positive control.

For MRC5 DNA, the highest number of mutations occurred in DNA from cells treated with 100 µM MDA, followed by a decreasing number up to 1000 µM, of which the majority were G insertion mutations, with some transitions (A to G and C to T) and transversions (C to A). For MRC5 SV2 DNA from cells treated with MDA, the greater number of mutations were found for 200 µM MDA and then 1000 µM MDA, of which all of the mutations were insertions, mainly G. A number of repeated mutations were identified, the majority of which resulted in an amino acid change to this sequence. For the positive control, H_2O_2, the majority of mutations in MRC5 DNA were transversions (Mostly G to T or C), and half of the mutations in MRC5 SV2 cells were insertions (mainly G) and the remainder were transitions and transversions. Thus, a clear difference was observed in mutations occurring due to MDA and H_2O_2, so eliminating radical attack, but also between the two cell lines which was due to the difference in p53 response.

An increase in changes to the amino acid sequence of this section of DNA was predicted, with increasing concentrations of MDA and H_2O_2, which resulted in an increased number of predicted changes to the secondary structure of this sequence, and an overall increase to the isoelectric points of the amino acid sequences, and an increase to the number of predicted hydrophobic regions.

CHAPTER 6

CONCLUSIONS & FUTURE WORK

6.1. Conclusions

Overall, low concentrations of MDA appeared to induce cell proliferation in both cell lines, whereas higher concentrations of MDA appeared to inhibit proliferation and viability with a dose-dependent response, but MRC5 cells to a much greater extent, perhaps due to the sequestration of p53 in MRC5 SV2 cells by the viral large T antigen. Cell surface morphology was altered, becoming more pitted and irregular in shape with increasing MDA concentration. A qualitative analysis showed what appear to be micronuclei were observed in cells treated with MDA, in a dose-dependent manner. The nuclear area also appeared to increase and cells appeared to express an increased amount of phosphatidyl serine indicating the early stages of apoptosis. p53 expression was observed to increase in individual cells, treated with increasing amounts of MDA, but overall p53 fold induction appeared to decrease when expression was measured by RT-qPCR, perhaps due to decreased cell viability, although p53 induction was still greater than the negative control. Thus, treatment with MDA results in alterations at the cellular level. Whilst previous studies have utilised these techniques, the novelty of this work is the combination of these methods to study the effects of treating MRC5 and MRC5 SV2 cells with MDA. In particular, the effects of MDA on cell surface morphology using AFM, nuclear morphology and p53 expression studies.

A sensitive method of M_1dG adduct detection has been developed using LC-MS-MS, however, M_1dG adducts were undetectable in these cell lines. Insufficient DNA may have been extracted for detection, or DNA repair mechanisms in the cell may act to remove M_1dG adducts from DNA. MDA may have been sequestered as protein-MDA adducts, reducing the effective dose of MDA reacting with DNA. M_1dG adducts have been quantified in CT-DNA treated with MDA, showing a dose-response relationship, although with a relatively high concentration of DNA compared to MRC5 and MRC5 SV2 DNA. Thus DNA-MDA reactions occur in the absence of biological events, however, cellular processes may interfere with DNA-MDA interactions.

Genomic DNA, extracted and purified from MRC5 and MRC5 SV2 cells which had been treated with MDA, showed increasing fragmentation with increasing MDA concentration, when imaged by AFM. This indicates that MDA is able to reach the nucleus and interact with DNA and cause alterations at the DNA level, although cellular responses to the presence of MDA may cause the fragmentation of DNA.

For the first time, the 5' UTR region of the human *TP53* gene was amplified by PCR and sequenced from MRC5 and MRC5 SV2 DNA extracted from cells treated with MDA. Mutations were found in this segment of DNA, generally increasing with increasing MDA concentration, and to a greater extent in MRC5 DNA than MRC5 SV2 DNA. Thus MDA has an effect on DNA but it is not known as to whether this is directly via M_1dG adducts (which were not detected), or by other cellular processes. The mutation pattern does not match that found in smoking-related lung cancer cells, which might be expected as the cell lines used were lung fibroblasts, however, insertion i.e. frameshift mutations

and transition mutations were observed which have been associated with passive smoking related and non-smoking related lung cancers respectively. Additionally, the majority of mutations found were at guanine residues, which would be expected as MDA has a greater reactivity with guanine than any of the other nucleotide bases. No direct comparison can be made between the mutations found here and the *TP53* mutation database, as the section of the *TP53* gene sequenced was the 5' UTR which includes exon 1, whereas the data held in the database covers the protein coding exons 2-11. Additionally, the majority of mutation data for *TP53* and lung cancer is for tobacco smoke, which contains a complex mix of carcinogenic compounds, such as PAHs, where the effects of these compounds may differ from or have a greater effect than MDA and the contribution of MDA to the mutations seen may have been masked by the impact of these other compounds.

6.2. Future Work

A number of different assays were carried out to determine the effects of MDA at the cellular level in human lung fibroblast MRC5 and MRC SV2 cell lines. A clear effect was found, however, further work may be carried out to complement and improve upon these findings.

Due to the potential reaction of proteins in FBS with MDA, the effect of FBS on cell proliferation was analysed in Section 3.2. After 48 h incubation in serum-free media, both cell lines appeared to no longer proliferate when compared to those grown in complete media, although they still remained viable which allowed their use in further

analyses. The use of a protein-free FBS-substitute, which are now readily available, could be used as an alternative to serum-free media, to allow both cell lines to continue proliferating up to 48 h, and beyond. The effect of MDA on MRC5 and MRC5 SV2 cells could be assessed over longer periods of exposure.

The culturing of the two cell lines may be scaled-up in order to produce sufficient amounts of mRNA for RT-qPCR p53 expression analysis, with the addition of higher concentrations of MDA to treat the cells (100-1000 µM), so that these results may be compared directly to the immunofluorescence assay for p53 expression. In addition to this, further expression studies could be carried out using RT-qPCR, for example apoptosis-related proteins such as *Bcl-2*, *Bax*, *JNK* and *ERK* (Cheng *et al.*, 2011). Any potential differences in expression may reveal the effects of MDA on these proteins and thus give further information as to the effects of MDA on apoptosis, they may also reveal the effects of p53 sequestration on the mechanisms of apoptosis. As it has been suggested that the use of a single housekeeping gene, such as *GAPDH*, is no longer the preferred method of normalising the target gene expression due to variations in expression due to experimental factors (Kozera and Rapacz, 2013). Multiple housekeeping genes should be used instead, for example *glucose-6-phosphate isomerase*, proteasome subunits *PSMB2* and *PSMB4*, and *RAS* oncogene family member *RAB7A* have been suggested (Eisenberg and Levanon, 2013), which could be used to improve the robustness of the RT-qPCR analysis.

MDA was observed to have an effect upon the nuclear morphology of MRC5 and MRC5 SV2 cells, with the nuclear area increasing and the number of what appeared to be

micronuclei increasing with increasing MDA concentration. The alteration in nuclear area may have been due to the flattening and spreading of the cell due to cytoskeletal changes, therefore 3-D imaging of the cells would be required to confirm this by measuring nuclear volume rather than area. Additionally, a full micronucleus assay could be carried out, as described in Section 3.6., in order to quantify the number of micronuclei formed in response to treatment with MDA.

MDA was observed to have a clear effect upon cell morphology, observed by both LM, where live cells were imaged *in vitro*, and AFM, where the cell surface of air-dried cells were also imaged. Work may be continued here to assess the effect of MDA on cell morphology and topography by carrying out force-measurements using AFM to look at the mechanical properties of the cell. The effect of MDA upon the cell cytoskeleton could also be assessed by immunofluorescence with confocal microscopy. Monoclonal antibodies against actin and β tubulin may be used to stain these cytoskeletal components following exposure of cells to different concentrations of MDA, to determine its effect on the cytoskeleton and thus cell morphology.

AFM was also used to image DNA from MRC5 and MRC5 SV2 cells treated with MDA, and found that there was increased DNA fragmentation with increasing MDA concentrations. A feasibility study was carried out to see if M_1dG antibodies could be used to locate M_1dG adducts on the same DNA strands, however, it was not possible to locate any adducts in this study. Immunoaffinity purification of the DNA samples could be carried out to isolate M_1dG adduct-containing DNA strands (Hochleitner *et al.*, 1991) prior to AFM analysis to increase the likelihood of locating antibodies bound to M_1dG

DNA adducts. This could also be used in conjunction with chemical force microscopy (CFM), an ultra-sensitive method using a chemically functionalised AFM tip (Hinterdorfer *et al.*, 1996). M_1dG antibodies could be attached to an AFM tip and used to locate M_1dG adducts on DNA strands. Additionally, isolation of specific regions of DNA, such as the TP53 gene, for AFM and CFM analysis could be carried out.

A LC-MS-MS method was developed for the detection and quantification of M_1dG adducts in DNA samples. The method was successful in that M_1dG adducts were detected in CT-DNA samples that had been treated with MDA, in a dose-dependent manner. However, DNA extracted from MRC5 and MRC5 SV2 cells that had been treated with MDA was insufficient in concentration for adduct detection by this method and the LC-MS-MS instrumentation available. In order to produce sufficient data for publication of this method, and the effect of MDA on M_1dG adduct levels in these cell lines, additional work is being undertaken. Initially, the method of DNA extraction is being examined using the M_1dG-DNA standard to determine whether there was any loss of adduct via this method. If any loss of adduct is detected, an alternative method of DNA extraction will need to be used for further analysis. The culturing of the cell lines may need to be scaled-up significantly in order to produce sufficient DNA to be used to detect M_1dG adducts. The use of more sensitive instrumentation may also be required for M_1dG adduct detection, as the LOD and LOQ of the instrumentation used here were relatively high. Immunoaffinity purification of the DNA samples could be carried out to isolate M_1dG adduct-containing DNA prior to analysis and thus improve adduct detection levels.

Finally, a section of the *TP53* gene from DNA extracted from MRC5 and MRC5 SV2 cells treated with MDA was sequenced and mutations were found. However, the mutation pattern did not match the mutations found in the *TP53* gene in smoking-related lung cancer cells, which might be expected as the cell lines were human lung fibroblasts. This may be due to the section of the *TP53* gene differing from those used previously in the p53 database, the 5' UTR in this study and the protein coding exons 2-11 in previous studies. However, differences were identified in the mutation patterns of MRC5 and MRC5 SV2 in response to MDA, which can be attributed to the differing p53 responses of the two cell lines. There is thus sufficient novel mutation data to present for publication, however a number of further analyses could be carried out to enhance the work. PCR amplification and mutation sequencing of the same sequences of the *TP53* gene as used in previous studies could be carried out and compared. Additionally, it may be possible that cellular DNA repair mechanisms could repair some of the mutations found here, and/or mutations occurring prior to DNA extraction may have already been repaired. A series of different MDA treatment times could therefore be used to monitor this effect, along with returning the treated cells to complete media for a set period of time post-treatment.

REFERENCES

Agarwal, S. and Draper, H. H. (1992). Isolation of a malondialdehyde-deoxyguanosine adduct from rat liver DNA. *Free Radical Biology & Medicine* **13**: 695-699.

Akingbade, D., Kingsley, P. J., Shuck, S. C., Cooper, T., Carnahan, R., Szekely, J. and Marnett, L. J. (2012). Selection of monoclonal antibodies against 6-oxo-M_1dG and their use in LC-MS/MS assay for the presence of 6-oxo-M_1dG *in vivo*. *Chemical Research in Toxicology* **25**: 454-461.

Alberts, B., Johnson, A., Lewis, J., Raff, M., Roberts, K. and Walter, P. (2002). *Molecular Biology of the Cell*. New York, Garland Science. 1300-1302.

Alberts, B., Johnson, A., Lewis, J., Raff, M., Roberts, K. and Walter, P. (2002). *Programmed Cell Death (Apoptosis)*, Garland Science. 1010-1014.

Alonso, J. L. and Goldmann, W. H. (2003). Feeling the forces: atomic force microscopy in cell biology. *Life Sciences* **72**: 2553-2560.

Arif, J. M., Dresler, C., Clapper, M. L., Gairola, C. G., Srinivasan, C., Lubet, R. A. and Gupta, R. C. (2006). Lung DNA adducts detected in human smokers are unrelated to typical polyaromatic carcinogens. *Chemical Research in Toxicology* **19**: 295-299.

Atasayar, S., Orhan, H. and Ozgunes, H. (2004). Malondialdehyde Quantification in Blood Plasma of Tobacco Smokers and Non-Smokers. *FABAD Journal of Pharmaceutical Sciences* **29**: 15-19.

Ayala, A., Munoz, M. F. and Arguelles, S. (2014) Lipid peroxidation: production, metabolism,and signalling mechanisms of malondialdehyde and 4-hydroxy-2-nonenal. *Oxidative Medicine and Cellular Longevity* **2014**, 1-31.

Badcock, N. R., Zoanetti, G. D. and Martin, E. S. (1997). Nonchromatographic assay for malondialdehye-thiobarbituric acid adduct with HPLC equivalence. *Clinical Chemistry* **43**: 1655-1657.

Barber, R. D., Harmer, D. W., Coleman, R. A. and Clark, B. J. (2005). GAPDH as a housekeeping gene: analysis of GAPDH mRNA expression in a panel of 72 human tissues. *Physiological Genomics* **21**: 389-395.

Benamira, M., Johnson, K., Chaudhary, A., Bruner, K., Tibbetts, C. and Marnett, L. J. (1995). Induction of mutations by replication of malondialdehyde-modified M13 DNA in *Escherichia coli*: determination of the extent of DNA modification, genetic requirements for mutagenesis and types of mutations induced. *Carcinogenisis* **16**(1): 93-99.

Billingsley, D. J., Bonass, W. A., Crampton, N., Kirkham, J. and Thomson, N. H. (2012). Single-molecule studies of DNA transcription using atomic force microscopy. *Physical Biology* **9**: 1-15.

Binnig, G., Quate, C. F. and Gerber, C. F. (1986). Atomic Force Microscope. *Physical Review Letters* **56**(9): 930-933.

Bladier, C., Wolvetang, E. J., Hutchinson, P., de Haan, J. B. and Kola, I. (1997). Response of a Primary Human Fibroblast Cell Line to H_2O_2: Senescence-like Growth Arrest or Apoptosis? *Cell Growth & Differentiation* **8**: 589-598.

Blattner, C. (2008). 'Junk' DNA meets the p53 network. *Molecular Systems Biology* **4**: 2.

Bono, R., Romanazzi, V., Munnia, A., Piro, S., Allione, A., Ricceri, F., Guarrera, S., Pignata, C., Matullo, G., Wang, P., Giese, R. W. and Peluso, M. (2010). Malondialdehyde-Deoxyguanosine Adduct Formation in Workers of Pathology Wards: The Role of Air Formaldehyde Exposure. *Chemical Research in Toxicology* **23**: 1342-1348.

Butler, M. (2004). *Animal Cell Culture & Technology*. Oxon, UK, BIOS Scientific Publishers. 55-79.

Caldini, R., Chevanne, M., Mocali, A., Tambaccini, D. and Paoletti, F. (1998). Premature induction of aging in sublethally H_2O_2-treated young MRC5 fibroblasts correlates with increased glutathione peroxidase levels and resistance to DNA breakage. *Mechanisms of Aging and Development* **105**: 137-150.

Chang, H. Y., Chi, J., Dudoit, S., Bondre, C., van de Rijn, M., Botstein, D. and Brown, P. O. (2002). Diversity, topographic differentiation, and positional memory in human fibroblasts. *Proceedings of the National Academy of Sciences* **99**(20): 12877-12882.

Chaudhary, A., K, Nokubo, M., Reddy, G. R., Yeola, S. R., Morrow, J. D., Blair, I. A. and Marnett, L. J. (1994). Detection of endogenous malondialdehyde-deoxyguanosine adducts in human liver. *Science* **265**: 1580-1582.

Chen, F. and Shi, X. (2002). Intracellular signal transduction of cells in reponse to carcinogenic metals. *Critical Reviews in Oncology/Hematology* **42**: 105-121.

Cheng, J., Wang, F., Yu, D.-F., Wu, P.-F. and Chen, J.-G. (2011). The cytotoxic mechanism of malondialdehyde and protective effect of carnosine via protein cross-linking/mitochondrial dysfunction/reactive oxygen species/MAPK pathway in neurons. *European Journal of Pharmacology* **650**: 184–194.

Cherneva, R. V., Georgiev, O. B., Petrov, D. B., Dimova, I. I. and Toncheva, D. I. (2009). Expression levels of p53 messenger RNA detected by real time PCR in tumor tissue, lymph nodes and peripheral blood of patients with non-small cell lung cancer - new perspectives for clinicopathological application. *Biotechnology & Biotechnological Equipment* **23**: 1247-1249.

Cho, Y., Gorina, S., Jeffrey, P. D. and Pavletich, N. P. (1994). Crystal structure of a p53 tumour suppressor-DNA complex: understanding tumorigenic mutations. *Science* **265**: 346-355.

Choi, W.-Y., Oh, S.-H., Seo, Y.-C., Kang, D.-H., Lee, S.-Y., Jung, K.-H., Cho, J.-S., Ahn, J.-H. and Choi, G.-P. (2011). Effects of methanol on cell growth and lipid production from mixotrophic cultivation of *Chlorella* sp. *Biotechnology and Bioprocess Engineering* **16**(5): 946-955.

Cighetti, G., Allevi, P., Anastasia, L., Bortone, L. and Paroni, R. (2002). Use of methyl malondialdehyde as an internal standard for malondialdehyde detection: validation by isotope-dilution gas chromatography-mass spectrometry. *Clinical Chemistry* **48**: 2266-2269.

CLCBIO (2014). CLC Main Workbench. www.clcbio.com, CLCBio.

Cooke, M. S., Olinski, R. and Loft, S. (2008). Measurement and meaning of oxidatively modified DNA lesions in urine. *Cancer Epidemiology, Biomarkers & Prevention* **17**: 3-14.

Courtois, S., Caron de Fromentel, C. and Hainaut, P. (2004). p53 protein variants: structural and functional similarities with p63 and p73 isoforms. *Oncogene* **23**: 631-638.

Croft, D. R., Crighton, D., Samuel, M. S., Lourenco, F. C., Munro, J., Wood, J., Bensaad, K., Vousden, K. H., Sansom, O. J., Ryan, K. M. and Olson, M. F. (2011). p53-mediated transcriptional regulation and activation of the actin cytoskeleton regulatory RhoC to LIMK2 signaling pathway promotes cell survival. *Cell Research* **21**(4): 666-682.

Cancer Research UK. (2011). "Cancer Research UK." [Online]. (Updated) Available at: http://info.cancerresearchuk.org/cancerstats/incidence/risk/. [Accessed: 27th February 2011]

Cancer Research UK. (2014). "Cancer Research UK." [Online]. (Updated) Available at: http://info.cancerresearchuk.org/cancerstats/incidence/risk/. [Accessed: 4th March 2014]

Dagan Feng, D. and Zaytoon, J. (2006). *Modelling and Control in Biomedical Systems 2006*, Elsevier.508

Dalman, M. R., Deeter, A., Nimishakavi, G. and Duan, Z. (2012). Fold change and p-value cutoffs significantly alter microarray interpretations. *BMC Bioinformatics* **13**(Suppl 2):S11.

de Hoffmann, E. and Stroobant, V. (2007). *Mass Spectrometry: Principles and Application*. West Sussex, UK, John Wiley & Sons Ltd

Dedon, P. C., Plastaras, J. P., Rouzer, C. A. and Marnett, L. J. (1998). Indirect mutagenesis by oxidative DNA damage: formation of the pyrimidopurinone adduct of deoxyguanosine by base propenal. *Proceedings of the National Academy of Sciences* **95**: 11113-11116.

del Rio, D., Stewart, A. J. and Pellegrini, N. (2005). A review of recent studies on malondialdehyde as toxic molecule and biological marker of oxidative stress. *Nutrition, Metabolism & Cardiovascular Diseases* **15**: 316-328.

Denissenko, M. F., Pao, A., Tang, M. and Pfiefer, G. P. (1996). Preferential formation of benzo(a)pyrene adducts at lung cancer mutational hotspots in P53. *Science* **274**: 430-432.

Eisenberg, E. and Levanon, E. Y. (2013). Human housekeeping genes, revisited. *Trends in Genetics* **29**(10): 569-574.

Ekstrom, T., Garberg, P., Egestad, B. and Hoberg, J. (1988). Recovery of malondialdehyde in urine as a 2,4-dinitrophenylhydrazine derivative analysed with high performance liquid chromatography. *Chemico-Biological Interactions* **66**: 177-187.

Elmore, S. (2007). Apoptosis: A Review of Programmed Cell Death. *Toxicologic Pathology* **35**: 495-516.

Elson, D. and Chargaff, E. (1952). On the deoxyribonucleic acid content of sea urchin gametes. *Experientia* **8** (4): 143–145.

Enge, M., Bao, W., Hedstrom, E., Jackson, S. P., Moumen, A. and Selivanova, G. (2009). MDM2-Dependent Downregulation of p21 and hnRNP K Provides a Switch between Apoptosis and Growth Arrest Induced by Pharmacologically Activated p53. *Cancer Cell* **15**: 171-183.

Esterbauer, H., Schaur, R. J. and Zollner, H. (1991). Chemistry and biochemistry of 4-hydroxynonenal, malonaldehyde and related aldehydes. *Free Radical Biology & Medicine* **11**: 81-128.

Evan, G. I. and Vousden, K. H. (2001). Proliferation, cell cycle and apoptosis in cancer. *Nature* **411**: 342-348.

Ezzati, M., Henley, S. J., Lopez, A. D. and Thun, M. J. (2005). Role of smoking in global and regional cancer epidemiology: current patterns and data needs. *International Journal of Cancer* **116**: 963-971.

Farnebo, M. (2009). Wrap53, a novel regulator of p53. *Cell Cycle* **8**(15): 2343-2346.

Fenaille, F., Mottier, P., Turesky, R. J., Ali, S. and Guy, P. A. (2001). Comparison of analytical techniques to quantify malondialdehyde in milk powders. *Journal of Chromatography A* **921**: 237-245.

Fenech, M. (2000). The in vitro micronucleus technique. *Mutation Research* **455**: 81-95.

Fenech, M. and Bonassi, S. (2011). The effect of age, gender, diet and lifestyle on DNA damage measured using micronucleus frequency in human peripheral blood lymphocytes. *Mutagenesis* **26**(1): 43-49.

Fink, S. P., Reddy, G. R. and Marnett, L. J. (1997). Mutagenicity in *Escherichia coli* of the major DNA adduct derived from the endogenous mutagen malondialdehyde. *Proceedings of the National Academy of Sciences USA* **94**: 8652-8657.

Flicek, P. M., Amode, R., Barrell, D., Beal, K., Brent, S., Carvalho-Silva, D., Clapham, P., Coates, G., Fairley, S., Fitzgerald, S., *et al*. (2012). Ensembl 2012. *Nucleic Acids Research*. **40:** D84-D90.

Freeman, T. L., Haver, A., Duryee, M. J., Tuma, D. J., Klassen, L. W., Hamel, F. G., White, R. L., Rennard, S. I. and Thiele, G. M. (2005). Aldehydes in Cigarette Smoke React with the Lipid Peroxidation Product Malonaldehyde to form Fluorescent Protein Adducts on Lysines. *Chemical Research in Toxicology* **18**: 817-824.

Gallus, S., Altieri, A., Boscetti, C., Franceschi, S., Levi, F., Negri, E. *et al.* (2003). Cigarette tar yield and risk of upper respiratory tract cancers: case-control studies from Italy and Swizerland. *Annals of Oncology* **14**: 209-213.

García-Inclán, C., López-Hernández, A., Alonso-Guervós, M., Allonca, E., Potes, S., Melón, S., López, F., Llorente, J. L. and Hermsen, M. (2014). Establishment and genetic characterization of six unique tumor cell lines as preclinical models for sinonasal squamous cell carcinoma. *Scientific Reports* **4**: 4925.

Giuliano, M., Stellavato, A., Cammarota, M., Lamberti, M., Miraglia, N., Sannolo, N. and De Rosa, M. (2009). Effects of low concentrations of benzene on human lung cells in vitro. **188**(2): 130–136.

Gomez-Sanchez, A., Hermosin, I., Lassaletta, J. and Maya, J. (1993). Cleavage and Oligomerization of Malondialdehyde. *Tetrahedron* **49**: 1237-1250.

Goodhew, P. J., Humphrey, J. and Beanland, R. (2001). *Electron Microscopy and Analysis*. London, Taylor Francis

Gottschalg, E. (2002). Detection, stability and factors influencing the formation of promutagenic endogenous DNA damage, University of Leicester. **PhD**. 199-210.

Guolin, L., Hui, L., Baohe, W. and Dazhong, Y. (2006). Effects of malondialdehyde on growth and proliferation of human bone marrow mesenchyme stem cells in vitro. *Frontiers of Biology in China* **2**: 131-136.

Gutteridge, J. M. C. (1995). Lipid peroxidation and antioxidants as biomarkers of tissue damage. *Clinical Chemistry* **41**: 1819-1828.

Gutteridge, J. M. C., Hays, A. D. and Lunec, J. (1977). Fluorescent malondialdehyde polymers from hydrolsed 1,1,3,3-tetramethoxypropane. *Analytica Chimica Acta* **94**: 209-211.

Hainaut, P. and Hollstein, M. (2000). p53 and human cancer: the first ten thousand mutations. *Advances in Cancer Research*. San Diego, Academic Press Inc. **77:** 81-137.

Hainaut, P. and Pfeifer, G. P. (2001). Patterns of p53 G→T transversions in lung cancers reflect the primary mutagenic signature of DNA-damage by tobacco smoke. *Carcinogenesis* **22**(3): 367-374.

Hamid, R., Rotshteyn, Y., Rabadi, L., Parikh, R. and Bullock, P. (2004). Comparison of alamar blue and MTT assays for high through-put screening. *Toxicology in Vitro* **18**: 703-710.

Hanahan, D. and Weinberg, R. A. (2000). The Hallmarks of Cancer. *Cell* **100**: 57-70.

Hannan, L. M., Jacobs, E. J., Thun, M. J. (2009). The association between cigarette smoking and risk of colorectal cancer in a large prospective cohort from the United States. *Cancer Epidemiology, Biomarkers and Prevention* **18** (12): 3362-3367.

He, R., Xu, Y. J., Qiang, M. and Han, C. S. (2011). Malondialdehyde as a fluorescent probe for misfolded protein in cells. *Biophysical Journal* **100**(3 (S1)): 398a.

Hecht, S. S. (2008). Progress and challenges in selected areas of tobacco carcinogenesis. *Chemical Research in Toxicology* **21**: 160-171.

Heid, C. A., Stevens, J., Livak, K. J. and Williams, P. M. (1996). Real time quantitative PCR. *Genome Research* **6**: 986-994.

Himmelstein, M. W., Boogaard, P. J., Cadet, J., Farmer, P., Kim, J. H., Martin, E., A, Persaud, R. and Shuker, D. E. G. (2009). Creating context for the use of DNA adduct data in cancer risk assessment: II. Overview of methods of identification and quantitation of DNA damage. *Critical Reviews In Toxicology* **39**: 679-694.

Hinterdorfer, P., Baumgartner, W., Gruber, H. J., Schilcher, K. and Schindler, H. (1996). Detection and localization of individual antibody-antigen recognition events by atomic force microscopy. *Proceedings of the National Academy of Science U S A* **93**: 3477-3481.

Hoberg, A., Ottender, M., Marnett, L. J. and Poulsen, H. E. (2004). Measurement of the malondialdehyde- 2'-deoxyguanosine adduct in human urine by immuno-extraction and liquid chromatography/atmospheric pressure chemical ionisation tandem mass spectrometry. *Journal of Mass Spectrometry* **39**: 38-42.

Hochleitner, K., Thomale, J., Nikitin, A. Y. and Rajewsky, M. F. (1991). Monoclonal antibody-based selective isolation of DNA fragments containing an alkylated base to be quantified in defined gene sequences. *Nucleic Acids Research* **19**: 4467-4472.

Hock, A. K., Vigneron, A. M., Carter, S., Ludwig, R. L. and Vousden, K. H. (2011). Regulation of p53 stability and function by the deubiquitinating enzyme USP42. *EMBO* **30**: 4921-4930.

Hu, W. G. and Lu, Q. P. (2014). Impact of oxidative stress on the cytoskeleton of pancreatic epithelial cells. *Experimental and Therapeutic Medicine* **8**(5): 1438-1442.

Huber, M. D. and Gerace, L. (2007). The size-wise nucleus: nuclear volume control in eukaryotes. *Journal of Cell Biology* **179**(4): 583-584.

Huschtscha, L. I. and Holliday, R. (1983). Limited and unlimited growth of SV40-transformed cells from human diploid MRC-5 fibroblasts. *Journal of Cell Science* **63**: 77-99.

Hwang, E. and Bowen, P. (2007). DNA damage, a biomarker of carcinogenesis: its measurement and modulation by diet and environment. *Critical Reviews in Food Science and Nutrition* **47**: 27-50.

Ierardi, V., Ferrera, F., Millo, E., Damonte, G., Filaci, G. and Valbusa, U. (2013). Bioactive surfaces for antibody-antigen complex detection by atomic force microscopy. *Journal of Physics: Conference Series* **439**: 1-11.

Jackson, S. P. (2009). The DNA damage response: new moleculare insights and new approaches to cancer therapy. *Biochemical Society Transactions* **37**: 483-494.

Janero, D. R. (1990). Malodialdehyde and thiobarbituric acid-reactivity as diagnostic indices of lipid perioxidation and peroxide tissue injury. *Free Radical Biology & Medicine* **9**: 515-540.

Ji, C., Rouzer, C. A., Marnet, L. J. and Pietenpol, J. A. (1998). Induction of cell cycle arrest by the endogenous product of lipid peroxidation, malondialdehyde. *Carcinogenesis* **19**: 1275-1283.

Jordan, S. J., Whiteman, D. C., Purdie, D. M., Green, A. C., Webb, P. M. (2006). Does smoking increase risk of ovarian cancer? A systematic review. *Gynecologic Oncology* **103**: 1122-1129.

Khaldi, N. and Shields, D. C. (2011). Shift in the isoelectric-point of milk proteins as a consequence of adaptive divergence between the milks of mammalian species. *Biology Direct* **6**(1): 40-49.

Kim, M., Chung, J., Yang, J., Chung, S., Kwag, N. and Yoo, J. (2003). Hydrogen Peroxide-Induced Cell Death in a Human Retinal Pigment Epithelial Cell Line, ARPE-19. *Korean Journal of Ophthalmology* **17**: 19-28.

Kim, S. I., Yoon, J.-I., Tommasi, S. and Besaratina, A. (2012). New experimental data linking secondhand smoke exposure to lung cancer in nonsmokers. *The FASEB Journal* **26**: 1845-1854.

Klinov, D. V., Dubrovin, E. V. and Yaminsky, I. V. (2003). Scanning probe microscopy of DNA on mica and graphite. Scanning Tunneling Microscopy/Spectroscopy and Related Techniques: 12th International Conference. Koenraad, P. M. and Kemerink, M. Eindhoven, American Institute of Physics. **696:** 452-456.

Knutson, C. G., Akingbade, D., Crews, B. C., Voehler, M., Stec, D. F. and Marnett, L. J. (2007). Metabolism *in vitro* and *in vivo* of the DNA base adduct, M_1G. *Chemical Research In Toxicology* **20**: 550-557.

Knutson, C. G. and Marnett, L. J. (2010) DNA Damage Caused by Endogenously Generated Products of Oxidative Stress, in The Chemical Biology of DNA Damage (eds N. E. Geacintov and S. Broyde), Wiley-VCH Verlag GmbH & Co. KGaA, Weinheim, Germany. 105-126.

Knutson, C. G., Wang, H., Rizzo, C. J. and Marnett, L. J. (2007). Metabolism and Elimination of the Endogenous DNA Adduct, 3-(2-Deoxy-β-D-

erythropentofuranosyl)-pyrimido[1,2-α]purine-10(3H)-one, in the Rat. *Journal of Biological Chemistry* **282**: 36257-36264.

Kozera, B. and Rapacz, M. (2013). Reference genes in real-time PCR. *Journal of Applied Genetics* **54**: 391-406.

Kruse, J.-P. and Gu, W. (2009). Modes of p53 regulation. *Cell* **137**: 609-622.

Kyte, J. and Doolittle, R. (1982). A simple method for displaying the hydrophobic character of a protein. *Journal of Molecular Biology* **157**: 105-132.

Lazaro-Dieguez, F. and Egea, G. (2007). Comparative study of the impact of the actin cytoskeleton on cell shape and membrane surface in mammalian cells in response to actin toxins. *Modern Research and Educational Topics in Microscopy*. **1:** 362-369.

Lee, D. H., O'Connor, T. R. and Pfeifer, G. P. (2002). Oxidative DNA damage induced by copper and hydrogen peroxide promotes CG → TT tandem mutations at methylated CpG dinucleotides in nucleotide excision repair-deficient cells. *Nucleic Acids Research* **30**(16): 3566-3573.

Leuratti, C., Singh, R., Lagneau, C., Farmer, P. B., Plastaras, J. P., Marnett, L. J. and Shuker, D. E. G. (1998). Determination of Malondialdehyde-induced DNA damage in human tissues using an immunoslot blot assay. *Carcinogenesis* **19**: 1919-1924.

Leuratti, C., Watson, M. A., Deag, E. J., Welch, A., Singh, R., Gottschalg, E., Marnett, L. J., Atkin, W., Day, N. E., Shuker, D. E. G. and Bingham, S. A. (2002). Detection of malondialdehyde DNA adducts in human colorectal mucosa: relationship with

diet and the presence of adenomas. *Cancer Epidemiology, Biomarkers & Prevention* **11**: 267-273.

Levine, A. J. and Oren, M. (2009). The first 30 years of p53: growing ever more complex. *Nature Reviews* **9**: 749-758.

Lewin, M. H., Bailey, N., Bandaletova, T., Bowman, R., Cross, A. J., Pollock, J., Shuker, D. E. G. and Bingham, S. A. (2006). Red meat enhances the colonic formation of the DNA adduct O6-carboxymethyl guanine: implications for colorectal cancer risk. *Cancer Research* **66**: 1859-1865.

Li, Z., Henning, S. M., Zhang, Y., Zerlin, A., Li, L., Gao, K., Lee, R., Karp, H., Thames, G., Bowerman, S. and Heber, D. (2010). Antioxidant-rich spice added to hamburger meat during cooking results in reduced meat, plasma, and urine malondialdehyde concentrations. *American journal of Clinical Nutrition* **91**: 1180-1184.

Liu, M., Poo, W.-K. and Lin, Y.-l. (2015). Pyrazine, 2-ethylpyridine, and 3-ethylpyridine are cigarette smoke components that alter the growth of normal and malignant human lung cells, and play a role in multidrug resistance development. *Experimental and Molecular Pathology* **98**(1): 18–26.

Liu, Y. and Bodmer, W. F. (2006). Analysis of P53 mutations and their expression in 56 colorectal cancer cell lines. *Proceedings of the National Academy of Sciences* **103**(4): 976-981.

Liu, Z., Tan, S., Zu, Y., Fu, Y., Meng, R. and Xing, Z. (2010). The interactions of cisplatin and DNA studied by atomic force microscopy. *Micron* **41**: 833-839.

Livak, K. J. and Schmittgen, T. D. (2001). Analysis of relative gene expression data using Real-Time Quantitative PCR and the 2^{2DDCt} method. *Methods* **25**: 402-408.

Lodish, H., Berk, A., Zipursky, S. L., Matsudaira, P., Baltimore, D. and Darnell, J. (2000). Molecular Cell Biology. 4th ed. New York, USA. W H Freeman and Company. 140-152.

Lowe, S. W. and Lin, A. W. (2000). Apoptosis in cancer. *Carcinogenesis* **21**(3): 485-495.

Lykkesfeldt, J. (2001). Determination of malondialdehyde as dithiobarbituric acid adduct in biological samples by HPLC with fluorescence detection: comparison with ultraviolet-visible spectrophotometry. *Clinical Chemistry* **47**: 1725-1727.

Lykkesfeldt, J. (2007). Malondialdehyde as biomarker of oxidative damage to lipids caused by smoking. *Clinica Chimica Acta* **380**: 50-58.

Lykkesfeldt, J., Viscovich, M. and Poulsen, H. E. (2004). Plasma malondialdehyde is induced by smoking: a study with balanced antioxidant profiles. *British Journal of Nutrition* **92**: 203-206.

Lyubchenko, Y. L. (2011). Preparation of DNA and nucleoprotein samples for AFM imaging. *Micron* **42**: 196-206.

Ma, B., Villalta, P. W., Balbo, S. and Stepanov, I. (2015). Analysis of a malondialdehyde-deoxyguanosine adduct in human leukocyte DNA by liquid chromatography nanoelectrospray-high-resolution tandem mass spectrometry. *Chemical Research in Toxicology* **27**(10): 1829-1836.

Macallan, D. C., Fullerton, C. A., Neese, R. A., Haddock, K., Park, S. S. and Hellerstein, M. K. (1998). Measurement of cell proliferation by labelling of DNA with stable isotope labelled glucose: Studies *in vitro*, in animals, and in humans. *Proceedings of the National Academy of Sciences* **95**: 708-713.

Madden, T. (2002). The BLAST Sequence Analysis Tool. The NCBI Handbook [Internet]. McEntyre J, O. J. Bethesda (MD): National Center for Biotechnology Information (US)**:** Chapter 16. Available from: http://www.ncbi.nlm.nih.gov/books/NBK21097/

Maglott, D., Ostell, J., Pruitt, K. and Tatusova, T. (2010). Entrez-Gene: gene-centred information at NCBI. *Nucleic Acids Research*: doi: 10.1093/nar/gkq1237.

Mahmoudi, S., Henriksson, S. and Corcoran, M. (2009). Wrap53, a natural p53 antisense transcript required for p53 induction upon DNA damage. *Molecular Cell* **33**: 462-471.

Mao, H., Reddy, G. R., Marnett, L. J. and Stone, M. P. (1999). Solution structure of an oligodeoxynucleotide containing the malondialdehyde deoxyguanosine adduct N^2-(3-oxo-1-propenyl)-dG (ring-opened M_1G) positioned in a $(CpG)_3$ frameshift hotspot of the *salmonella typhimurium hisD3052* gene. *Biochemistry* **38**: 13491-13501.

Mao, Y., Song, G., Cai, Q., Liu, M., Luo, H., Shi, M., Ouyang, G. and Bao, S. (2006). Hydrogen peroxide-induced apoptosis in human gastric carcinoma MGC803 cells. *Cell Biology International* **30**: 332-337.

Marnett, L. J. (1999). Lipid peroxidation- DNA damage by malondialdehyde. *Mutation Research* **424**: 83-95.

Marnett, L. J. (2002). Oxy radicals, lipid peroxidation and DNA damage. *Toxicology* **181-182**: 219-222.

Marnett, L. J. (2012). Inflammation and cancer: chemical approaches to mechanisms, imaging and treatment. *The Journal of Organic Chemistry* **77**: 5224-5238.

Martin, A. C. R., Facchiano, A. M., Cuff, A. L., Hernandez-Boussard, T., Olivier, M., Hainaut, P. and Thornton, J. M. (2002). Integrating mutation data and structural analysis of the TP53 tumor-suppressor protein. *Human Mutation* **19**: 149-164.

Mascotti, K., McCullough, J. and Burger, S. R. (2000). HPC viability measurement: trypan blue versus acridine orange and propidium iodide. *Transfusion* **40**: 693-696.

Mendes, R., Cardoso, C. and Pestana, C. (2009). Measurement of malondialdehyde in fish: a comparison study between HPLC methods and the traditional spectrophotometric test. *Food Chemistry* **112**: 1038-1045.

Mermelstein, C. S., Rebello, M. I. L., Amoral, L. M. and Costa, M. L. (2003). Changes in cell shape, cytoskeletal proteins and adhesion sites of cultured cells after extracellular Ca^{2+} chelation. *Brazilian Journal of Medical and Biological Research* **36**: 1111-1116.

Michaud, D. S., Pietinen, P., Taylor, P. R., Virtanen, M., Virtamo, J. and Albanes, D. (2002). Intakes of fruits and vegetables, carotenoids and vitamins A, E, C in relation to

the risk of bladder cancer in the ATBC cohort study. *British Journal of Cancer* **87**: 960-965.

Moll, U. M. and Petrenko, O. (2003). The MDM2-p53 Interaction. *Molecular Cancer Research* **1**: 1001-1008.

Moloney, M., McDonnell, L. and O'Shea, H. (2004). Atomic force microscopy of BHK-21 cells: an investigation of cell fixation techniques. *Ultramicroscopy* **100**: 153-161.

Montano, M., Cisneros, J., Ramirez-Venegas, A., Pedraza-Chaverri, J., Mercado, D., Ramos, C. and Sansores, R. H. (2010). Malondialdehyde and superoxide dismutase correlate with FEV(1) in patients with COPD associated with wood smoke exposure and tobacco smoking. *Inhalation Toxicology* **22**(10): 868-874.

Moore, S. A., Humphreys, E., Friesen, M. D., Shuker, D. E. G. and Bingham, S. A. (2008). The effect of n-6 polyunsaturated fatty acid on blood levels of malondialdehyde-deoxyguanosine adducts in human subjects. *The Open Biomarkers Journal* **1**: 28-35.

Moore, S. A., Xeniou, O., Zeng, Z. T., Humphreys, E., Burr, S., Gottschalg, E., Bingham, S. A. and Shuker, D. E. G. (2010). Optimizing immunoslot blot assays and application to low DNA adduct levels using an amplification approach. *Analytical Biochemistry* **403**: 67-73.

Morelli, C., Barbisan, F., Laccheri, L. and Tognon, M. (2004). SV40-immortalised human fibroblast as a source of SV40 infectious virions. *Molecular Medicine* **10**: 112-116.

Mosmann, T. (1983). Rapid colormetric assay for cellular growth and survival: Application to proliferation and cytotoxicity assays. *Journal of Immunological Methods* **65**: 55-63.

Munnia, M., Bonassi, S., Verna, A., Quaglia, R., Pelucco, D., Ceppi, M., Neri, M., Buratti, M., Taioli, E., Garte, S. and Peluso, M. (2006). Bronchial malondialdehyde DNA adducts, tobacco smoking and lung cancer. *Free Radical Biology & Medicine* **41**: 1499-1505.

Naderi, N. J., Farhadi, S. and Sarshar, S. (2012). Micronucleus assay of buccal mucosa cells in smokers with the history of smoking less and more than 10 years. *Indian Journal of Pathology and Microbiology* **55**(4): 433-438.

NCBI (2014). National Center for Biotechnology Information. MD, USA, US National Library of Medicine.

Nelson, N. J. (2006). Migrant Studies Aid the Search for Factors Linked to Breast Cancer Risk. *Journal of the National cancer Institute* **98**(7): 436-438.

Nersesyan, A., Kundi, M., Atefie, K., Schulte-Hermann, R. and Knasmuller, S. (2006). Effect of staining procedures on the results of micronucleus assays with exfoliated oral mucosa cells. *Cancer Epidemiology, Biomarkers & Prevention* **15**: 1835-1840.

Niedernhofer, L. J., Daniels, J. S., Rouzer, C. A., Greene, R. E. and Marnett, L. J. (2003). Malondialdehyde, a product of lipid peroxidation, is mutagenic in human cells. *The Journal of Biological Chemistry* **278**: 31426-31433.

Nielsen, F., Mikkelsen, B. B., Nielsen, J. B., Andersen, H. R. and Grandjean, P. (1997). Plasma malondialdehyde as biomarker for oxidative stress: reference interval and effects of life-style factors. *Clinical Chemistry* **43**: 1209-1214.

Nikoshkov, A. and Hurd, Y. L. (2006). p53 splice variants generated by atypical mRNA processing confer complexity of p53 transcripts in the human brain. *Biochemical and Biophysical Research Communications* **351**: 383-386.

Nolan, T., Hands, R. E. and Bustin, S. A. (2006). Quantification of mRNA using real-time RT-PCR. *Nature Protocols* **1**(3): 1559-1582.

O'Brate, A. and Giannakakou, P. (2003). The importance of p53 location: nuclear or cytoplasmic zip code? *Drug Resistance Updates* **6**: 313-322.

Oates, K. D. and Van der Kraak, G. D. (2003). Utility of the TBARS assay in detecting oxidative stress in the white sucker (*Catostomus commersoni*) populations exposed to pulp mill effluent. *Aquatic Toxicology* **63**(4): 447-463.

Onyango, A. N. and Baba, N. (2010). New hypotheses on the pathways of formation of malondialdehyde and isofurans. *Free Radical Biology & Medicine* **49**(10): 1594-1600.

Ottender, M. B., Knutson, C. G., Daniels, J. S., Hashim, M., Crews, B. A., Remmel, R. P., Wang, H., Rizzo, C. and Marnett, L. J. (2006). *In vivo* oxidative metabolism of a major peroxidation-derived DNA adduct M_1dG. *Proceedings of the National Academy of Sciences* **103**: 6665-6669.

Palazzo, A. F. and Gregory, T. R. (2014) The case for junk DNA. *Public Library of Science Genetics* **10**(5). doi: 10.1371/journal.pgen.1004351.

Pamplona, R. (2011). Advanced lipoxidation end-products. *Chemico-Biological Interactions* **192**: 14–20.

Parkin, D. M., Boyd, L., Darby, S. C., Mesher, D., Sasieni, P., Walker, L. C. and Peto, R. (2011). The fraction of cancer attributable to lifestyle and environmental factors in the UK in 2010. *British Journal of Cancer* **105**: S2-S81.

Pastre, D., Pietrement, O., Fusil, S., Landousy, F., Jeusset, J., David, M.-O., Hamon, L., Le Can, E. and Zozime, A. (2003). Adsorption of DNA to mica mediated by divalent counterions: A theoretical and experimental study. *Biophysical Journal* **85**: 2507-2518.

Pavanello, S., Favretto, D., Brugnone, F., Mastrangelo, G., Dal Pra, G. and Clonfero, E. (1999). HPLC/fluorescence determination of anti-BPDE-DNA adducts in mononuclear white blood cells from PAH-exposed humans. *Carcinogenesis* **20**(3): 431-435.

Peluso, M., Srivatanakul, P., Munnia, A., Jedpiyawongse, A., Ceppi, M., Sangrajrang, S., Piro, S. and Boffetta, P. (2010). Malondialdehyde-deoxyguanosine adducts among workers of a Thai industrial estate and nearby residents. *Environmental Health Perspectives* **118**: 55-59.

Phillips, D. H., Farmer, P. B., Beland, F. A., Nath, R. G., Poirier, M. C., Reddy, M. V. and Turteltaub, K. W. (2000). Methods of DNA adduct determination and their

application to testing compounds for genotoxicity. *Environmental and Molecular Mutagenesis* **35**: 222-233.

Pietrasanta, L. I., Smith, B. L. and MacLeod, M. C. (2000). A novel approach for analysing the structure of DNA modified by benzo[a]pyrene diol epoxide at single-molecule resolution. *Chemical Research In Toxicology* **13**: 351-355.

Pipas, J. M. (2009). SV40: Cell transformation and tumorigenesis. *Virology* **384**: 294–303.

Pleasance, E. D., Stephens, P. J., O'Meara, S., McBride, D. J., Meynert, A., Jones, D., Lin, M., Beare, D., Lau, K. W., Greenman, C., Varela, I., Nik-Zainal, S., Davies, H. R., Ordonez, G. R., Mudie, L. J., Latimer, C., Edkins, S. and Stebbings, L. (2010). A small-cell lung cancer genome with complex signatures of tobacco exposure. *Nature* **463**: 184-190.

Pouladi, N., Kouhsari, S. M., Feizi, M. H., Gavgani, R. R. and Azarfam, P. (2013). Overlapping region of p53/Wrap53 transcripts: mutational analysis and sequence similarity with microRNA-4732-5p. *Asian Pacific Journal of Cancer Prevention* **14**: 3503-3507.

Prentki, M., Chaponnier, C., Jeanrenaud, B. and Gabbiani, G. (1979). Actin microfilaments, cell shape, and secretory processes in isolated rat hepatocytes. Effect of phalloidin and cytochalasin D. *Journal of Cell Biology* **81**: 592-607.

Pryor, W. A. and Stone, K. (1993). Oxidants in cigarette smoke. Radicals, hydrogen peroxide, peroxynitrate and peroxynitrite. *Annals of the New York Academy of Sciences* **686**(1): 12-27.

Rajeevan, M. S., Ranamukhaarachchi, D. G., Vernon, S. D. and Unger, E. R. (2001). Use of real-time quantitative PCR to validate the results of cDNA array and differential display PCR technologies. *Methods* **25**(4): 443-451.

Rasband, W. S. (1997). ImageJ. Bethesda, Maryland, USA., U.S. National Institutes of Health. Available at: http://imagej.nih.gov/ij/, 1997-2014.

Riggins, J. N., Pratt, D. A., Voehler, M., Daniels, J. S. and Marnett, L. J. (2004). Kinetics and mechanism of the general-acid-catalyzed ring-closure of the malondialdehyde-DNA adduct, N^2-(3-oxo-1-propenyl)deoxyguanosine (N^2OPd^G), to 3-(2'-deoxy-β-D-erythro-pentofuranosyl)pyrimido[1,2-α]purin-10(3H)-one (M_1dG). *Journal of the American Chemical Association* **126**: 10571-10581.

Rittie, L., Monboisse, J., Gorisse, M. and Gillery, P. (2002). Malondialdehyde binding to proteins dramatically alters fibroblast functions. *Journal of Cellular Physiology* **191**: 227-236.

Rivlin, N., Brosh, R., Oren, M. and Rotter, V. (2011). Mutations in the p53 Tumor Suppressor Gene. *Genes and Cancer* **2**(4): 466-474.

Rong, S., Zou, L., Zhang, Y., Zhang, G., Li, X., Li, M., Yang, F., Li, C., He, Y., Guan, H., Guo, Y., Wang, D., Cui, X., Ye, H., Liu, F., Pan, H. and Yang, Y. (2015). Determination of purine contents in different parts of pork and beef by high performance liquid chromatography. *Food Chemistry* **170**: 303-307.

SABiosciences. (2015). *Pathway central: p53 signalling.* Available at: http://www.sabiosciences.com/pathway.php?sn=p53_Signaling. Last accessed 30th April 2015.

Santos, N. C. and Castanho, M. A. R. B. (2004). An overview of the biophysical applications of atomic force microscopy. *Biophysical Chemistry* **107**: 133-149.

Sapkota, M., Hottor, T. K., DeVasure, J. M., Wyatt, T. A. and McCaskill, M. L. (2014). Protective role of CYP2E1 inhibitor diallyl disulfide (DADS) on alcohol-induced malondialdehyde-deoxyguanosine (M_1dG) adduct formation. *Alcoholism, Clinical and Experimental Research* **38**: 1550-1558.

Seljeskog, E., Hervig, T. and Mansoor, M. A. (2006). A novel HPLC method for the measurement of thiobarbituric acid reactive substances (TBARS). A comparison with a commercially available kit. *Clinical Biochemistry* **39**: 947-954.

Sharma, R. A. and Farmer, P. B. (2004). Biological relevance of adduct detection to the chemoprevention of cancer. *Clinical Cancer Research* **10**: 4901-4912.

Shaw, K. L., Grimsley, G. R., Yakovlev, G. I., Makarov, A. A. and Pace, C. N. (2001). The effect of net charge on the solubility, activity, and stability of ribonuclease Sa. *Protein Science*. **10:** 1206-1215.

Sheridan, M. T. and West, C. M. L. (2001). Ability to undergo apoptosis does not correlate with the intrinsic radiosensitivity (SF2) of human cervix tumor cell lines. *International Journal of Radiation Oncology* **50**: 503 – 509.

Shuker, D. E. G. and Benford, D. J. (1997). DNA modification in carcinogen risk assessment in relation to diet: recent advances and some perspectives from a MAFF workshop. *Biomarkers* **2**: 265-278.

Siddique, Y. H., Ara, G., Beg, T., Gupta, J. and Afzal, M. (2009). Assessment of cell viability, lipid peroxidation and quantification of DNA fragmentation after the treatment of anticancerous drug mitomycin C and curcumin in cultured human blood lymphocytes. *Experimental and Toxicologic Pathology* **62**(5): 503-508.

Singh, R., Leuratti, C., Josyula, S., Sipowicz, M. A., Bhalchandra, A. D., Kasprzak, K. S., Schut, H. A. J., Marnett, L. J., Anderson, L. M. and Shuker, D. E. G. (2001). Lobe-specific increases in malondialdehyde DNA adduct formation in the livers of mice following infection with *Helicobacter hepaticus*. *Carcinogenesis* **22**(8): 1281-1287.

Soussi, T., Dehouche, K. and Beroud, C. (2000). p53 website and analysis of p53 gene mutations in human cancer: forging a link between epidemiology and carcinogenesis. *Human Mutation* **15**: 105-113.

Stafford, J. B., Eoff, R. L., Kozekova, A., Rizzo, C. J., Guengerich, F. P. and Marnett, L. J. (2009). Translesion DNA synthesis by human DNA polymerase *n* on templates containing a pyrimidopurinone deoxyguanosine adduct, 3-(2'-deoxy-β-D-*erythro*-pentofuranosyl)pyrimido-[1,2-α]purin-10(3*H*)-one. *Biochemistry* **48**: 471-480.

Starr, D. A. and Fridolfsson, H. N. (2010). Interactions Between Nuclei and the Cytoskeleton Are Mediated by SUN-KASH Nuclear-Envelope Bridges. *Cell and Developmental Biology* **26**: 421-444.

Surget, S., Khoury, M. P. and Bourdon, J.-C. (2014). Uncovering the role of p53 splice variants in human malignancy: a clinical perspective. *OncoTargets and Therapy* **7**: 57-68.

Szekely, J., Wang, H., Peplowski, K. M., Knutson, C. G., Marnett, L. J. and Rizzo, C. J. (2008). "One-pot" syntheses of malondialdehyde adducts of nucleosides. *Nucleosides, Nucleotides, and Nucleic Acids* **27**: 103-109.

Takagi, M., Absalon, M. J., McLure, K. G. and Kastan, M. B. (2005). Regulation of p53 translation and induction after DNA damage by ribosomal protin L26 and nucleolin. *Cell* **123**: 49-63.

Termini, J. (2000). Hydroperoxide-induced DNA damage and mutations. *Mutation Research/Fundamental and Molecular Mechanisms of Mutagenesis* **450**(Issues 1–2): 107–124.

Tomankova, K., Kolarova, H., Vujtek, M. and Zapletalova, H. (2007). Study of cancer cells used atomic force microscopy. *Modern Research and Educational Topics in Microscopy*: 23-28.

Traverso, N., Menini, S., Maineri, E. P., Patriarca, S., Odetti, P., Cottalasso, D., Marinari, U. M. and Pronzato, M. A. (2004). Malondialdehyde, a lipoperoxidation-derived aldehyde, can bring about secondary oxidative damage to proteins. *Journals of Gerontology Series A: Biological Science and Medical Science* **59**(9): B890-895.

Tug, T., Karatas, F., Terzi, S. M. and Ozdemir, N. (2005). Comparison of serum malondialdehyde levels determined by two different methods in patients with COPD: HPLC or TBARS methods. *Science* **36**: 41-44.

Tuma, D. J., Kearley, M. L., Thiele, G. M., Worrall, S., Haver, A., Klassen, L. W. and Sorrell, M. F. (2001). Elucidation of reaction scheme describing malondialdehyde-acetaldehyde-protein adduct formation. *Chemical Research In Toxicology* **14**: 822-832.

Untergasser, A., Cutcutache, I., Koressaar, T., Ye, J., Faircloth, B. C., Remm, M. and Rozen, S. G. (2012). Primer3 - new capabilities and interfaces. *Nucleic Acids Research* **40**(15): e115.

Vaca, C. E., Fang, J., Mutanen, M. and Valsta, L. (1995). ^{32}P-Postlabelling determination of DNA adducts of malondialdehyde in humans: total white blood cells and breast tissue. *Carcinogenesis* **16**: 1847-1851.

Vahakangas, K. H., Bennett, W. P., Castren, K., Welsh, J. A., Khan, M. A., Blomeke, B., Alavanja, M. C. R. and Harris, C. C. (2001). p53 and K-ras mutations in lung cancers from former and never-smoking women. *Cancer Research* **61**: 4350-4356.

VanMeerloo, J., Kaspers, G. J. and Cloos, J. (2011). Cell sensitivity assays: the MTT assay. *Methods in Molecular Biology* **731**: 231-245.

Van Vleet, T. R., Watterson, T. L., Klein, P. J. and Coulombe, J. R. A. (2006). Aflatoxin B_1 alters the expression of p53 in cytochrome P450-expressing human lung cells. *Toxicological Sciences* **89**(2): 399-407.

VanderVeen, L. A., Hashim, M. F., Shyr, Y. and Marnett, L. J. (2003). Induction of frameshift and base pair substitution mutations by the major DNA adduct of the

endogenous carcinogen malondialdehyde. *Proceedings of the National Academy of Sciences* **100**(24): 14247-14252.

Verhoven, B., Schlegel, R. A. and Williamson, P. (1995). Mechanisms of phosphatidylserine exposure, a phagocyte recognition signal, on apoptotic T lymphocytes. *Journal of Expermental Medicine* **182**(2): 1597-1601.

Vogel, A. I. (1956). *Practical Organic Chemistry*. 3rd ed. London, UK, Longman. 1061.

Vogelstein, B., Papadopoulos, N., Velculescu, V. E., Zhou, S., Jr., L. A. D. and Kinzler, K. W. (2013). Cancer Genome Landscapes. *Science* **339**: 1546-1558.

Wang, Y., Rosengarth, A., Luecke, H. (2007). Structure of the human p53 core domain in the absence of DNA. *Acta Crystallographica. Section D, Biological Crystallography* **63**: 276-281.

Watkins, S. C. and St Croix, C. M. (2013). *Current Protocols Select: Methods and Applications in Microscopy and Imaging*. New Jersey, USA, John Wiley & Sons Inc. 5-19.

Watson, J. D. and Crick, F. H. C. (1953). A structure for deoxyribose nucleic acid. *Nature* **171**: 737-738.

Webb., H. K., Truong, V. K., Hasan, J., Crawford, R. J. and Ivanova, E. P. (2011). Physico-mechanical characterisation of cells using atomic force microscopy - current research and methodologies. *Journal of Microbiological Methods* **86**: 131-139.

Webster, M., Witkin, K. L. and Cohen-Fix, O. (2009). Sizing up the nucleus: nuclear shape, size and nuclear-envelope assembly. *Cells Science* **122**: 1477-1486.

Weglarz, L., Molin, I., Orchel, A., Parfiniewicz, B. and Dzierzewicz, Z. (2006). Quantitative analysis of the level of *p53* and *p21^{waf1}*mRNA in human colon cancer HT-29 cells treated with inositol hexaphosphate. *Acta Biochimica Polonica* **53**(2): 349-356.

Wei, J., Zaika, E. and Zaika, A. (2012) p53 family: role of protein isoforms in human cancer. *Journal of Nucleic Acids* **2012**, 1-19.

Wilson, S. M. and Bacic, A. (2012). Preparation of plant cells for transmission electron microscopy to optimize immunogold labeling of carbohydrate and protein epitopes. *Nature Protocols* **7**: 1716-1727.

Xu-Monette, Z. Y., Medeiros, J. L., Li, Y., Orlowski, R. Z., Andreeff, M., Bueso-Ramos, C. E., Greiner, T. C., McDonnell, T. J. and Young, K. H. (2012). Dysfunction of the TP53 tumour suppressor gene in lymphoid malignancies. *Blood* **119**(16): 3668-3683.

Yang, P., He, X. Q., Peng, L., Li, A. P., Wang, X. R., Zhou, J. W. and Liu, Q. Z. (2007). The role of oxidative stress in hormesis induced by sodium arsenite in human embryo lung fibroblast (HELF) cellular proliferation model. *Journal of Toxicology and Environmental Health A* **70**(11): 976-983.

Ye, J., Coulouris, G., Zaretskaya, I., Cutcutache, I., Rozen, S. and Madden, T. (2012). Primer-BLAST: a tool to design target-specific primers for polymerase chain reaction. *BMC Bioinformatics* **13**: 134.

Zarkovic, N., Cipak, A., Jaganjac, M., Borovic, S. and Zarkovic, K. (2013). Pathophysiological relevance of aldehydic protein modifications. *Journal of Proteomics* **92**: 239 – 247.

Zhang, Y., Chen, S., Hsu, T. and Santella, R. M. (2002). Immunohistochemical detection of malondialdehyde-DNA adducts in human oral mucosa cells. *Carciniogenesis* **23**: 207-211.

Zhou, X., Taghizadeh, K. and Dedon, P. C. (2005). Chemical and biological evidence for base propenals as the major source of the endogenous M_1dG adduct in cellular DNA. *The Journal of Biological Chemistry* **280**: 25377-25382.

Zhu, H. and Gooderham, N. (2002). Neoplastic transformation of human lung fibroblast MRC-5 SV2 cells induced by benzo(a)pyrene and confluence culture. *Cancer Research* **62**: 4605-4609.

APPENDIX 1

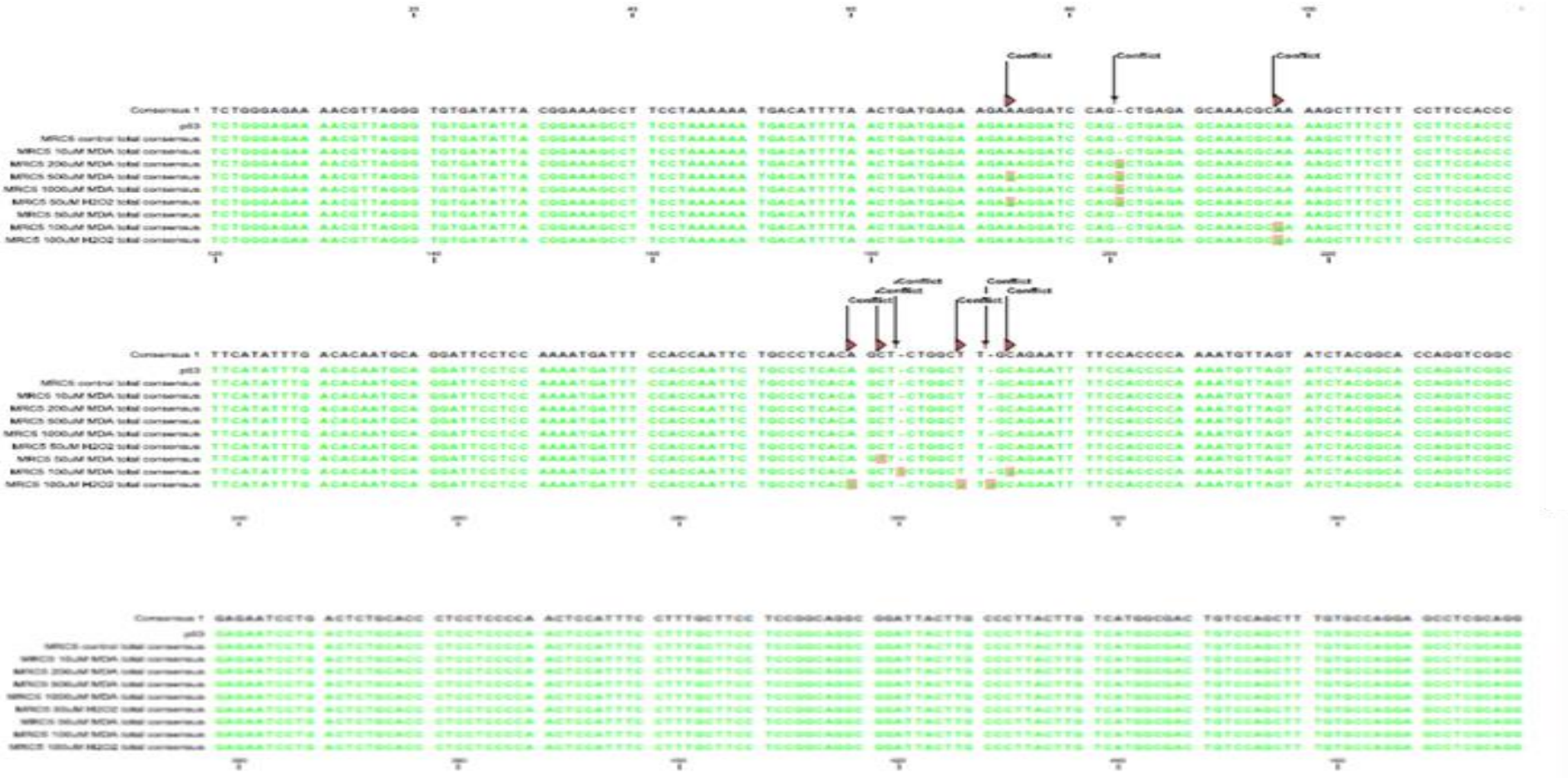

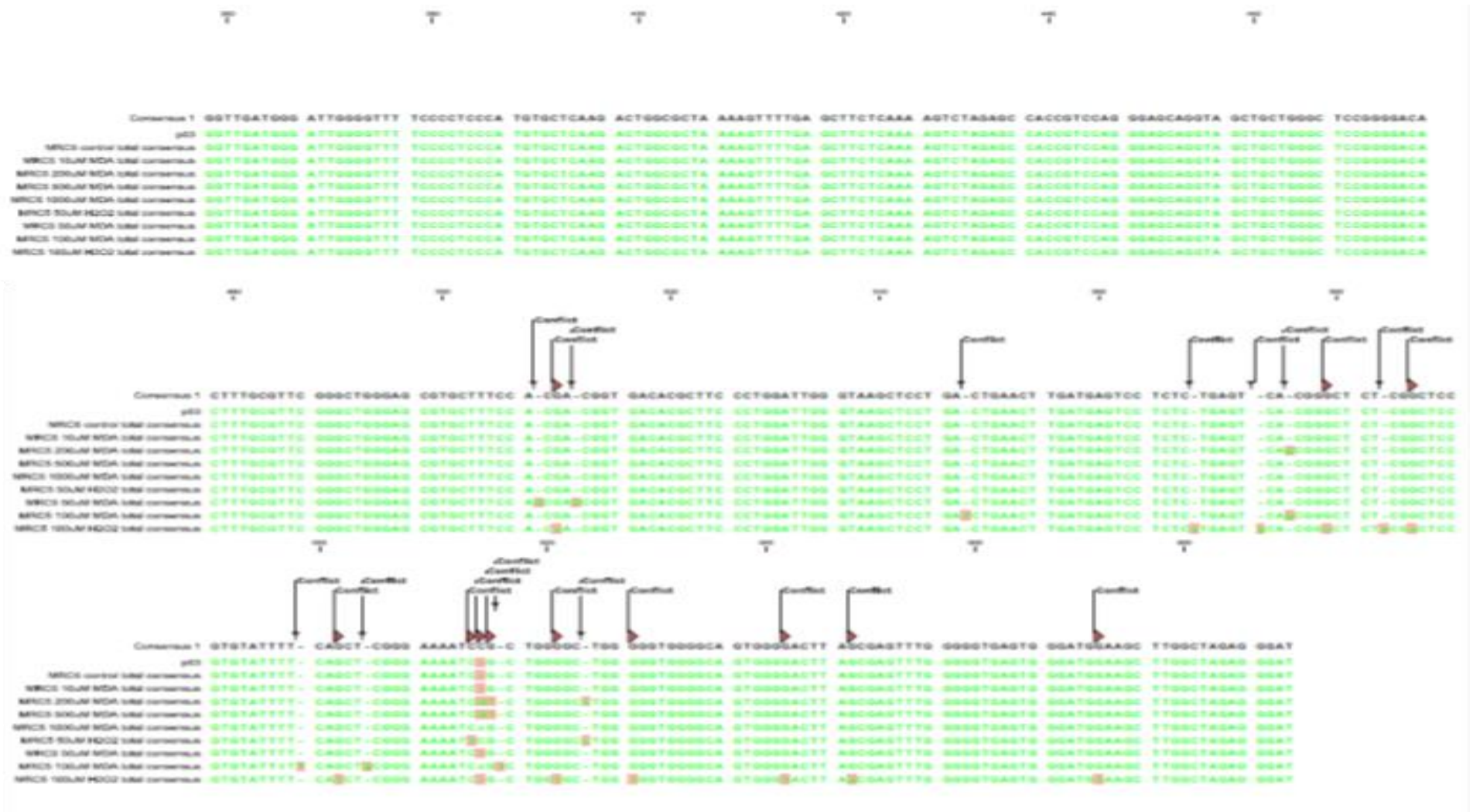

Figure 49. Nucleotide sequence of residues 4640-5328 of *TP53* gene, sequenced from DNA of MRC5 cells treated with MDA (0-1000 µM) and H_2O_2 (50-100 µM) for 48 h, aligned to the *TP53* GenBank sequence. Mutations in the sequence are highlighted as conflicts.

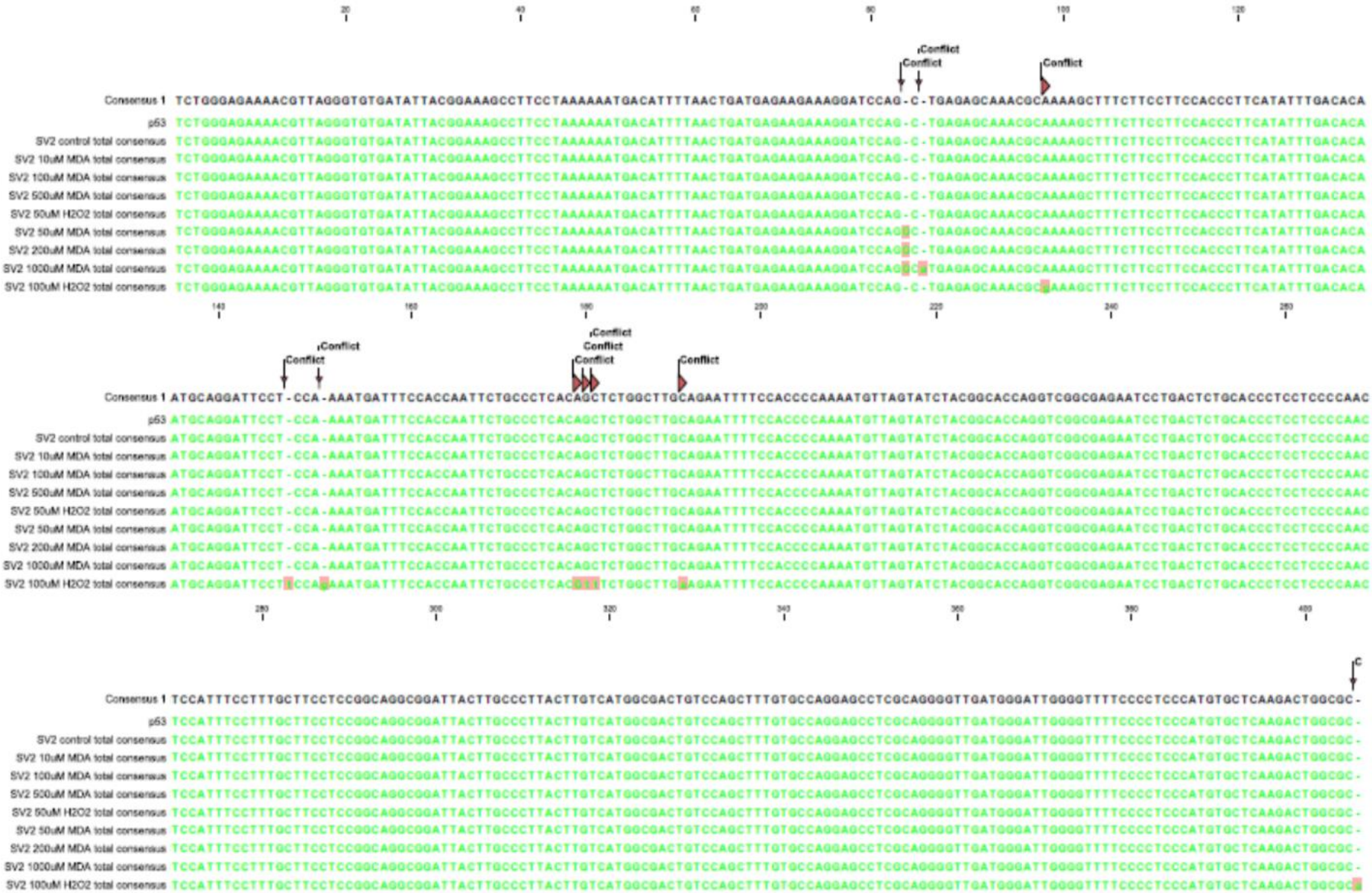
Conflict
Consensus 1
p53
SV2 control total consensus
SV2 10uM MDA total consensus
SV2 100uM MDA total consensus
SV2 500uM MDA total consensus
SV2 50uM H2O2 total consensus
SV2 50uM MDA total consensus
SV2 200uM MDA total consensus
SV2 1000uM MDA total consensus
SV2 100uM H2O2 total consensus

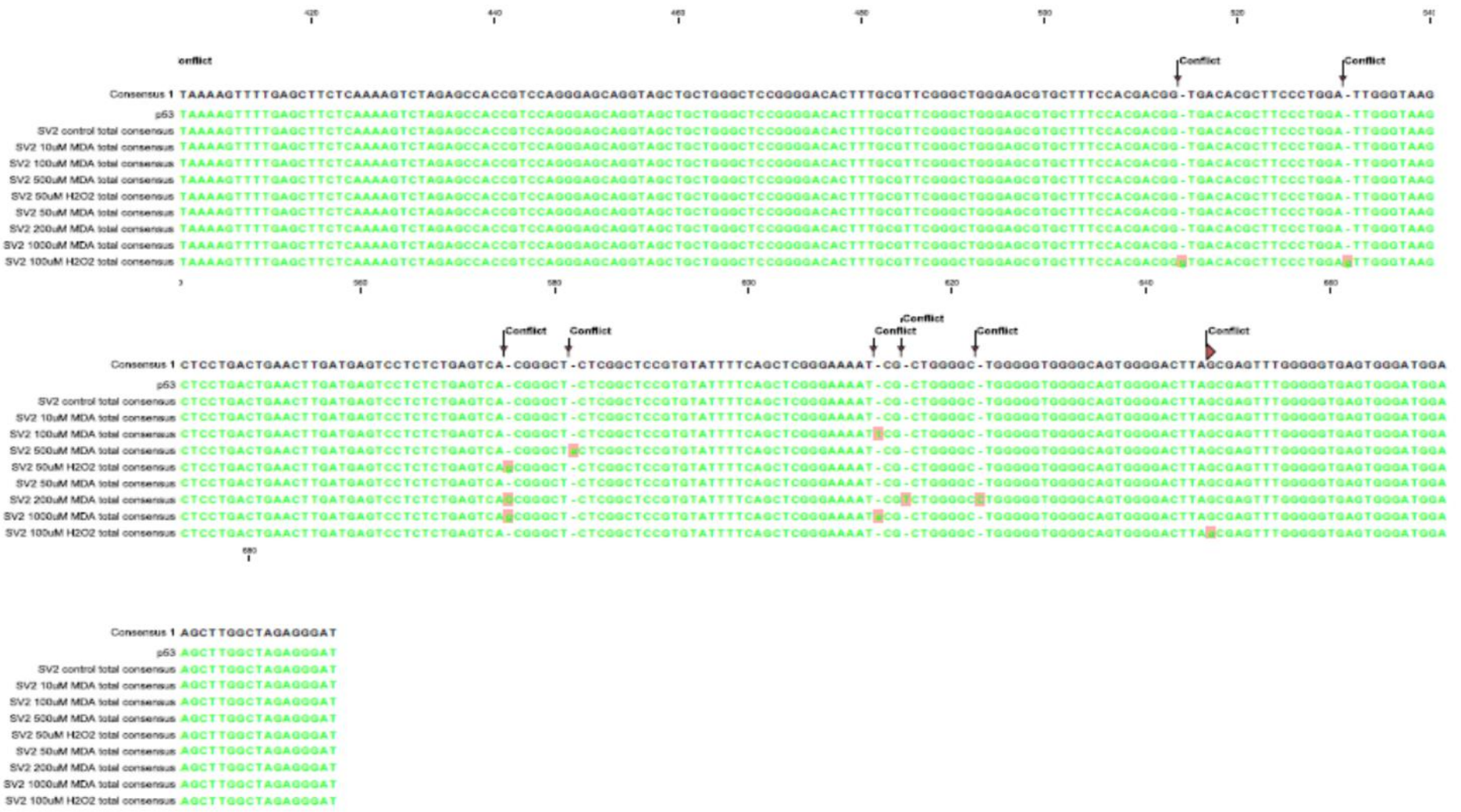

Figure 50. Nucleotide sequence of residues 4640-5328 of *TP53* gene, sequenced from DNA of MRC5 SV2 cells treated with MDA (0-1000 µM) and H_2O_2 (50-100 µM) for 48 h, aligned to the *TP53* GenBank sequence. Mutations in the sequence are highlighted as conflicts.

APPENDIX 2

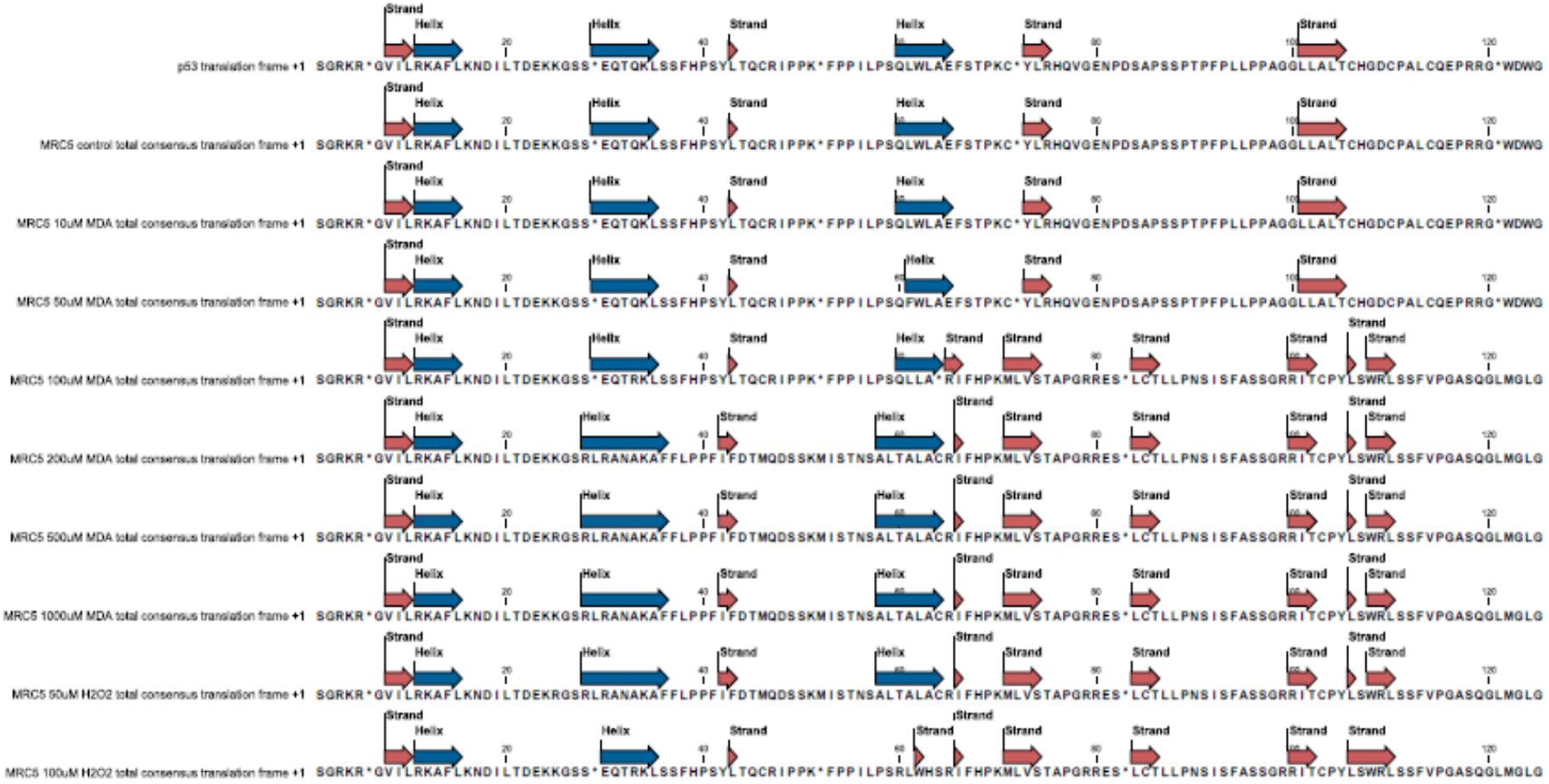
p53 translation frame +1 SGRKR*GVILRKAFLKNDILTDEKKGSS*EQTQKLSSFHPSYLTQCRIPPK*FPPILPSQLWLAEFSTPKC*YLRHQVGENPDSAPSSPTPFPLLPPAGGLLALTCHGDCPALCQEPRRG*WDWG
MRC5 control total consensus translation frame +1 SGRKR*GVILRKAFLKNDILTDEKKGSS*EQTQKLSSFHPSYLTQCRIPPK*FPPILPSQLWLAEFSTPKC*YLRHQVGENPDSAPSSPTPFPLLPPAGGLLALTCHGDCPALCQEPRRG*WDWG
MRC5 10uM MDA total consensus translation frame +1 SGRKR*GVILRKAFLKNDILTDEKKGSS*EQTQKLSSFHPSYLTQCRIPPK*FPPILPSQLWLAEFSTPKC*YLRHQVGENPDSAPSSPTPFPLLPPAGGLLALTCHGDCPALCQEPRRG*WDWG
MRC5 50uM MDA total consensus translation frame +1 SGRKR*GVILRKAFLKNDILTDEKKGSS*EQTQKLSSFHPSYLTQCRIPPK*FPPILPSQFWLAEFSTPKC*YLRHQVGENPDSAPSSPTPFPLLPPAGGLLALTCHGDCPALCQEPRRG*WDWG
MRC5 100uM MDA total consensus translation frame +1 SGRKR*GVILRKAFLKNDILTDEKKGSS*EQTRKLSSFHPSYLTQCRIPPK*FPPILPSQLLA*RIFHPKMLVSTAPGRRES*LCTLLPNSISFASSGRRITCPYLSWRLSSFVPGASQGLMGLG
MRC5 200uM MDA total consensus translation frame +1 SGRKR*GVILRKAFLKNDILTDEKKGSRLRANAKAFFLPPFIFDTMQDSSKMISTNSALTALACRIFHPKMLVSTAPGRRES*LCTLLPNSISFASSGRRITCPYLSWRLSSFVPGASQGLMGLG
MRC5 500uM MDA total consensus translation frame +1 SGRKR*GVILRKAFLKNDILTDEKRGSRLRANAKAFFLPPFIFDTMQDSSKMISTNSALTALACRIFHPKMLVSTAPGRRES*LCTLLPNSISFASSGRRITCPYLSWRLSSFVPGASQGLMGLG
MRC5 1000uM MDA total consensus translation frame +1 SGRKR*GVILRKAFLKNDILTDEKKGSRLRANAKAFFLPPFIFDTMQDSSKMISTNSALTALACRIFHPKMLVSTAPGRRES*LCTLLPNSISFASSGRRITCPYLSWRLSSFVPGASQGLMGLG
MRC5 50uM H2O2 total consensus translation frame +1 SGRKR*GVILRKAFLKNDILTDEKRGSRLRANAKAFFLPPFIFDTMQDSSKMISTNSALTALACRIFHPKMLVSTAPGRRES*LCTLLPNSISFASSGRRITCPYLSWRLSSFVPGASQGLMGLG
MRC5 100uM H2O2 total consensus translation frame +1 SGRKR*GVILRKAFLKNDILTDEKKGSS*EQTRKLSSFHPSYLTQCRIPPK*FPPILPSRLWHSRIFHPKMLVSTAPGRRES*LCTLLPNSISFASSGRRITCPYLSWRLSSFVPGASQGLMGLG

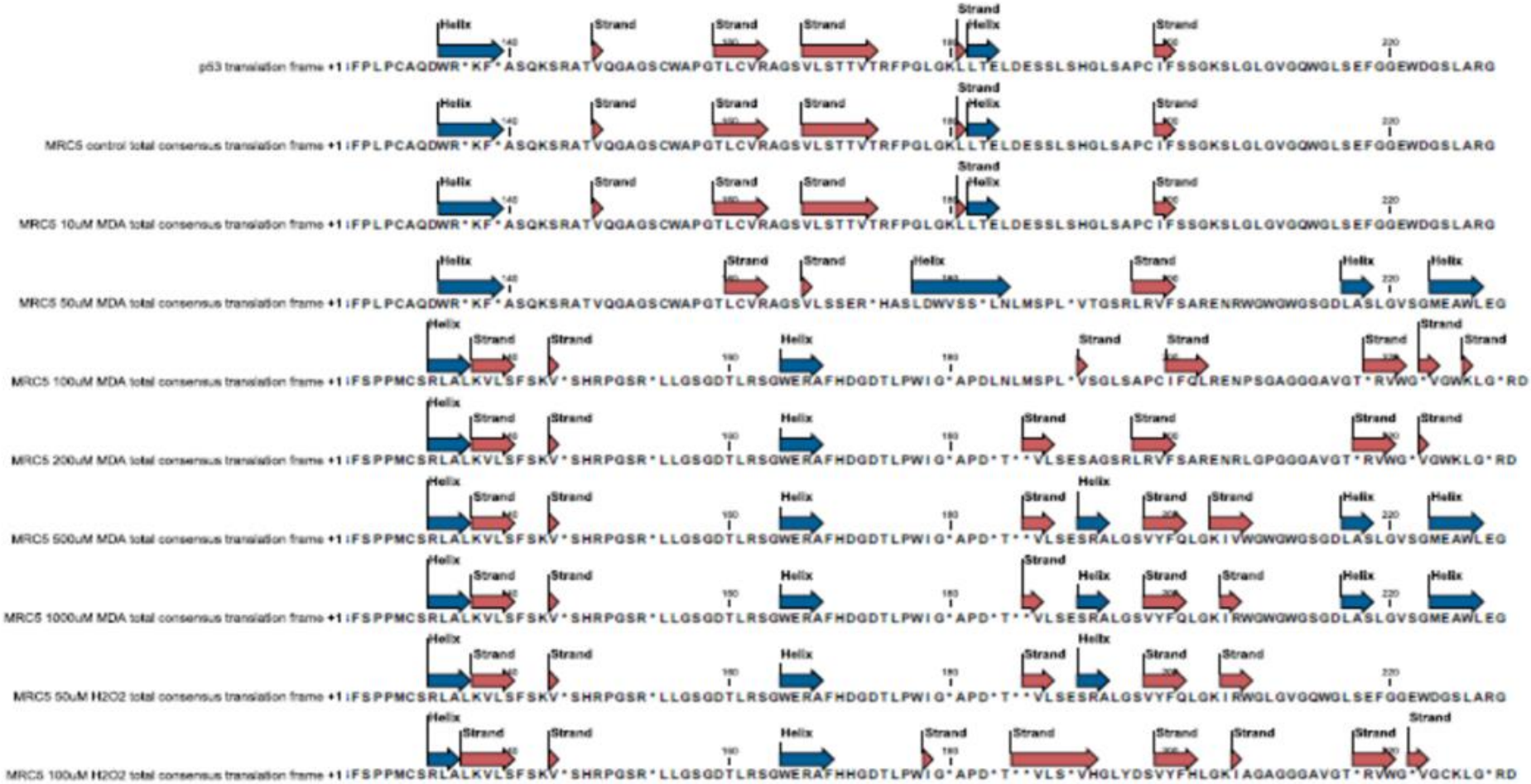

Figure 51. Primary structure of residues 4640-5328 of the *TP53* gene extracted from MRC5 cells treated with MDA (0-1000 µM) and H_2O_2 (50-100 µM) for 48 h. Secondary structures are illustrated with arrows in pink (β –strand) or blue (α- helix).

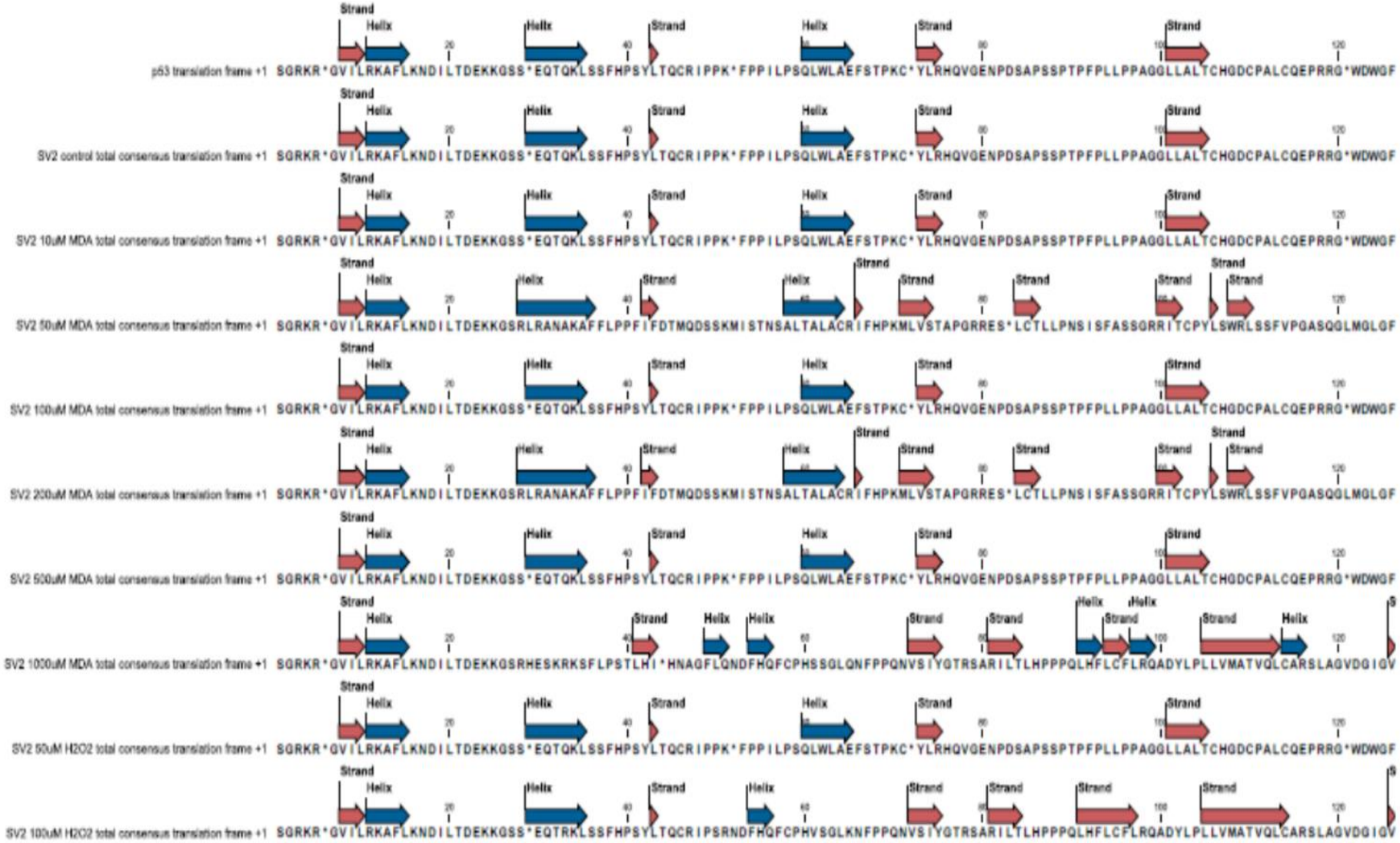
p53 translation frame +1 SQRKR*QVILRKAFLKNDILTDEKKGSS*EQTQKLSSFHPSYLTQCRIPPK*FPPILPSQLWLAEFSTPKC*YLRHQVGENPDSAPSSPTPFPLLPPAGQLLALTCHGDCPALCQEPRRQ*WDWGF
SV2 control total consensus translation frame +1 SQRKR*QVILRKAFLKNDILTDEKKGSS*EQTQKLSSFHPSYLTQCRIPPK*FPPILPSQLWLAEFSTPKC*YLRHQVGENPDSAPSSPTPFPLLPPAGQLLALTCHGDCPALCQEPRRQ*WDWGF
SV2 10uM MDA total consensus translation frame +1 SQRKR*QVILRKAFLKNDILTDEKKGSS*EQTQKLSSFHPSYLTQCRIPPK*FPPILPSQLWLAEFSTPKC*YLRHQVGENPDSAPSSPTPFPLLPPAGQLLALTCHGDCPALCQEPRRQ*WDWGF
SV2 50uM MDA total consensus translation frame +1 SQRKR*QVILRKAFLKNDILTDEKKGSRLRANAKAFFLPPFIFDTMQDSSKMISTNSALTALACRIFHPKMLVSTAPGRRES*LCTLLPNSISFASSGRRITCPYLSWRLSSFVPGASQGLMGLGF
SV2 100uM MDA total consensus translation frame +1 SQRKR*QVILRKAFLKNDILTDEKKGSS*EQTQKLSSFHPSYLTQCRIPPK*FPPILPSQLWLAEFSTPKC*YLRHQVGENPDSAPSSPTPFPLLPPAGQLLALTCHGDCPALCQEPRRQ*WDWGF
SV2 200uM MDA total consensus translation frame +1 SQRKR*QVILRKAFLKNDILTDEKKGSRLRANAKAFFLPPFIFDTMQDSSKMISTNSALTALACRIFHPKMLVSTAPGRRES*LCTLLPNSISFASSGRRITCPYLSWRLSSFVPGASQGLMGLGF
SV2 500uM MDA total consensus translation frame +1 SQRKR*QVILRKAFLKNDILTDEKKGSS*EQTQKLSSFHPSYLTQCRIPPK*FPPILPSQLWLAEFSTPKC*YLRHQVGENPDSAPSSPTPFPLLPPAGQLLALTCHGDCPALCQEPRRQ*WDWGF
SV2 1000uM MDA total consensus translation frame +1 SQRKR*QVILRKAFLKNDILTDEKKGSRHESKRKSFLPSTLHI*HNAGFLQNDFHQFCPHSSGLQNFPPQNVSIYQTRSARILTLHPPPQLHFLCFLRQADYLPLLVMATVQLCARSLAGVDGIGV
SV2 50uM H2O2 total consensus translation frame +1 SQRKR*QVILRKAFLKNDILTDEKKGSS*EQTQKLSSFHPSYLTQCRIPPK*FPPILPSQLWLAEFSTPKC*YLRHQVGENPDSAPSSPTPFPLLPPAGQLLALTCHGDCPALCQEPRRQ*WDWGF
SV2 100uM H2O2 total consensus translation frame +1 SQRKR*QVILRKAFLKNDILTDEKKGSS*EQTRKLSSFHPSYLTQCRIPSRNDFHQFCPHVSGLKNFPPQNVSIYQTRSARILTLHPPPQLHFLCFLRQADYLPLLVMATVQLCARSLAGVDGIGV

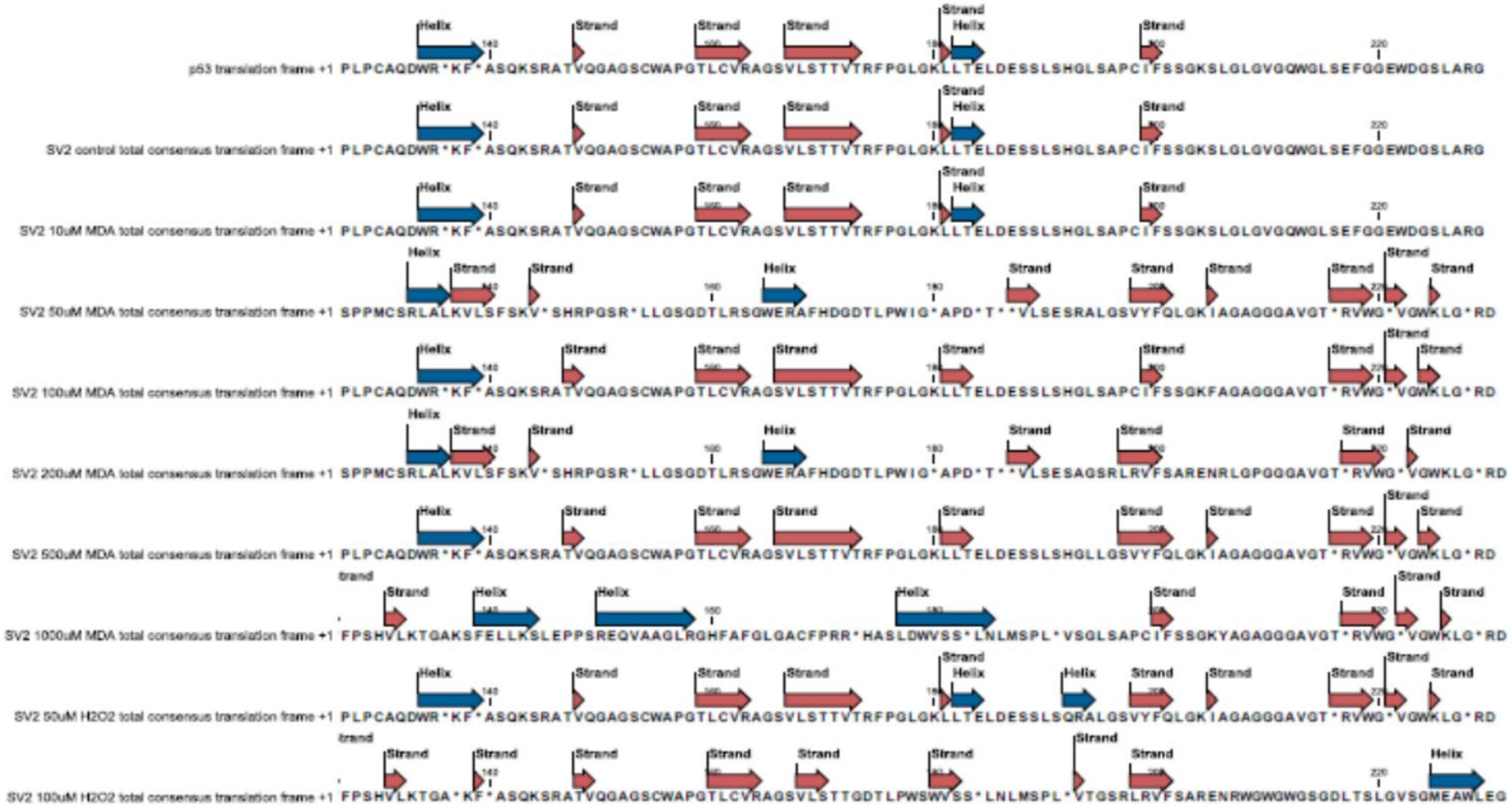

Figure 52. Primary structure of residues 4640-5328 of the *TP53* gene extracted from MRC5 SV2 cells treated with MDA (0-1000 µM) and H_2O_2 (50-100 µM) for 48 h. Secondary structures are illustrated with arrows in pink (β –strand) or blue (α- helix).